Ultrastructural, molecular and functional heterogeneities of cerebellar granule cell presynaptic terminals

Kevin Dorgans

Université de Strasbourg
École Doctorale des Sciences de la Vie et de la Santé
Unité de recherche : CNRS UPR3212

THÈSE

Présentée par **Kevin DORGANS** soutenue le **03 Octobre 2017**

En vue d'obtenir le grade de docteur de l'université de Strasbourg
Spécialité : Neurosciences

Ultrastructural, molecular and functional heterogeneities of cerebellar granule cell presynaptic terminals

Thèse dirigée par

Dr POULAIN Bernard	CNRS, Université de Strasbourg
Dr DOUSSAU Frédéric	CNRS, Université de Strasbourg (Encadrant)

Rapporteurs

Dr CATHALA Laurence	CNRS, Université Pierre et Marie Curie (UPMC)
Dr HERZOG Etienne	CNRS, Université de Bordeaux

Autres membres du jury

Dr GASMAN Stéphane	CNRS, Université de Strasbourg
Pr HALLERMANN Stefan	CLI, Université de Leipzig
Dr DOUSSAU Frédéric	CNRS, Université de Strasbourg (Encadrant)

ACKNOWLEDGMENTS

Tout d'abord, je tiens à remercier Dr Laurence Cathala, Dr Etienne Herzog ainsi que Pr Hallermann Stefan et Dr Stéphane Gasman pour avoir accepté d'évaluer mon travail de thèse. Je remercie également Pr Bernard Poulain d'avoir dirigé ma thèse.

Merci Fred pour ces (presque) quatre ans d'aventure dans les synapses (qui ne se ressemblent pas), les réseaux, les fibres parallèles (qu'on stimule sans échecs !), les synapsines. Merci de m'avoir accueilli dans ta chouette famille, et surtout pour ta patience et ta bienveillance qui ne te font jamais défaut.

Merci Philippe pour tous tes bons plans (scientifiques), de m'avoir initié aux analyses tordues et de me pousser à aller de plus en plus loin (qui qu'il s'agisse !).

Merci au reste de l'équipe toujours présente : Ludovic Spaeth, Fernando Giuliani, Sébastien Roux, Didier Desaintjan, Aline Huber, Jean-Louis Bossu. Et surtout à ceux qui sont pas/plus là : Alvaro Sanz Diez, Inés Gonzalez Calvo, Orkan Ozcan pour leur aide mais surtout leur présence.

Merci à toute l'équipe de l'Aïkido (Sadek, Emilienne, Schwartz) et à l'équipe de l'escalade (Léa, Guillaume, Thomas Matthieu) de m'avoir accompagné durant ce que je pouvais vous consacrer de temps libre !

Et surtout, merci à Sarah et Ben et Élise pour votre présence, votre bienveillance et vos encouragements de tous les instants. Avec vous, tout est différent.

TABLE OF CONTENTS

INDEX OF FIGURES

LIST OF ABBREVIATIONS

AMPA	α-Amino-3-hydroxy-5-methyl-4-isoxazole propionic acid
BC	Basket-Cell
CB1	Cannabinoid Receptor Type-1
CDK	Cyclin-Dependant Kinase
CaMK	Ca 2+ /calmodulin-dependent protein kinase
EphB	Erythropoietin-Producing Human hepatocellular receptors (type B receptor)
FFI	FeedForward Inhibition
GABA	Gamma-Aminobutyric Acid
GC	Granule-cell
GC-MLI	Granule-cell to Molecular Layer Interneuron (synaptic terminals)
LTD	Long-Term Depression
LTP	Long-Term Potentiation
MAP	Mitogen-Activaed Protein
MF	Mossy-Fibers
MLI	Molecular Layer Interneuron
Munc-13	Mammalian Uncoordinated 13
NCAM	Neural Cell Adhesion Molecule
NMDA	N-Methyl-D-Aspartate
PC	Purkinje-Cell
PDZ	PSD-95, Dlf, ZO-1 (domain)
PKA	Protein Kinase A
Pr	(neurotransmitter) Release Probability
PV	Parvalbumin
RIM	Rab3 Interacting Molecule
RIM-BP	Rab3 Interacting Molecule Binding Protein
RP	Reserve Pool (aka. Resting Pool of presynaptic vesicles)
RRP	Readily Releasable Pool (of presynaptic vesicles)
SC	Stellate-Cell
SC-LTD	Stellate-Cell Long-Term Depression
SNARE	Soluble Nethylmaleimide-sensitive-factor-Attachement protein Receptor
SOM	Somatostatin
SSE	Short-term Suppression of Excitation
STP	(presynaptic) Short-Term Plasticity
STSP	Synapse-specific Short Term Plasticity
SV	Synaptic Vesicle
Syn2KO	Knockout mouse for Synapsin gene coding type-2 isoform
TKO	Triple-Knockout mouse model
VAMP	Vesicle Associated Membrane Protein
VGCC	Voltage-Gated Calcium channel
VGluT	Vesicular Transporter for Glutamate
VIAAT	Vesicular Inhibitory Amino Acid Transporter

PREFACE *(English version)*

The way neuronal network process and store information is a major issue in the study of brain function. Studying the mechanisms of communication between neurons is essential to understanding the various functions endowed by the central nervous system: from the simplest motor reflexes to higher cognitive process.

Synapses play a critical role in neural communication. In the simplistic vision of neuronal networks, a presynaptic neuron connects a post-synaptic neuron with chemical synapses, functional units dedicated to information transfer. Indeed, synapses provide a millisecond-scale process of neuron-to-neuron communication by transforming an input electrical information -the action potentials- into a chemical signal -the neurotransmitters.

One of the goals of the team "Physiologie des réseaux de neurones" where I performed my PhD is to characterize the molecular determinants of neurotransmitter release behaviors during information processing at the presynaptic level, also termed as *short term synaptic plasticity*. In parallel, we investigate the mechanisms of information processing in the cerebellar cortex, a neuronal structure involved in motor control. In the cerebellar cortex, feedforward inhibition has a central function in computing the output message coded by Purkinje cell activity. Molecular layer interneurons are responsible of feedforward inhibition and control the precise instructions given by Purkinje cells for motor adjustments. Thus, I worked on the mechanisms of short term plasticity at granule cell-to- molecular layer interneuron (GC-MLI) synapses that control feedforward inhibition.

Presynaptic terminals are highly sensitive units: experience, microenvironment, neuromodulators, developmental processes are prone to modify the synapse. For example, post-synaptic neurons can directly impact the quantity of neurotransmitter released with retrograde messengers. Also, patterns of action potentials emitted at specific frequencies can enhance or depress the release of neurotransmitters for minutes and hours.

Importantly, the frequency of the input information received at a given synapse will determine its future ability to release neurotransmitters. In most of the brain structures, relevant information is encoded through high frequency bursts of activity. *Short term presynaptic plasticity* is the consequence of a presynaptic adaptation following the integration high frequency action potentials. Some synapses react positively to such patterns by releasing more neurotransmitters while other synapses depress.

Previous studies have characterized a large panel of short term plasticity behaviors in the central nervous system. Most of the time, inter-synaptic variations depend on :
i) The nature of the synapses that are being stimulated. (The nature of the presynaptic and the post-synaptic cell)
ii) The stimulation pattern (frequency and number of stimuli) used to evoke neurotransmitter release.

GC-MLI synapses from the cerebellar cortex are specialized in high frequency information transfer. These presynaptic terminals are well known for their ability to sustain glutamate release following sensorimotor integration traduced by high frequency bursts of action potentials. Hence, I studied the presynaptic properties of single GC-MLI terminals and their ability to drive the feedforward system. All my observations were characterized by a strong inter-synaptic variability at the single-synapse level and were at the origin of my PhD project:

"Ultrastructural, molecular and functional heterogeneities at granule cell presynaptic terminals"

Surprisingly, unitary GC-MLI synapses endowed very different short term plasticity behaviors following the same stimulation pattern leading to the idea that granule cell terminals are hypervariable units. I described this heterogeneity in a molecular, ultrastructural and functional frameworks. Also, I characterized the consequence of multimodal short term plasticity onto the recruitment of feedforward network.

Also, I have identified SynapsinII as a candidate for inter-synaptic molecular heterogeneity. I assessed the same ultrastructural, functional and network drive properties at granule cell terminals in mice lacking SynapsinII. These mice displayed a strong reduction of granule cell intersynaptic heterogeneity meaning that a selective expression of presynaptic molecules can determine inter-synaptic variations of short term plasticity at a given population of synapses.

In the following introduction of my PhD work I will first describe the basic physiology of neurotransmitter release (Part I) and cerebellar cortex (Part II). I will focus onto molecular layer interneurons (MLI) as post-synaptic neuronal target (Part III) and describe their ability to integrate electrical inputs. Finally, we will see that granule cells synapses are specialized in high-frequency information transfer (Part IV) and that short term plasticity is susceptible to vary from one synaptic terminal to another (Part V).

PREFACE *(French version)*

Afin d'étudier les fonctions cérébrales, il est nécessaire de comprendre les mécanismes de traitement de l'information au sein de neurones en réseau. Un bonne compréhension des mécanismes de communication entre neurones permet en effet de mieux apprécier les diverses fonctions du système nerveux central : depuis les réflexes moteurs les plus simples jusqu'aux processus cognitifs les plus complexes.

Les synapses jouent un rôle fondamental dans la communication neuronale. Dans un réseau composé de multiples neurones, les neurones présynaptiques se connectent à des neurones post-synaptiques à l'aide de synapses chimiques ; ce sont des unités fonctionnelles dédiées au transfert d'information. Les synapses permettent une communication de neurone à neurone extrêmement rapide (à l'échelle de la milliseconde), et transforment un signal électrique (les potentiels d'action) en message chimique (les neurotransmetteurs).

Un des objectifs de l'équipe « Physiologie des réseaux de neurones » dans laquelle j'ai effectué ma thèse, est de caractériser les déterminants moléculaires de la libération de neurotransmetteurs durant le transfert d'une information électrique au niveau présynaptique aussi dénommé *plasticité à court terme*. En parallèle, l'équipe s'intéresse aux mécanismes de traitement de l'information nerveuse dans le cortex cerebelleux, une structure du cerveau impliquée dans le contrôle moteur. Dans le cortex cerebelleux, l'inhibition en mode *feedforward* a un rôle essentiel dans la computation du message de sortie encodé par l'activité de décharge des cellules de Purkinje. Les interneurones de la couche moléculaire sont responsables de l'inhibition *feedforward* et contrôlent les instructions précises données aux cellules de Purkinje en vue d'établir des ajustements moteurs. Ainsi, j'ai travaillé sur les mécanismes de plasticité à court terme aux terminaisons synaptiques entre cellules en grain et interneurones de la couche moléculaire (synapses GC-MLI) ce sont des synapses excitatrices qui sont à l'origine du contrôle de l'inhibition *feedforward*.

Les terminaisons présynaptiques sont des unités fonctionnelles extrêmement sensibles : leur microenvironnement, des neuromodulateurs ainsi que des processus développementaux peuvent affecter leur fonctionnement. Par exemple, les neurones post-synaptiques peuvent directement moduler la quantité de neurotransmetteurs libérés par les neurones présynaptiques via des messagers rétrogrades. De plus, stimuler une synapse donnée à une fréquence précise peut augmenter ou diminuer le gain de la neurotransmission pendant plusieurs minutes et certaines fois des heures.

La fréquence d'une information électrique reçue sous la forme de potentiels d'actions au niveau des terminaisons présynaptiques va conditionner sa capacité à libérer des neurotransmetteurs. On parle de *plasticité à court terme*. En effet, lorsqu'elles intègrent des séries de potentiels d'action à haute fréquence, les terminaisons présynaptiques adaptent leurs mécanismes de libération de neurotransmetteurs. Pour une

même stimulation, certaines synapses réagissent en augmentant la quantité de neurotransmetteurs libérés tandis qu'à l'inverse, d'autres synapses dépriment.

Des études ont caractérisé une très grande gamme de comportements de *plasticité à court terme* dans diverses synapses du système nerveux central. La plupart du temps, de telles variations inter-synaptiques dépendent de :
i) la nature des synapses stimulées (la nature du neurone présynaptique et celle du neurone post-synaptique)
ii) le patron de stimulation utilisé (la fréquence et le nombre de stimuli appliqués)

Les terminaisons synaptiques GC-MLI du cortex cerebelleux sont spécialisées dans le transfert d'informations à très hautes fréquences. Ces synapses sont reconnues pour leur capacité à soutenir la libération de glutamate au cours d'une intégration sensorimotrice qui se traduit par des bouffées de potentiels d'action à de très hautes fréquences. Ainsi, j'ai étudié les propriétés présynaptiques de synapses unitaires GC-MLI ainsi que leur capacité à activer l'inhibition *feedforward*. J'ai observé de manière récurrente des variations inter-synaptiques à l'échelle de synapses unitaires et ces résultats sont à l'origine de mon projet de thèse :

« Heterogeneités ultrastructurales, moléculaires et fonctionnelles aux terminaisons synaptiques des celules en grain »

De manière intéressante, les synapses unitaires GC-MLI présentaient des comportements de plasticité à court terme extrêmement différents à la suite de stimulations des cellules en grain strictement identiques (séries de potentiels d'action à 100Hz). Ainsi, après avoir caractérisé leur hétérogénéité ultrastructurale et fonctionnelle j'en ai déduit que ces synapses pouvaient être considérées comme des unités hypervariables. J'ai également étudié les conséquences de cette variabilité de fonctionnement présynaptique sur l'activation du réseau inhibiteur *feedforward*.

De plus, j'ai identifié un candidat moléculaire à l'hétérogénéité présynaptique : la SynapsineII. J'ai testé l'hétégorénéité ultrastructurale et fonctionnelle sur des souris knockout pour la SynapsineII : ce modèle présente une très forte réduction de la variabilité du fonctionnement des synapses GC-MLI. Ces données montrent qu'une expression synapse-spécifique de molécules présynaptiques telles que la SynapsineII peut créer des variations de plasticité à court terme au sein d'une même population de synapses.

Dans l'introduction qui suit, je décrirai les bases de la neurotransmission (Partie I), et de la physiologie du cortex cerebelleux (Partie II). Je m'attarderai sur la description des interneurones de la couche moléculaire en tant que des cibles post-synaptiques (Partie III) et décrirai leur capacité à intégrer des informations électriques. Enfin, nous verrons que les terminaisons présynaptiques des cellules en grain sont spécialisées dans le transfert d'information à très haute fréquence (Partie IV) et que la plasticité à court terme

INTRODUCTION

Part1. The presynaptic terminal: an ultrastructural unit designed for chemical transmission

Synapses faithfully transfer input electrical information by releasing neurotransmitters in an ultra fast temporal window (less than 1ms). The incredible ability of synaptic terminals to transmit information and recover within very short time windows is inherent to their evolutionary conserved ultrastructural and molecular properties.

Neurotransmitters are filled inside small synaptic vesicles and the cycle of synaptic vesicles is a multi-step process tightly regulated within the presynaptic compartment. 1) First, synaptic vesicles are gathered from the vesicular reserve to the presynaptic cytomatrix where they are targeted to the active zone. 2) The active zone contains release sites, and synaptic vesicles are docked and primed for vesicular fusion relying on SNARE molecular complexes. 3) Upon network activity, the presynaptic terminals are depolarized by action potentials. Such a depolarization generates an entry of calcium through voltage-dependent calcium channels (VDCCs) at release sites and in turn, the fusion of primed synaptic vesicles in hundreds of microseconds. 4) Following excoytosis, synaptic vesicle membrane and molecular components of the release machinery are rapidly retrieved via several endocytic pathways. Finally, recycling synaptic vesicles in the periphery of release sites through endocytic processes is essential for the refilling of vesicle populations.

During neuronal activity, neurotransmitters are released in the synaptic cleft and produce post-synaptic currents after their binding to post-synaptic receptors. There is a very close relationship between the quantity of neurotransmitter released by synaptic depolarization and the size of post-synaptic currents. The quantity of released neurotransmitters can be assessed by electrophysiological measurements of post-synaptic currents (PSCs). Classically, a simple equation sums up :

$$i_{syn} = n \,.\, p_r \,.\, q$$

i_{syn} the size (in Ampere) of the ePSC
q the size of unitary vesicular fusion event (in Ampere)
n the number of release-ready vesicles
p_r the fusion probability of release ready vesicles

While the quantum size (Q), is both related to presynaptic (the quantity of neurotransmitters inside synaptic vesicles) and postsynaptic variables (the active conductance of ionotropic post-synaptic receptors), the neurotransmitter release probability following a single action potential (P_r) and the number of release sites (n) are strictly presynaptic parameters.

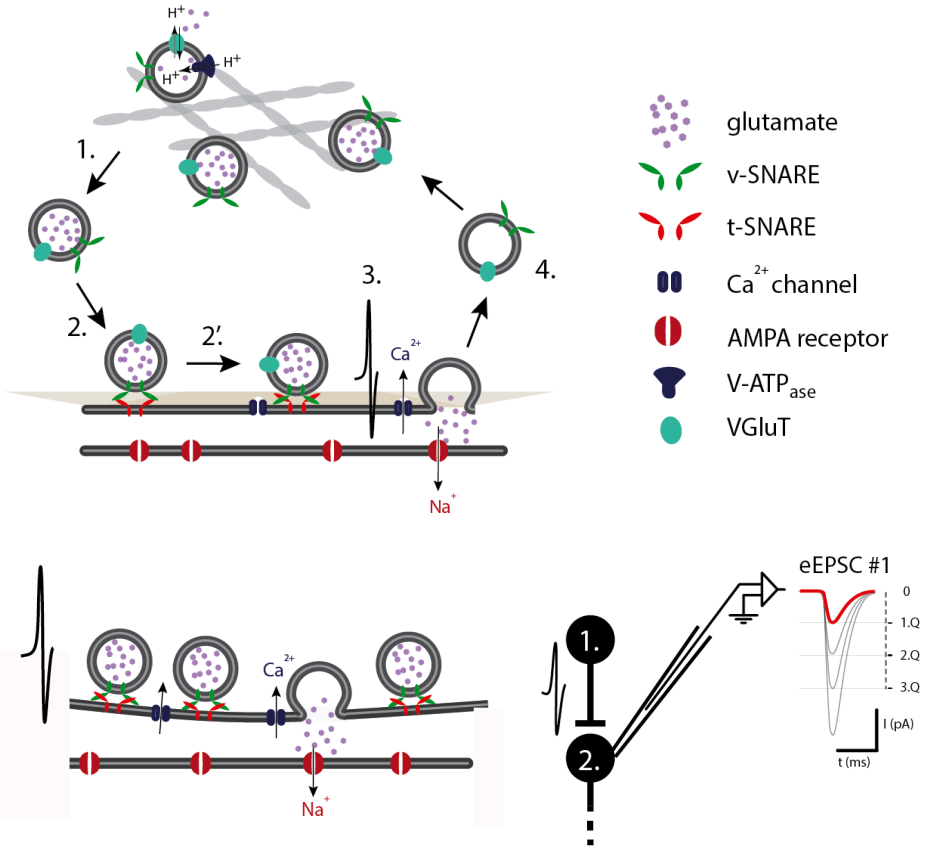

Figure 1. *Top* - **The cycle of synaptic vesicles.** Vesicles are targeted to the active zone (1) where they are docked to the presynaptic membrane (2) and primed from regulated exocytosis (2'). Upon a single spike depolarization, calcium entries trigger neurotransmitter release (3). Finally, endocytosis compensates the fusion of synaptic vesicles by refilling reserve populations.

Bottom – **Excitation-secretion coupling : the equation of neurotransmitter release.** Several (*n) d*ocked and primed vesicles (here, n=4) are ready for fusion. The theoretical release probability (P_r) correspond to the fraction of these vesicles that undergo fusion upon single spike depolarization (here, P_r = 0.25). The quantum value is the ePSC size corresponding to the fixation of the content of a single vesicle to post-synaptic ionotropic receptors.

In the next paragraphs, I will describe the physiological elements that define neurotransmitter release parameters. Also, I will attach a particular importance to presynaptic short term plasticity ; an active and dynamic process that actively shape neurotransmission during information processing by neural networks. I will show that upon repetitive activity, neurotransmitter release parameters are not fixed in time. Finally, presynaptic release parameters follow inter-synaptic variations and this heterogeneity is the main focus point of my PhD.

1.1 Synaptic vesicles

Synaptic vesicles contain neurotransmitters. They are traditionally considered as homogeneous batch of ultrastructural units dedicated to regulated exocytosis. Recent works have characterized the proteome of single synaptic vesicles and lighten their molecular specifications (Takamori, Holt, Stenius, Lemke, Grønborg, Riedel, Urlaub, Schenck, Brügger, et al., 2006).

First, these studies show that neurotransmitters are densely filled inside small synaptic vesicles (~40nm) by vesicular transporters (VGLUT 1-3 for glutamate, VGAT for GABA). Vesicular transporters use proton gradients for vesicular loading so that V-ATPase activity is necessary for lumen acidification, vesicles are equipped with one or two copies of the V-ATPase. These molecules determine the exact quantity of neurotransmitter loaded inside single vesicles. Also termed as neurotransmitter *quantum*, this quantity is supposed to be stable within one synaptic terminal even though it can be subject to various modulation processes (Takamori, 2016).

Second, these studies show that synaptic vesicles are enriched with a high diversity of trafficking proteins, including vSNAREs (VAMP, synaptobrevin), multiple isoforms of Synapsins (that bind cytoskeletal elements, as I will describe below), small Rab-GTPases and also calcium sensitive proteins such as Synaptotagmins, the calcium sensors for vesicular fusion.

Hence, synaptic vesicles are in constant interaction with their cytoskeletal environment and with macromolecular complexes specialized in vesicular fusion. Importantly, there is a huge isoform diversity within the proteins associated to synaptic vesicles. This diversity could be dependent on the synapse which has been purified and is suspected to arise from inter-synaptic heterogeneity.

From biosynthesis to fusion, the trafficking of synaptic vesicles is tightly regulated and follows different steps of maturation. Here, I will describe the presynaptic machinery that turns synaptic vesicles in fully releasable units upon synaptic activity.

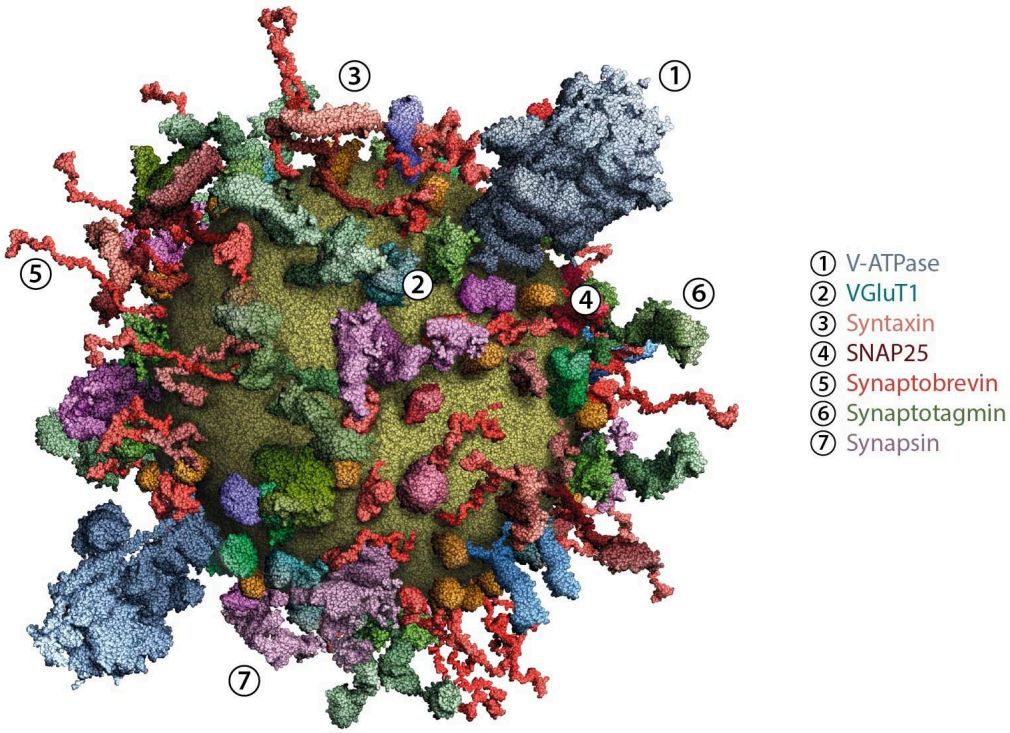

Figure 2. The synaptic vesicle and its molecular components. Three-dimensional reconstruction of a synaptic vesicle with a realistic stoichiometry of its molecular components. V-ATPase and VGluT1 contribute in vesicular neurotransmitter refilling while Syntaxin and SNAP25 are required for vesicular fusion. Various synaptic vesicle associated proteins are involved in vesicular trafficking. The average size of a synaptic vesicle is 40nm. (Takamori, Holt, Stenius, Lemke, Grønborg, Riedel, Urlaub, Schenck, Brü, et al., 2006)

1.2 The presynaptic active zone

The presynaptic active zone is a specialized area of presynaptic terminal devoted to the release of neurotransmitter. It contains the neurotransmitter release machinery and faces the post-synaptic density and especially post-synaptic receptors. Because it holds the fusion sites for synaptic vesicles, the active zone is the keystone element of excitation-secretion coupling (Südhof, 2012). When one action potential depolarizes the presynaptic terminal, voltage gated calcium channels produce presynaptic calcium currents. Calcium currents are detected by protein complexes that will trigger the fusion of some synaptic vesicles anchored at the active zone. As we will see later on, a tight coupling between synaptic vesicles and calcium channels is required for fast synchronous neurotransmission.

Before undergoing exocytosis, synaptic vesicles follow several maturation steps that get them closer from active zone release sites. First, they are targeted the active zone cytomatrix by molecular tethers. Then, synaptic vesicles are carried close to the inner leaflet of synaptic membrane where they are *docked* thanks to specific macromolecular complexes. At the end, *priming* synaptic vesicles include molecular adjustments that will increase their release probability upon synaptic activation.

1.2.1 Targeting synaptic vesicles to the active zone

Targeting synaptic vesicles to the active zone is an important step of the synaptic vesicle cycle because all the machinery necessary for vesicle exocytosis is condensed in this area. Electron micrographs of the active zone show a 400~700 nm diameter neuron-to-neuron junction with electron-dense material called the cytomatrix. Proteomic assays have shown that the active zone cytomatrix is enriched in cytoskeletal elements (such as tubulin, actin microfilaments), various proteins stabilizing cytoskeleton (such as Synapsins and spectrin for microfilaments, tau and MAP6 for microtubules) and also proteins promoting oligomerization (such as septins). Such a network of filaments traps synaptic vesicles and constrains a physical proximity with the vesicle fusion sites. In addition, the active zone cytomatrix is stabilized by transmembrane proteins that both act as scaffolds promoting a cohesion between the pre/post-synaptic elements and act as signal transducers (for example, N-CAMs). This focal enrichment shows that the active zone is evolutionarily designed as a dynamic « focal hot spot » for vesicular trafficking (Laßek, Weingarten, & Volknandt, 2014). Indeed, electron tomography reveals an ultra-dense meshwork of 30~60nm filaments bringing synaptic vesicles to the active zone while shorter filaments cross-link synaptic vesicles one another (Siksou et al., 2007). These studies have characterized various synapse-specific proteins including Synapsins and Bassoon taking part in vesicle cross-linking and vesicle-to-membrane linkage.

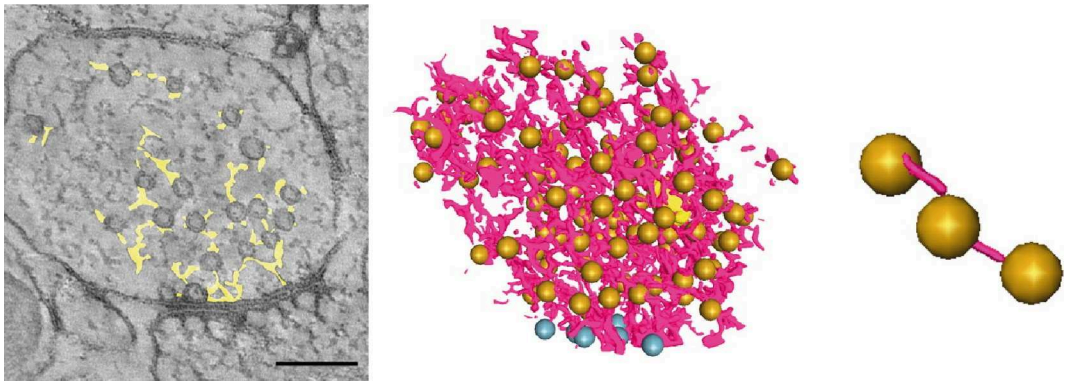

Figure 3. The presynaptic cytomatrix. A dense meshwork of filament cross-links synaptic vesicles within the presynaptic volume. The cytomatrix is essential for vesicular trafficking within presynaptic terminals.
Left - Electron micrograph representing a presynaptic terminal and its synaptic vesicles (scale-bar : 200nm) with the superimposed cytomatrix obtained from 3D stacks (yellow).
Center – Representation of synaptic vesicles (yellow) and docked synaptic vesicles (blue) interlaced with filaments (pink).
Right – Neighboring synaptic vesicles are cross-linked with molecular connectors (pink).
(Siksou et al., 2007)

1.2.2 Docking synaptic vesicles at release sites

Gathering and stabilizing synaptic vesicles at the active zone (also called *docking* phase) is a crucial step for neurotransmission process because it brings them at very close distances from calcium channels. Indeed, the presynaptic active zone contains a pool of synaptic vesicles ready for fusion. These vesicles have been extensively studied onto electron micrographs and consists in series of docked vesicles at very close distances from synaptic membrane (when the membrane-to-vesicle distance is less than 10nm) (Schneggenburger, Han, & Kochubey, 2012). Very specific molecular complexes regulate the docking of synaptic vesicles and the number of docked vesicles is a key parameter in determining neurotransmitter release properties of unitary synapse (Szule et al., 2012; Weyhersmüller, Hallermann, Wagner, & Eilers, 2011).

Cutting-edge techniques have identified several release sites within single hippocampal synaptic terminals by using nanoscale optical detection of quantal release events during functional assays (Maschi & Klyachko, 2017a). Here, the authors have shown that release sites have a physical identity and synaptic vesicles fuse on the same presynaptic membrane domain from one trial to another. This finding elegantly shows that the active zone cytomatrix has an essential function in the maintenance over time of molecular docking slots (n ; the number of release sites). Docking sites are composed of cytoskeletal elements such as actin microfilaments and also an assembly of synapse-specific proteins such as Rim1, Munc13, Bassoon, Piccolo and Synapsins.

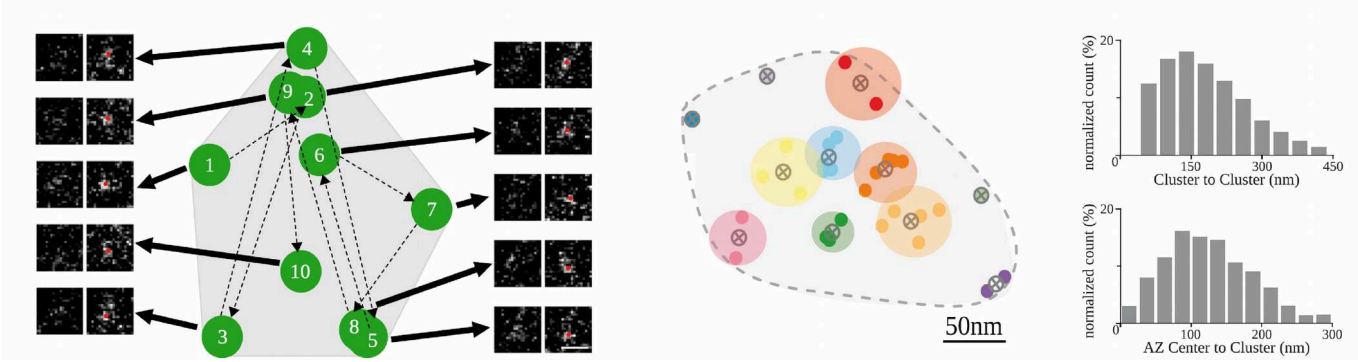

Figure 4. Synaptic vesicles fuse at several release sites from a single terminal.
Left – Nanoscale detection of 10 successive fusion events observed with VGluT1-pHfluorin nanoscale imaging. Fusion events follow a wide distribution within the presynaptic active zone.
Right – Fusion events are clustered at release sited. In the same experiments, hierarchical clustering identified several release sites on the basics of the x,y position of release events. Discrete release sites are homogeneously distributed at the active zone.
(Maschi & Klyachko, 2017b)

1.2.3 Molecular and positional priming of synaptic vesicles

Once the vesicles are docked, they undergo a *priming* step, molecular adjustments that make them ready for fusion. Rim and Munc13 are key molecules in the regulation of vesicular priming even though they are not the only molecular interactors involved in this process.

-Positional priming : Several proteins such as Rim and Munc13 are specifically enriched at the active zone and are qualified as the core components of synaptic active zone (Südhof, 2012). They contribute in the construction of functional release sites by clustering calcium channels at very short distances from synaptic vesicles which optimizes fast and synchronous neurotransmission of the release pool. Indeed, the distance between the synaptic vesicles and the calcium channels is essential for the definition of fusion probability at release sites (P_r). Tightening the vesicle-channel distance increases release probability and enhances the synchronicity of neurotransmission.

-Molecular priming : Presynaptic molecules optimize the excitation/secretion coupling by adjusting the distance and the molecular links between the synaptic vesicles and the presynaptic membrane. Munc13 (the mammalian homolog of Unc13, initially discovered in *C. elegans*) is a calcium binding protein that regulates vesicle anchoring at release sites by its interaction with syntaxin, the membrane protein of vesicle fusion.

Munc13 also binds β-spectrin, and this interactions with cytoskeleton help to stabilize synaptic vesicles onto release site through molecular adjustments (Garner, Kindler, & Gundelfinger, 2000).

Rim is also a calcium binding protein known for its interactions with Rab3, a small protein associated to synaptic vesicles involved in the regulation of vesicle fusion. Rim also strongly binds calcium channels at the active zone thanks to its interactor, the Rim binding protein (Rim-BP) and is suspected to play a role in the regulation of vesicle/channel coupling which is a crucial step in determining neurotransmitter release probability. Indeed, the recruitment of calcium channels at the active zone is likely to be Rim-dependant (Kaeser et al., 2011).

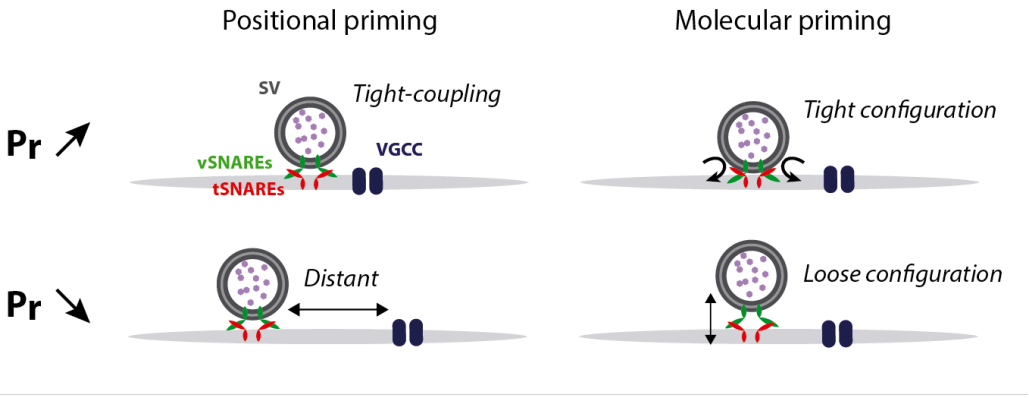

Figure 5. Positional and molecular priming of synaptic vesicles.
Different priming configurations will modulate release probability of synaptic vesicles. *Positional priming* takes in account the physical distance between synaptic vesicles and calcium channels while *molecular priming* is a conformational adjustment of release machinery. Several molecules such as RIM, RIM-BP, Munc13, Rab, Synapsin, are involved in priming synaptic vesicles.

Rim and Munc13 are highly sensitive to synaptic activity because of their calcium binding domains and their sensitivity to phorbol-esthers (such as DAG, a metabolite of metabotropic Gq receptors). Indeed, such proteins are able to modulate presynaptic calcium influx which affects neurotransmitter release probability. They are the target of potential presynaptic modulations adjusting the gain of neurotransmitter release following action potential depolarization.

1.2.4 Presynaptic calcium influx triggers neurotransmitter release

Depolarizing a synaptic bouton induces neurotransmitter release through the activation of calcium channels. Calcium ions are detected by the vesicular calcium sensors, Synaptotagmins, that change conformation following the binding of calcium onto their C2 domains. Several synaptotagin isoforms coexist at central synapses and their biophysical properties strongly affect the synchronicity of neurotransmitter release (Chen, Arai, Satterfield, Young, & Jonas, 2017). Thus, the molecular nature of the calcium sensors is also a key parameter in the definition release probability (Schneggenburger et al., 2012).

Clusters of calcium channels define the number of release sites and are positioned within the active zone. By using freeze-fracture electron microscopy combined to immunogold labeling, recent studies have established a link between release sites and clusters of P/Q-type calcium channels at central synaptic terminals (Miki et al., 2017). The number of physical release sites observed in electron microscopy correlates with the number of release sites calculated during electrophysiological experiments showing that the physical organization of the active zone will define the release properties of presynaptic terminals.

The alpha sub-unit of calcium channel consists in a transmembrane ion-selective pore that generates presynaptic calcium microdomains upon depolarization. The first hypothesis of calcium microdomains exocytosis emerged following observations at the squid giant synapse and the frog neuromuscular junction (Fogelson & Zucker, 1985). At central synapses such as the calyx of Held of adult rats, calcium concentration inside microdomains reach tens of µM (about 50~60 µM). Nanodomains of calcium can be observed at the channel level and neurotransmitters will be released with more or less efficiency depending on the vesicular priming status. Spatiotemporal properties of calcium influx have very strong consequences onto synaptic physiology because it restricts the temporal window for synchronous neurotransmission and regulate the presynaptic release properties (Eggermann, Bucurenciu, Goswami, & Jonas, 2012).

Presynaptic calcium channels have numerous binding partners, and some of these molecules influence channel opening kinetics and the spatial arrangement of channel clusters. Indeed, the efficiency of excitation/secretion relies on the very short distances between calcium channels and release-ready vesicles. Several molecular actors are direct binding partner for P/Q channels and have been identified to modulate positional priming by increasing (or decreasing) the distance with calcium channels. This is the case of SynapsinII, which directly binds P/Q channels which increases the distance with synaptic vesicles (Medrihan et al., 2013).

Importantly, the properties of the presynaptic calcium influx which directly control the probability of release depend on the subtype of VGCC (A. M. Weber et al., 2010). At presynaptic terminals the main channel subtypes contributing in neurotransmitter secretion are N, P/Q and R-type channels. Such differences between channel subtypes can lead to interesting developmental switches during synaptic maturation (Iwasaki, Momiyama, Uchitel, & Takahashi, 2000). Also, a mix of different channel sub-units can give the synapse very specific release properties as it has been shown at cerebellar granule cell synaptic terminals (Satake & Imoto, 2014) and also in another brain structures (Scheuber, Miles, & Poncer, 2004).

1.2.5 Vesicular fusion

Synaptic vesicles fuse to the presynaptic membrane thanks to the SNARE complex (for Soluble N-ethylmaleimide-sensitive-factor-Attachement protein REceptor). This complex of proteins have a general function in exocytosis and intracellular trafficking. They mediate exocytosis in neurons but also in various neuroendocrine, paracrine systems. SNAREs are one of the core components of the vesicular fusion machinery that are very well conserved across species and similar in various membrane trafficking processes (Rizo & Xu, 2015). Synaptobrevin (also called VAMP for Vesicle Associated Membrane Protein) is the SNARE element attached to synaptic vesicles (v-SNARE) while the other elements of the complex Syntaxin and SNAP-25 are included at the presynaptic membrane (t-SNARE). They form coiled-coil helix bundles that generates sufficient energy to bring the vesicle and synaptic membrane altogether. The formation of a pore allows the secretion of vesicular content. Even if the mechanisms of fusion and pore formation are not well elucidated, SNARE complexes are thought to be the minimal elements required for vesicular fusion (Rizo & Xu, 2015; T. Weber et al., 1998).

1.3 Populations of vesicles within presynaptic terminals

In the classical vision of vesicular release, synaptic vesicles are stored within the synaptic terminal until they get mobilized at the active zone during intense activity. Thus, intrinsic synaptic mechanisms are able to regulate populations of vesicles and fine tune neurotransmitter release by controlling vesicular availability (Chamberland & Tóth, 2016).

Electron microscopy which allowed to visualize the ultrastructural content of presynaptic terminals helped to distinguish populations of vesicles depending on their distance to the active zone. In parallel, electrophysiological assays allowed to study the properties of releasable populations of vesicles by using various stimulation protocols.

There are heterogeneous populations of synaptic vesicles with different contributions in neurotransmitter release, depending on the nature of the synaptic terminal and the protocol used for stimulating these terminals.

As we will see in the next paragraph, vesicles populating presynaptic terminals are not set equal. Variability at the level of the priming stage (positional priming and molecular priming) but also in the way vesicles are clustered around the active zone account for a functional specification of glutamate release behavior (Jung, Szule, Marshall, & McMahan, 2016).

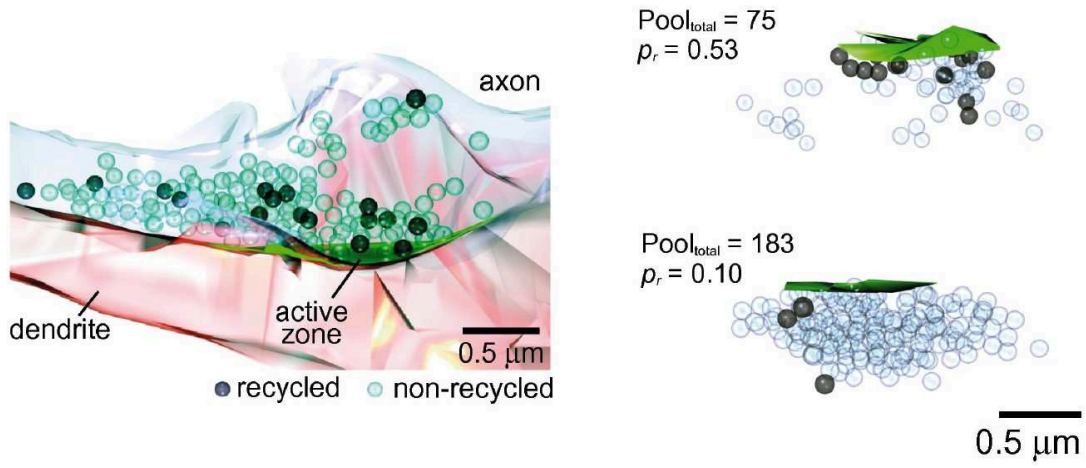

Figure 6. Structure/function relationships within a population of presynaptic terminals from hippocampal cultures. By examining the number of recycled vesicles (black) on electron micrographs the authors could assess the number of released vesicles per synaptic terminal following action-potential stimulation. The fraction of released vesicles (p_r) was not correlated with the absolute number of vesicles per bouton (reserve pool : $Pool_{total}$) but was correlated with the number of docked vesicles per synapse (Branco et al., 2010).

This study illustrates the relationships between the ultrastructural organization of presynaptic terminals and the presynaptic release properties. Even if some ultrastructure/function parallels can be made, it is hardly conceivable to predict presynaptic functioning with ultrastructure exclusively.

1.3.1 Ultrastructurally defined pools of vesicles

i) The *morphological readily releasable pool (RRP)*. As we have seen before, a fraction of synaptic vesicles are at very close distances from the plasma membrane (<50nm) and are considered as the previously described *docked synaptic* vesicles. Electron microscopy assays have identified several grid-like macromolecular complexes linking these docked synaptic vesicles to the presynaptic density (Zampighi et al., 2008). Again, these observations show that presynaptic terminals are specifically designed for vesicle anchoring prior to membrane fusion.

ii) The *reserve pool* of synaptic vesicles (also *resting pool*) is linked to actin microfilaments at distance from the active zone and provides a source of synaptic vesicles during intense synaptic activity. Mobilization of reserve vesicles during synaptic activation fosters the replenishment of docked vesicles which counterbalances depletion caused by sustained activity (Moulder & Mennerick, 2006). While the synapse is resting, Synapsins provide a physical constraint by cross-linking synaptic vesicles to actin microfilaments. However, an activity-dependant phosphorylation of Synapsins will dissociate the reserve pool which makes synaptic vesicles free to move within the presynaptic button (S Hilfiker et al., 1999).

iii) The *recycling pool* is usually described in periphery from release sites and composed of vesicle emerging from compensatory endocytosis. Recycling vesicles is known to be enhanced during synaptic activity and provide another source of synaptic vesicles for the replenishment of both *readily releasable pool* and *reserve pool*. Clathrin-mediated endocytosis can be identified with electron microscopy while FM-dyes or pH-sensitive dyes are better suited for the characterization of the recycling pool. In any case, endocytosis is essential for morphological stability and ultrastructural integrity during intense activity (Xie et al., 2017).

1.3.2 Functionally defined pools of releasable synaptic vesicles

In-vitro experimental methods combining voltage clamp of a postsynaptic neurons and electrical stimuli of a presynaptic inputs helped to characterize different populations of vesicles contributing to neurotransmission.

i) The *functional readily releasable pool (RRP)* is defined as the fraction of synaptic vesicles that release their neurotransmitter content following one action potential. The size of the RRP has been debated since decades and has been studied thanks to depletion experiments using, for example, prolonged burst stimuli during electrophysiological recordings of postsynaptic neurons. This RRP size varies depending on the nature of the synaptic terminal but often accounts for a very small proportion of the total vesicle number (~1-2%). However, the size of the functional RRP is not systematically correlated to the number of docked vesicles observed in electron microscopy (M. a Xu-Friedman & Regehr, 2004).

ii) The *reluctant* pool of synaptic vesicles (also called *replacement pool*) which is not immediately releasable by one single action potential. However, several physiological or non-physiological conditions such as high-frequency bursting activity, extracellular potassium or hyperosmotic shocks can trigger release of reluctant populations of synaptic vesicles (Moulder & Mennerick, 2006). This population of synaptic vesicles is suspected to be at higher distances from release sites and especially from calcium channels (or in different priming states) but still at sufficiently short distances from release sites to be released upon high-frequency activation during short term plasticity experiments.

1.4 Synapsins : Multifunction molecules regulating the synaptic vesicles cycle

We have seen that the presynaptic terminals are equipped with a very specific molecular machinery dedicated to regulated exocytosis. Decades of research in the field have characterized a large panel of synapse-specific molecular interactors. The quantification and localization of synaptosomal proteins showed an enrichment in synaptic vesicle associated proteins and trafficking proteins. There is also an important spatial segregation within the synaptic volume (Wilhelm et al., 2014) meaning that various proteins are involved at multiple stages of vesicular trafficking. For example, this is the case at mammalian central synapses that show different topological arrangements for different presynaptic molecules (Bassoon, Aczonin, RIM, Munc13) suggesting that structure/function relationships closely interact in determining synaptic properties (Limbach et al., 2011). Finally, some molecules have very specific roles within the synaptic vesicle cycle (i.e. SNAREs, the machinery of vesicular fusion) while other proteins (such as Synapsins) have more diversified presynaptic functions as we will see below.

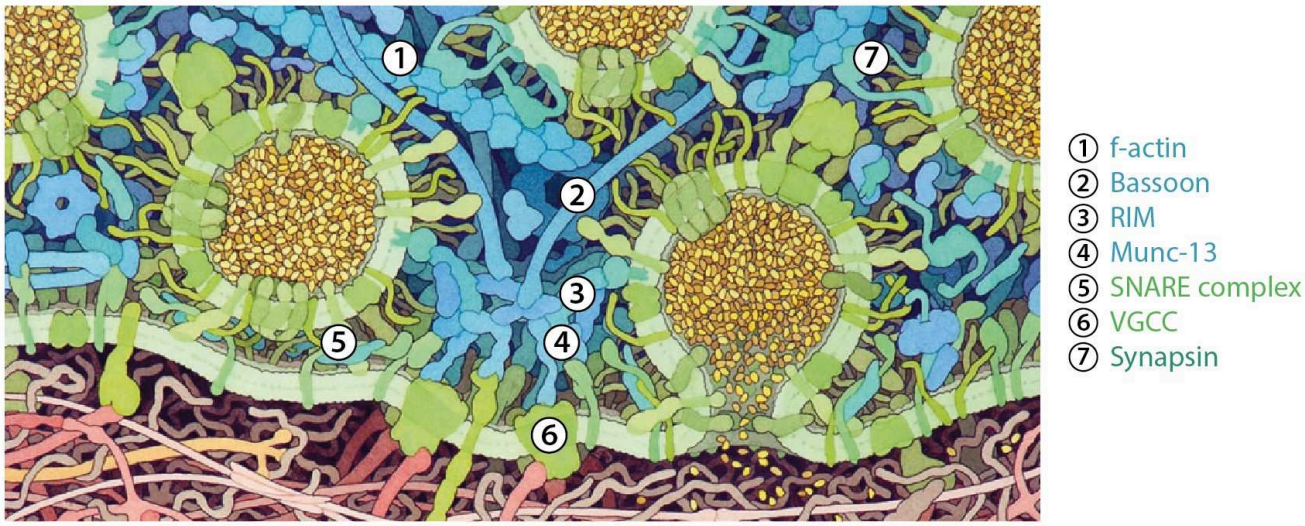

Figure 7. Presynaptic organization of synapse-specific molecules. Illustration showing that various molecules are involved at different stages of neurotransmission and follow a spatial segregation within the presynaptic volume. Some are involved in the trafficking of synaptic vesicles (blue) while others are associated to synaptic vesicles (green) and contribute in neurotransmitter release. Neurotransmitters are represented in yellow. (Goodsell, 2009)

1.4.1 Diversity of Synapsin isoforms

Synapsins are a family of synapse-specific phosphoproteins encoded by three different genes in vertebrates (Candiani et al., 2010; Kao et al., 1999), Synapsin I, II, III. Their expression in brain tissues gives rise to multiple mRNA transcripts and splice variants (*synIa/b, synIIa/b, synIIIa/f*) (Li et al., 1995; Porton, Wetsel, & Kao, 2011). Synapsins share common features, such as phosphorylation domains for MAP-kinases, PKA and CaMK I,IV (domains A,B) or molecular scaffolding (domain D) that binds to SH3-containing adapters (Cesca, Baldelli, Valtorta, & Benfenati, 2010; S Hilfiker et al., 1999; Medrihan, Ferrea, Greco, Baldelli, & Benfenati, 2014). More importantly the common feature of Synapsins is to interact with synaptic vesicles (Schiebler, Jahn, Doucet, Rothlein, & Greengard, 1986), bind actin microfilaments (domain C) (Shupliakov, Haucke, & Pechstein, 2011) and promote the polymerization of actin microfilaments (Bähler & Greengard, 1987; Chilcote, Siow, Schaeffer, Greengard, & Thiel, 1994). These proteins are well known for their

Despite a functional redundancy between synapsin transcripts, the domain combination of each single synapsin isoform is unique. Their variability in domain composition generates subtle functional specifications : for example some synapsin domains are essential for synaptic targeting of the molecule (Gitler, Xu, et al., 2004). Also, synapsin domain E has been suspected to act during the last steps of vesicle priming and modifies the kinetics of neurotransmitter release in Aplysia (Sabine Hilfiker et al., 1999). Finally, synapsinII binds presynaptic P/Q-type calcium channels in mice hippocampal neurons which desynchronizes the evoked release of glutamate (Medrihan et al., 2013).

1.4.2 Synapsins regulate populations of synaptic vesicles

Synapsins are not specifically enriched at the active zone but various isoforms of Synapsins (with various domain composition) have distinct presynaptic functions in vesicular trafficking (Dolphin & Greengard, 1981; Navone, Greengard, & De Camilli, 1984) and are well known for their contributions to the regulation of vesicle pools at presynaptic terminals (Bykhovskaia, 2011; Shupliakov et al., 2011).

i) Synapsins promote actin polymerization (Bähler & Greengard, 1987; Chilcote et al., 1994) favoring the establishment of reserve populations (Bykhovskaia, 2011) within the presynaptic volume and also the stabilization of cytomatrix at the active zone. Triple-knockout terminals for the three genes coding all the synapsin isoforms show a dramatic reduction of the number of reserve pool synaptic vesicles (Fornasiero et al., 2012).

ii) Synapsins regulate the exchange of synaptic vesicles between the different pools of vesicles (Humeau et al., 2001; Ryan, Li, Chin, Greengard, & Smith, 1996; Shupliakov et al., 2011). Synapsins are sensitive to presynaptic activity as they dissociate from synaptic vesicles upon phosphorylation by CaMKII (Sabine Hilfiker et al., 1999). Their specific ability to cross-link synaptic vesicles at the active zone (Hallermann & Silver, 2013) provides a dynamic tethering onto the presynaptic cytomatrix which enhances vesicular targeting to the neurotransmitter release sites.

iii) Synapsins organize macromolecular clusters at the active zone which largely affects vesicular priming. Interestingly, some isoforms such as SynapsinII have direct interactions with calcium channels meaning that they can modulate the distance between calcium channels and synaptic vesicles (Medrihan et al., 2013). As we have seen before, *positional priming* has important consequences in the regulation of neurotransmitter release, especially during short term plasticity process.

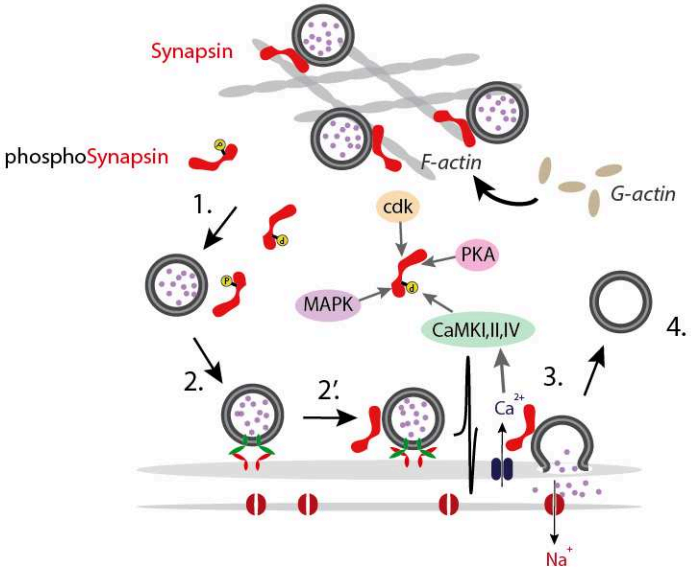
Synapsin
phosphoSynapsin
F-actin
G-actin
1.
cdk
PKA
MAPK
CaMKI,II,IV
2.
2'.
3.
4.
Ca 2+
Na +

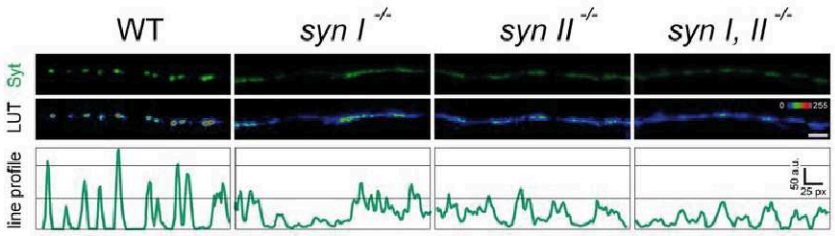
WT
syn I -/-
syn II -/-
syn I, II -/-
Syt
LUT
line profile
50 a.u.
25 px

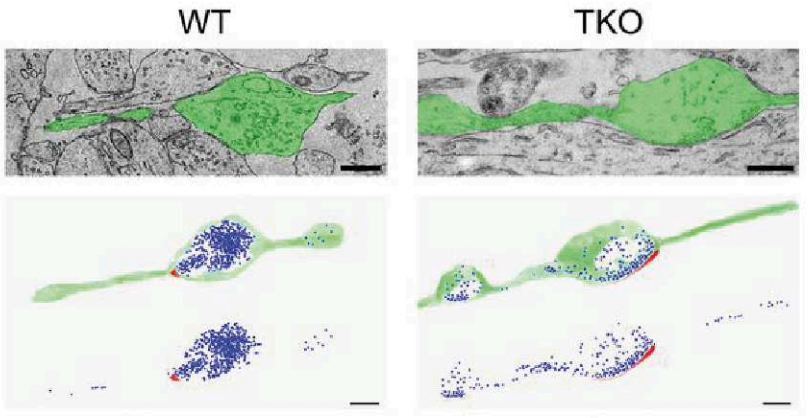
WT
TKO

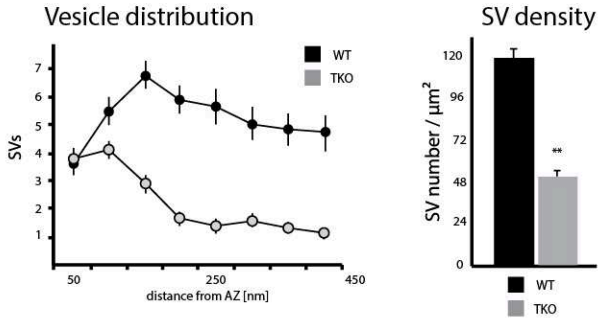
Vesicle distribution
WT
TKO
SVs
distance from AZ [nm]
SV density
SV number / µm²
**
WT
TKO

Figure 8. Functions of Synapsins at presynaptic terminals.
Top - Synapsins interfere at different stages of vesicular trafficking. First, they cross-link vesicles to actin microfilaments. Synapsins are phosphorylated upon synaptic activity (1) and loose their ability to link vesicles. Synaptic vesicles are recruited at the active zone (2) where Synapsins will affect the docking and priming steps of neurotransmission.
Bottom – Synapsins are essential for the maintenance of reserve populations at presynaptic terminals. Imaging synaptic vesicles from various Synapsin knockouts show a dispersion of synaptic vesicles within the axonal process for syn I, synII and synIII knockout mice.
A deletion of the three genes encoding Synapsins (TKO) severely alters vesicular distribution and vesicular density at presynaptic terminals from hippocampal cultures. (Fornasiero et al., 2012)

1.5 Short-term synaptic plasticity

Neuronal networks are subject to a permanent activity and neurons fire at various frequencies, ranging from background activity noise to physiologically relevant information. Presynaptic terminals sometimes undergo fast frequency changes and the presynaptic machinery of a given terminal will adapt -or not- to follow rate-coding modulations inherent to network activity. One major feature of presynaptic terminals is that it filters information depending on the properties of its intrinsic neurotransmitter release machinery. Indeed, neurotransmitter release mechanisms are remarkably able to adapt themselves following repetitive depolarization of presynaptic terminals. Termed as *short term plasticity*, this effect is highly dependent on the stimulation pattern (Zucker & Regehr, 2002) but can also be sensitive to various heterosynaptic and trans-synaptic neuromodulators that will affect durably neurotransmission efficiency (Yang & Calakos, 2013).

Unlike the other forms of plasticity that involve long-term or mid-term modifications of neurotransmitter release (i.e. induced by post-tetanic potentiation of high frequency theta bursts), short-term synaptic plasticity is a millisecond-scale modulation of the synaptic weight caused by a transient modification of presynaptic release parameters ; essentially release probability (P_r) and the number of release sites (n). Only in the case of short term plasticity, this adaptation is transient and presynaptic parameters recover within a very short time window (milliseconds). In the case of long-term plasticity, the adaptation is maintained over a longer period of time (minutes to hours and sometimes longer).

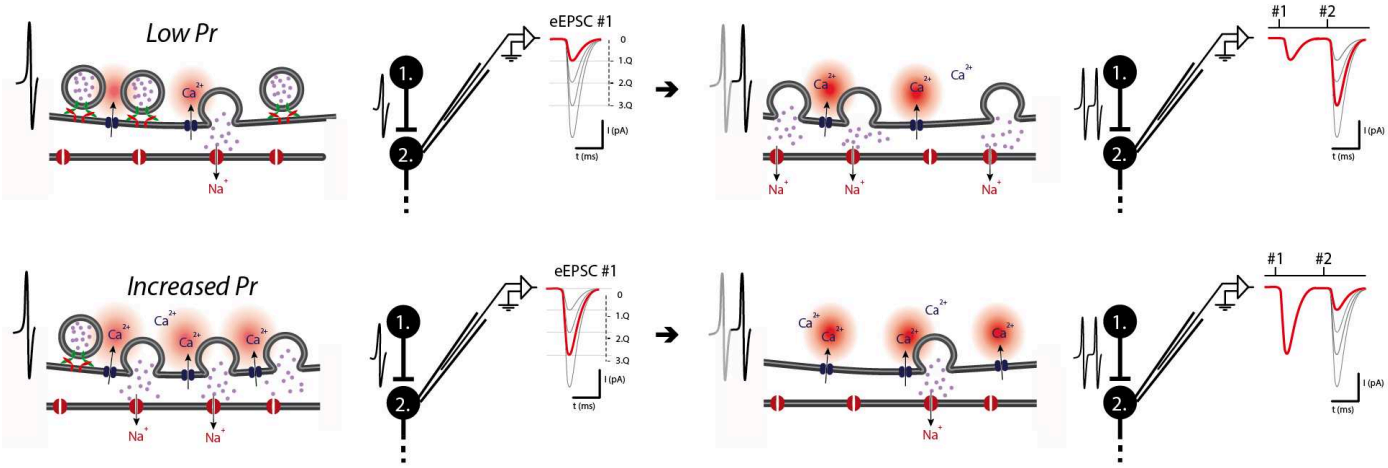

Figure 9. Basic mechanisms of short term plasticity.
Facilitation of calcium entries in calcium nanodomains and the size of release ready populations of vesicles contribute in the direction of short term plasticity. Two examples of synaptic terminals with low (top) and high (bottom) initial release probability. Calcium facilitation and low initial release probability contribute in neurotransmitter release facilitation during paired-pulse experiments (top) while a high initial release probability will induce the depletion of the ready-to-release population of vesicles during the same paired-pulse protocol.

Synaptic terminals provide an ultra-fast adaptation to ongoing fluctuations of environmental (or internal) stimuli: presynaptic terminals release more or less neurotransmitters following modifications in the input firing frequency. In the central nervous system, one fascinating feature of presynaptic terminals is that they display a wide variety of short term plasticity behaviors. For example, two different synaptic terminals receiving the same input firing pattern can show different short term behaviors ; classically, we oppose depressing synapses to facilitating synapses (M. A. Xu-Friedman, Harris, & Regehr, 2001).

In the case of high-frequency stimuli, presynaptic depression or facilitation emerge from a subtle interplay between release probability (P_r) and the number of synaptic vesicles available on release sites (n). We have seen that presynaptic terminals are equipped with a limited number of ready-to-release vesicles. In the case of a *low-P_r* terminal, only few synaptic vesicles will fuse upon a single depolarization. If a subsequent spike depolarizes the synapse a few milliseconds later, neurotransmission is sustained (and sometimes facilitates) because more vesicles are available for release at the fusion sites. However, in the case of a *high-P_r* terminal, the great majority of ready-to-release vesicles will fuse at the first depolarization which deplete the docking sites. In that case, depletion of the ready-to-release pool induces a depression of neurotransmitter release.

Unlike facilitation, synaptic depression can be caused by a simple passive depletion of the vesicles available for release because in some conditions, very short time windows do not allow the replenishment of the ready-to-release vesicles. However, depression can be explained by an active modulation process. Previous studies from the team have shown that an active extinction (switch-off) of the synaptic vesicles release sites induces depression of neurotransmitter release without vesicular depletion (Doussau, Humeau, Benfenati, & Poulain, 2010).

At the ultrastructural level, two synaptic terminals with identical synaptic vesicle distribution can present different release probability (Branco, Marra, & Staras, 2010; M. A. Xu-Friedman et al., 2001). However, release probability is correlated to the number of docked vesicles at the active zone (Branco et al., 2010) but not the absolute size of the synapse or the vesicle pools. These results show that both ultrastructural and molecular properties of presynaptic terminals determine the synaptic release properties. In order to study presynaptic physiology, one should take in account both ultrastructural and molecular properties of presynaptic terminals: taken apart, these two parameters do not explain the functional properties of a synaptic connection.

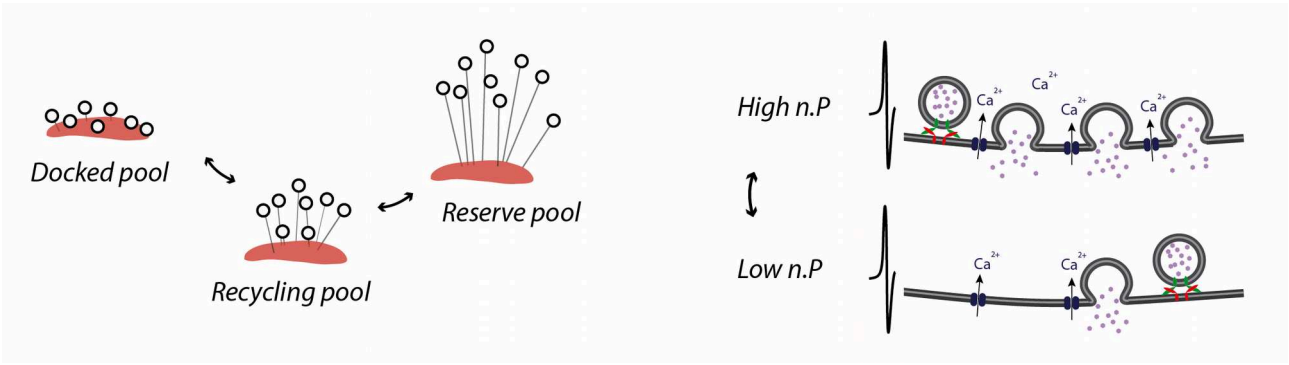

Figure 10. Ultrastructural and molecular properties shape presynaptic short term plasticity.
Left - The ultrastructural organization of presynaptic terminals shape presynaptic short term plasticity of synaptic terminals (Branco et al., 2010; M. a Xu-Friedman & Regehr, 2004). This simple illustration shows that the physical distance between synaptic vesicles and the active zone (red) may vary from one vesicle pool to another. The docked population of synaptic vesicles is closest from the active zone release sites while the reserve population is at longer distances. Decreasing the physical distance between the active zone and the vesicles fosters ultra-fast neurotransmitter release during repetitive presynaptic activity.

Right – Interaction between the number of release sites (n) and release probability (P) will determine the apparent number of synchronously fused synaptic vesicles (n.P). The apparent n.P is strongly affected by positional and molecular priming.

It is important to note that during repetitive activation of presynaptic terminals, both the ultrastructure and release parameters are subject to dynamic modulations.

1.5.1 Short term plasticity and the presynaptic calcium influx

Upon repetitive synaptic activation, presynaptic release parameters (P_r, and n) are reshaped. While the presynaptic calcium influx itself is known to contribute in short term facilitation, diverse populations of releasable vesicles with various release probabilities create an internal heterogeneous P_r that interfere short term plasticity. Thus, release probability does not build-up linearly (as calcium does) during repetitive activation of presynaptic terminals because of internal variability within the synapse.

Calcium ions play a crucial role in neurotransmitter release facilitation which has been explained through several mechanistic hypothesis.

i) The *residual calcium hypothesis* states that a repetitive activation of presynaptic calcium channels increases the concentration and size of calcium inflow. Several experiments using competing calcium buffers or changing external calcium concentration show that a bigger calcium influx is correlated with an enhancement of neurotransmitter release. Recent findings have enlighten the importance of membrane-associated calcium sensors in synaptic plasticity. At central synapses, the low affinity calcium sensor Synaptotagmin7 has been shown to be required for synaptic facilitation through its ability to sense residual calcium (Jackman & Regehr, 2017).

ii) The *calcium buffer saturation* hypothesis states that a repetitive calcium influx can saturate mobile or immobile calcium buffers (such as calbindins) while calcium buffers largely restrict the spatial propagation of the calcium influx during single spike activation.

iii) Other hypothesis include modifications in the properties of the presynaptic calcium current itself. For example, the broadening of spike waveform or the modulation of channel alpha subunit can modify its opening kinetics.

1.5.2 Different populations of vesicles contribute in short term plasticity

Facilitation can be explained by an activity dependent increase in the number of release sites (n) at some synaptic terminals specialized in high-frequency information transfer (Miki et al., 2016; Valera, Doussau, Poulain, Barbour, & Isope, 2012). Such a non-linear build up in *n* is explained by a two-pool vesicle model and accounts for a high-passing information transfer at these specific terminals. Electrophysiological studies have shown that both reluctant and readily releasable pool contribute to vesicular release facilitation during repetitive activation of various synapses such as the Calyx of Held (Trommershauser, Schneggenburger, Zippelius, & Neher, 2003). At the Calyx of Held, the coexistence of *high release probability vesicles* and *low release probability vesicles* shape short term plasticity during prolonged release. High release probability vesicles are immediately released upon depolarization, while low release probability vesicles are released later on in the depolarization sequence thanks to a calcium enhancement of vesicular recruitment (Gelman, 2011).

A recent study has shown the existence of a *replacement pool* at cerebellar granule cell terminals which is at close distances from release sites and dependent on actin and myosin linkage (Miki et al., 2016). This study lightens the role of actin microfilaments in the refilling process of release sites during sustained high frequency activity which counterbalances depletion.

Interestingly, Synapsins are involved in actin polymerization and vesicle cross-linking. Because Synapsins provide spatial rearrangements of synaptic vesicles, they are a good candidate for the regulation of populations of synaptic vesicles and the segregation of synaptic vesicles in ultrastructurally and functionally distinct pools.

Testing the existence of a *reluctant* pool at central synapses using electrophysiological recordings is a real challenge because most of the depletion protocols recruit both reluctant and RRP pools of vesicles. In the team, we have designed stimulation protocols enabling us to isolate specific release from the *reluctant* pool. We used these protocols to assess such a two-pool model at granule cell presynaptic terminals (including *readily releasable* and *reluctant* vesicles) contributes in neurotransmitter release adaptation to frequency changes. These specific synaptic properties are inherent to granule cell synaptic boutons, specialized in high-frequency information transfer and will be described in the next paragraphs.

1.6 Inter-synaptic heterogeneity of short term plasticity

Previously, we have seen that synaptic terminals are dynamical filters that transmit – or not – information depending on their short-term plasticity properties. The direction of presynaptic short term plasticity (facilitation or depression) will depend on the interaction between the different release parameters and the ultrastructural and molecular properties of presynaptic terminals are the main factors of presynaptic diversity (Atwood & Karunanithi, 2002).

Decades of research have described inter-synaptic variations of synaptic short term plasticity. There is a high diversity of short term plasticity behaviors into the central nervous system (Dittman, Kreitzer, & Regehr, 2000). These variation have been observed between neural structures and often associated to a specific neuronal subtype and between different neuronal networks like in hippocampal synapses (Debanne, Guérineau, Gähwiler, & Thompson, 1996; Hanse & Gustafsson, 2001a, 2001b, 2001c) or the Calyx of Held terminals (Taschenberger, Woehler, & Neher, 2016).

Inter-synaptic variations of short term plasticities have a central function in neuronal networks :
i) They regulate excitability by stabilizing excitation/inhibition imbalance.
ii) They filter relevant information in terms of network processing. For example, facilitating synaptic terminals high-pass information transfer during bursting activity.
iii) They set temporal coding in networks by enhancing relevant information. This is the case for short term depressing synapses with a high synaptic weight that show a very strong depression.

1.6.1 *Hard-wired* properties versus experience

Early theories of Hebbian neuronal computations supposed that information storage within neuronal network depends on variations of synaptic strength defined by active learning processes (Teyler & Discenna, 1984). Following this idea a population of synapses would have a wide range of synaptic weights, at a given instant in time and depending on the terminal which is activated.

Nowadays, we know that a highly integrated processing of electrical signal can provide long term changes such as Long-Term Potentiation (LTP) or Long-Term Depression (LTD) processes. It has been proven that active regulations of synaptic weight (by trans-synaptic or homeostatic mechanisms) can lead to extremely variable synaptic states such as synaptic silencing (Liao, Hessler, & Malinow, 1995) and even synaptic pruning.

For example, in the cerebellar cortex, a big proportion of granule cell presynaptic terminals is silent meaning that stimulating such a connection doesn't induce any relevant eEPSCs. More interestingly, active

and inactive synapses form a stereotypical functional map that can be dynamically modulated (Valera et al., 2016). Awakening synapses is possible using LTP-induction protocols : this form of heterogeneity (active versus silent synapses) is both *hard-wired* and follows active learning rules that shape synaptic variability. Interestingly, this specific example shows that a *hard-wired* stereotyped connectivity map is prone to activity-dependent modifications.

Also, redistribution of synaptic efficacy (RSE) has been observed in the neocortex where synapses belonging to homogeneous populations display very different gain and short term plasticity properties (Markram & Tsodyks, 1996; Tsodyks & Markram, 1997). Importantly, experience can reshape the synaptic gain of individual terminals but not only: modifying presynaptic release parameters of one terminal has consequences onto its short term properties. These adjustments require the interaction with the post-synaptic target through retrograde signaling (Branco, Staras, Darcy, & Goda, 2008; Futai et al., 2007; Regehr, Carey, & Best, 2009; Soler-Llavina & Sabatini, 2006) and follow specific rules of heterosynaptic adaptation like branch-dependent equalization (Branco et al., 2008) or contact-specificity (Soler-Llavina & Sabatini, 2006). Finally, terminals of homogeneous synaptic populations may display different functional behaviors because they express different dynamical states depending on network experience.

The ultrastructural organization of synaptic vesicles originating from the same axonal process can be reshaped by experience. Inter-synaptic shuffling of vesicles was described *in-vitro* (Staras et al., 2010) *in-vivo* (Herzog et al., 2011) and allows the redistribution of synaptic vesicles at individual synapses. Defined as a "superpool" of synaptic vesicles, their ability to diffuse from synapse-to-synapse the axonal compartment is enhanced synaptic activity (Fornasiero et al., 2012). Intersynaptic mobility can be modulated by synapse-specific proteins (Orenbuch et al., 2012; Siksou et al., 2013) and is a potential source of inter-synaptic variability through possible synapse-specific redistribution of vesicular ensembles. For example, at the mossy fiber synapse, kinetics of vesicle diffusion are tuned by vesicular density and impact short term plasticity (Rothman, Kocsis, Herzog, Nusser, & Silver, 2016). Also, Synapsins are involved in the restriction of reserve populations within varicosity volumes (Fornasiero et al., 2012; Orenbuch et al., 2012).

Interestingly, previous studies also describe a for of inter-synaptic shuffling of presynaptic molecules (Kalla et al., 2006; Star, Newton, & Murthy, 2005). Combined to synapse and experience dependent retrograde modulations, the highly dynamical redistribution of vesicles and molecules within the axonal and synaptic compartments is prone to modulate presynaptic release properties in a synapse-specific fashion.

To conclude, even if neuronal networks display some *hard-wired* properties in term of architectonics, the dynamical properties of neuronal systems are highly sensitive to experience. Both presynaptic and post-synaptic compartments are subject to homeostatic readjustments that tune neurotransmitter release machinery at the level of unitary synaptic contacts.

1.6.2 Functional connectivity models

Inter-synaptic variations of short term plasticity have been classified in various connectivity models (Larsen & Sjöström, 2015) of synapse-specific short term plasticity (STSP).

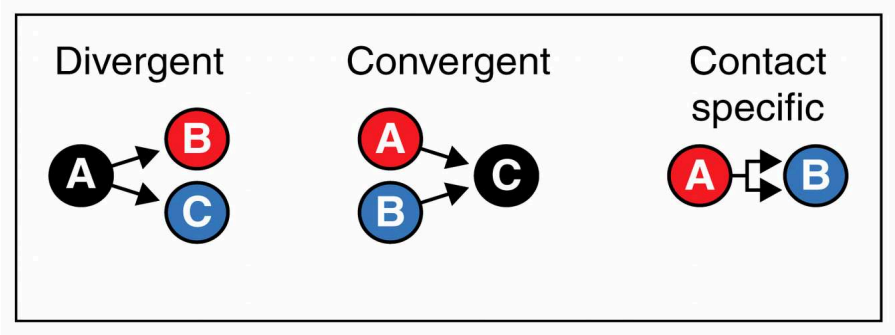

Figure 11. Different organization modes for synapse-specific short term plasticity (STSP).
In local networks neurons, STSP can be;
i) divergent : where the plasticity of a given synaptic population is dependent of their targets (also called target-dependence).
ii) *convergent ;* where the pre-synaptic neuronal subtype will determine the functional properties of its synaptic contacts.
iii) contact-specific. Some studies have identified synapse-specific variations within a population of synaptic terminals. *Contact-specificity* is probably the resulting of a very subtle modulations following network processing (like sensory experience) and reflects a more integrated form of network adaptations (pre and post-synaptic).
(Larsen & Sjöström, 2015)

The most described form of inter-synaptic heterogeneities is probably *target-dependence*. Here, the nature of the post-synaptic neuron sets the plasticity of its presynaptic inputs through trans-synaptic mechanisms (Blackman, Abrahamsson, Costa, Lalanne, & Sjöström, 2013). In most of the case, categories of small inhibitory interneurons are suspected to receive a batch of synaptic inputs expressing the exact same short term plasticity dynamics (For example, neocortical SOM-positive inputs are facilitating while PV-positive inputs are depressing). The mechanisms of target-dependence are barely known even if this organizational model has been extensively described in the hippocampus, neocortex and once in cerebellum.

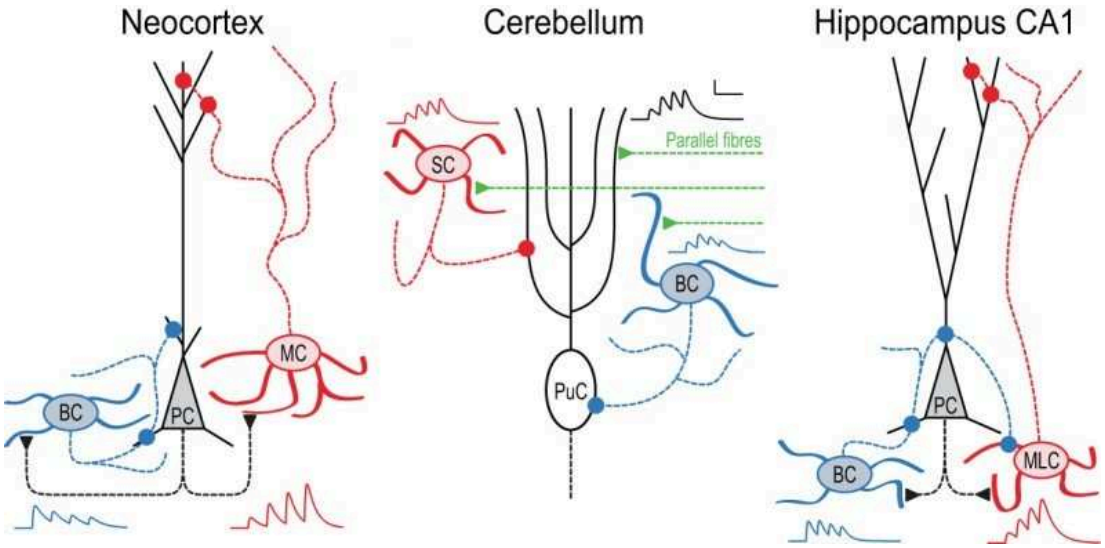

Figure 12. Target-dependance of short term synaptic plasticity.
Several studies have characterized a target-dependant mode of short-term plasticity organization in several micronetworks of neocortex, cerebellum and hippocampus. Here, the functional identity of presynaptic terminals will adapt depending on the nature of the post-synaptic target (Blackman et al., 2013). For example, depressing synapses of a pyramidal neuron contact basket cells in the cortical column while facilitating synapses of the same pyramidal neuron contact Martinotti cells. Target-dependence has also been described in cerebellum where parallel fiber synaptic contacts are depressing if their post synaptic targets are basket cells and facilitating if their targets are stellate cells (Bao et al., 2010) and also in hippocampal pyramidal neurons.

Target-dependence isn't the sole organizational model ruling functional connectivity laws. Multiple works describe heterogeneity of short term dynamics depending on the origin of the pre-synaptic input. For example, convergent neurons originating from different nuclei can express various neurotransmitter release behaviors. *Origin-dependent* heterogeneity has been described at thalamocortical projections (Kielland, Erisir, Walaas, & Heggelund, 2006), tectopulvinar synapses (Wei, Masterson, Petry, & Bickford, 2011) and also at pre-cerebellar mossy-fiber projections (Chabrol, Arenz, Wiechert, Margrie, & DiGregorio, 2015).

1.6.3 Molecular identity of presynaptic terminals

In both *target* and *origin-dependent* modes of functional connectivity, neurotransmitter release behaviors have been associated to synapse-specific expression of presynaptic molecules (Atwood & Karunanithi, 2002). Indeed, different isoforms of presynaptic proteins involved in neurotransmission coexist in the central nervous system and these molecules often present distinct properties:

i) Molecules related to the regulation of the presynaptic calcium influx (like VGCC,s subunits alpha/beta, Synaptotagmins, calcium buffers) or modifying the priming stage (Munc13, RIM, RIM-BP) at release sites will strongly affect neurotransmitter release probability and short term plasticity (Dulubova et al., 2005; Graf, Daniels, Burgess, Schwarz, & DiAntonio, 2009; Ishiyama, Schmidt, Cooper, Brose, & Eilers, 2014).

For example, Munc13-3 is involved in the *target-dependance* of cerebellar granule cell presynaptic terminals onto postsynaptic molecular layer interneurons. The genetic deletion of presynaptic proteins such as Munc13 only have a partial loss-of-function effect within a population of excitatory terminals (Bao, Reim, & Sakaba, 2010). Munc13-3 deletion has a very specific effect onto parallel fiber-to-basket cell synapses that switch from short term depression during high frequency bursts to facilitation. Other populations, such as parallel fiber-to-stellate cell synaptic contacts remain unaffected by the deletion suggesting a synapse-specific function of some molecular interactors.

ii) Organizers of the active zone (Bassoon, Piccolo, Actin) will contribute in determining the number of release sites and regulate the clustering of synaptic vesicles nearby the active zone (Mukherjee et al., 2010).

iii) Protein partners of synaptic vesicles (Synapsins) will contribute in the ultrastructural arrangements of vesicle pools. Over all the molecular candidates, Synapsins are probably the most important contributors of inter-synaptic heterogeneity. These proteins are already known to tune short term synaptic plasticity in a synapse-specific manner (Kielland et al., 2006), especially in neocortical areas where they control the excitation/inhibition imbalance (Gitler, Takagishi, et al., 2004). Interestingly, Synapsins are not necessary for neurotransmission but their numerous functions (such as regulating populations of vesicles, regulating vesicular docking/priming stages, modifying neurotransmitter release parameters) make them very central actors for the fine-tuning of inter-synaptic functional heterogeneity.

For example, a triple deletion of the three genes coding for all Synapsin isoforms has a massive impact onto the ultrastructural organization of presynaptic terminals in the hippocampus (Fornasiero et al., 2012). The ability of Synapsins to cross-link synaptic vesicles and associate them to active filament is essential for the coherence of reserve populations.

Also, Synapsins are equipped with specific targeting sequences (Gitler, Xu, et al., 2004). A synapse-specific targeting of synapsin isoforms might organize synapse-specific short term plasticity in line with experiments in various brain structures (Gitler, Takagishi, et al., 2004; Kielland et al., 2006; Wei et al., 2011).

Finally, one important issue in synaptic physiology is to link the expression of presynaptic molecules with the functioning of a given presynaptic terminal. Even if the functional role of many different presynaptic molecules is very well depicted in the literature, the way heterogeneous expression of presynaptic molecules modulate the information flow in neuronal networks remains barely known. Such an investigation requires molecular, ultrastructural and functional correlates that need to me replaced in the framework of a specific brain network.

Part 2. The cerebellar cortex

2.1 Generalities on cerebellum

The cerebellum is generally considered as a sensorimotor brain structure involved in motor adjustments and motor learning (Albus, 1971a; John C. Eccles, Ito, & Szentágothai, 1967; Wolpert, Miall, & Kawato, 1998). Its main function is to coordinate ensembles of body elements requested during specific tasks like motor adjustments during conditioning tasks or *on-line* adjustments of fine movements during motor learning. Also, cerebellum is largely involved in the control of passive motor behaviors like postural tonus, proximal musculature, gravitational adjustments and various autonomic processing (Bastian, 2006; Wolpert et al., 1998). In human patients, many cases of cerebellar lesions induce limb tremors, ataxia and deficiencies in different motor adaptations. Indeed, recent *in-vivo* studies have enlighten the role of cerebellum (and more specially cerebellar cortex) in sensorimotor prediction. This ability to anticipate incoming stimuli helps in the detection of unexpected events in order to generate appropriate body responses (Giovannucci et al., 2017a). The specific predictive function of cerebellum in a dynamical environment have also been described in humans (Bastian, 2006). Such a function requests a permanent integration of a massive amount of internal inputs such as the efferent copy of motor commands and external sensory information of the current body state (Thach, Goodkin, & Keating, 1992).

In mammals, the cerebellum is composed of two anatomical parts:
i) the deep cerebellar nuclei contain the output projection neurons of the cerebellum. Deep cerebellar nuclei projection neurons contact an incredible number of brain areas including the thalamus, the red nucleus, pontine nuclei and various other nuclei from the midbrain, the brainstem and the spinal cord that are especially involved in motor control.

ii) The input stage of cerebellum, the cerebellar cortex, is a highly foliated and dense multi-layered structure responsible of the integration and processing of a large variety of inputs.

2.2 Anatomy of cerebellar cortex

The cerebellar cortex receives two main excitatory inputs, mossy fibers coming from various precerebellar nuclei, and climbing fibers coming from the inferior olive. Mossy and climbing fiber projections show topographically organized maps. There is a perfect match between transversal Purkinje cell ZebrinII stripes and climbing fiber projections, while mossy fibers inputs are organized in longitudinal and bilateral bands (Apps & Hawkes, 2009). These bands form functional units (Valera et al., 2016) (called *modules*): they

are spread over the 10 lobules of cerebellar cortex and share a common neuronal architecture underlying similar mechanisms of information processing.

i) Mossy fibers relay different modalities coming from the spinal-cord and brainstem with contralateral projections and the nature of sensory information transferred by mossy fibers depends on the precerebellar nuclei origin. Indeed, there is a highly conserved somatotopy of cerebellar mossy fiber inputs from the macroscopic to the microzone level.

ii) The inner-most layer of the cerebellar cortex is the granule cell layer, at the input stage of the cerebellar cortex. It directly receives mossy fibers coming from various precerebellar nuclei by making several synaptic contacts onto the excitatory granule cells. Because of the very high number of granule cells and because of the anatomical structure of glomeruli (that clusters one mossy fiber contact to several granule cell dendrites), there is an important degree of divergence at the mossy-fiber-to-granule cell synapse.

Some inhibitory neurons also have their soma inside the granule cell layer and coordinate populations of granule cells by providing feedback inhibitions. Golgi cells are the main GABAergic inhibitory cell type within the granular layer. They provide feedback inhibition of cerebellar granule cells within cerebellar modules. Other types of cells have been characterized such as lugaro cells that provide a medio-lateral inhibition and are very sensitive to monoamines, and also globular cells.

iii) The second layer of cerebellar cortex is composed of an array of Purkinje cells with dendrites in a parasagittal orientation. Cerebellar Purkinje cells are spontaneously active inhibitory cells (both *in-vivo* and *in-vitro)* and represent the sole output of cerebellar cortex. As they inhibit neurons from the deep cerebellar nuclei, rate and timing adjustments of their firing account for a precise modulation of the downstream targets. Indeed, deep cerebellar nuclei neurons are highly sensitive to Purkinje cell firing pauses, synchronicity and regularity (Dykstra, Engbers, Bartoletti, & Turner, 2016; Sudhakar, Torben-Nielsen, & De Schutter, 2015).

iv) The outermost layer of cerebellar cortex is the molecular layer, beyond pia mater. It contains the huge dendritic trees of Purkinje cells where excitatory inputs (from granule cells and climbing fibers) and inhibitory inputs (from molecular layer interneurons) converge: First, climbing fiber inputs provide a very strong and one-to-one excitation of Purkinje cells by directly contacting their dendritic tree. Second, a massive amount of granule cells contact Purkinje cells by spanning their axons, the parallel fibers, perpendicular to Purkinje cell dendritic arbor. Parallel fibers also contact various inhibitory interneurons responsible of *feedforward inhibition* onto Purkinje cells.

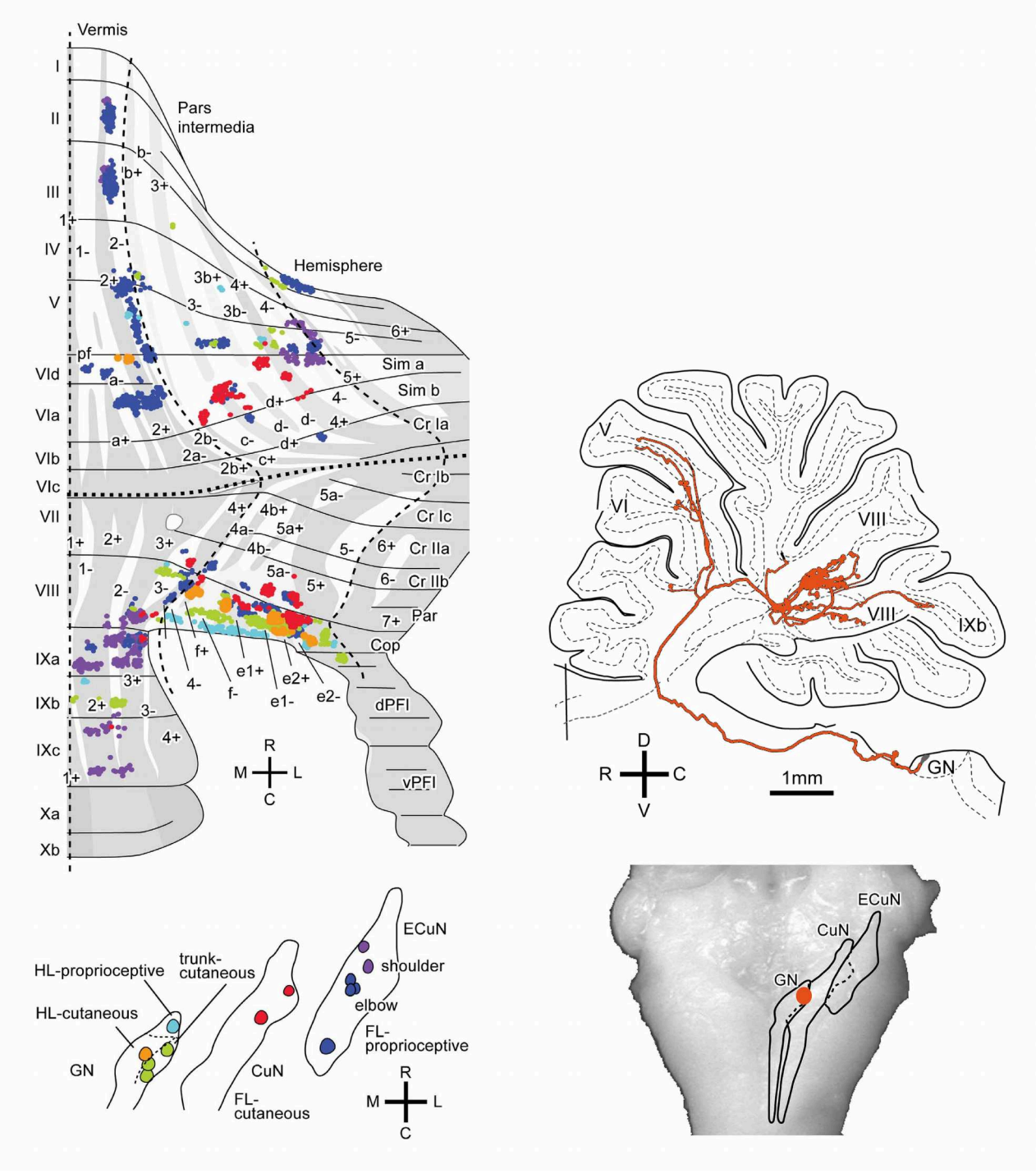

Figure 13. Topography of mossy fiber projections at the input stage of the cerebellar cortex.
Left – Posterior view of an unfolded cerebellar cortex showing the projection sites of multiple mossy fibers originating from different localization within precerebellar pontine nuclei (bottom). Some cortical zones show an overlap of populations of mossy fibers with different pre-synaptic origins. Such a projection pattern suggest a multimodal overlapping at the level of the cerebellar cortex
Right – Sagittal section of cerebellum showing the divergence of a single mossy fiber traced from the precerebellar gracile nucleus projecting to different lobules of the cerebellar cortex.
(GN – Gracile nucleus, CuN – Cuneate nucleus, ECuN – external cuneate nucleus,)

2.3 The feedforward network

Electrical compound stimulation of parallel fibers within the molecular layer induce a direct monosynaptic excitatory current onto the postsynaptic Purkinje cells. This current is immediately followed (a few milliseconds after excitation) by a strong disynaptic inhibition provided by the activation of molecular layer interneurons (Mittmann, Koch, & Häusser, 2005). The properties of feedforward inhibition provide a temporal restriction for desynchronized excitatory inputs onto Purkinje cells and also enhance the precision of Purkinje cell evoked firing (Dizon & Khodakhah, 2011). Also, the feedforward network is a potential source of synaptic learning for somatosensory contextual representations (Brunel et al., 2004; J.C. Eccles, Llinàs, R., & Sasaki, 1966; Isope & Barbour, 2002; Thach et al., 1992).

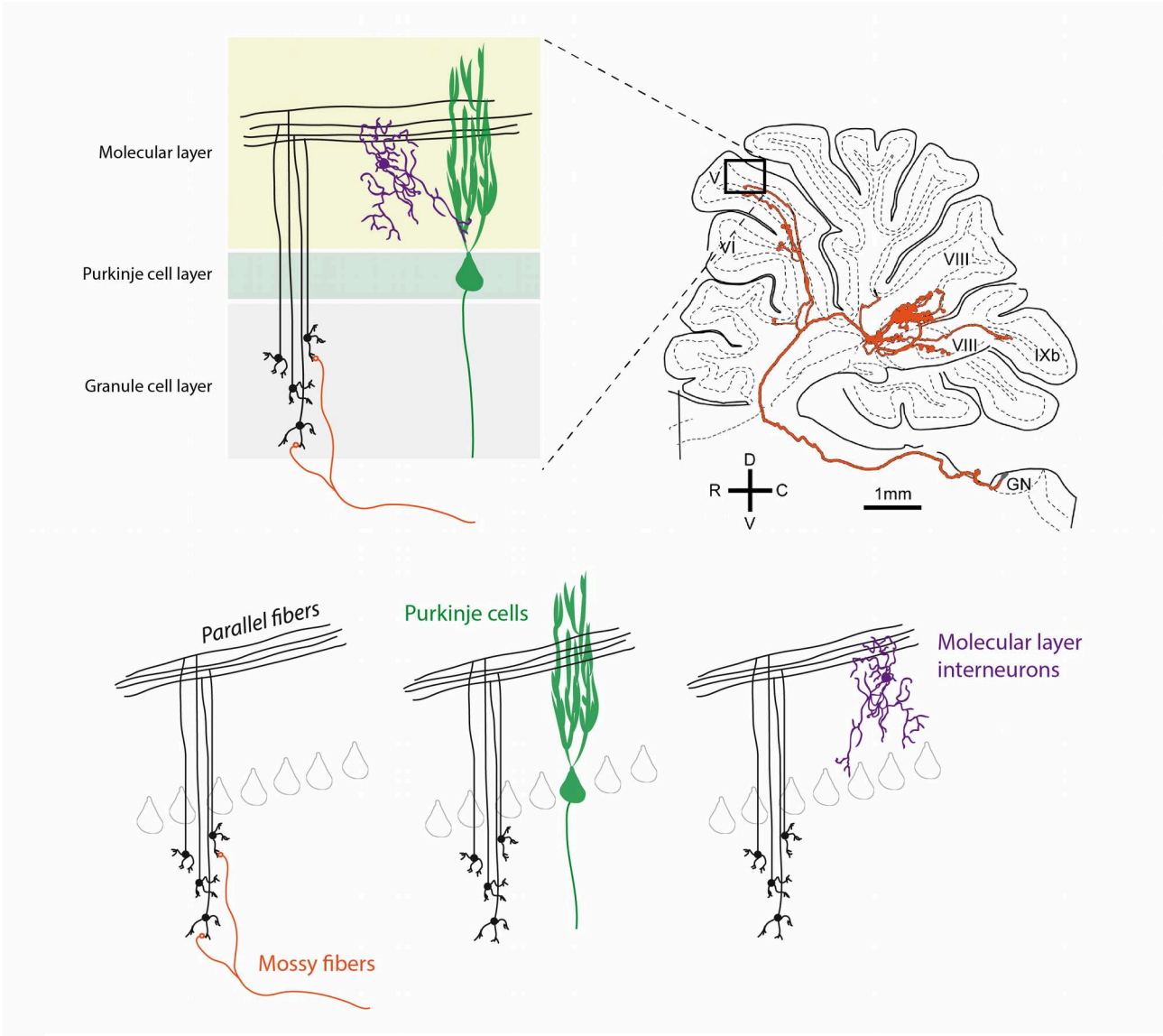

Figure 14. The feedforward network of the cerebellar cortex.
Top – illustration of the neuronal elements composing the feedforward network of cerebellar cortex.
Granule cells are contacted by the excitatory mossy fibers (orange) and in turn, provide an excitatory drive onto Molecular layer interneurons (purple) and Purkinje cells (green), the sole output elements of cerebellar cortex.

2.3.1 Molecular layer interneurons mediate feedforward inhibition

Molecular layer interneurons play a central role in constructing feedforward inhibition. They receive excitatory inputs from granule cells and contact both Purkinje cells and other interneurons with GABAergic terminals. Following sensory activation, parallel fibers discharge series of action potentials at very high frequencies (Arenz, Bracey, & Margrie, 2009; Chadderton, Margrie, & Häusser, 2004a; Jörntell & Ekerot, 2006; Rancz et al., 2007). In turn, they drive molecular layer interneurons which follow granule cell firing by an immediate frequency build-up, sometimes up to hundred hertz. This provides a strong di-synaptic inhibition onto Purkinje cells which often masks direct excitation from parallel fibers (Chu, Bing, & Qiu, 2011).

Molecular layer interneurons display an irregular basal firing activity at frequencies between 5~30Hz *in-vitro* (Carter & Regehr, 2002) and *in-vivo* (Jelitai, Puggioni, Ishikawa, Rinaldi, & Duguid, 2016) but slightly lower on anesthetized animals (Blot et al., 2016; J.C. Eccles, Llinàs, & Sasaki, 1966). During *in-vivo* recordings, locomotion induces an acceleration of granule cell firing rates providing a direct excitatory drive onto molecular layer interneurons and finally a disynaptic inhibition on Purkinje cells. Thus, frequency coding by molecular layer interneurons is unidirectional (like granule cells) because no decrease of basal firing rate is reported following sensorimotor integration. (Jelitai et al., 2016).

Feedforward inhibition fine tunes the spike output firing pattern of Purkinje cells. Unlike granule cells, and molecular layer interneurons, Purkinje cells bidirectionally encode sensorimotor information : this means that some Purkinje cells display an acceleration or a decrease of their firing rate following a specific *in-vivo* sensory stimulus (Chen, Augustine, & Chadderton, 2016).

Molecular layer interneurons control the direction of Purkinje cells firing output pattern. *In-vivo* optogenetic inactivation of molecular layer interneurons (via a specific expression of ArchRhodopsine) suppressed bidirectionnal coding properties of Purkinje cells. Without any feedforward inhibition, there is no deceleration of Purkinje cell spike output pattern following sensory activation meaning that the coding possibilities are dramatically reduced. In addition, the same *in-vivo* inactivation induced very strong behavioral changes (such as motion rate during locomotion) at different moments of illumination (Jelitai et al., 2016). This outstanding effect clearly shows that fine tuning the feedforward inhibition provided by molecular layer interneurons controls the precise instructions given by Purkinje cells for motor adjustments. Thus, variations of molecular layer interneuron inhibitory strength and timing lag onto Purkinje cells might reflect a very specific neuronal code within cerebellar networks.

2.3.2 Granule cells drive the feedforward network

Granule cell firing acceleration encodes motion

Granule cells are at the input stage of cerebellar cortex. *In-vivo* recordings on awake animals have shown that granule cells have very low baseline firing. When the animal is immobile, granule cell firing frequency is low, approaching 0.14Hz (Chadderton et al., 2004a; Jelitai et al., 2016; Powell, Mathy, Duguid, & Häusser, 2015). During locomotion, granule cell firing increases. They display multiple firing patterns, from mini-bursts to permanent activation with a highly variable rate of acceleration. In any case, information coding by granule cells is unidirectional, meaning that no granule cell silencing or deceleration but only acceleration has been observed. Granule cells illustrate the perfect excitatory drive of feedforward networks.

*Granule cells encode massive sensorimotor representation*s

Early computational models assigned small assemblies of granule cells to encode very specific contextual information (Albus, 1971b; Fujita, 1982; Ito; Marr, 1969). The neuroanatomical properties of their synaptic inputs, the mossy fibers, enable *sparse-coding* because combinations of mossy fibers are needed to activate single granule cells and each granule cell is contacted by different (3~5) mossy fibers (Chadderton, Margrie, & Häusser, 2004b; Xu-Friedman & Regehr, 2003). Such a *sparse-coding* enables pattern discrimination and would refine information storage and processing within the cerebellar cortex. Recent studies have shown that a subset of granule cells are active during specific limb movements to encode gait representation. This representation originates from a massive integration of contextual sensory inputs during locomotion (Powell et al., 2015) that would be rather considered as *dense* coding (Spanne & Jörntell, 2015). Indeed, granule cells encode massive contextual information that can be used for sensory prediction during conditional learning (Giovannucci et al., 2017b). Strikingly, the latter study shows that predictive activation of granule cells is systematically correlated to a successful conditioned response. This outstanding discovery shows that : *i*) a huge proportion (two-thirds) of granule cells continuously encode both external and internal representation. And *ii*) in case of motor learning, some granule cells carry predictions of specific motor behaviors (such as a conditioned responses) although it was already known that granule cell activity precedes motor behaviors (Thach et al., 1992).

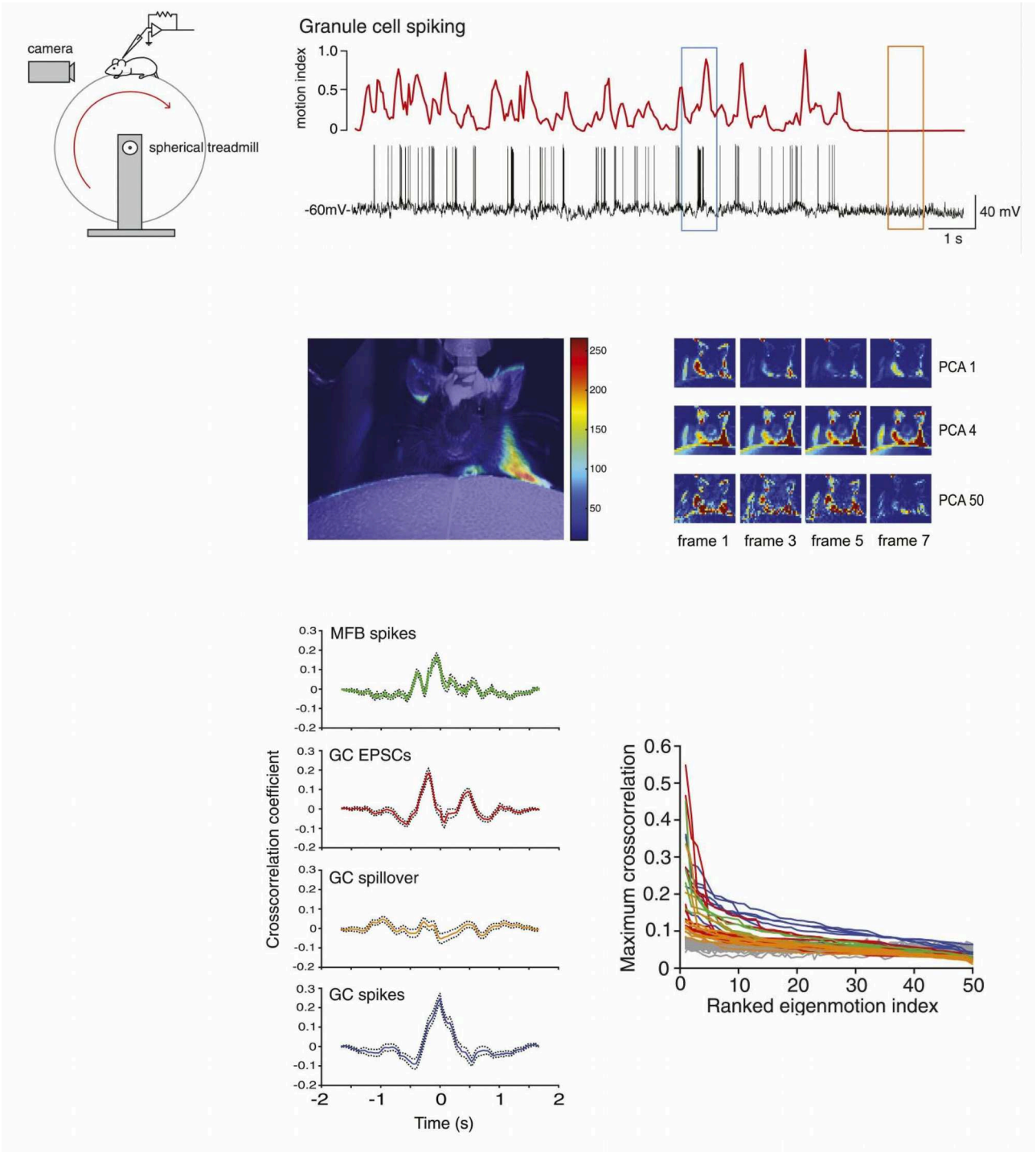

Figure 15. Granule cells encode limb motion in freely-moving animals.
Top – Illustration showing a freely-moving mouse on a head restrained setup. Simultaneous recordings of animal motion and granule cell firing show an important correlation between motion activity and granule cell bursting activity recorded *in-vivo*. Motion index is based on the analysis of recorded movements onto video acquisitions.
Middle – Principal component analysis from video recording of animal motion describe the main source of variability of limb movements. The most important source of motion is explained by the first principal components (mainly by PC1).
Bottom – Cross-correlation between the motion index and various parameters inherent to the granule cell excitatory drive. Granule cell EPSCs and Granule cell firing are the parameters most correlated to limb movement (left). Granule cell firing activity and EPSC bursts are motion-specific (right) ; the first eigenvalues of the PCA kinematics are highly correlated to granule cell parameters (Powell et al., 2015).

2.4 Regulation of granule cell activity

2.4.1 Activation of granule cells by mossy fiber inputs

Granule cells have a very small somata and short dendrites which minimizes dendritic spatiotemporal filtering which make them electrotonically compact and highly excitable (Delvendahl, Straub, & Hallermann, 2015). Electrotonic compactness of granule cells, ultrastructural properties of the glomeruli and presynaptic properties of mossy fibers contribute altogether in a reliable transfer of sensory information from mossy fibers to granule cells (Chadderton et al., 2004b; Delvendahl et al., 2015; Gabbiani, Midtgaard, & Knöpfel, 1994). Both AMPA and NMDA receptors are involved in excitatory transmission at this synapse with an important contribution of glutamate spillover in generation of bursts of activity (DiGregorio, Nusser, & Silver, 2002; Powell et al., 2015). Thus, signal-to-noise ratio is enhanced by an accurate detection of high frequency mossy fiber EPSC bursts while spontaneous eEPSCs at mild and low frequencies have more complex consequences on signal integration (Schwartz et al., 2012). *In-vivo* recordings during evoked sensory stimulation induce very high-frequency firing (sometimes up to ~700Hz) at single mossy fiber terminals (Rancz et al., 2007). Hence, those synapses act in a « detonator fashion » : during locomotion, granule cells burst at high frequencies (hundreds of hertz) following mossy fiber activity (Powell et al., 2015; Rancz et al., 2007).

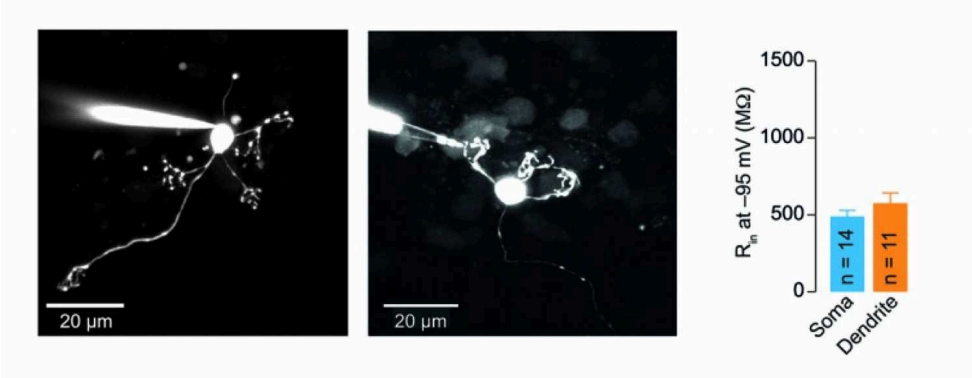

Figure 16. Electronic compactness of single granule cells.
Somatic (left image) and dendritic (right image) patch clamp of single granule cells reveal a weak dendritic filtering. The cells are filled with a constitutive dye and reconstructed under a 2-Photon microscope. Internal resistance are calculated using both configurations (right). Somatic and dendritic and very high and similar in the two configurations showing that there is a very weak attenuation of electrical information during dendritic filtering following MF-GC activation (Delvendahl et al., 2015).

2.4.2 Granule cells encode unimodal and multimodal information

Single granule cells can receive both unimodal and multimodal information (Chabrol, Arenz, Wiechert, Margrie, & DiGregorio, 2015; Ishikawa, Shimuta, & Hä Usser, 2015). Previous studies have shown that 17 % of granule cells in CrusI and II, cerebellar regions receiving mostly somatosensory inputs can also respond to auditory inputs (Chadderton et al., 2004b; Rancz et al., 2007). Paraflocculi, known for their dominant vestibular inputs have 10 % of multimodal granule cells (and at 1 % trimodal : auditory, somatosensory and vestibular).

Other neuronal tracing studies (Chabrol et al., 2015; Huang et al., 2013) have shown that distinct mossy fibers originating from distinct pre-cerebellar nuclei (pontine nuclei and vestibular nuclei) can connect to one single granule cell. These results are in line with electrophysiological signatures of multimodality. As it was suggested fifty years ago by founder theories (Albus, 1971b; Marr, 1969) single granule cells encode different input features in order to code accurate representations of the body state (for example during locomotion).

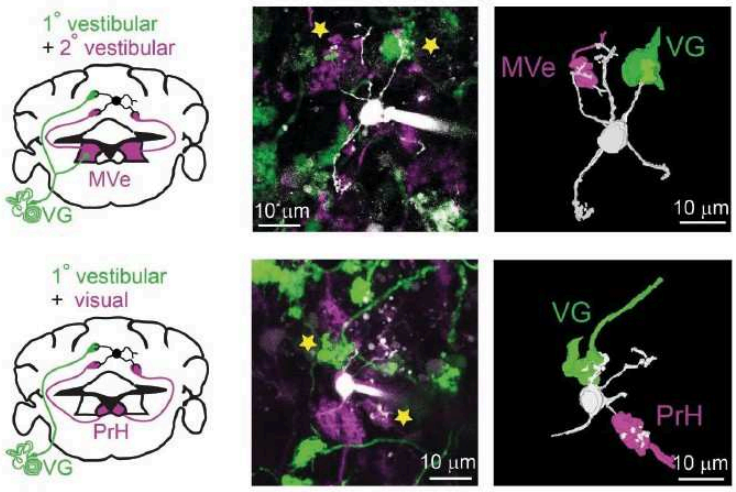

Figure 17. Granule cell are contacted by multiple mossy fiber inputs from different pre-cerebellar nuclei.
The goal of this experiment is to determine whether unitary granule cells are contacted by presynaptic mossy fibers from different origins (Multisensory granule cells) or by fibers incoming from the same nucleus (Monosensory). Double viral injection were performed in distinct pre-cerebellar nuclei following two conditions (VG – Vestibular Ganglion and Mve, – Medial vestibular nucleus or VG and PrH – Nucleus prepositus hyperglossi). Both pairs of nuclei projections show a convergence at the level of unitary granule cells. Mossy fiber tracing and three dimensional reconstructions confirm that granule cells (white) are activated by multisensory inputs (green and purple mossy fiber inputs) coming from distinct pre-cerebellar origins (Chabrol et al., 2015).

Chabrol & al. have demonstrated *in-vitro* a synapse-specific short term plasticity at mossy fiber synaptic terminals depending on their nucleus origin (or the nature of the modality they encode) (Chabrol et al., 2015). Combining *in-vivo*, *in-vitro* and computational models they show a temporal coding of both unimodal and multimodal sensory inputs in granule cell neurons. The diversity of multisensory information transferred by cerebellar granule cells is directly linked to the specific interplay between activated mossy fibers. According to specific combinations of unimodal sensory inputs, the delay and the firing output pattern can vary onto one single granule cell which diversifies the readout of the output firing pattern.

2.4.3 Population coding during sensory activation

In-vivo calcium imaging studies demonstrated that sensory activation of granule cells leads to a preferential activation of neighboring parallel fibers (Wilms & Häusser, 2015). A clustered activation of parallel fibers produces glutamate spillover and retrograde signaling that triggers long term synaptic modifications. By studying coincident activation, the authors have found that only 22 % of the imaged granule cells are connected by the same mossy fiber. The somata of two neighboring parallel fibers are not at the same position inside the granule cell layer because of developmental issues (Espinosa & Luo, 2008). Thus, different mossy fibers encoding the same modality might activate spatially distributed granule cells in the granule cell layer projecting neighboring axons inside the granule cell layer. During sensorimotor integration, a clustered excitation of the various post-synaptic targets of granule cells might have crucial consequences onto information processing. We will see later on that long term dynamics of synaptic transmission are highly dependent on the distance between neighboring fibers. (Abrahamsson, Cathala, Matsui, Shigemoto, & DiGregorio, 2012; Pachoud, Sharma, Bergerot, Knöpfel, & Marcaggi, 2014; Wilms & Häusser, 2015). Thus, the dynamic regulation of excitation/inhibition balance onto Purkinje cells and molecular layer interneurons is dependent on the spatio-temporal pattern of activated fibers.

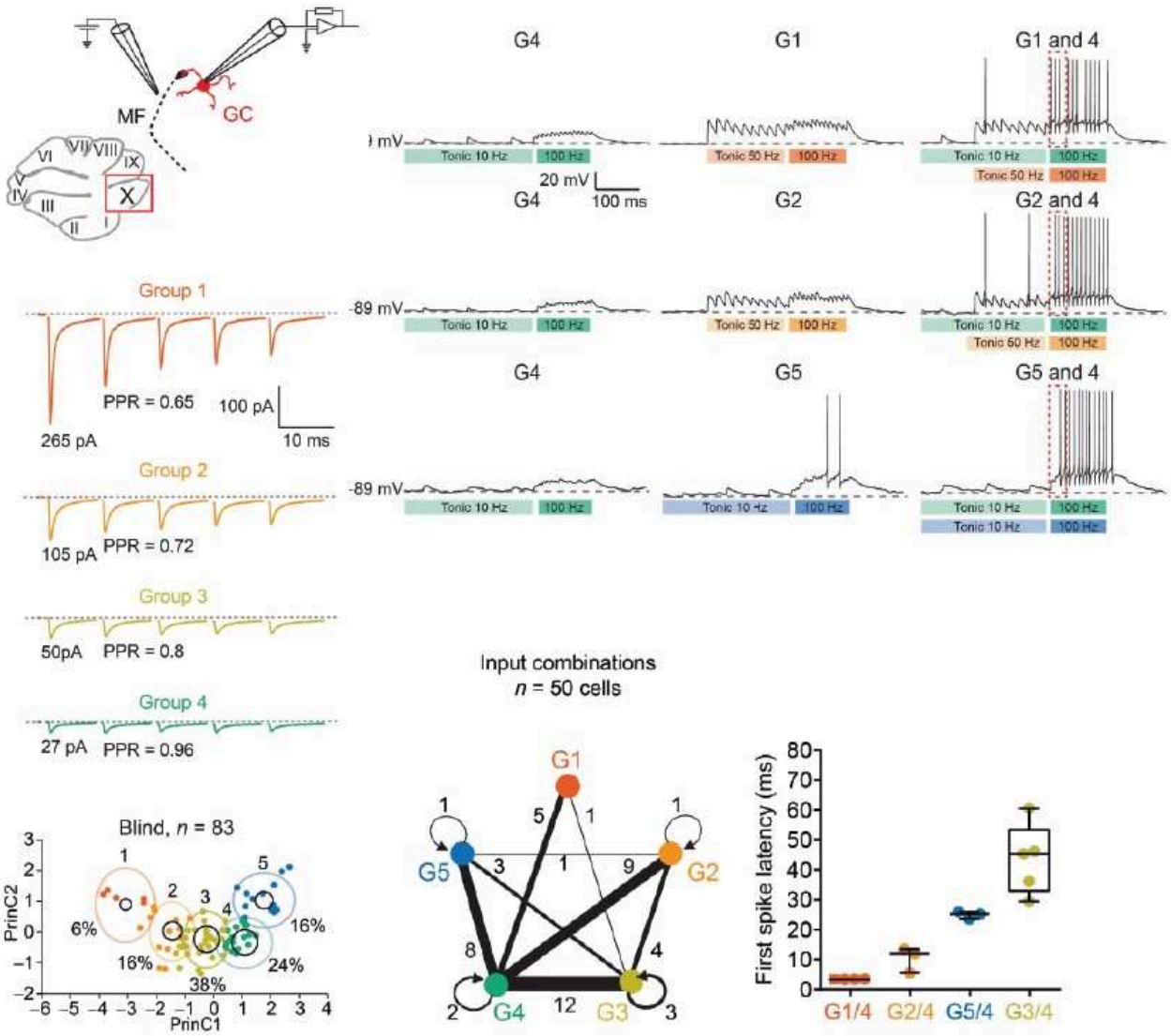

Figure 18. Combinations of mossy fiber inputs with different presynaptic origins and different short term properties induce different output firing patterns at the level of single granule cells.

Top – Illustration showing the stimulation of individual mossy fibers stimulated electrically and the patched granule cell.

Left - Different populations of mossy fiber synaptic terminals are identified based on their short term plasticiy behavior following bursts of electrical stimuli that mimic physiological mossy-fibre activities. Short term presynaptic behaviors are classified depending on the time-course of glutamate release during eEPSC bursts. Then, synapses are clustered in different groups using Principal Component Analysis and Kmeans clustering.

Bottom - On a population of 50 cells, different combination of input plasticities could be encountered on single granule cells. Different short term plasticity behaviors are isolated with KMean clustering and several inputs characterized by different functional properties could be connected onto the same granule cells.

Right - Simultaneous stimulations of double mossy fiber inputs induce different output firing patterns that vary depending on the delay of the first spike. Coincident activation of specific mossy fibers regulate temporal coding at the GC stage of sensorimotor integration.

(Chabrol et al., 2015)

Part 3. Molecular layer interneurons

Molecular layer interneurons from the cerebellar cortex are the core component of feedforward network. The first morphological descriptions of molecular layer interneurons were made one century ago by Santiago Ramòn y Cajal (1911). Golgi preparations visualized under light microscopy helped to better appreciate their similarities and diversity (Chan-Palay & Palay, 1972). Later on, molecular layer interneurons were all identified as GABAergic cells (Obata, Ito, Ochi, & Sato, 1967) integrating direct excitatory inputs from granule cells. Altogether, morphological and electrical properties of interneurons shape the integration of excitatory inputs (Abrahamsson, Cathala, Matsui, Shigemoto, & DiGregorio, 2012; Sultan & Bower, 1998).

3.1 Morphological classification of molecular layer interneurons

Historical observations of molecular layer interneurons by Santiago Ramòn y Cajal divided them in two categories : basket cells and stellate cells. Studying the morphology of their axon and dendritic arbour helped to refine classification criteria over the years (Chan-Palay & Palay, 1972; Rieubland, Roth, & Häusser, 2014; Sultan & Bower, 1998). Their main distinction criteria remains the peculiar axonal projection : Basket cells connect to the soma of Purkinje cells on parasagittal rows while Stellate cells connect onto local Purkinje cell dendritic arbor. The pericellular « basket » axon characterizing Basket cells have chemical and ephaptic contacts (providing an electric shunt of membrane voltage drops) (Blot & Barbour, 2014) around Purkinje cell soma and form « pinceau » structures around the axon with very specific ephaptic contacts. In the classical vision of cerebellar cortex, Stellate cells are devoid of this basket-like somatic axons.

In addition, several intermediate morphotypes of basket and stellate neurons have been identified with specificities in dendritic orientation, depth of axonal projection and radial expansion of the neuronal processes (Chan-Palay & Palay, 1972; Sultan & Bower, 1998). For example, stellate cells with a soma neighboring the pia-mater («superficial stelate cells ») tend to have a bi-polar dendritic arbour. Cells in deeper areas («deep stellate cells ») tend to have fusiform dendrites with a bigger dendritic arbor.

Despite this categorical classification, controversial studies pinpoint the absence of clear distinctions between basket and stellate cells. For example, Basket cells can be found preferentially in the inner one third of molecular layer but other basket neurons can be found more externally (sometimes in the outer one third). These cells are no more « pure » Baskets as they also display both stellate-like and basket-like morphological properties (for example, « superficial » and « deep » stellate cells can have descending axons that connect Purkinje somas in proportions close to 15 % and 19 % respectively) (Chan-Palay & Palay, 1972; Paula-

Barbosa, Tavares, Ruela, & Barroca, 1983). In addition, some basket collateral can also inhibit Purkinje cells dendritic tree (Sotelo, 2015).

Finally, the diversity of molecular layer interneurons is better described as a continuum sharing common anatomical features (Sultan & Bower, 1998) rather than a clear dichotomy between basket and stellate cells. During the time of my PhD, I performed my experiments with the idea that morphological diversity of molecular layer interneurons would be better described by a top-down continuum of neurons (from the *pia-mater* to the Purkinje cell layer), keeping in mind that the relative depth of the interneuron would be the best parameter representative of its nature and function in the network.

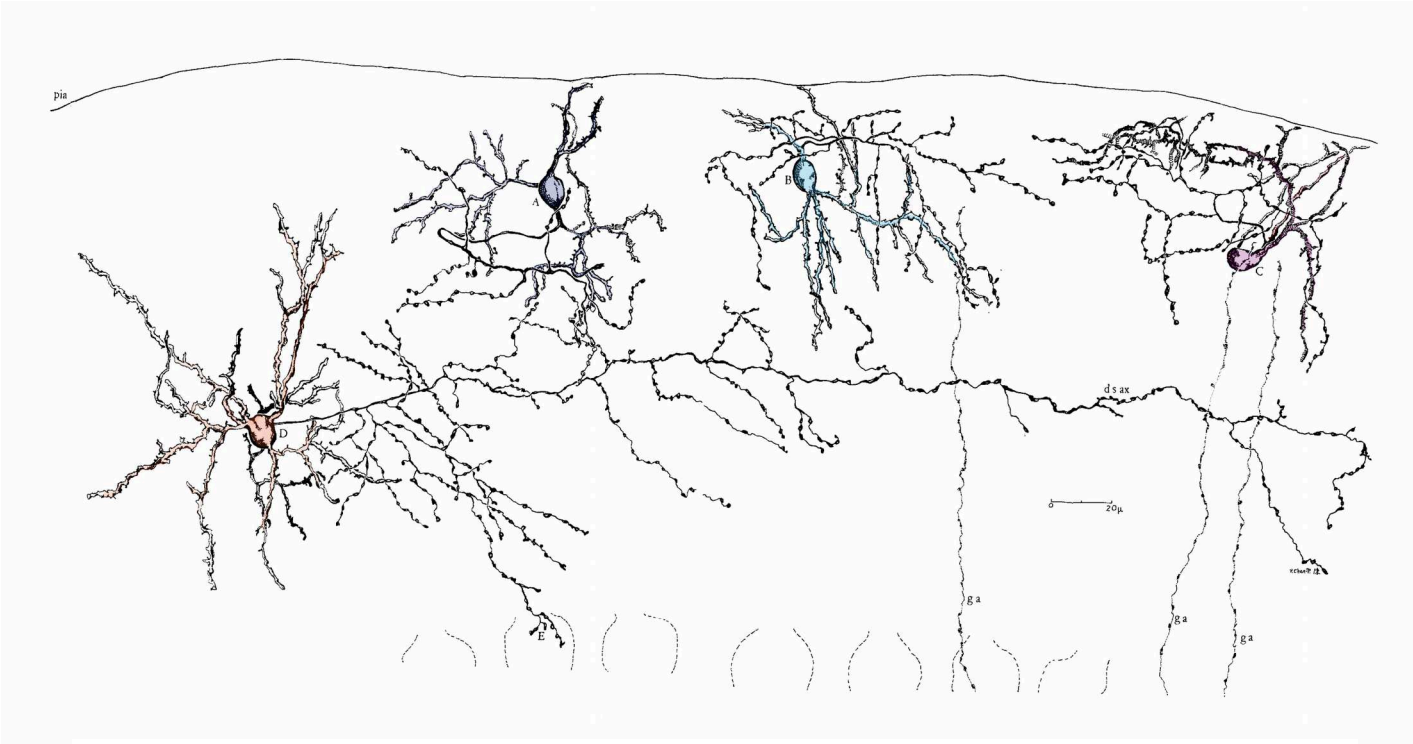

Figure 19. Morphological properties of molecular layer interneurons.
Illustration of four stellate cells with different morphology onto a sagittal cross-section of rat cerebellar cortex. Interestingly, some superficial stellate cells are equipped with a descending axon targeting Purkinje cells' soma (Chan-Palay & Palay, 1972).

3.2 Development of molecular layer interneurons

Axonal projections

The topographical refinements of cerebellar cortex microcircuitry are mainly postnatal (van Welie, Smith, & Watt, 2011). Morphological differentiation of molecular layer interneurons is orchestrated by micro-environmental extrinsic cues combined to genetical determinants (Huang, Di Cristo, & Ango, 2007). Guidance cues such as cell adhesion molecules, EphB, neurofascins, play a crucial role in axonal targeting of basket axons toward the soma of Purkinje cells. More precisely, Purkinje cells express AnkyrinG, a downstream effector will create macromolecular complexes that will facilitate the aggregation of N1CAM with voltage gated sodium channels onto axonal processes. If the axonal prolongations are close from Purkinje cell soma, a neurofascin gradient will act as an attracting cue towards the axon initial segment. In the case of dendritic connections, Bergmann glia will help to refine axonal trajectories towards Purkinje cells through interactions with N1CAM. Axonal development is highly sensitive to the molecular environment and activity inside a developmental framework. Thus, morphological differentiation of molecular layer interneurons is dependent on the micro-environment of molecular layer (Purkinje cells, granule cells, Bergmann glia, other interneurons); gradients of extracellular cues might explain the previously stated top-down continuum of interneuron morphology (Williams, de Wit, & Ghosh, 2010).

Gene expression

One study analyzing the gene expression resources from the Allen Brain Atlas has characterized potential molecular markers expressed by all molecular layer interneurons (Schilling & Oberdick, 2009). Some genetic markers are commonly expressed: for example, genes coding for GABA/Glycine co-transporter VIAAT, GABA decarboxylase Gad1 and Grm2, the metabotropic receptor for glutamate type2 are expectedly expressed by inhibitory interneurons.

Interestingly, other genes are preferentially expressed by deep molecular layer interneurons, neurons nearby Purkinje cells. This is the case for genes coding for cell adhesion molecules known for their involvement in axonal development (such as EphB2, Nef3). The presence of these genes could be correlated to a peculiar axonal morphology of these neurons such as the « Baskets » of the « pinceau » formations. Other genes might be correlated with differences in membrane excitability and sensitivity to various chemical species (such as Acid sensitive ion channels or metabotropic receptor for glutamate Type8). For example, the expression of voltage-gated potassium channel subunits genes Kcnab3 and Kcna2 suggests functional differences and seem to be linked with the presence of an axonal *pinceau*. Deeper molecular layer interneurons are enriched in these potassium channels subunits, one should expect variations of excitable properties (Rowan, Tranquil, & Christie, 2014).

For now, variations in gene expressions between interneurons do not depict any specific functional property. They cannot account for reliable pos-synaptic markers for separate homogenous populations. Instead, they illustrate a need of specific protein expressions related do development or their position in molecular layer depth. To conclude, the best parameter characterizing molecular layer interneurons is certainly their deepness in the molecular layer. Indeed, even if some neurons connect Purkinje cell somas while other don't, there are no clear cuts between morphotypes or subcategories based on molecular classification.

3.3 Electrical properties of individual molecular layer interneurons

In this part, we will see that molecular layer interneurons are highly-dynamic functional units that deal with electric information at unitary level and also at population level. As they are responsible of feedforward inhibition, their electrical properties contribute to the temporal precision of Purkinje cell spike discharges, excitation/inhibition imbalances, gain tuning of firing activity (Isaacson & Scanziani, 2011; Mittmann, Koch, & Häusser, 2005).

Altogether, the morphological properties of molecular layer interneurons, their passive and active conductance properties contribute to dendritic signal integration and computation leading to a given spike output firing pattern. Both passive and active conductances expressed by molecular layer interneurons provide a strong reactivity to granule cell excitatory inputs. Feedforward inhibition is driven by granule cells and adjusts Purkinje cell firing with a very strong temporal accuracy (Häusser et al., 1997).

3.3.1 Computation of MLI spike output firing pattern

Membrane properties of MLI

Passive cable properties of molecular layer interneurons model their excitability and their integration properties. The main biophysical properties that shape the temporal reliability of synaptic integration are :

i) Their somatodendritic volume : Because of their small somatodendritic volume, molecular layer interneurons are electrically compact and have high input resistances *in-vivo* (Chu, Bing, Liu, & Qiu, 2012) (with a mean R_{input} ~ 256 MΩ and sometimes over 1GΩ) which make them very sensitive to synaptic activity and input conductance (Kreitzer et al., 2002; Llano & Gerschenfeld, 1993). Interestingly, even small quantal-like currents can also evoke an increase in firing frequency of molecular layer interneurons (up to 610 % of their basal activity) (Crowley, Carter, & Regehr, 2007).

ii) The axonal volume : In contrast to the small size of their soma, molecular layer interneurons have a huge axons (with a length sometimes approaching 500µm in young rats). Axotomization of molecular layer interneurons increases the variability of their firing onset and modifies the filtering of their synaptic currents (Mejia-Gervacio et al., 2007). Indeed, tha axonal compartment acts as a « current sink » providing a supplementary capacitance to the neuron which increases the temporal reliability of synaptic inputs. The presence such an axonal capacitance sharpens the decay of synaptic input currents which increases the accuracy of temporal coding inside the network.

Active conductances regulating neuronal computations

Specific expression of active conductance such as voltage gated potassium and calcium channels help interneurons increase their spike-timing precision and recovery from depolarization (Llano, Tan, & Caputo, 1997; Tan & Llano, 1999). In cerebellar molecular layer interneurons, high levels of voltage gated channels have been reported (Midtgaard, 1992). As these channels are involved in the active repolarization of cell membranes, they enhance the sensitivity of neurons to consecutive inputs.

Different subtypes of voltage gated potassium channels coexist on the membrane of molecular layer interneurons. Kv1 are involved in membrane repolarization, spike waveform modulation and contribute especially in shaping the firing output pattern of interneurons especially. They are expressed at the axonal initial segment and allow repetitive firing activities (Rowan et al., 2014). Unlike Kv1, Kv3 channels are not involved in firing regulation and they tune neurotranmission at molecular layer interneuron inhibitory terminals. They restrict presynaptic calcium entries by shortening action potentials at molecular layer interneuron inhibitory terminals. Potassium and calcium conductances have also been reported to interact during signal computations. Following integration of electrical signals, the firing delay depends on an interplay between A-type potassium currents and T-type calcium currents (M. L. Molineux, 2005).

Can excitable properties of MLI predict their affiliation to a specific neuronal category ?

Previously, we have seen that the morphological distinctions between molecular layer interneurons are not clearly established. Here again, there are no clear functional boundaries between potential « Basket » or « Stellate » cells. Still, interesting relationships with their proximity to Purkinje cell soma (notably depending on their depth inside the molecular layer) denote some possible heterogeneities in functional connectivity. Differences in expression of potassium channels subunits alpha2 and beta have been observed (Schilling & Oberdick, 2009) and might lead to variations in excitability. Yet, no differences in basal firing frequencies or sensitivity to current injections have been reported between various interneurons found at different positions along the depth of the molecular layer (Bao, Reim, & Sakaba, 2010; Chu et al., 2012; Eccles, Llinàs, & Sasaki, 1966)

To conclude, excitability of molecular layer interneurons might follow more complex rules probably emerging from a collaboration between voltage gated potassium, calcium channels and metabolic fluctuation of the micro-environment of the molecular layer (Anderson et al., 2013; Michael L. Molineux, Fernandez, Mehaffey, & Turner, 2005). Studies taking into account morphological properties of molecular layer interneurons suggest no clear morpho/functional relationships (between the excitable properties of

interneurons and their Basket and Stellate morphological property) and it was clearly demonstrated *in-vivo* (Chu et al., 2012).

Finally, during the time of my PhD, I considered that the best parameter that illustrates cell-to-cell variability in the population of molecular layer interneurons is the position in the depth of molecular layer (aka. 1-The distance of the neuron soma to Purkinje cell layer).

3.3.2 Networks of molecular layer interneurons

We have seen that interneuron activation is orchestrated by simple biophysic rules and active conductances. Molecular layer interneurons are also known to be highly interconnected by both electrical and chemical synapses. Signal integration can follow complex dynamics because molecular layer interneurons present both important synaptic interconnexions and electrical continuities.

Synchronization of activity through gap junctions

Dye coupling experiments have shown mutual connections between interneurons which are electrically coupled (Mann-Metzer & Yarom, 1999). Pairs of interneurons synchronize their firing activity without the involvement of inhibitory chemical transmission. Indeed, the expression of connexin36 onto molecular layer interneuron dendrites creates electrotonic networks of 1 to 4 neighboring neurons (Alcami & Marty, 2013). Networks of coupled interneurons are likely to follow specific patterns of connectivity depending on their depth inside molecular layer. Some contradictory studies show higher coupling coefficient in neurons from the outer molecular layer (Mann-Metzer & Yarom, 1999) or from the inner molecular layer (Alcami & Marty, 2013). In both cases, specific connectivity motifs shape the electric network. Indeed, triple patch experiments confirm a preference for electrical clustering in small networks of interneurons (Rieubland et al., 2014). Connectivity allows the synchronicity of clustered interneurons contributing to coherent inhibition of Purkinje cells.

The synchronization/desynchronization state of coupled interneurons highly depends on their excitatory drive as it has been shown onto electrically coupled cerebellar Golgi cells (Vervaeke et al., 2010). Synchronization might help to sample the activity of a large number of parallel fibers : spatial and temporal activation of molecular layer interneurons by parallel fibers is crucial for the definition of their inhibitory dynamics of molecular layer interneurons.

Sub-network synaptic connectivity

Chemical synapses also contribute to the local regulation of grouped interneuron in response to parallel fiber activation. Recent studies report a hierarchy in the local circuitry of mutual inhibition (Rieubland et al., 2014). There is a preference for *transitive* inhibition patterns showing a specific direction of inhibition in local networks of interneurons. This direction is dependent on the position of interneurons in the depth of molecular layer. Transitions are top-down inside the sagittal plane, meaning that interneurons near the pia mater preferentially connect deeper interneurons (closer to Purkinje somas) because their axons are oriented

towards Purkinje cells. In line with morphological characterizations describing a morphological continuum (Sultan & Bower, 1998), this study depicts an internal connectivity within parasagittal bands of connected interneurons.

3.3.3 Dendritic integration of excitatory signals

Molecular layer interneurons receive excitatory inputs from granule cells terminals. However, these inputs do not have the same influence onto the post-synaptic neuron. Indeed, post-synaptic cable properties and active conductances introduce themselves non-linearities of signal integration. As the main focus of my PhD was inter-synaptic variability of pre-synaptic short term dynamics, post-synaptic non-linearities could strongly influence my results. However, we will see in the next paragraphs that my experimental conditions are free from post-synaptic interference.

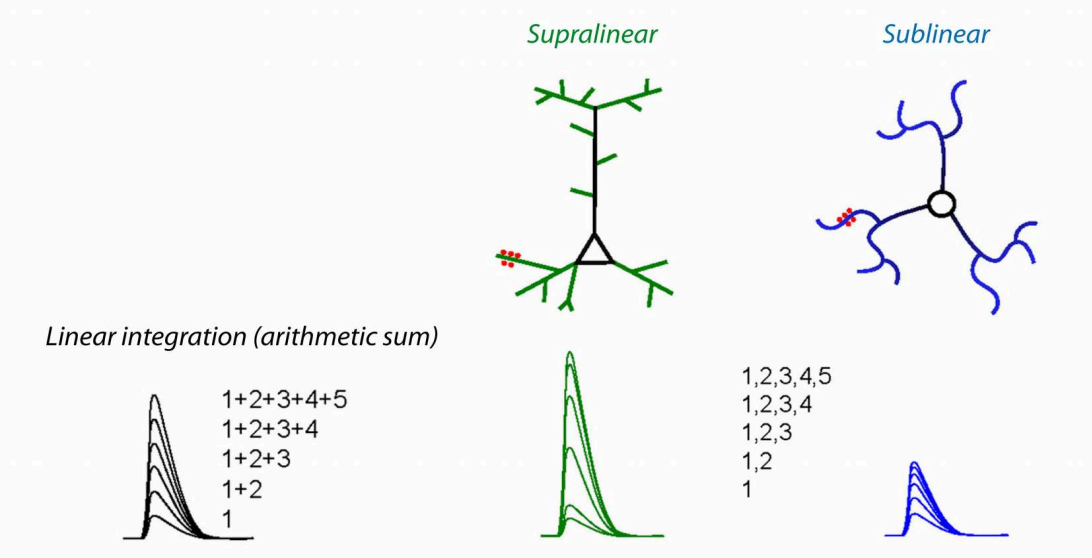

Figure 20. Non-linearities of dendritic signal integration.
Two examples of non-linearities observed at cortical pyramidal cells (green) and molecular layer interneuron from cerebellar cortex (blue). Supralinear integration happens when the observed sum of the evoked events is higher than the predicted arithmetic sum (black) while sublinear integration follows the opposite effect (Tran-Van-Minh et al., 2015a).

Passive cable properties shape dendritic voltage integration

Abrahanssom & al. have shown important differences in electrical integration between somatic and dendritic compartments of stellate cells (Abrahamsson et al., 2012). Passive dendritic cable properties can influence the size of eEPSCs and also short term plasticities. Because of the very small diameter of dendritic

processes (0.2 ~ 0.9µm) , important depolarizations caused by local dendritic inputs can locally attenuate the ionic driving force. For strong or repetitive inputs, dendritic integration of eEPSPs is sublinear : the observed depolarization is weaker than the expected one.

Sublinear integration has two main consequences : First, it alters spatial integration by diminishing the impact of coincident synaptic inputs onto the same dendritic portion. Second, it modifies temporal integration and short term plasticity by enhancing current filtering during successive EPSCs. However, this effect doesn't concern somatic contacts where the driving force is resistant to strong depolarizations due to the important post-synaptic volume.

Dendritic integration depends on the synaptic strength and the timing of inputs. This study shows that coincident synaptic inputs are more efficient when they are scattered on different post-synaptic dendrites rather than condensed onto the same dendritic segment of molecular layer interneurons.

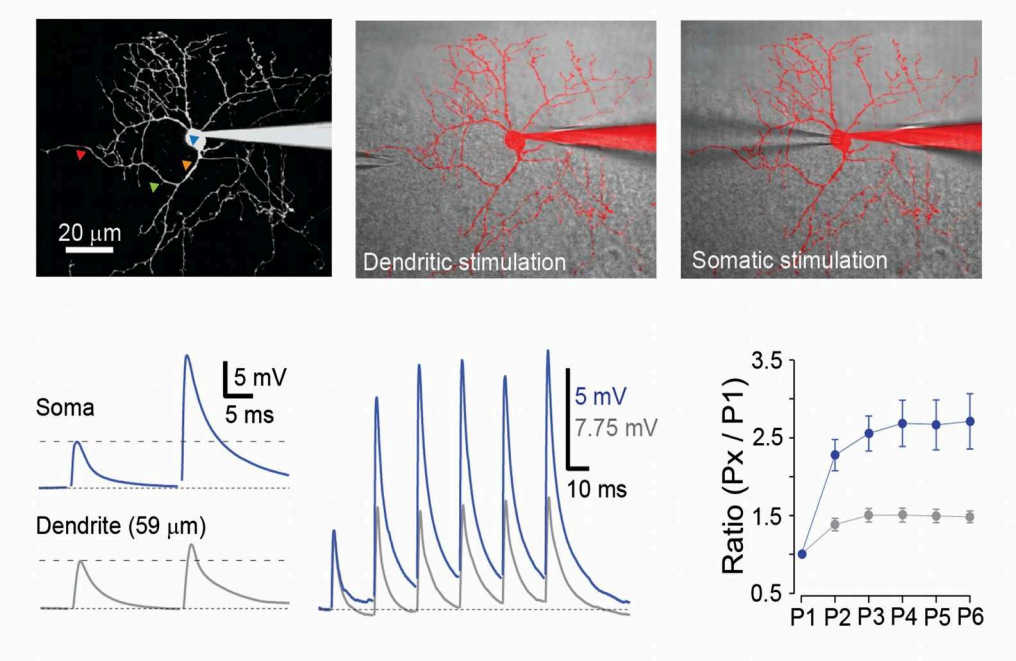

Figure 21. Sublinear integration of excitatory inputs at the granule cell to molecular layer interneuron synapse.
Top – 2-Photon acquisition of a patched molecular layer interneuron with different positions of the electrical stimulation pipette (somatic or dendritic). GC presynaptic terminals are repeatedly stimulated with electrical pulses while post-synaptic MLI are recorded in current-clamp configuration. Short term presynaptic plasticity of GC inputs depends on the distance of the stimulation pipette from the post-synaptic neuron. Dendritic stimuli are delivered at very high distances fro the soma (>50µm) while somatic stimuli are delivered at close distances (<10µm).
Bottom – Sublinear integration shapes short term plasticity of dendritic excitatory inputs. Paired pulse of ePSPs is higher when the electrical pipette is at very close distances from the soma. The time course of ePSPs is modified depending on the position of the presynaptic input and the authors show that the alteration of the 'Paired Pulse Ratio' during current clamp experiments is linked to a local decrease of the driving force in small dendritic segments.
(Abrahamsson et al., 2012)

Calcium dynamics of dendritic integration

Parvalbumin is an endogenous calcium buffer expressed by all functionally mature molecular layer interneurons (Collin et al., 2005). Postsynaptic calcium buffering by Parvalbumin sharpens calcium currents and is correllated with the firing frequency envelope of molecular layer interneuron activity (Franconville, Revet, Astorga, Schwaller, & Llano, 2011).

Calcium buffers such as parvalbumin have a strong impact in regulating postsynaptic calcium dynamics evoked by unitary synaptic inputs. Activating single granule cell presynaptic terminals evokes a strong but spatially restricted calcium signal inside molecular layer interneuron dendrite through to the opening of calcium permeant AMPA receptors (Soler-Llavina & Sabatini, 2006). The spread of calcium signal is limited at 5.8µm around the contact zone (with a maximum of 7.8 µm) while the distance between two active contacts is estimated at ~10µm on *in vitro* acute slices. The compartimentalization of calcium signals restricts the induction of long-term plasticity dynamics, such as stellate-cell long term depression SC-LTD, to single synaptic contacts (Soler-Llavina & Sabatini, 2006) which is a CB1 receptor and mGluR1 receptor dependent plasticity or SSE (Short-term Suppression of Excitation). The occurrence of one or another plasticity effect depends on the firing frequency of the stimulation protocol (Tran-Van-Minh, Abrahamsson, Cathala, & DiGregorio, 2016).

Interestingly, sublinear voltage integration and supralinear calcium integration coexist at stellate cell dendrites (Abrahamsson et al., 2012; Tran-Van-Minh et al., 2016). Voltage gated conductances including NMDA receptors and L-type calcium channels boost calcium signal during repetitive synaptic activation. *In fine*, the observed calcium signal is bigger than the signal predicted from a linear extrapolation.

Network consequences of signal integration

During sensory integration, interneurons are activated by clusters of *en-passant* terminals arising from parallel fibers meaning that several coactivated excitatory synapses possibly contact the same dendritic branch (Wilms & Häusser, 2015). Interestingly, sublinear voltage integration will bypass the effect of clustered *en-passant* terminal activation. Combined to supralinear calcium-induced SSE, these effects might help to diminish the gain of over represented unimodal stimuli (Tran-Van-Minh et al., 2016). Molecular layer interneurons are better activated by scattered parallel fiber contacts favorizing multimodal representation.

While voltage integration is necessary for the computation of input signals in an output firing pattern, calcium integration shapes short term plasticities onto dendritic compartments. There are some

important links between the firing pattern and firing frequency of stimulated parallel fibers and the type of postsynaptic plasticity induced. For example, mid frequency protocols (30Hz bursts) induce an homosynaptic SC-LTD lasting minutes (Soler-Llavina & Sabatini, 2006) while higher frequencies (more than 50Hz) induce heterosynaptic SSE lasting a few seconds (Tran-Van-Minh et al., 2016). Thus, high frequency activation of granule cells has relevant consequences on signal transmission in cerebellar network by modifying the synaptic strength of unitary contacts with a very strong dependence on spatial integration.

In conclusion, molecular layer interneurons are more sensitive to scattered and/or decorrellated sensory inputs (Tran-Van-Minh et al., 2015b). Again, this show that the recruitment of feedforward inhibition is tightly dependent on the spatiotemporal patterns of granule cells activities.

Conclusions regarding dendritic integration of excitatory signals

Sensorimotor integration is encoded by granule cells in high frequency bursts of activity. A we will see later, the core of my PhD work shows that the nature of short term plasticities inherent to unitary granule cell boutons is a key parameter in the control of interneuron activation. We have seen in the previous paragraphs that both active and passive membrane properties gate the input excitatory signal. So how could I assume that intersynaptic variations of short term plasticities are « purely » pre-synaptic ?

i) Sublinear integration of excitatory inputs is dependent on the volume of the post-synaptic compartments (Abrahamsson et al., 2012). Homogeneous dendritic compartments won't affect signal integration. Indeed, signal integration is constant above 20µm distance from the soma. During my PhD, I stimulated terminals at a respectable distance from the somatic compartment ; at such distances I was sure to get rid of any post-synaptic compartmental variations.

ii) Active conductances gate supralinear integration of dendritic signals. However, whole cell voltage-clamp experiments (at -70mV) combined to intra-cellular calcium buffering and NMDA receptor antagonist application prohibited such a supralinear effect,

iii) Bursts of granule cell activity are prone to trigger pre-synaptic gain adjustments through trans-synaptic mechanisms (i.e. retrograde signaling with endocannabinoïds) through SSE or SC-LTD. To discard any variations of plasticity induction from the functional mapping of short term plasticities, I used various blockers of presynaptic neuromodulation or/and long term plasticity induction (Endocannabinoïd receptor CB1, mGlur1-5 receptors, $GABA_B$ receptors, NMDA receptors).

Part 4. Granule cell synaptic terminals

4.1 Morphology of granule cell projections and synapses

Axonal projections of granule cells

Granule cell axonal projections have been extensively described by early tracing studies on rat cerebella (Pichitpornchai, Rawson, & Rees, 1994). Granule cell axons are unmyelinated and composed of two segments. First, the ascending axon emerging from granule cell somata, goes perpendicularily to granule cell layer and separates into the molecular layer as a « T-shaped » bifurcation. Then, it laterally runs along the folia of cerebellar cortices forming the well known « parallel fibers ». In the rat, beams of parallel fibers can bilaterally extend up to 4.7mm (with a 2.08 mm mean length) and in smaller animal, such as mice, it easely reaches 1mm size. Both ascending axons and parallel fibers present a high density of varicosities, corresponding to « ascending » and « en-passant » synaptic terminals, respectively.

During my PhD, I focused essentially on the molecular, ultrastructural and functional heterogeneity of these terminals.

Development of granule cell axonal projections

During postnatal development, immature granule cells are stored inside the external plate (external granule cell layer, just under the pia mater). Clones of granule cells migrate together towards the inner granule cell layer (Espinosa & Luo, 2008) in such a way that parallel fibers are progressively stacked in the molecular layer. Parallel fibers from similar granule cells will run at the same level inside the molecular layer while the cell bodies of two granule cell clones will be dispersed inside the granule cell layer (Wilms & Häusser, 2015). This particular developmental process is at the origin of specific network connectivity inside the cerebellar cortex. Recent studies even suspect clones of granule cells to be connected by afferent mossy fiber coding for the same modalities (Wilms & Häusser, 2015). In that way, sensory-evoked granule cell stimulation would induce a clustered activation of parallel fibers onto their targets (molecular layer interneurons and Purkinje cells).

High density of granule cell boutons in the molecular layer

Using transgenic mice expressing a fusion protein Synaptophysin-GFP that exclusively stains synaptic boutons and cytosolic tdTomato, recent works describe the distribution of synaptic contacts onto single parallel fibers (Li et al., 2010). This study is in line with former papers showing an incredibly high density of granule cell synaptic contacts inside the molecular layer of rats (granule cell synaptic density is over 0.931 contact per μm^3 of tissue) (Napper & Harvey, 1988). The reasons for that are certainly the very high number of granule cells in cerebellar cortex giving rise to the same number of parallel fibers (Harvey & Napper, 1988) and also the high number of varicosities per granule cell axon: onto one single granule cell, we can count hundreds of varicosities (between 250 and 500). In consequence, *en-passant* varicosities are very small and vary in size a lot (from $0.46\mu m^2$ to $0.82\mu m^2$) which is often correlated with the axonal diameter and the distance from granule cell somata (Pichitpornchai et al., 1994).

Ultrastructure of granule cell synaptic terminals

Electron microscopy studies on adult Wistar rats have estimated that about 80% of granule cell synaptic contacts are made with Purkinje cells (Harvey & Napper, 1988; Napper & Harvey, 1988). The rest of them are made with various neuron types into the molecular layer. One single Purkinje cell receives a massive amount of granule cell excitatory terminals : between 154 and 175 thousands of granule cell inputs. About 20 % of these inputs are coming from the ascending axon of local granule cells (Huang, Wang, & Huang, 2006; Pichitpornchai et al., 1994), while 80 % of then come from « en passant » terminals.

Granule cell synaptic terminals contain a very high density of synaptic vesicles. Latest estimations from electron microscopy studies have counted about 480 (±160) vesicles per varicosity while only 8 (±2.9) vesicles are docked at the active zone (M a Xu-Friedman, Harris, & Regehr, 2001).

Despite a very good characterizations of docked vesicles at *en-passant* terminals, the ultrastructural arrangements of synaptic vesicles away from the active zone are poorly depicted in the litterature. From electron microscopy micrographs, I described inter-synaptic ultrastructural heterogeneities at granule cell-to-molecular layer interneuron synaptic terminals. With complementary immunogold experiments directed against SynapsinII, I have shown that variations in synaptic ultrastructure are associated with the presence or not of this specific molecular marker.

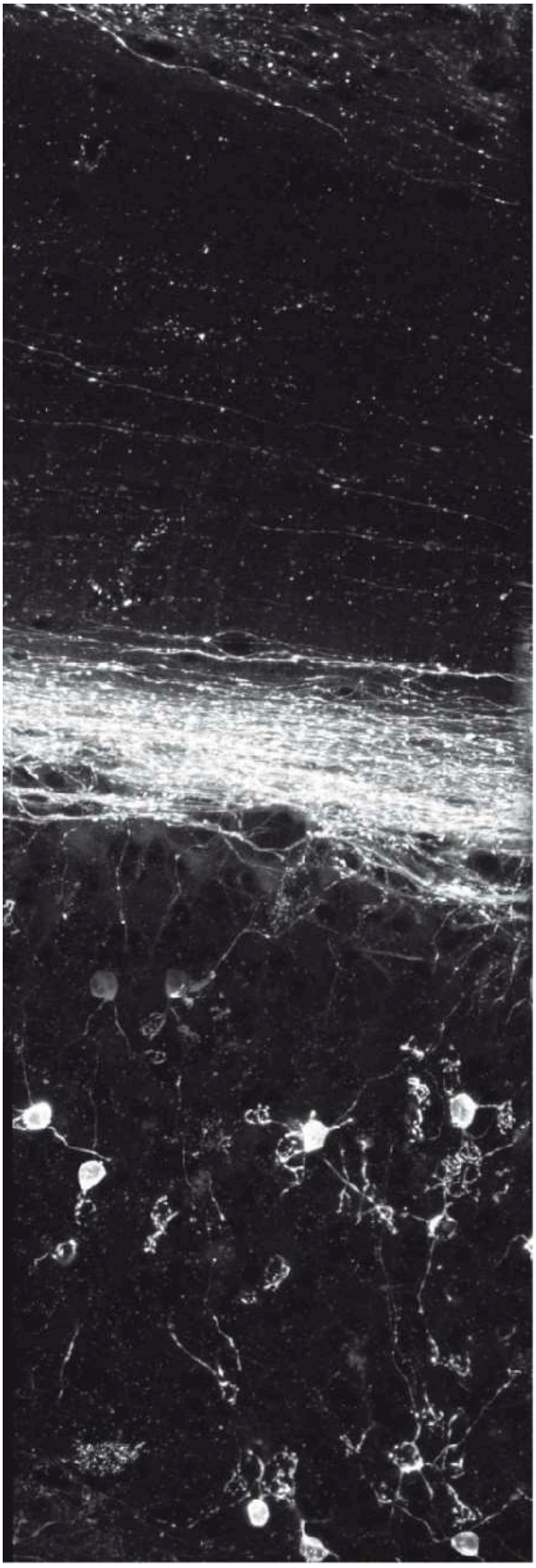

Figure 22. Cerebellar granule cells and their axonal projections in the molecular layer.
DiI injections in the molecular layer retrogradely trace granule cell projections and stains a subpopulation of isolated granule cells. Parallel fibers are organized in beams within the molecular layer. They project an ascending axon that splits, forming the parallel fibers.

This three-dimensional acquisitions under confocal microscope shows a very high density of parallel fibers within the cerebellar cortex and an important number of granule cell varicosities per granule cell axon.

(E.Savier, K.Dorgans. 2015 - Unpublished)

4.2 Short term synaptic plasticity at granule cell synapses

4.2.1 Facilitation of glutamate release at granule cell synaptic terminals

Granule cell terminals are facilitating synapses which are very well suited for sensory-like information transfer at high frequencies (Valera, Doussau, Poulain, Barbour, & Isope, 2012). Synaptic facilitation can be assessed by repetitive stimulation of parallel fibers. Paired stimuli of parallel fiber synaptic terminals show an enhancement of neurotransmitter release at the second pulse and the mechanisms of this facilitation have been extensively explored (Atluri & Regehr, 1996; Isope & Barbour, 2002; Jackman & Regehr, 2017; Zucker & Regehr, 2002). Facilitation highly depends on the time window separating two stimuli and high-frequencies tend to enhance glutamate release at the second pulse. Hence, granule cell synaptic terminals high-pass information transfer towards the various post-synaptic targets in the molecular layer. At the synaptic level, relevant sensory-like stimuli are enhanced while background noise of neuronal activity is by-passed.

Several mechanisms have been proposed to explain synaptic facilitation. 1) The regulation of presynaptic calcium influx affects short term plasticities (Jackman & Regehr, 2017), and also 2) an adaptation of vesicular pools to high-frequency modes of release (Miki et al., 2016). In one or another hypothesis, the nature of presynaptic proteins composing one given terminal will determine its functional specifications. Indeed, we will see in the following section that specific presynaptic proteins provide molecular mechanisms of ultra-fast neurotransmission. The small glutamatergic granule cell boutons are very well equipped with such mechanisms.

4.2.2 Short term facilitation and presynaptic calcium influx

Contribution of multiple calcium channels in glutamate release

Multiple calcium channels are known to contribute altogether to evoked vesicular release at granule cell synaptic terminals. Among the large panel of voltage-gated calcium channels, mostly N, P/Q and R types are involved in presynaptic vesicular release which is also the case at granule cell synaptic terminal (Mintz, Sabatini, & Regehr, 1995). P/Q channels are known to interact with a large variety of presynaptic proteins such as SynapsinII, RIM1α and form molecular clusters at vesicle release sites (Kaeser et al., 2011; Medrihan et al., 2013; Schmidt et al., 2013).

Using specific channel blockers (ω-agatoxin-IVA), early studies have shown than P/Q type channels ($Ca_V2.1$) contribute at more than 90 % to synchronous vesicular release while N-Type calcium channels ($Ca_V2.2$) less than 10 % (Mintz et al., 1995) However, both P/Q and N-type contribute to 50 % of presynaptic calcium influx. Hence, P/Q inward currents are specifically dedicated to synchronous vesicular release and contribute to the high neurotransmitter release probability of granule cell terminals.

Highly reliable calcium signaling at parallel fiber boutons

Calcium channels are positioned at very short distances from synaptic vesicles at the active zone (Kulik et al., 2004). There is a tight coupling between P/Q calcium channels and synaptic vesicles on nanoscale ranges (30~50nm) which optimizes excitation-secretion-fusion coupling (Ishiyama, Schmidt, Cooper, Brose, & Eilers, 2014; Schmidt et al., 2013). Upon spike-induced synaptic depolarization, voltage gated calcium channels open and calcium flows in nanodomains within the active zone (Eggermann, Bucurenciu, Goswami, & Jonas, 2012). Calcium inward transients are detected by vesicular calcium sensors, synaptotagmin that trigger vesicular release for a fraction of readily releasable vesicles (docked and primed vesicles). Calcium signals are sharpened and stabilized by the endogenous buffer Calretinin (Bastianelli, 2003; Schmidt et al., 2013). The combination of all of these features produces a highly-reliable calcium signal at *en-passant* terminals.

More importantly, signal intensity is also reproducible during high-frequency repetitive activation (more than 300 Hz) of synaptic terminals which corresponds to multisensory-like activity of granule cells. At these frequencies, calcium dyes sum linearly during calcium imaging assays (Brenowitz & Regehr, 2007; Miki et al., 2016; Zhang & Linden, 2009).

In conclusion : 1) calcium signaling is stable over time so that it doesn't limit vesicular release, 2) calcium signaling reliably follows granule cell firing pattern over a wide range of frequencies.

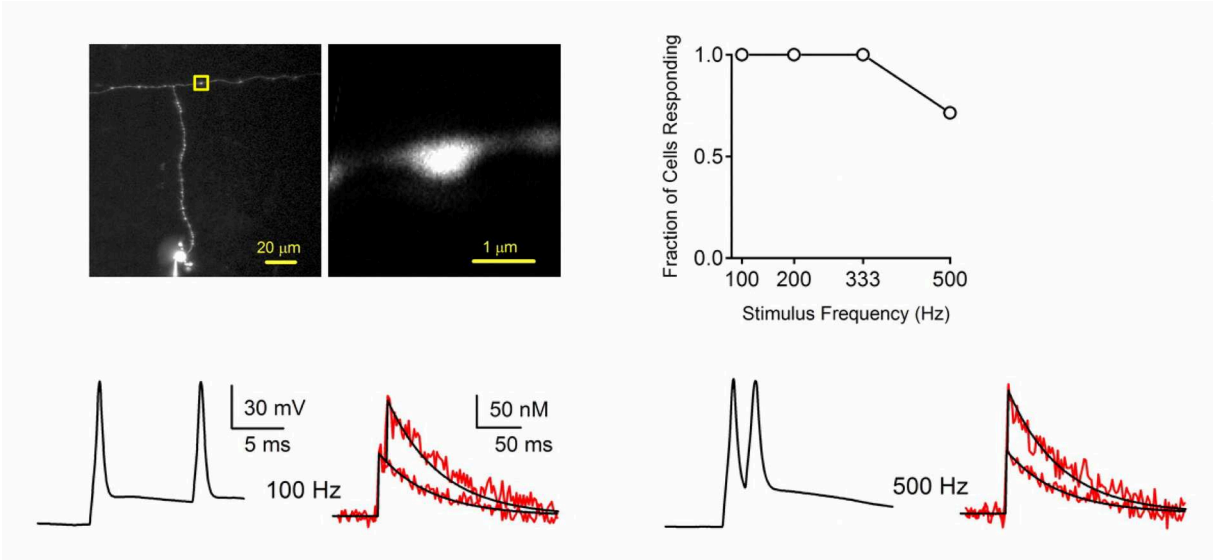

Figure 23. Reliability of calcium signaling within single granule cell axon varicosity.
Ratiometric calcium imaging (using Fluo-5F) during high-frequency stimulation of single granule cells. Repetitive activation of granule cells induce a reliable calcium response at individual terminals over a wide range of high frequencies (>100Hz) (Brenowitz & Regehr, 2007). Calcium signals responds to direct fiber excitation and follows a linear summation when the terminals are repeatedly stimulated.

« Superpriming » of release-ready vesicles

The spatial localization of calcium channels inside the presynapse is crucial to understand links between short term facilitation and channel subtype. N-type channels are positioned distally from release sites at the Calyx of Held terminals (more than 100nm) (Wu, Westenbroek, Borst, Catterall, & Sakmann, 1999). Indeed, P/Q channel are tightly clustered at vesicular release sites inside the active zone of granule cell boutons (Kulik et al., 2004).

Using the exogenous calcium buffer EGTA-AM and specific toxin blockers for calcium channels (Shin'ichiro Satake & Imoto, 2014), Satake & al suspect the collaboration of two different P/Q channels-vesicles associations at the granule cell-to-molecular layer interneuron synapse : 1) a subset of tightly coupled P/Q channels contribute to synchronous multivesicular release 2) the rest of P/Q channels exclusively contribute to glutamate release facilitation because they are positioned more distally from release sites. Interestingly, distal N-type calcium channels are involved in both synchronous and asynchronous release facilitation which shapes the decay of evoked currents.

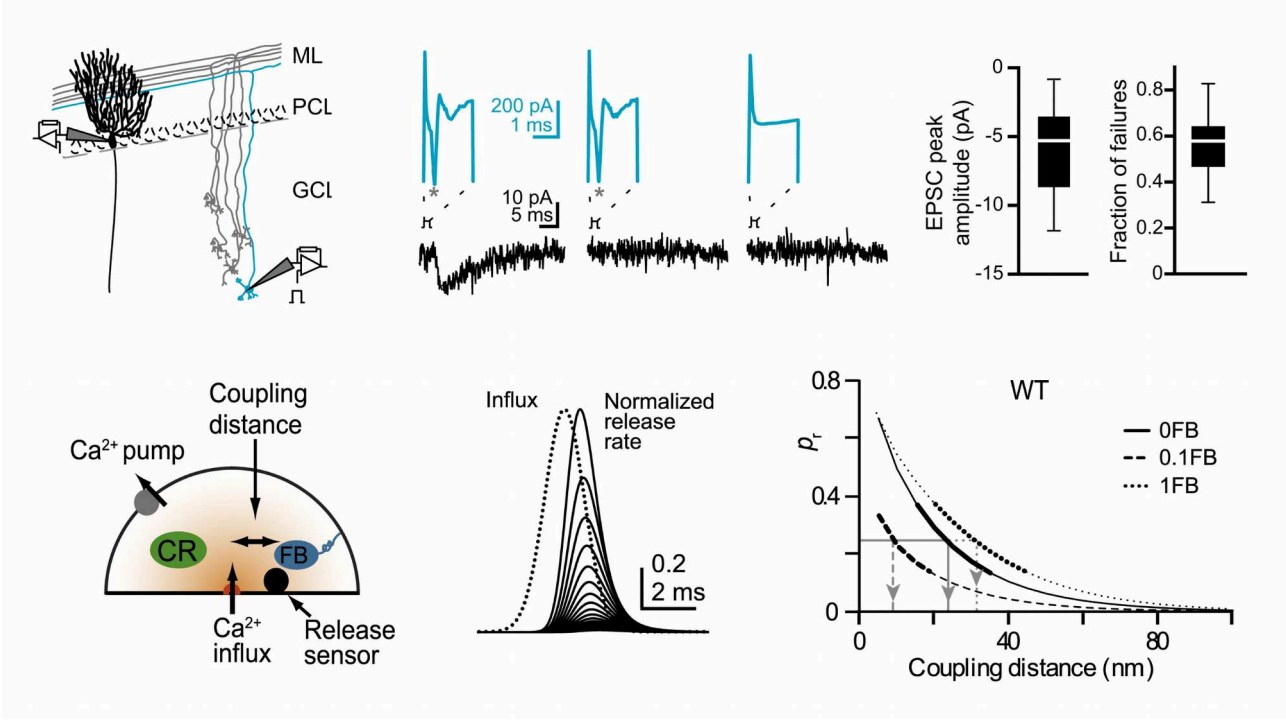

Figure 24. Nanodomain coupling between presynaptic release-ready vesicles and presynaptic calcium channels at granule cell presynaptic terminals.
Top - Pairs of synaptic connections between cerebellar granule cells and Purkinje cells were used to determine the release properties of single presynaptic contacts. The presynaptic patch controls granule cell excitability while the post-synaptic cell is voltage-clamped. Such a configuration enables a precise calculation of the proportion of neurotransmission failures following pre-synaptic excitation. Release probability is deduced from the fraction of failures.
Bottom - Mathematical models show a correlation between the neurotransmitter release rate and vesicle-channel coupling. This model takes in account the category of calcium buffers (here, Calretinin, CR), the distance between the calium sensor and the calcium channel, the kinetics of calcium clearance. At the estimated physiological release probability of single contacts, the vesicle-channel coupling distance is less than 40nm (Schmidt et al., 2013).

Thus, proximity between P/Q type channels and calcium sensors increase release probability (also called « superpriming » or sometimes « positional priming ») and is a keystone parameter for synchronous multivesicular release regulation at granule cell presynaptic terminals (Shin'ichiro Satake & Imoto, 2014; Shin'Ichiro Satake, Inoue, & Imoto, 2016). *Tight* vesicle-channel links will increase the probability of release at the first pulse and decrease short term facilitation. At the opposite, *loose* configurations will decrease release probability and enhance release facilitation during repetitive activation.

A mix of *tight* and *loose* configurations at granule cell synaptic terminals provides both a high release probability and short term facilitation which make these synapses well suited for high frequency information transfer.

Regulation of « superpiming »

Vesicle-channel distances shape short term synaptic plasticities and several synapse-specific molecules enriched in the active zone contribute in regulating *« superpriming »*. At granule cell synaptic terminals, RIM and RIM-BP proteins are also interactors for P/Q channels and clusterize vesicles and calcium channels altogether at the active zones through PDZ domains (Kaeser et al., 2011). Another protein isoform, Munc13-3, is involved in protein-protein interactions at the active zone and its expression enhances glutamate release probability at granule cell-to-basket cell synaptic terminals (Ishiyama et al., 2014). Munc13-3 tightens the distance between readily releasable vesicles and calcium channels down to 10~15nm.

In conclusion, some synapse-specific proteins are dedicated to « superpriming » by modifying the physical conformation of release sites. Some of them are also sensitive to presynaptic activity through phosphorylation cascades. This is the case of SynapsinII that binds P/Q calcium channels and constraints vesicles at release sites (Medrihan et al., 2013).

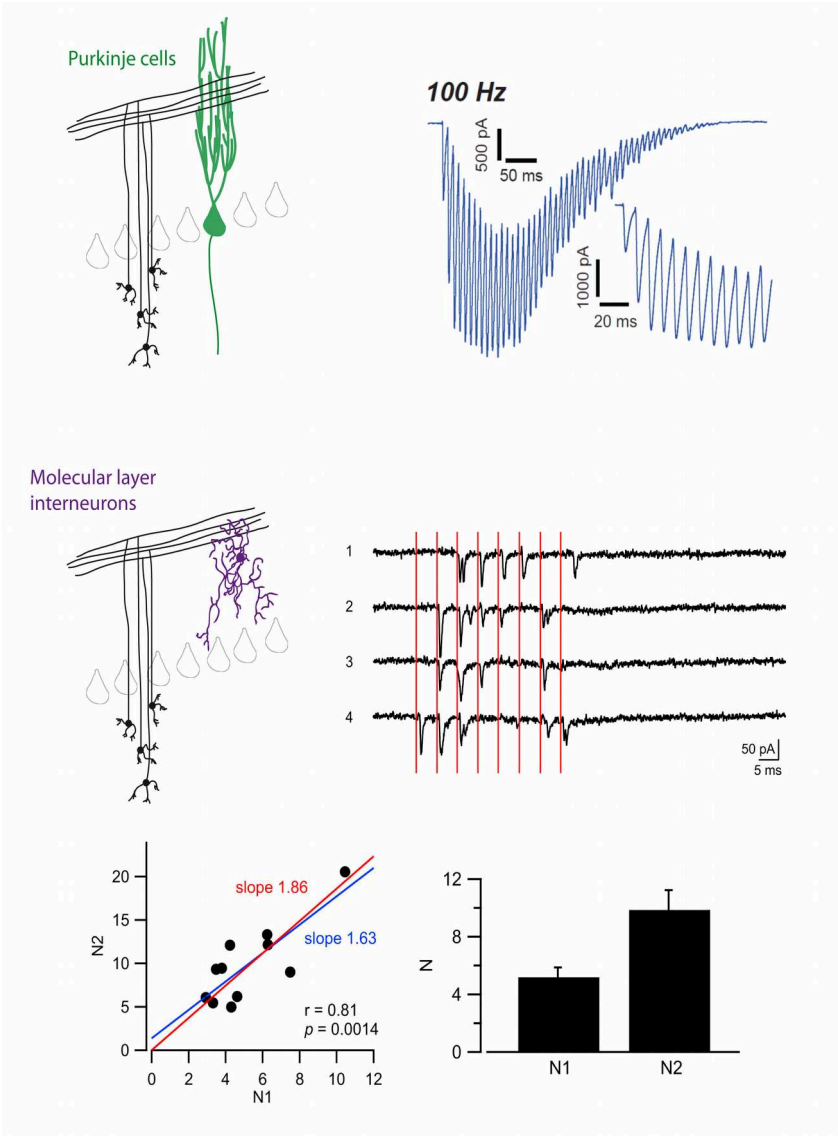

Figure 25. Facilitation of glutamate release at granule cell presynaptic terminals during high-frequency activity.
Top - 100Hz train-stimulation of parallel fibers during PC voltage-clamp experiments produces short term facilitation of glutamate release at granule cell synaptic terminals (Doussau et al. In review). Short term facilitation of glutamate release is sustained during more than 10 pulses.
Bottom – Synaptic facilitation of glutamate release is linked to an activity dependent increase in the number of release sites (N) at the granule cell to molecular layer interneuron synapse even contribute to paired-pulse (the N2/N1 ratio) (Miki et al., 2016).

4.2.3 Two populations of vesicles contribute in synaptic facilitation

Adaptation to high-frequency glutamate release

Granule cell synaptic terminals produce multivesicular release (Foster, Crowley, & Regehr, 2005; Shin'Ichiro Satake et al., 2016) with a very high release probability (Schmidt et al., 2013; Valera et al., 2012) but very few RRP vesicles are physically docked/primed at the active zone (Matthew a Xu-Friedman & Regehr, 2004). This low number of RRP vesicles is not limiting because these synapses can sustain multivesicular release during high frequency evoked eEPSC bursts (Bao, Reim, & Sakaba, 2010). Understanding how these synapses can release glutamate during repetitive activity with very few vesicles available on release sites is a major issue in the team.

Indeed, granule cell terminals can enhance the number of release-ready vesicles during repetitive stimuli and in a frequency dependent manner (Brachtendorf, Eilers, & Schmidt, 2015; Valera et al., 2012). Using various calcium concentrations for variance fluctuation analysis, previous works from the team have shown that high-frequency stimuli (more than 20Hz) recruits supplementary (*N*) vesicles for release (Valera et al., 2012). This phenomenon is well explained by a two-pool vesicle models (Pan & Zucker, 2009) and has been demonstrated in granule cell to interneuron synapses (Miki et al., 2016) where an acto-myosin dependent *replacement pool* of synaptic vesicles contributes in the fast replenishment of docking sites during activity. During my PhD, we assessed the presence of a *reluctant* population of synaptic vesicles (that may be equivalent to the *replacement pool*). This population is exclusively used during high frequency stimuli, high-passing information transfer at granule cell terminals.

Contribution of vesicular tethering in ultra-fast neurotransmission

Vesicular « tethers » such as Bassoon provide an efficient way to prevent synapses from vesicular depletion during prolonged or high frequency activity (Hallermann & Silver, 2013). Sustaining prolonged activity with molecular tethers is a common feature of sensory Ribbon synapses (in bipolar neurons from retina for example) which contain chain-like arrangements of synaptic vesicles that speed vesicle replenishment of release sites.

Synaptic terminals of cultured hippocampal neurons are depressing synapses at frequencies above 10Hz. At these terminals, a double genetic deletion of Bassoon and Piccolo didn't have any effect on basal transmission or train stimuli at 10Hz (Mukherjee et al., 2010). In contrast, cerebellar mossy fiber that sustain neurotransmission at high frequencies (over 100Hz), the deletion of Bassoon affected the replenishment of RRP and neurotransmission sustainability during train stimuli (Hallermann et al., 2010).

Active replenishment of RRP by tethering is suspected to be an active calcium process, and could explain the contribution of supplementary (*N*) vesicles during high-frequency glutamate release at granule cell terminals (Valera et al., 2012). Tethering could be one mechanisms used by synapses from sensory systems to optimize information transfer at very high frequencies, by bringing synaptic vesicles close to calcium channels (Hallermann & Silver, 2013).

Other proteins are also involved in tethering synaptic vesicles at the active zone such as actin, myosin and Synapsins (Shupliakov & Brodin, 2010). Actin and myosin contribute in forming a so-called *replacement pool* inside a two-step model at granule cell-to-molecular layer interneuron terminals (Miki et al., 2016).

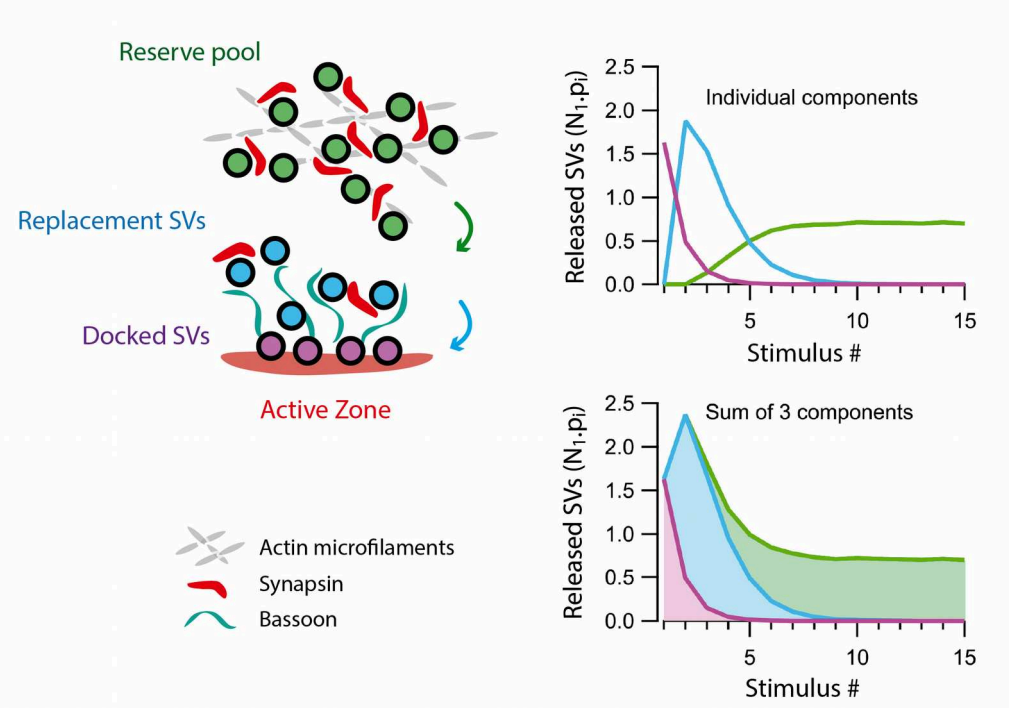

Figure 26. A two-pool model explains presynaptic facilitation of glutamate release at granule cell terminals.
Left – Illustration of the different populations of synaptic vesicles within a granule cell presynaptic terminals contributing to glutamate release during repetitive high-frequency activity. Docked synaptic vesicles (Purple) are in the vicinity from release sites, while replacement vesicles (aka. Reluctant synaptic vesicles. Blue) are tethered around the active zone. Finally, the reserve population of synaptic vesicles (Green) is located at higher distances from the release sites inside the presynaptic volume. The replenishment of the two populations is sequential (arrows).
Some molecules that hypothetically contribute in the maintenance of reluctant populations are also represented (Actin, Synapsins, Bassoon)

Right - Contribution of the three populations of synaptic vesicles into glutamate release at granule cell terminals. The replacement pool of synaptic vesicles operates immediately at the second stimulus while the reserve pool contributes in the steady-state of neurotransmitter release.

Part 5. Heterogeneity of glutamate release at granule cell terminals

5.1 Variability within cerebellar networks

The incredible ability of the cerebellar system to compute sensory information, generate motor command and provide feedback adjustments during limb movements would certainly be impossible without non-linearities and heterogeneities which are also inherent to many other neuronal networks (Chabrol, Arenz, Wiechert, Margrie, & DiGregorio, 2015; Jelitai, Puggioni, Ishikawa, Rinaldi, & Duguid, 2016; Tran-Van-Minh, Abrahamsson, Cathala, & DiGregorio, 2016). Despite their highly conserved architectures between individuals, neuronal ensembles display massive sources of variability; down to the subcellular, molecular, and biochemical level. Studying variability at multiple scales is crucial to understand how a given network computes information to achieve its physiological role. The cerebellar cortex is the perfect example to illustrate how variability and non-linearity can influence information treatment at different levels. For example, we have seen that :

i) At the network level, synaptic plasticities of the mossy fiber-to-granule cell synaptic contacts are heterogeneous and depend on the nucleus origin of mossy fibers (Chabrol et al., 2015). Such a heterogeneity has dramatic consequences on network computation. Here, the integration of sensorimotor mossy fiber inputs in granule cells is non-linear because appropriate combinations of input activation induce specific granule cell firing motifs.

ii) At the neuronal level, computation of both electric signal and calcium signal by molecular layer interneurons is non-linear (Abrahamsson, Cathala, Matsui, Shigemoto, & DiGregorio, 2012; Tran-Van-Minh et al., 2016). This non-linear computation has dramatic effects on spatiotemporal integration of granule cell excitatory inputs during physiological activity.

iii) At the synaptic level, heterogeneous populations of vesicles at granule cell presynaptic terminals help to sustain glutamate release during very high frequencies of stimulation (>20Hz) (Chamberland & Tóth, 2016; Valera, Doussau, Poulain, Barbour, & Isope, 2012). In the team, we have shown that two populations of vesicles heterogeneously contribute to neurotransmission depending on stimulation frequency. Low frequency stimuli (2Hz) depress synaptic transmission in a *band-stop* manner while high frequency stimuli (>20Hz) enhance glutamate release by recruiting a reluctant pool of vesicles that *high-passes* neurotransmission.

Granule cells use very complex mechanisms to sustain the transfer of relevant information and attenuate noisy background. However, the heterogeneity of short term plasticities at granule cell terminals is poorly depicted in literature. Are all the granule cell presynaptic terminals functionally equivalent ?

During compound experiments at the granule cell to Purkinje cell synapses, I analyzed glutamate release during *low frequency depression* protocols and high frequency bursts. Frequency stimulation of beams of parallel fibers showed an impressive functional variability during synaptic plasticity experiments. Two different protocols showed impressive inter-synaptic variability with a strong reproducibility between trials. These experiments were at the starting point of my PhD and helped me to build working hypothesis :

i) Is variability in short term plasticity expressed at the unitary synapse level ?
ii) What are the molecular mechanisms supporting inter-synaptic heterogeneity ?

5.2 Heterogeneity of functional dynamics at granule cell synaptic terminals

Previous works described inter-synaptic variations of functional dynamics within the population of granule synaptic boutons. Taking the example of granule-cell to Purkinje cell presynaptic plasticity we can note that *paired-pulse* ratios vary a lot from one preparation to another (Sims & Hartell, 2005; Valera et al., 2012) but the interpretation of such a variability remains unclear:
Is is the consequence of slight differences in experimental paradigms (calcium concentrations, stimulation protocols, buffer composition), or the consequence of internal variability of presynaptic dynamics?

Some studies have characterized inter-synaptic variations in functional properties of granule cell presynaptic terminals. This is the case with the probability of neurotransmitter release (Sims & Hartell, 2006), multivesicular release (Malagon, Miki, Llano, Neher, & Marty, 2016; Miki et al., 2016; Nahir & Jahr, 2013; Satake, Inoue, & Imoto, 2016) and also sustainability of neurotransmitter release during repetitive activity (Bao, Reim, & Sakaba, 2010) which underlie a possible inter-synaptic diversity in neurotransmitter release machinery.

Taken altogether, heterogeneous morphology, ultrastructure, molecular composition and functional properties of these terminals account for the diversification of short term synaptic plasticity dynamics of one population of synapses.

In the next part, I will cite two potential origins of presynaptic functional heterogeneity at granule cell terminals as they have been described in literature:

i) *Wired-heterogeneity:* The nature of the synaptic terminal and is role in the network underlie potential correlations between network architecture and synaptic plasticity. In the presynaptic point of view it can be the position of the terminal on the axonal segment of the granule cell. And in a postsynaptic point of view : functional dynamics can be associated to the nature of the post-synaptic neuron in a « target-dependant » organization that has also been observed in neocortical and hippocampal networks.

ii) *Metaplasticity:* Experience and development can shape the functional dynamics of presynaptic terminals through trans-synaptic signaling and a pre-post crosstalk. The information flow through the cerebellar network might shape synaptic plasticities of granule cell terminals depending on long term synaptic plasticity processes and affect both molecular, ultrastructural and functional properties of presynaptic terminals. Network adaptation and modulation following incoming stimuli may be part of active learning processes in cerebellar cortex.

5.3 ***Wired*** **heterogeneity**

5.3.1 Ascending axon versus *en-passant* terminals

In-vitro studies have described variations in functional and morphological features between distinct synaptic boutons from the same granule cell population. Ascending axon terminals are larger than parallel fiber synapses with an elevated vesicular density (Gundappa-Sulur, De Schutter, & Bower, 1999; Pichitpornchai, Rawson, & Rees, 1994) and connect onto different Purkinje cell post-synaptic compartments. Sims & al have characterized a lack of susceptibility to long term plasticity protocols, including potentiation and depression protocols, at ascending axon terminals (Sims & Hartell, 2005, 2006). Those variations are due to the difference in size of post-synaptic compartments. Induction protocols are possible at *en-passant* synapses because a great majority of them are connected to large dendrites enabling endocannabinoïd retrograde signaling through synaptic crosstalk (Marcaggi & Attwell, 2005, 2007). On the contrary, large ascending axon synapses are resistant to induction protocols because of the important scattering of their synaptic contacts onto small Purkinje cell dendrites.

The scattering of synaptic contact will dramatically affect their sensitivity to long term modulations. Spatially dispersed contacts on the same Purkinje cell dendrite limits the ability to induce retrograde modulations unlike condensed inputs. This attests of an inter-dependence between network architecture and long term modulations at granule cell terminals.

The nature of short term plasticities at granule cell terminals can be linked to network connectivity. In the same paper, Sims & Hartell have shown a higher neurotransmitter release probability at ascending axon presynaptic terminals. This stronger synaptic weight at granule-cell to Purkinje cell connections on a very specific anatomical component (the ascending axon) illustrates inter-synaptic differences inside the same population of granule cell buttons. In this example the authors describe a form of « hard wired » functional heterogeneity. Short term plasticities can pre-determined in some cases by the position of synaptic boutons on the axonal segment.

5.3.2 Target-dependant short term plasticity

Following bursts of high frequency stimuli (>50Hz), granule cell synaptic terminals endow various glutamate release behaviors. They can either sustain glutamate release over several stimulus, or follow a pronounced depression. Using *in-vitro* compound stimuli, Bao & al. have shown a link between the short term plasticity of granule cell inputs and the nature of their post synaptic targets (Bao et al., 2010). Termed as a « target-dependent plasticity », the authors describe a sustained glutamate release behavior onto Purkinje neurons and stellate interneurons that is opposed to a depressing release mode when the post-synaptic

target is a basket interneuron. Such a target dependent organization would provide a tonic inhibition of Purkinje dendrites by stellate cells while the strong somatic inhibition provided by basket cells would be phasic during sensory integration.

In addition, there is a loss of short term depression at the granule cell-to-basket cell synaptic terminal in the knockout mouse model for Munc13-3 showing that a synapse-specific expression of a presynaptic protein can shape information processing at the network level. Here, a synape-specific expression of Munc13-3 at granule cell-to-basket cell synaptic terminals would set synaptic depression during high-frequency release activity.

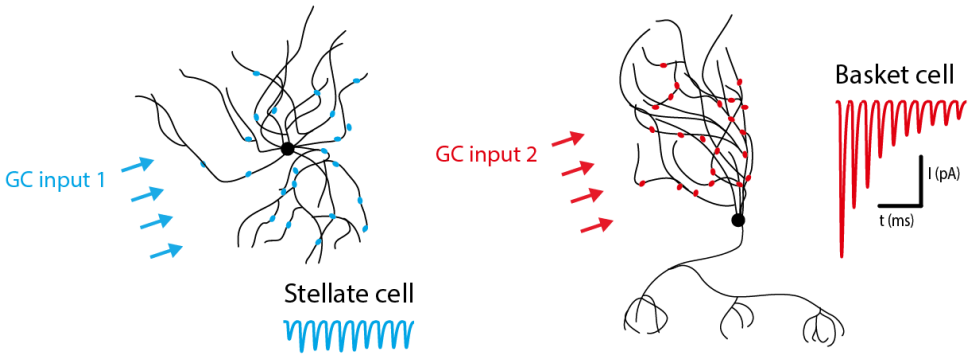

Figure 27. Target-dependence of short term plasticity of granule cell inputs
For now, the model for functional organization of granule cell presynaptic inputs is target-dependence, meaning that the nature of the post-synaptic neuron (Basket cell, stellate cell or Purkinje cell) will determine the functional property of its synaptic inputs (Bao et al., 2010). In this idea, all of the inputs contacting a stellate cell are facilitating and sustain glutamate release will the inputs contacting basket cells are more phasic.

In conclusion, functional connectivity in cerebellar networks can be *hard-wired*. However, in the cerebellum as in other brain structures, short term plasticity is not only synapse-specific but also depends on active learning rules where environmental stimuli can induce long-standing changes in presynaptic specialization (Blackman, Abrahamsson, Costa, Lalanne, & Sjöström, 2013).

The predominance of *target-dependent* models as the main organization mode for many different networks suggests that post-synaptic neurons influence pre-synaptic terminals. A pre/post cross-talk might influence presynaptic dynamics through a fine tuned regulation of glutamate release parameters as it has been observed in neocortical and hippocampal areas (H J Koester & Sakmann, 2000; Helmut J Koester & Johnston, 2005; Rozov, Burnashev, Sakmann, & Neher, 2001; Watanabe, Rozov, & Wollmuth, 2005).

5.4 Acquired heterogeneity

5.4.1 Metaplasticity

Prior studies describe important fluctuations of presynaptic properties at the unitary synapse level. *In-vitro* 2-Photon imaging studies of presynaptic calcium dynamics shows important heterogeneities between *en-passant* buttons from a same granule cell (Brenowitz & Regehr, 2007) while electron microscopy coupled to electrophysiology describe inter-synaptic variations in the number of release sites (Miki et al., 2017) with no pre-determined scheme for synaptic organization.

In parallel, some studies show that individual presynaptic boutons are not equipped with the same receptors. Zhang and Linden show differences in pre-synaptic sensitivity to adenosine and endocannabinoïd signaling from one *en-passant* synapse to another (Zhang & Linden, 2009, 2012b). Presynaptic A1 (for adenosine) and CB1 (for endocannabinoïds) are both coupled to Gq proteins, their activation reduces calcium influx diminishing glutamate release. There is a presynaptic heterogeneity in the sensitivity to several neuromodulators which is correlated with the varicosity size (stated as a time-variant parameter) but not with their identity inside the network (no link with *en passant* versus ascending terminals and no dependence with the target neuron). This means that some terminals will be sensitive to long term modulations while others won't. Similarly, NMDA presynaptic receptors are not expressed at all the presynaptic receptors, even onto the same parallel fiber (Bouvier et al., 2016).

Here, the authors introduce the concept of *metaplasticity* at granule cell terminals (Zhang & Linden, 2012a). This broad vision of synaptic plasticity takes into account morphology, ultrastructure, functioning and sensitivity to various neuromodulators. Synaptic terminals are subject to permanent dynamic interactions in such a way that the history of one given terminal will affect its future functional properties. Populations of presynaptic terminals from the same neuronal subtypes are not homogeneous because they have experienced different presynaptic input firing patterns and different local neuromodulation processes (Goussakov, Fink, Elger, & Beck, 2000; Hunter & Milton, 2001).

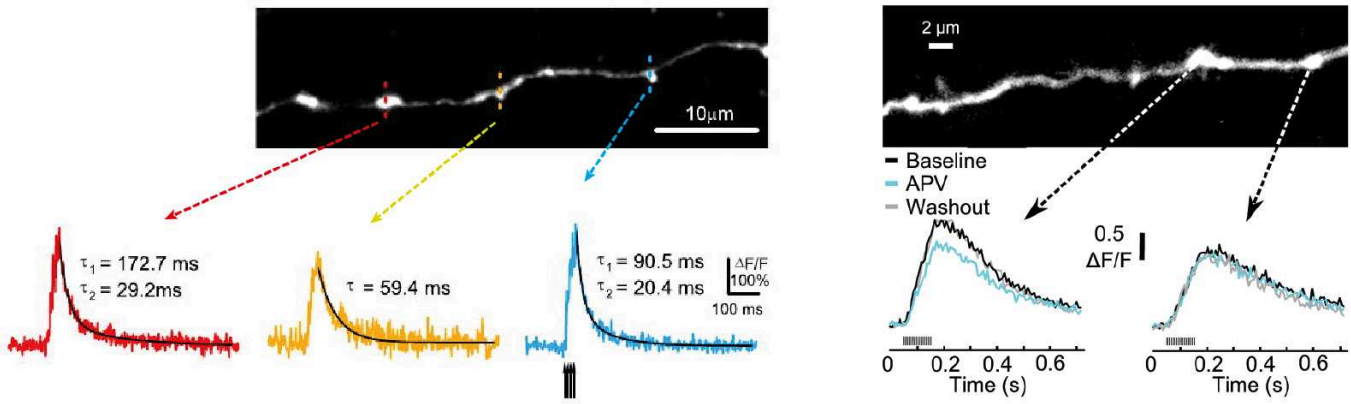

Figure 28. Inter-synaptic variability of granule cell presynaptic boutons.
In these two different studies, individual presynaptic boutons of the same parallel fiber express different presynaptic properties. Granule cells are patched and filled with a calcium dye and a constitutive dye for calcium imaging. Unitary varicosities are visualized under 2-Photon microscope.
Left – Different calcium transients (amplitude and kinetics) evoked by action-potential stimulation at individual parallel fibers underlie inter-synaptic differences in calcium regulation between neighboring presynaptic boutons (Zhang & Linden, 2012a).
Right – Differences in sensitivity to the NMDA receptor blocker APV between two neighboring presynaptic boutons. Individual synapses do not present the same molecular equipment (Bouvier et al., 2016).

Indeed, signal integration at the granule cell to interneuron synaptic terminal is compartmentalized and some forms of long term plasticities can alter neurotransmitter release behaviors with a strong spatial discrimination. Thus, presynaptic parameters can be deferentially modulated between terminals contacting a same neuron (Soler-Llavina & Sabatini, 2006). Burst stimulations (25×30Hz) of single terminals will induce a presynaptic depression of glutamate release by an endocannabinoïd retrograde mechanism that relies on postsynaptic calcium influx (Soler-Llavina & Sabatini, 2006). The spatial restriction of calcium influx inside molecular layer interneurons bypasses heterosynaptic plasticity. In that way, only synapses that have experienced a bursting behavior will undergo depression.

ARTICLE I

Ultrastructural, molecular and functional heterogeneities of cerebellar granule cell presynaptic terminals.

This article contains the core results of my PhD. Initially, the goal was to link a presynaptic function with molecular elements of the presynaptic machinery. However, it appeared quickly that granule cell terminals displayed very different forms of short term behaviours and this inter-synaptic heterogeneity became a topic of interest.

Provided the insights in presynaptic heterogeneity of neurotransmitter release at granule cell terminals, I suspected that short term plasticities are not stereotyped but vary in a dynamical range within the whole population of granule cell synaptic terminals. This dynamical range relies onto the molecular particularities of the network. Thus, the resulting readout of neurotransmitter secretion during bursting activity is susceptible to change with time and experience generating a contrasted patchwork of short term dynamics at a given moment in time (Brenowitz & Regehr, 2007).

During my PhD, I characterized a wide range of short term dynamics at the granule cell-to-molecular layer interneuron synaptic terminal during *in-vitro* train stimulation protocols. By blocking all forms of trans-synaptic long-term plasticities (with antagonists for endocannabinoïds, metabotropic receptors of glutamate, $GABA_B$ receptors and NMDA blocker), I was able to « freeze » long term pre-synaptic plasticities. In that way, synapses were maintained in their current dynamical steady-state and with no long term modulations by high-frequency stimulation protocols.

As we have seen before, short term presynaptic plasticity is the readout of very complex molecular interaction that shape the ultrastructure and the function of presynaptic terminals. Synapsins are good candidates for presynaptic heterogeneity: I used a Knockout model for SynapsinII in order to investigate the physiological relevance of presynaptic diversity of granule cell presynaptic terminals in three different aspects : ultrastructural, molecular and functional.

Studying unitary synapses – The most important issue while working onto unitary GC-MLI presynaptic terminals is to find a pair of synaptically connected neurons. Pairing methods were developed at GC-BC (Ishiyama, Schmidt, Cooper, Brose, & Eilers, 2014; Schmidt et al., 2013) and GC-PC (Isope & Barbour, 2002). Unfortunately, these time-consuming techniques have low throughput and their success rate is worse when the post-synaptic neuron receives a lower number of synaptic contacts; this is the case with pairs of GC-MLI connections. Indeed, these methods tend to work better when the neurons are close one from another. By puffing glutamate into the granule cell layer, it is possible to find pairs of connected GC-BC neurons (Schmidt et al., 2013). However, such a technique is most of the time limited to GCs in the upper GC layer and MLI in the lower part of molecular layer (BCs). This configuration restricts the category of recorded synaptic terminals; mostly local contacts from ascending axons onto deep MLI only.

Because I was interested in inter-synaptic heterogeneity my priority concern was to maximize the subtype of recorded synapses.

Regarding the literature, some external parameters could be associated to particular short term presynaptic plasticity behaviours:

1) The position of postsynaptic MLI into the depth of molecular layer.

2) The position of the presynaptic contact (parallel fiber) into the depth of the molecular layer.

3) The distance between the presynaptic cell and the post synaptic interneuron (aka. The position of the presynaptic bouton on the parallel fiber).

4) The relationship between the position of pre and postsynaptic neurons and the zebrin patterns.

For each connection, I associated at least, parameters 1-2 and 3 when possible. Due to technical issues, I didn't take in account parameter 4.

Methods - In order to study a large variey of unitary GC s-MLI synapses, I used two different techniques:

1) I uncaged glutamate onto very small patches of GC layer in horizontal slice configuration to conserve the integrity of parallel fibers.

2) I also used the minimal configuration onto sagittal slices in order to locally evoke glutamate release assisted by 2Photon microscopy.

In both techniques, GC presynaptic terminals were stimulated at high frequencies (≥100Hz)

Principal Component Analysis - I chose multivariate statistical techniques to analyse short term plasticity data because it allowed me to take in account the whole time-course of evoked release dynamics. Principal Component Analysis (PCA) is a robust tool used for multidimensional dataset analysis and data mining. Most of my analyses use PCA transformation because it is a reliable way to represent complex datasets by minimizing data loss (that happens during fitting or averaging for example).

Article 1. *"Ultrastructural molecular and functional heterogeneities of granule cell presynaptic terminals"*

Ultrastructural, molecular and functional heterogeneities of cerebellar granule cell presynaptic terminals

Kevin Dorgans[1], Valérie Demais[2], Yannick Bailly[1,2], Bernard Poulain[1], Philippe Isope[1] and Frédéric Doussau[1].

[1] Institut des Neurosciences Cellulaires et Intégratives, CNRS UPR 3212, Université de Strasbourg, 67084 Strasbourg, France

[2] Plateforme Imagerie in vitro, CNRS UPS 3156, 67084 Strasbourg, France

INTRODUCTION

In neural network, feedback or feedforward inhibition exerts powerful control over the timing and frequency firing of principal cell and to understand how information is processed in these circuits it is fundamental to decipher the rules governing spike output tuning of inhibitory interneurons. Because interneurons are small cells with high input resistance, they can fire in response to quantal event (Carter & Regehr, 2002) originating from unitary excitatory inputs. Consequently, during repetitive activities, presynaptic short-term plasticity (STP) at single synapse sculpts the firing pattern of interneurons. Since numerous studies have shown that the profile of presynaptic short-term plasticity is synapse specific, it is important to describe the behaviour of neurotransmitter release at unitary level in the context of local circuit. Here we studied how heterogeneous forms of STP at unitary excitatory inputs shape the spike output pattern of cerebellar molecular layer interneuron.

In the cerebellum, granule cell (GCs), the most numerous cells in central nervous system, contact inhibitory molecular layer interneurons (MLIs) and Purkinje cells (PCs), considered as principal cell as they constitute the sole output of the cerebellar cortex. GCs have a T-shape axon that ascents to the molecular layer and then bifurcates to form a parallel fiber (PF) that runs for several millimetres along cerebellar folia. In the cerebellar cortex, GCs represent the first stage for computation of incoming sensorimotor information conveyed by mossy fibers (MF). In response to peripheral stimulations or during locomotion, GCs emit burst of action potentials (Chadderton, Margrie, & Häusser, 2004; Jörntell & Ekerot, 2006; Powell, Mathy, Duguid, & Häusser, 2015; Rancz et al., 2007) and the differential processing of these high-frequency activities by synapses involved in the direct excitatory pathway (GC-PC synapses) or in the bi-synaptic feedforward inhibition (GC-MLI synapse and MLI-PC synapses) (Atluri & Regehr, 1996; Bornschein et al., 2013; Ishiyama, Schmidt, Cooper, Brose, & Eilers, 2014; Ritzau-Jost et al., 2014; Valera, Doussau, Poulain, Barbour, & Isope,

2012) shape the output message of the cerebellar cortex carried by PCs (Jelitai, Puggioni, Ishikawa, Rinaldi, & Duguid, 2016; Mittmann, Koch, & Häusser, 2005).

Based on positional and morphological criteria, MLIs have been classified into two cell types, stellate cells (SC) and basket cells (SC) (Chan-Palay & Palay, 1972; Eccles, Llinàs, & Sasaki, 1966; Hamori, 1975). BCs could be identified following 2 criteria. First, BC somata are located in deepest part of the molecular layer and second, their axon terminals form a dense network of GABAergic synapses (the basket) surrounding the soma of a nearby PC before ending in a so-called pinceau structure that wraps the axon initial segment of PC axon. At the opposite, somas of SCs are located in the upper part of the molecular layer and their axon contact PC dendrites.

The profile of STP at PF-SC synapses and PF-BC synapses have been shown to be different during high-frequency train of stimulation of beam of PFs (Bao, Reim, & Sakaba, 2010) and such target cell-dependent STP associated with an ultra-fast ephatic inhibition exerted by the BC pinceau on PC axon (Blot & Barbour, 2014) is supposed to shape the somatodendritic excitability of PC. However, the concept of target cell–dependent STP of GC terminals is challenged by different experimental findings. First, there is a controversy over the strict segregation of MLI into SC and BC. The classification of MLI based on axonal morphology and position of the soma in the molecular layer would rather suggest that MLI represent a single population of cells that varies gradually with their position in the molecular layer. While MLI localized in the vicinity of PC layer have a tendency to form basket-like and MLI localized near the pia form dendritic connection, number of MLIs localized the middle part of the molecular layer cannot be accurately classified as BC or SC (Sotelo, 2015; Sultan & Bower, 1998). Second, functional heterogeneity of GC terminals may also relie on the position of boutons in the ascending branch or in the PF (Sims & Hartell, 2005; Zhang & Linden, 2009, 2012). Third, presynaptic calcium dynamic among individual boutons from a same GC is highly heterogeneous and respond differently to neuromodulators (agonist of CB1, A1, NMDA and mGlur4 receptors). This suggest, that besides the target cell, other parameters control STP at unitary GC synapses.

Here we showed that the response onset of a single MLI is differentially tuned by multimodal GC inputs and that input-specific behaviours of single MLI are the consequence of heterogeneities in the ultrastructure and the molecular content of GC bouton. More precisely, we demonstrated that SynapsinII, a presynaptic protein involved in synaptic vesicle trafficking, is heterogeneously expressed at GC-MLI synapses. Functional studies performed at unitary synapses shown that the presence or absence of SynapsinII determines the profile of STP and the spike output pattern at GC-MLI synapses. The convergence of functionally distinct excitatory inputs on a single MLI indicate that spatiotemporal properties of FFI and ultimately the control over PC spike output by inhibitory interneurons is highly heterogeneous and depend on the combination of multimodal inputs recruited by MF.

Article 1. *"Ultrastructural molecular and functional heterogeneities of granule cell presynaptic terminals"*

MATERIALS AND METHODS

This study was carried out in strict accordance with the national and international laws for laboratory animal welfare and experimentation and was approved by the Comité d'Ethique en Expérimentation Animale de Strasbourg CEEA35.

Slice preparation. Acute cerebellar slices were prepared from P20~P35 young adult WT or SYN2 -/- CD1 mice cerebella extracted in ice-cold (~1°C) ACSF containing 120 mM NaCl, 3 mM KCl, 26 mM NaHCO3, 1.25 mM 80 NaH2PO4, 2.5 mM CaCl2, 2 mM MgCl2, 10 mM glucose and 0.05 mM minocyclin bubbled with carbogen (95% O2, 5% CO2). Cerebella were sliced (Microm HM650V) inside an ice-cold low-sodium and zero-calcium slicing buffer containing 93 mM N-Methyl-D-Glucamine, 2.5 mM KCl, 0.5 mM CaCl2, 10 mM MgSO4, 1.2 mM NaH2PO4, 30 mM NaHCO3, 20 mM HEPES, 3 mM Na-Pyruvate, 2mM Thiourea, 5 mM Na-ascorbate, 25 mM D-Glucose and 1 mM Kynurenic acid. Slices of 300µm thick were either sagittal or horizontal depending on the experimental protocol and immediately transferred for recovery in an oxygen-saturated ACSF for 30 minutes at 34°C. Resting slices were maintained at room temperature (~25°C) until their use for experiment.

Electrophysiology. After 1H recovery at room temperature (~25°C), slices were transferred in a recording chamber continuously perfused with 32~34°C ACSF. In order to block all forms of long term synaptic plasticity and trans-synaptic mechanisms, we used blockers of $GABA_A$ (100µM picrotoxin), $GABA_B$ 10 µm CGP52432; 3-[[(3,4-Dichlorophenyl)-methyl]amino]propyl(diethoxymethyl)phosphinic acid), NMDA, (100 µM D-AP5; D-(-)-2-Amino-5-phosphonopentanoic acid) endocannabinoïd CB1 receptors (1 µM AM251 1-(2,4-Dichlorophenyl)-5-(4-iodophenyl)-4-methyl-N-(piperidin-1-yl)-1H-pyrazole-3-carboxamide) and mGluR1 receptors (2 µM JNJ16259685 (3,4-Dihydro-2H-pyrano[2,3-b]quinolin-7-yl)-(cis-4-methoxycyclohexyl)-methanone.

Moleular layer interneurons were patch-clamped (in lobules IV to VI in the cerebellar vermis) under a 2Photon microscope setup (Multiphoton Imaging System, Scientifica UK) with 10MΩ glass electrodes containing a cesium-based intra-cellular medium (140 mM CsCH3SO3, 10 mM Phosphocreatine, 10 mM HEPES, 10 mM BAPTA, 4 mM Na-ATP and 0.3 mM Na-GTP) with 50µM ATTO-594 fluorescent marker in order to visualize their dendritic arbour. In all experiments, cells were voltage-clamped at -70mV in whole cell configuration (Multiclamp 700B, Molecular Devices). Electrical stimulations were realized with a ~10MΩ monopolar electrode also filled with ATTO-594 for a very precise online adjustment of the distance between the stimulation pipette and isolated dendritic processes of molecular layer interneurons. The intensity of electric train-pulses was adjusted depending on the experiment and excitatory post-synaptic currents (eEPSCs) were evoked with a stimulator (REF STIMULATEUR) controlled by WinWCP freeware (John Dempster, Strathclyde Institute of Pharmacy and Biomedical Sciences, University of Strathclyde, UK).

Minimal configuration experiments were used to monitor short term plasticities at unitary granule cell synapses. To do so, we followed previously established procedures (Malagon, Miki, Llano, Neher, &

Marty, 2016; Miki et al., 2016). For each synapse, the intensity of electrical stimulation was maintained in an intensity window that avoided both stimulation failures and multiple-synapse stimulation (Supplementary figure 2).

Glutamate-uncaging assays were realized under a MOSAiC patterned illumination system (Andor Technologies) and coupled to patch-clamp experiments. Molecular layer interneurons were recorded in a bath containing 100µM extracellular RuBiGlutamate. In order to find connected pairs of granule-cell to molecular layer interneuron, we first used full-field arrays composed of very small photostimulation areas (15~25µm diameter) and sequentially illuminated single granule cell patches. Considering the weak connexion probability provided by such a configuration, the synaptic activity evoked by isolated granule cell bursting activity was most of the time single-synapse neurotransmitter release activity. Before patching interneurons in whole cell configuration, we used a second pipette for a loose-patch recording of firing activity during granule cell photostimulation. A *post-hoc* monitoring of photostimulation evoked EPSCs was systematically performed with Igor PRO (WaveMetrics), using the SpAcAn plugin (Dugue, 2005) http://www.spacan.net/ . We only conserved experiments where the evoked curents orginate from single synapses. When the analyzed eEPSCs displayed important kinetic variations suggesting multiple contact release, the recordings (both loose-patch and whole-cell recordings) were systematically discarded.

Prior studies described the very high sensitivity of MLI output firing pattern to unitary or simultaneous excitatory quanta (Carter & Regehr, 2002). However, the rate modulation of MLI firing activity following the activation of individual GC terminals remained unclear. In order to determine how single presynaptic inputs modulate single presynaptic neurons, we used sequential loose-patch and whole-cell patch under a photostimulation setup. This method has the advantage to keep the intracellular medium intact during MLI firing assessment We took advantage on the horizontal slice configuration to stimulate lateral GCs in a distant position from the recorded MLI.

After all experiments, we used 1µm resolution 2Photon Z-stacks to reconstruct the patched molecular layer interneurons with the *simple neurite tracer* plugin (Longair, Baker, & Armstrong, 2011) from ImageJ freeware (National Institute of Health, USA). Some neurons displayed Basket-like features such as a descending axonal process probably contacting Purkinje cells (Sultan & Bower, 1998) were qualified as *Basket-like* cells.

Electron microscopy. P20 WT and Syn2-/- mice were anaesthetized by intraperitoneal injection of Ketamine (2 ml/kg) and Xylazine (0.5 ml/kg) and fixed by transcardiac perfusion with 2,5% glutaraldehyde in phosphate buffer (PB) for ultrastructural analysis or with 0,1% glutaraldehyde and 4% paraformaldehyde in sodium phosphate buffer (PBS) for immunogold labelling. Transversal vibratome sections (75-µm thick) of fixed cerebellum were cut and processed either for ultrastructural analysis or for pre-embedding immunogold labelling.

Ultrastructural analysis. After three washes with PB, sections were postfixed (1% OsO4 in PB for 1 hour), dehydrated (ethanol at 25% for 10 min; 50% for 10 min, 70% for 10 min, 95% for 10 min and 100%for 3×10 min; propylene oxide for 3×10 min) and embedded (Araldite M: propylene oxide at 1:1 for 1 hours followed

by Araldite M for 2×2 hours at room temperature; polymerization at 60°C for 3 days). Ultrathin sections were contrasted with uranyl acetate and inspected on a transmission electron microscope.

Pre-embedding immunogold labelling. Sections were permeabilised with 0.2% saponin in PBS, rinsed in PBS and blocked in a blocking solution: 2% bovine serum albumin in PBS (PBS-BSA). The sections were incubated overnight with anti-Syn1 (1/250) or anti-Syn2 (1/100) antibodies (polyclonal, SynapticSystems) in 0.1% BSA in PBS. After washing in PBS-BSA, the sections were incubated in Ultra small nanogold F(ab') fragments of goat anti-rabbit or goat anti-mouse immunoglobulin G (IgG) (H and L chains; Aurion) diluted 1/100 in PBS-BSA. After several rinses in PBS-BSA and in PB, sections were postfixed in glutaraldehyde 2% in PB before washing in PB and distilled water. Gold particles were then silver enhanced using the R-Gent SE-EM kit (Aurion) before being washed in distilled water and PB. Finally, the sections were post-fixed in 0.5% OsO4 in PB for 10 min before classical processing for Araldite embedding (Sigma, St. Louis, MO, USA) and ultramicrotomy. The ultrathin sections were counterstained with uranyl acetate and observed with a Hitachi 7500 transmission electron microscope (Hitachi High Technologies Corporation, Tokyo, Japan) equipped with an AMT Hamamatsu digital camera (Hamamatsu Photonics, Hamamatsu City, Japan). In control sections processed without anti-Syn1 or anti-Syn2 primary antibodies or gold-labeled secondary antibod-ies, no gold particles were observed.

Analysis of electron micrographs. Images were exclusively collected from granule cell-to-molecular layer interneuron synaptic contacts (GC-MLI) thanks to ultrastructural recognition criteria. The aldehydic fixation reveals excitatory glutamatergic synapses in cerebellar molecular layer as asymmetrical synapses (Korogod, Petersen, & Knott, 2015). To differentiate GC-MLI from GC-PC excitatory terminals, we took advantage on the synapse-specific presence of mitochondrion within the post-synaptic compartment. Numerous mitochondrion are found at the MLI post-synaptic volume (Palay & Chan-Palay, 1974) while PC dendritic thorns are devoid of any mitochondrion (Liu & Shio, 2008; Palay & Chan-Palay, 1974). Electron micrographs were analysed with ImageJ freeware (National Institute of Health, USA). In order to assess vesicular distributions, we estimated the nearest distances from the centre of synaptic vesicles to the active zone cytomatrix for all synaptic vesicles contained in each GC-MLI synaptic terminals. Then we binned the number of vesicles (with 50nm distance bins) starting from the active zone cytomatrix as a reference point (0nm).

Immunohistochemistry. P20~P25 WT mice were fixed with an intracardiac perfusion of phosphate buffer saline (PBS) containing 4% paraformaldehyde (PFA). After a 3 hour post-fixation, cerebella were sliced in sagittal configuration (50µm thick). Slices were washed with series of PBS baths (3×10 minutes). Membranes were permeabilized with 0,1% TritonX100 and coated with 10% bovine serum albumin (BSA) 1% goat serum albumin (GSA) during 6 hours. Synapses were stained using the same solution containing anti-VGluT1 polyclonal antibodies diluted at 1/600 (SynapticSystems) and polyclonal pand-SynapsinI and pan-SynapsinII antibodies (SynapticSystems) diluted at 1/500. Secondary antibodies (Abcam) were applied after several washouts with PBS (4×10 minutes) during 3 hours in a solution containing 10%BSA. Slices were mounted and visualized under confocal microscope (Leica SP5, II)

Global data analysis. Analysis were performed with home-made python routines (WinPython 3.3.5, Python Software Fundation) based on custom scripts. Short term plasticity data (STP-db) was collected by extracting the charge value of each eEPSCs from 100Hz trains from 7 (or more) consecutive sweeps per synapse. This connexion presents a very high failure rate, especially at eEPSC1 so we arbitrarily detected signals above a 3 . σ_{noise} threshold where σ_{noise} is calculated on a fixed temporal window before the train stimulations. Multiplying consecutive trials (>5) onto the same terminals revealed synapse-specific envelopes of STP (Supplementary figures). Thus, we used the median eEPSC charge value for each stimulation as it reflects an embedded intra-synaptic property with an important source of inter-synaptic variability. The ultrastructural data (ULTRA-db) is gathered from electron microscopy micrographs and contains the absolute distance from each synaptic vesicle to the active zone cytomatrix.

Principal Component Analysis (PCA). PCA is a linear transformation algorithm which enables: i) a data reduction of the number of dimensions into a lower dimensional dataset composed of Principal Components. ii) a data transformation through covariance reduction. The first two Principal Components (PC1 and PC2) explain the highest variance of the original dataset. We used PCA in order to simplify STP-db and ULTRA-db sets of data and extract the most relevant inter-individual differences in the two databases. PCA were computed using the python-based *sklearn* plugin. First, input variables were normalized and centred using Vector Space Model (VSM) that linearly scales the observations (between 0 and 1, using 'l2' norm) but keeps the deviations between the different variables on single observations intact (Salton, Wong, & Yang, 1975). In the STP-db, the VSM allowed us to focus on the individual neurotransmitter release time-course and get rid of absolute eEPSC inter-synaptic differences (that could reflect post-synaptic variations in compartmental electrical properties). In the ULTRA-db, VSM allowed us to scale single-synapse vesicular repartitions to the total number of vesicles per synaptic terminal. Then, after a PCA transformation of normalized data, we plotted the first two principal components. Such a representation allows to visualize inter-synaptic differences in short term plasticities between the different synapses from the STP-db and differences in vesicular repartition between the different synapses of the ULTRA-db.

Article 1. *"Ultrastructural molecular and functional heterogeneities of granule cell presynaptic terminals"*

RESULTS

Unitary GC-MLI synapses heterogeneously drive MLI spiking output pattern

In order to evoke glutamate release at unitary GC terminals, we induced unitary GC bursting activity *in-vitro* by photostimulating very small patches in the GCL of cerebellar cortices from WT mice. We used small diameter blue light spots under a mosaic photostimulation setup (mean diameter: 28±3.9 µm) and recorded GCs in loose-patch configuration under the photostimulation zone (Supplementary Figure 1). By blocking inhibition, we could record prolonged GC bursting activity (mean number of action potentials per cell: 28±4 spikes, n=15) at high frequencies (135±19 Hz).

To characterize MLI responses to the activation of unitary GC synapses, we used the same uncaging protocols and recorded MLI in loose-patch configuration from horizontal slices. Uncaging glutamate onto very small area of the GCL evokes high frequency bursts of activity onto GCs and in turn, triggers glutamate release at single GC-MLI contacts (Figure1-A). MLI response to GC activation consisted in accelerations (mean baseline frequency: 12.75±5 Hz; acceleration frequency peak: 33.7±17 Hz, n=32). Our work provide the first evidence that MLI output firing pattern is modulated by unitary GC excitatory synapses during isolated GC bursting activity.

Finally, the same MLI were held in whole-cell voltage-clamp configuration. At the population level, bursts of eEPSCs did not follow the same time-course envelope suggesting intersynaptic differences in short term presynaptic plasticity between single GC synaptic units (Figure1-A). We used Principal Component Analysis (PCA, see methods) followed by Kmean clustering (KMC) on the binned (5ms) evoked current traces in order to describe neurotransmitter release behavior at the level of populations of GC terminals (Figure1-B). Glutamate release behavior was very well described by principal component 1 (PC1) so we separated the bursts of eEPSCs in three categories (Figure1-C). The *phasic* and depressing bursts (C1 with a positive PC1 value), the delayed and facilitating bursts (C2 with a low PC1 value), the *tonic* bursts (C3, with a negative PC1 value). Thus, we could identify heterogeneous presynaptic modes of glutamate release at the level of single presynaptic terminals, and the main source of variations was the onset of release peak facilitation.

For some synaptic contacts, we were able to retrieve the evoked MLI firing pattern recorded in loose-patch configuration (Figure1-C *right panel*). Strikingly, the delay of the firing peak frequency was strongly anti correlated ($R<0$, $p=0{,}0004389$) with the neurotransmitter release behavior described by the three categories obtained with voltage clamp experiments. Short term presynaptic plasticity of single GC units drives MLI firing acceleration; the delay of firing peak frequency in controlled by the presynaptic glutamate release behavior during high frequency bursts. Phasic synapses induce a very short (~20ms) delay, while tonic or facilitating presynaptic units induce a longer firing delay (~70 and ~100 ms respectively) (Figure1-D). To conclude our work provide a direct link between variations of evoked MLI firing acceleration and multimodal short term behaviors of presynaptic GC terminals.

Functional heterogeneity of GC-MLI STP profiles during high-frequency stimulations

Our results suggested that variations in short term presynaptic plasticites could have strong outcomes onto information processing in cerebellar networks. As photostimulation does not allow a very precise timelocking of GC stimuli, we assessed a more precise characterization of presynaptic functional variability during minimal stimulation already used by recent studies (Malagon, Miki, Llano, Neher, & Marty, 2016; Miki et al., 2016). Thus, we examined short term synaptic plasticity profiles of GC-MLI terminals during repetitive electrical stimuli at high frequency (10 pulses at 100Hz). MLI from cerebellar vermis (lobules IV-VI) were maintained in whole cell voltage-clamp configuration and loaded with Alexa594 fluorescent dye (n=49) (Figure 2). In order to avoid multi-contact stimulation, MLI processes were visualized under two-photon microscope and stimulation pipettes were positioned close to isolated dendrites. We evoked glutamate release at single synaptic contact by using the minimal stimulation configuration and characterized a specific functional identity for each terminal. In these conditions, we could record trains of eEPSCs from both Basket cells (Figure2 – *top*) and Stellate cells (Figure2 – *bottom*) and multimodal short term synaptic plasticities could be evoked onto the two types of neurons.

We observed a high diversity of short term plasticity profiles between synapses among a global population of GC-MLI contacts (n=96). In order to dissect the functional dynamic range over the population of synapses, we used principal component analysis (PCA) on all release profiles followed by a KMeans clustering (KMC) (Figure 3). In order to focus on release time course and compare STP one to another, we estimated release profiles by using a vector space model which normalizes all eEPSC charges along the train stimulation. Thus, a functional identity was given to each synaptic terminal (see methods). There are four dominant short term plasticity behaviors at GC-MLI contacts and the main sources of heterogeneity have three origins (1) the quantity of neurotransmitter released at the first pulse, (2) phasic facilitation between $eEPSC_2$ to $eEPSC_4$, and (3) sustainability of release after $eEPSC_4$.

At the population level 22.9% of the presynaptic terminals immediately displayed a marked depression of glutamate release at the second pulse (C2, n=21) the other 77.1% exerted facilitation of glutamate release (C1, C3, C4, n=74) (Figure 3-C). The nature of presynaptic STP was also dissimilar from one facilitating synapse to another. 21.6% of them displayed a particular ability to sustain glutamate release all along the electrical train pulse (C4, n=16). In this category, release facilitation is low and very few vesicles are released simultaneously. These synapses were termed as *tonic* contacts, maybe the monovesicular contacts previously described (Bender, Pugh, & Jahr, 2009; Nahir & Jahr, 2013). 54% of facilitating GC terminals sustained a strong facilitation of multivesicular during at least 3 pulses with sometimes sustained release all over the 10 eEPSCs (C1, n=40) as it was seen in other studies (Malagon et al., 2016; Satake, Inoue, & Imoto, 2016). However, in the rest of them, facilitation of multivesicular release was short, purely phasic and

restrained the three first eEPSCs (C3, n=18). Thus, STP is not uniform at GC-MLI synaptic terminals. The functional readout is the resulting of an interplay between different presynaptic parameters; multivesicular versus monovesicular release, low probability versus high probability of release and sustainability along the eEPSC burst.

At the unitary post-synaptic MLI level, there is a high dynamic range of synaptic input STP profiles (Figures 2,3). Most of the time, we could give a functional identity for more than one synapse connecting to the same neuron (2.06 ±1 contacts per neuron in average). In 86.2% of patched MLI, we could find at least two different categories of inputs on the same neuron (two categories: 62.1%, three categories: 24.1%). In only 13.8% of the time, STP was identical between synaptic inputs showing a high diversity of STP profiles at GC-MLI synapses.

Ultrastructural heterogeneity between GC-MLI presynaptic terminals

We performed electron microscopy onto parasagittal sections of P20 CD1 male WT mice (n=4). Synaptic contacts made by GCs onto molecular layer interneurons are characterized by the presence of mitochondrion inside both pre and post synaptic compartments which was a used as a criteria for identification (See methods). As we focused on the organization of vesicles contained in GC synapses, we measured the shortest distance from each vesicle contained in a given terminal to the active zone of the same terminal (Figure 4-A, B) and compared inter-synaptic vesicular distributions (n=109).

To characterize inter-synaptic variations, we performed principal component analysis (PCA) onto the vesicle distribution using 8 bins of 50nm range (from 0: the closest vesicles from release sites, to 400 nm: the farthest). We avoided errors linked to synapse size and cutting orientation by normalizing count values to the total number of vesicles per terminal. There is an independent fluctuation of two distinct vesicle pools from one synapse to another. PCA explains the overall variations of synaptic vesicular distributions with two major variable components PC1 and PC2 The first population of vesicles described by PC1 is found at >150nm from release sites (explains 39.4% of the overall variability of vesicle distributions), probably the reserve pool of synaptic vesicles. The second population is closer from release sites (PC2. Overall explained variance: 17.9%) is characterized by fluctuations of vesicle number in a 50-150nm range has been described as the recycling pool according to literature (Schikorski & Stevens, 2001).

These two populations of vesicles are depicted inside three categories of synapses defined by KMeans clustering (Figure 4-A, C, D). The first one (n=22 terminals) contains a higher number of vesicles at 50-150nm distances (n1=5.45 +/- 2.18, statistically distinct from n3=3.67 +/- 2.09 $p<0.001$) unlike Category

2 terminals (n=43) that contain more synaptic vesicles at higher distances (>150nm) (n2=5.6 +/- 1.38 vesicles per 50nm radius is statistically distinct than n1=1.95 +/- 1.38 or n3=1.76 +/- 1.65, ttest- p<0.001). Finally, category 3 terminals (n=44) do not show much vesicles inside the reserve pool neither recycling pool. Interestingly, one category of synaptic terminals has a lower number of docked synaptic vesicles (n1=4,7 +/- 1.749; n2=6,7 +/- 2.21; n3=7,2 +/- 2.02)). Another important report is the increase of vesicular density (vesicle count/μm^2) in another category of synapses(Category 2) (n2=30.45 vesicles/μm^2) compared to category 1 and 3 (n1=16.8, n3=17.1 vesicles/μm^2) with no change of mean synapse surface (s1=1.32 +/- 0.29; s2=1.37 +/- 0.48; s3=1.25 +/- 0.42).

EM data show a multi-pool segregation of synaptic vesicles within GC-to molecular layer interneuron terminals with important inter-synaptic fluctuations. We identified three main ultrastructural heterogeneities (1) differences in the number of docked synaptic vesicles (0-50nm), (2) differences in the size of the resting pool (>150nm), storing an important number of synaptic vesicles and (3), differences at population independent from the resting pool and closer to active zone (~100nm) probably the recently described replacement pool of SVs (Miki et al., 2016).

The heterogeneous expression of Syn2 modifies the distribution of SVs at GC-MLI terminals.

Presynaptic heterogeneity could arise from an intersynaptic heterogeneous expression of molecular candidates. Hence, we suspected a link between ultrastructural variations at GC terminals and a synapse-specific protein expression. Synapsins are well known for their role in vesicular cross-linking and have isoform specific sub-functions in vesicle pool regulation so we tested the presynaptic expression of several Synapsin isoforms at GC terminals.

The vesicular transporter for glutamate VGluT1 is known for its restricted expression at parallel fiber synaptic terminals inside the molecular layer (Hioki et al., 2003). Thus, we performed triple immunolabellings onto cerebellar sagittal crosssections of P20~P22 CD1 mice (N=4) with VGluT1, Synapsin1 and 2 antibodies and visualized under confocal microscope (Figure 5- A).

We used Pearson's R coefficient to assess colocalization between the different presynaptic markers. Synapsin1 / VGluT1 staining shows a significantly higher correlation coefficient (RSyn1=0.584 +/- 0.057) than the Synapsin2 / VGluT1 (RSyn2=0.435 +/- 0.075) labellings (Paired t-test: t=-19.015 ; p<0.001 ; n=52). The density of VGluT1+ punct colocalizing with Synapsin1 (DSyn1=0.38 +/- 0.09 puncta/μm^2 - *data not shown*) was also significantly higher than the density of VGluT1+ terminals containing Synapsin2 (DSyn2=0.31 +/- 0.76 puncta/μm^2 - *data not shown*) for the same ROI (Paired t-test: t=8.35; p<0.001 ; n=52). Pearson's correlation coefficient was calculated between Synapsin1 and Synapsin2 signal overlapping with VGluT1 signal for all ROIs (R=0.72 +/- 0.108 – *data not shown*).

Using Immunogold electron microscopy, we were able to study exclusively GC-MLI synaptic terminals (Figure 5- B). In this subpopulation of GC terminals, we observed a systematic labeling with anti-Synapsin1 gold beads. However, Synapsin2 was observed in 55.9% of those terminals only. Thus, Synapsin2 is also heterogeneously expressed at GC-MLI terminals. Some will contain Synapsin2 others not. On the same EM micrographs, we examined the distribution of synaptic vesicles at GC-MLI terminals stained by gold beads (Syn2+, n=75) and compared this distribution with unstained terminals (Syn2-, n=59). There is a significant decrease in the number of synaptic vesicles in the 150-200 nm range (150nm: $p<0.001$, 200nm: $p<0.05$ using MannWhitney test) and an increase in docked (0-50nm) synaptic vesicles at Syn2+ terminals.

Our results show that Synapsin2 is expressed at a subpopulation of GC synaptic terminals. This expression is associated with a reorganization of vesicular distribution: the distance between SVs and the active zone cytomatrix is decreased at Syn2+ terminals with more vesicles at release sites. There is an inter-synaptic heterogeneity caused by molecular factors and a large contribution of SynapsinII in ultrastructural variability.

Partial loss of functional variability at GC-MLI presynaptic terminals of Syn2 -/- mice

Knowing the heterogeneous inter-synaptic expression of SynapsinII and its role in the regulation of vesicular populations in WT animals, we used a knockout mouse model for SynapsinII (Syn2-KO) where presynaptic terminals are all devoid of SynapsinII isoforms. We assessed functional variability within the population of GC-MLI synaptic terminals of SYN2-KO mice with the minimal electrical stimulation protocols previously used for WT mice (Figure 6). To do so, we performed PCA transformation of Syn2-KO STP profiles based on a PCA fit of minimal WT data exclusively.

There is a partial loss of STP heterogeneity at GC terminals from Syn2-KO mice :
i) Syn2-KO STP profiles are superimposed to already existing WT STP profiles. Syn2-KO STP profiles are essentially synapses following glutamate release facilitation with a low initial release probability.
ii) Half of the WT STP profiles are lost in the Syn2-KO mice (Figure 6- B, C). The lost profiles are essentially phasic STP profiles that endow a strong neurotransmitter release behavior at the beginning on the burst. In conclusion, Syn2 modulates STP within a fraction of GC synaptic terminals by increasing release probability and glutamate release sustainability during prolonged stimulation.

In order to characterize the ultrastructural correlates of functional heterogeneity reduction, we assessed vesicular distribution of SVs by using EM micrographs from Syn2-KO GC-MLI presynaptic terminals (Figure 7). Interestingly the mean number of docked synaptic vesicles was significantly decreased in terminals lacking SynapsinII (Figure 7- B). Also, reserve population were altered at both replacement and resting pools and the mean distribution profile of Syn2KO GC-MLI terminals was only comparable to 1/3 of WT distribution profiles (Figure 7- C).

Finally, both the ultrastructural and functional organization of synaptic vesicles is modified by the absence of SynapsinII. There is a drastic reduction of inter-synaptic variability at GC terminals lacking SynapsinII.

We have shown that MLI firing is driven by GC-MLI single presynaptic units ; unitary synapses regulate the firing delay of post synaptic MLI. Knowing the partial loss of functional heterogeneity at GC-MLI terminals from Syn2-KO mice, we expected a disturbance of MLI output firing pattern at Syn2-KO GC terminals. For that, we photostimulated unitary GCs and monitored the evoked firing acceleration in MLI induced by SYN2-/- and SYN2+/+ synaptic contacts (Figure 8). Again, subsequent whole-cell voltage clamp experiments allowed us to record the time-course of photostimulation evoked currents is in line with our minimal experiments onto the SYN2-/ mouse line. A lack of Synapsin2 induces lower initial release probability and a delayed increase in synaptic facilitation characterized by a weaker facilitating slope of eEPSC charge build-up (Figure 8-A). Analyzing the associated evoked firing showed a similar delay in the firing entrainment of loose-patched SYN2-/- MLI associated to a lack of synchronicity of the evoked response.

To conclude, SynapsinII is expressed at a subpopulation of granule cell presynaptic terminals and contributes in the heterogeneous drive of feedforward inhibition. In the mouse model lacking SynapsinII, the presynaptic terminals tend to homogeneity; less variability alters the coding properties of MLI neurons through molecular, ultrastructural and functional modifications.

Article 1. *"Ultrastructural molecular and functional heterogeneities of granule cell presynaptic terminals"*

DISCUSSION

This work demonstrates for the first time that the pattern of firing of a single MLI is heterogeneously driven by functionally distinct excitatory synaptic inputs. Input-specific synaptic behaviour generates difference in the spike onset delay and potentially enhances the pattern decorrelation of sensorimotor inputs, that is, facilitates the representation of functionally distinct inputs by PC (Albus, 1971; Marr, 1969). By combining molecular, ultrastructural and functional studies, we showed that heterogeneous expression of SynapsinII in GC boutons underlies part of the diversity in STP observed at unitary GC-MLI synapses.

The rules governing diversity in presynaptic behaviour have been extensively studied in neocortical or hippocampal circuits. In most of cases, presynaptic determinants of synaptic efficacy among boutons issued from a single axon vary with the identity of the postsynaptic cell (Blackman, Abrahamsson, Costa, Lalanne, & Sjöström, 2013; Markram, Wang, & Tsodyks, 1998). Target cell type-dependent heterogeneity relies on differences in probability of release (p_r) (Koester & Johnston, 2005), responsiveness to neuromodulators (Scanziani et al., 1998; Delaney and Jahr, 2002; Pelkey et al., 2006; Buchanan et al., 2012) or ability co-release GABA and glutamate (Galvan and Gutierrez, 2016). Target cell type-dependent STP has also been described at cerebellar GC-MLI synapses by using stimulation of beam of PFs or cluster of GC somata; upon high-frequency stimulation compound synaptic responses exhibit a facilitating profile at GC-SC synapses whereas these responses depress at GC-BC synapses (Bao et al., 2010). Our results contradict the target-cell dependent STP at GC synapses since both single BC- or SC-like MLI receive multimodal unitary excitatory inputs. While we cannot explain the discrepancies between results obtained with compound stimulations versus unitary ones, our work suggest that the functional organization of single MLI inputs and the tuning of the FFI pathway are more complex than expected.

At the input stage of the cerebellar cortex, single GCs are able to expand the code of sensorimotor information to PC by enhancing pattern decorrelation of MF inputs. Computation of multisensory events by single GCs relies on the diversity of MF synaptic behaviour and on the ability of single GC to transduce a given mix of coincident multisensory inputs in unique first spike latency (Chabrol et al., 2015). Here we showed that the delay of firing acceleration of a single MLI is differentially tuned by individual GC inputs. PCA analysis of release profile at individual GC-MLI synapse permitted to determine four groups of synaptic behaviour (C1 to C4, Figure 3) during 100 Hz train. By analogy to what have been shown at MF-GC synapses where 5 groups of MF input profile have been categorized (Chabrol et al., 2015), we can postulate that a specific combination of groups of GC inputs (e.g. C1+C4 or C2+C3+C4) can tune the delay of firing and the spike output of a single MLI in a standardized way. In any case, the succession of delay coding at individual excitatory inputs at the first and

second stage of the cerebellar cortex should refine the salient features of a particular combination of events and ultimately enlarge the ability of PCs to represent and discriminate multisensory inputs.

Organization of synaptic diversity at unitary GC-MLI synapses

At individual MF-GC synapse, the synaptic behaviour of a given MF terminal is determined by its topographical origin (Chabrol et al., 2015). In this work, we could not find a specific organization of the heterogeneity of MLI excitatory inputs. Particularly, it is not known whether GC boutons issued from a single PF share the same synaptic behaviour when contacting MLIs or at the opposite, if these boutons are functionally heterogeneous. Nevertheless, several experimental findings support the last possibility. Firstly, calcium imaging performed on single PFs revealed that Ca^{2+} dynamics and regulation of Ca^{2+} influx by neuromodulators in synaptic varicosities from a same PF are highly heterogeneous (Brenowitz and Regehr, 2007; Zhang and Linden, 2009, 2012; Bouvier et al., 2016). Secondly, at GC-MLI synapses, the number of active release sites is heterogeneous (Malagon et al., 2016) and the possibility to increase the number of active release site upon paired-pulse stimulation is observed in a fraction of these synapses only (Miki et al., 2016). Third, the retrograde release of endocannabinoid by MLI dendrites induce presynaptic LTD at GC-MLI via the activation of presynaptic CB1 receptors (Soler-Llavina and Sabatini, 2006; Beierlein et al., 2007). The release of endocanbinoid is triggered by a strong entry of Ca^{2+} in MLI dendrite upon sustained activity of PF and since SC dendrites are able to compartmentalize postsynaptic Ca^{2+} signal to submicron stretches, endocannabinoid release and endocannabinoid-dependent presynaptic LTD is restricted to the sole unitary excitatory inputs activated during the induction protocol (Soler-Llavina and Sabatini, 2006). Hence, functional heterogeneities among GC terminals also originate from the history of firing of each GC. To summarize, the synaptic behaviour of individual GC bouton is probably tuned in a unique way by an intermingled combination of factors including presynaptic receptor composition, presynaptic Ca^{2+} dynamic, number of active release sites, retrograde signalling and history of firing. Our work indicates that synaptic diversity is also underpinned by the heterogeneous expression of SynapsinII at GC-MLI synapses.

Origin of SynapsinII expression diversity was not probed in this study. Potentially, the presence or absence of SynapsinII may be genetically determined at early developmental stages, leading to Syn2+ and Syn2- subclones of GCs. In this view, it is interesting to note that clonally related GCs (that is, GCs issued from the same GC progenitor) stack their axons in a specific sublayer in the molecular layer (Espinosa and Luo, 2008) suggesting that the presence or absence of SynapsinII may organized in beams of PFs. Since beam of neighbouring PF are activated during sensory stimulation (Wilms and Häusser, 2015), recruitment of SynapsinII+ or SynapsinII- may

be related to the activation of a given sensorimotor task. Alternatively, the targeting of SynapsinII may be controlled at individual bouton of a single PF by a complex interplay of mechanisms regulating the traffic of synapsins in axons (Gitler et al., 2004) or organizing the assembly of the presynaptic active zone (Owald and Sigrist, 2009).

Tuning of STP by SynapsinII

The heterogeneous expression as well as the heterogeneous function of SynapsinII in subtypes of neurons belonging to same neural network have been reported in numerous studies (Gitler et al., 2004; Kielland et al., 2006; Feliciano et al., 2017) but this work bring the first evidence that expression of SynapsinII within presynaptic terminal issued from the same population of neurons can be heterogeneous. As mentioned above, the heterogeneous expression of SynapsinII in GC terminal is required to enlarge the number of functionally distinct inputs on a single MLI.

SynapsinII tunes the first spike latency at unitary GC-MLI synapses by shaping the synaptic behaviour of GC bouton. Since the absence of SynapsinII leads to a reduced number of docked synaptic vesicles and to a strong reduction of EPSC charge at the first response of 100 Hz train, we postulate that SynapsinII controls the release of glutamate by regulating the number of release-ready synaptic vesicles.

In the Calyx of Held (Sakaba, 2006; Schneggenburger et al., 2012; Neher, 2015) and in GC terminal (Valera et al., 2012), the behaviour of glutamate release during high-frequency train relies on the segregation of releasable vesicles in two functionally distinct populations. At GC-PC synapse, releasable SV are segregated in a fully-releasable pool that can be released by a simple AP and in a reluctant pool that can be recruited in a millisecond time scale by high-frequency stimulations. At GC-MLI synapse, the reluctant pool probably corresponds to the so-called replacement pool which supply release sites with release-ready vesicles upon high-frequency activity (Miki et al., 2016). At both GC-MLI and GC-PC synapses, ultrafast recruitment of the replacement/reluctant pool underlies part of the large facilitation of glutamate release during high-frequency activities. In Synapsin2 KO mice, the reduction of the synaptic strength is larger than the reduction of the number of docked vesicles and we cannot exclude that SynapsinII also regulates postdocking priming stages. Based on the two-pool model, we propose that the lack of SynapsinII shifts the equilibrium between the fully-releasable pool and the reluctant one at the expanse of the first one. Nevertheless the fact that the lack of SynapsinII did not affect the charge of synaptic response after the third response of high-frequency train also suggests that recruitment of the reluctant pool is not impaired in SynapsinII deficient terminal.

Conclusion

First spike latency in MLI clearly depends on the pattern of STP at unitary synapse. This suggests that the temporal coding of the FFI may be controlled by a single GC. Considering the importance of time delays for internal models of motor adjustments (Kistler, van Hemmen, & De Zeeuw, 2000; Mauk & Buonomano, 2004; Wolpert, Miall, & Kawato, 1998) synapse-specific functional identity would have essential consequences onto learning and predictive functions of the cerebellum. Indeed, heterosynaptic long term plasticities are triggered within very short time windows (<100ms) (Rahmati et al., 2014; Suvrathan et al., 2016) and the inhibitory control of PC by MLI is essential for motor adjustments (Dizon & Khodakhah, 2011; Jelitai, Puggioni, Ishikawa, Rinaldi, & Duguid, 2016). While direct inhibition of MLI and PC is time-invariant (Blot et al., 2016), we showed that the "hypervariable" granule-cell to molecular layer interneuron connection expands the variety of time-lags for the excitation of MLI. Altogether, our results indicate that the high diversity of STP have network relevance for information processing in the molecular layer of cerebellar cortex and that presynaptic molecular machinery is itself adapted for inter-synaptic variability. We believe that these results provide new clues to understand how the fine tuning of the presynaptic machinery controls the computation of information in assemblies of neurons.

Article 1. *"Ultrastructural molecular and functional heterogeneities of granule cell presynaptic terminals"*

FIGURES

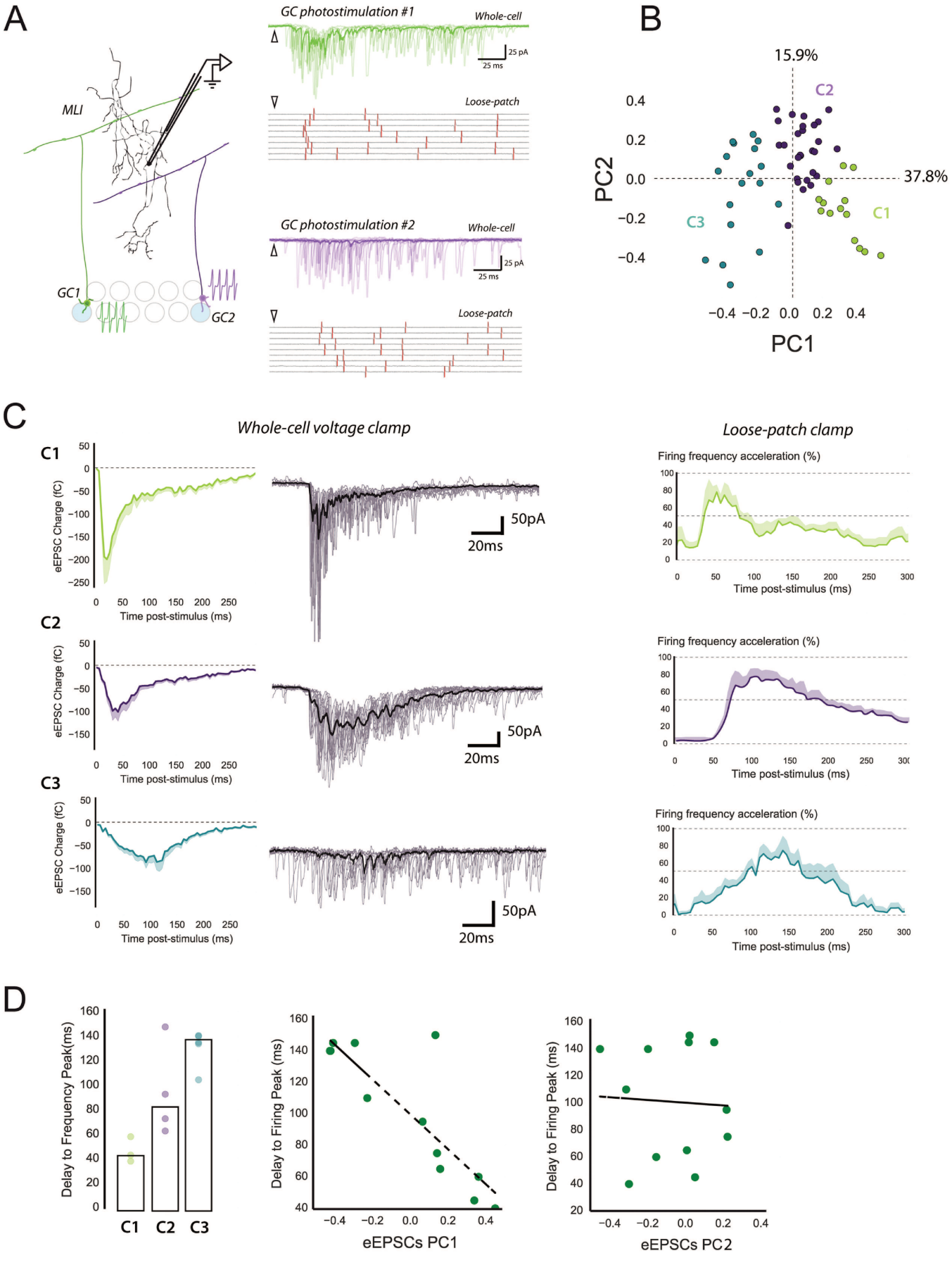
A
MLI
GC1
GC2
GC photostimulation #1
Whole-cell
25 pA
25 ms
Loose-patch
GC photostimulation #2
Whole-cell
25 pA
25 ms
Loose-patch
B
15.9%
C2
37.8%
C3
C1
PC2
PC1
0.4
0.2
0.0
−0.2
−0.4
−0.4 −0.2 0.0 0.2 0.4
C
Whole-cell voltage clamp
Loose-patch clamp
C1
C2
C3
eEPSC Charge (fC)
Time post-stimulus (ms)
50pA
20ms
Firing frequency acceleration (%)
Time post-stimulus (ms)
D
Delay to Frequency Peak(ms)
C1 C2 C3
Delay to Firing Peak (ms)
eEPSCs PC1
eEPSCs PC2

Figure 1. Unitary synapse stimulation evokes different output firing patterns on single MLIs.

A. Example of one photostimulation experiment where unitary GCs are stimulated upon light dissociation of RuBiGlutamate. Post-synaptic MLIs are sequentially recorded in loose-patch configuration and whole cell configuration in order to respectively record the spike output firing pattern associated to the input eEPSC train. Here, we monitored two different eEPSC time courses, one phasic and depressing GC1 terminal (*top*) and one tonic GC2 synapse (*bottom*). Strikingly, the output firing pattern is time-locked to the phasic component for GC1 while the delay of evoked firing was more variable for GC2.
B. Principal Component Analysis of the evoked charge time course for 63 unitary contacts (see methods). The eEPSC bursts could be differentiated depending on their tonic or phasic component into three different clusters using K-Means clustering (Panel C).
C. Within the population of synaptic terminals, some responded with a phasic and depressing eEPSC burst (cluster1), others facilitated and still have a lower phasic component (cluster2). The third cluster is characterized by a tonic release of glutamate.
Retrieving loose patch recordings of the firing output pattern associated to the eEPSC bursts from the three clusters (right panel) showed a high variability in the delay of the peak frequency acceleration that suggests different modes of temporal coding.
D. Heterogeneous presynaptic boutons with different short term plasticities evoke variations of temporal coding by MLIs. Left; bar plot representing the three different clusters of eEPSC classified by the short term plasticity of input eEPSC burts. There is a high correlation between temporal coding and eEPSC bursting activity (represented by principal components 1 but not principal component 2) at the level of single synapses (right scatter plots).

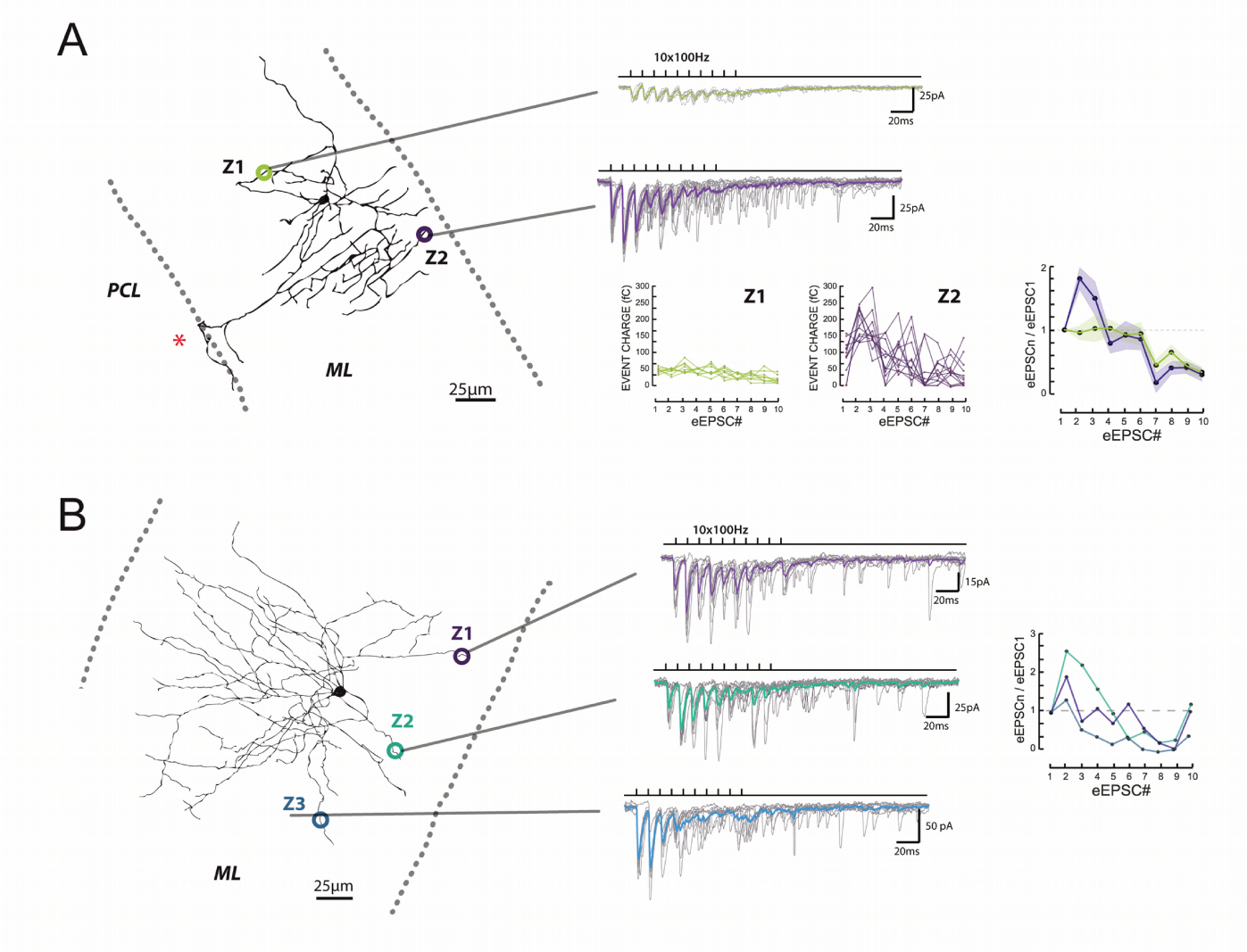

Figure 2. Inter-synaptic heterogeneity of GC synaptic terminals during high frequency activation of single presynaptic contacts.

Example of two reconstructed cells (A; one Basket-like, and B; one Stellate-like *bottom*) where different GC presynaptic show different short term synaptic plasticity behaviors. One depressing and one sustaining GC synapic terminals are connected to the same post-synaptic target (top backet-like neuron). Facilitating, depressing and also intermediate synapses contact the same post-synaptic target (Bottom stellate-like neuron). Scatter plot show a trial-to-trial reproducibility of short term plasticity profiles for single terminals. Rigth plots show the median values of eEPSC charge for the eEPSC1-10 of single contacts normalized to eEPSC1.

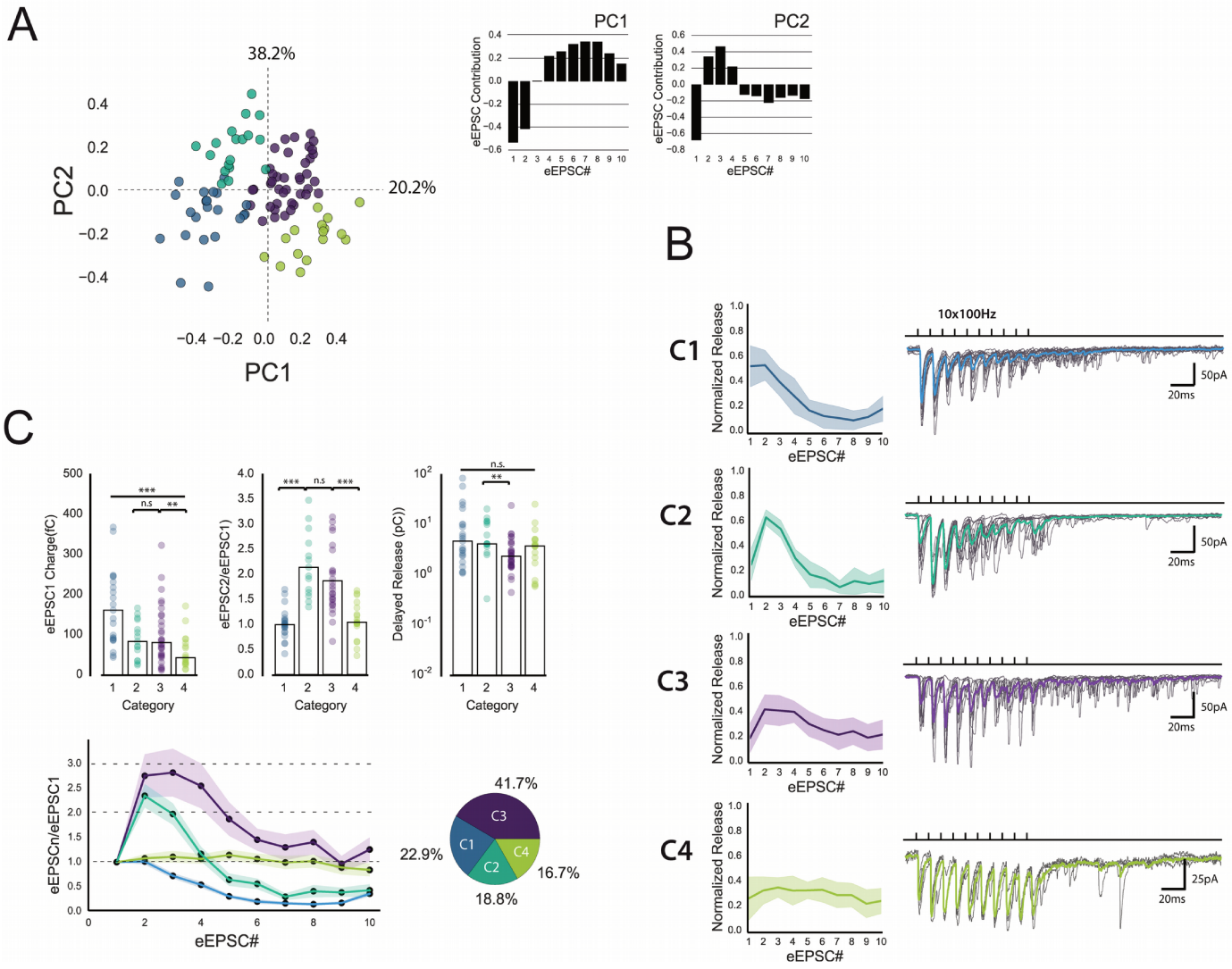

Figure 3. Inter-synaptic functional heterogeneity within a population of GC synaptic terminals.

A. PCA transformation of short term synaptic plasticity profiles. Scatter plot of the first two principal components (PC1, PC2) of GC synaptic terminal populations (n=99). The first two components explain 58,4% of the total variance of short term plasticity. Synapses with positive PC1 values sustain glutamate release during the 10 eEPSC from the burst while PC1 synapses are depressing synapses. Positive PC2 synapses are facilitating synapses during $eEPSC_{2,3}$ while negative PC2 synapses follow a strong short term depression.
B. Four categories of short term plasticity behaviours are determined by K-Mean clustering. Two categories sustain glutamate release throughout the burst (C1 and C4) while the two others endow phasic release during the initial pulses (C2, C3). There is a strong short term facilitation in category C3 opposed to a strong depression in the synapses from category C2. Synapses from category C4 provide a sustaining "monovesicular" glutamate release. Circular diagram representing the proportion of individual short term synaptic plasticity behaviour within the whole population of synaptic terminals (bottom right).

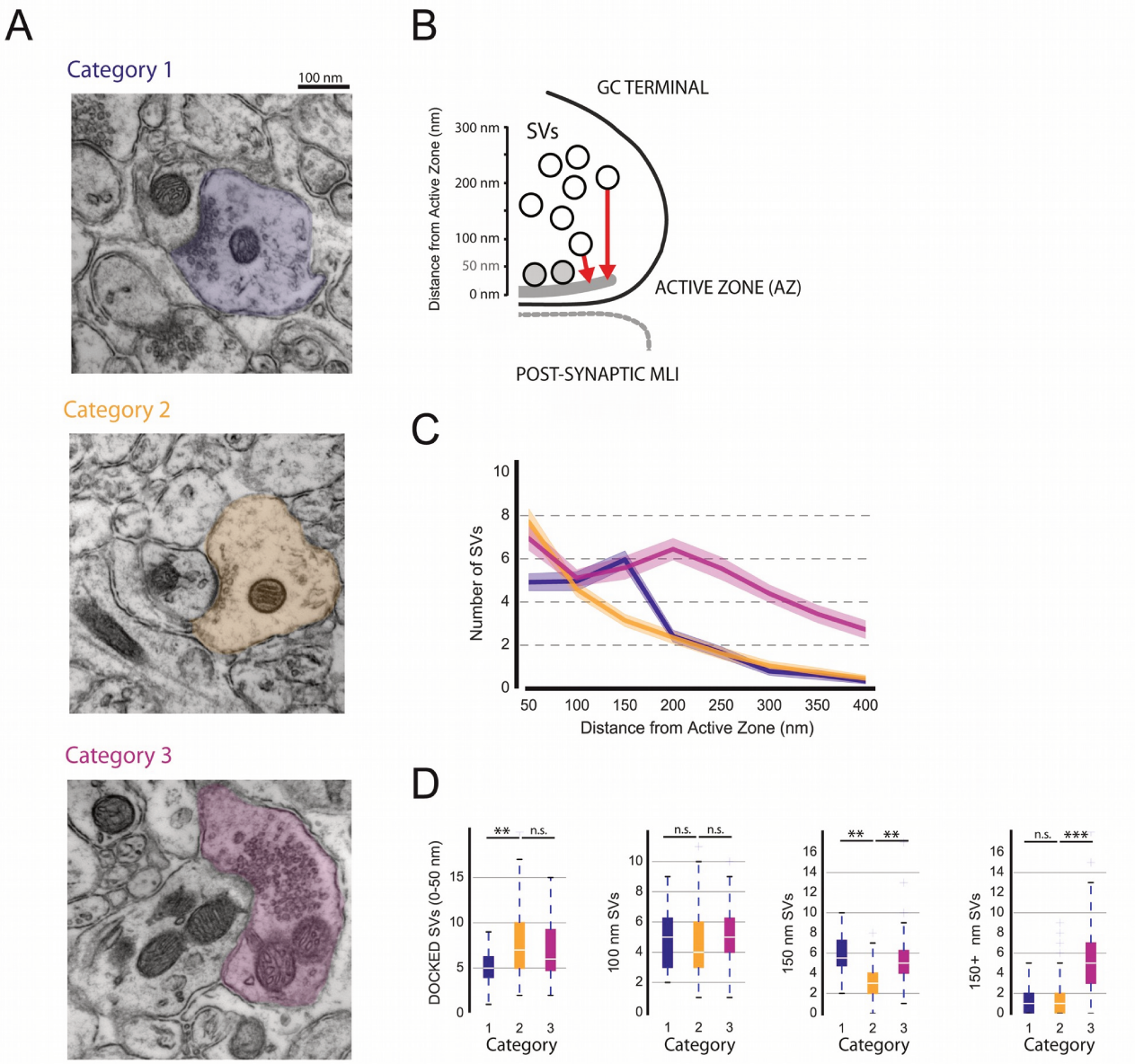

Figure 4. Inter-synaptic ultrastructural heterogeneity of vesicular distribution at single GC-MLI terminals.

Populations of GC presynaptic terminals can be classified in three different categories (A) depending on vesicular distribution within the presynaptic volume (B). We have identified inter-synaptic variations of vesicular clustering at three different areas of the presynaptic volume, leading to a three preferential distributions. First, some synaptic terminals (Category 1) have fewer docked (0-50nm) synaptic vesicles (D) but this same terminals have significatively more synaptic vesicles at 150nm but no reserve populations (compared to Category 3)

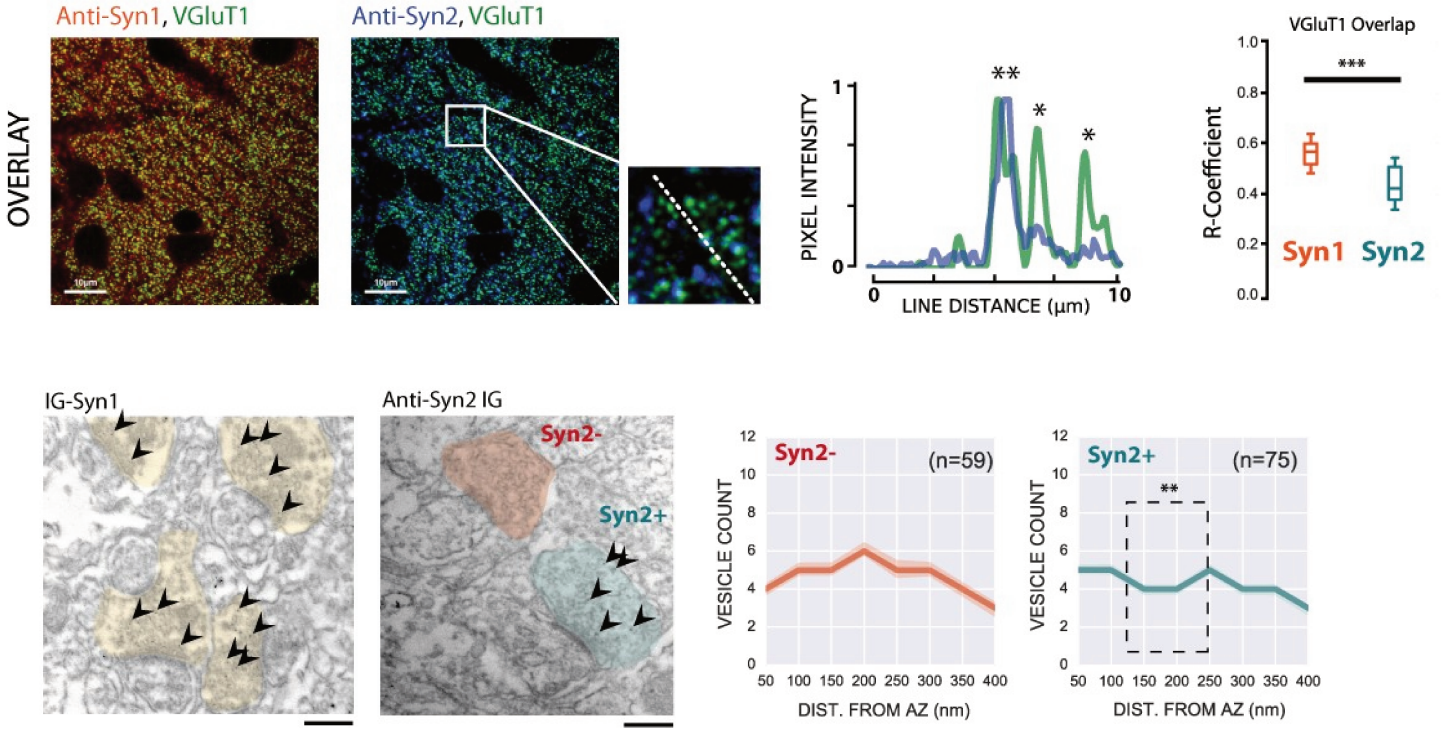

Figure 5. Inter-synaptic molecular heterogeneity between GC-MLI terminals.

Synapsin2 is expressed by a subset of synaptic terminals while Synapsin1 is an ubiquitous synaptic marker for GC synaptic boutons. Immunohistochemistry assays show a partial colocalization between Syn2 and VGluT1, an exclusive presynaptic marker for GC terminals (top right) but a full colocalisation with Syn1.
Electron microscopy micrographs from immunogold assays also present a synapse-specific expression of Synapsin2 within a subset of GC-to-MLI presynaptic terminals (bottom micrographs), but a full colocalisation with Syn1 at this category of synapses (scalebar – 500nm).
Importantly, synaptic boutons stained by Anti-Syn2 gold beads present variations in vesicular distribution. In boutons expressing Synapsin2, there are significantly more synaptic vesicles at the 0-50nm range (docked vesicles), but significantly less vesicles at 150-200nm.

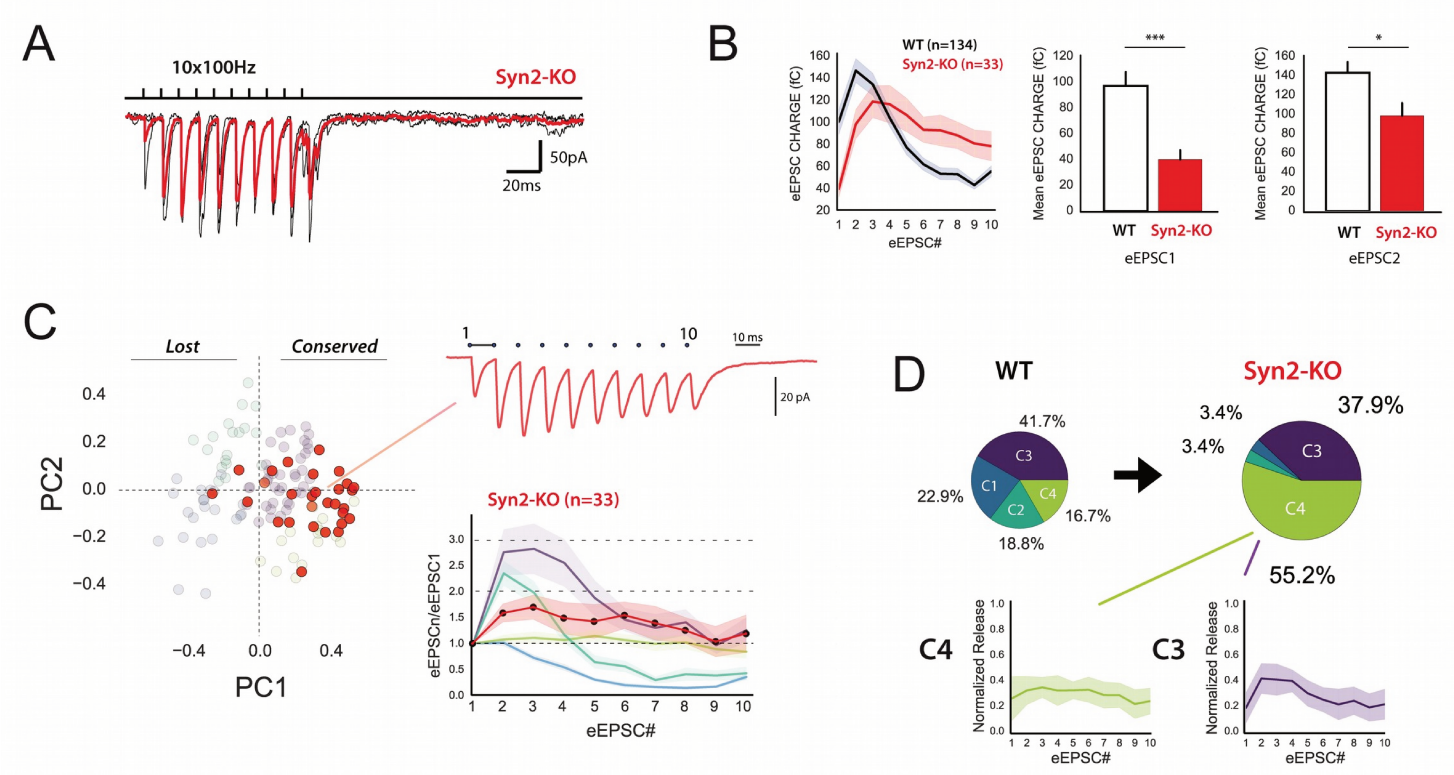

Figure 6. Partial loss of functional variability at SYN2 -/- GC-MLI presynaptic terminals.

A. Example of SYN2-/- synaptic terminal recorded in minimal configuration onto one MLI using the same parameters as the ones used for Figure2-3.
B. Average eEPSC charges evoked following 10 consecutive eEPSCs at WT (black) and SYN2 -/- (red) synapses. The bar plots show that significantly less glutamate is released following pulse#1 and pulse#2.
C. PCA transformation of SYN2-/- short term synaptic plasticity profiles with the PCA fit used for WT animals. SYN2-/- boutons represent only half of the WT functional mapping cloud of points. There is a significant loss of variability in a population of synaptic terminals devoid of Synapsin2.
D. Reduction of representative WT clusters illustrating a loss of short term plasticity functional variability. In mice lacking Synapsin2, only two different forms of short term plasticity are maintained: synapses with a delayed facilitation (C3), and synapses sustaining release (C4).

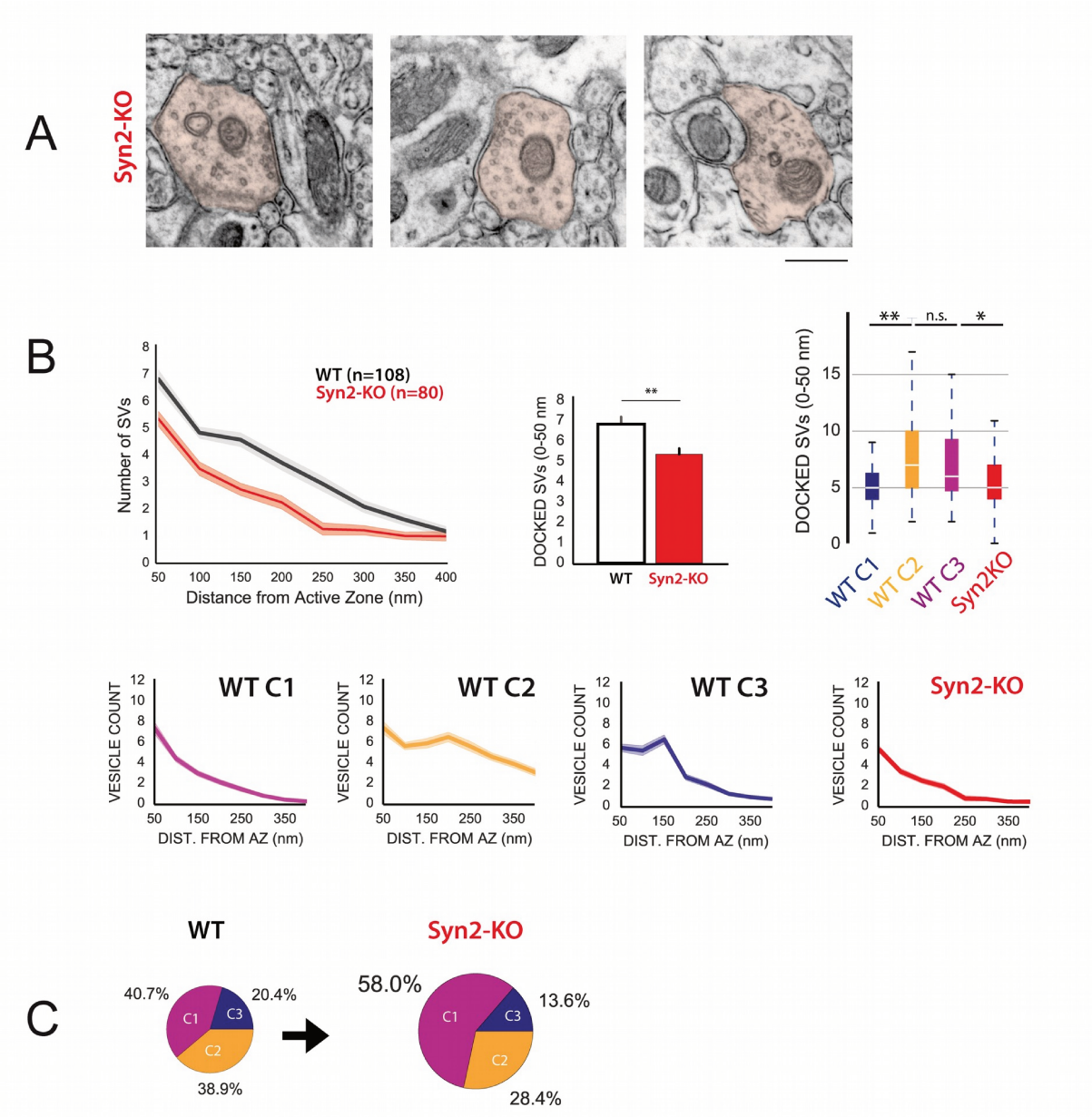

Figure 7. Reduction of ultrastructural heterogeneity at SYN2 -/- GC-MLI presynaptic terminals.

A. Three representative micrographs of GC-MLI presynaptic terminals from the cerebellar cortex of SYN2 -/- mice.

B. Alteration of presynaptic ultrastructure at granule cell presynaptic terminals from SYN2-/- animals. Vesicular distribution from the SYN2-/- presynaptic terminals (red) superimposed with the average WT. The box plots illustrate an important decrease in the number of docked vesicles (0-50nm) combined to an alteration of distal vesicular pools (replacement and reserve pools).

C. Pie chart containing the proportion of WT and SYN2-/- synapses in each ultrastructural category. Category1 is 18% more represented meaning that the regulation of vesicular populations is severely affected at SYN2- GC-MLI terminals. The mean synaptic vesicle distribution profile of Syn2KO terminals (red) is similar to one of the three WT profiles obtained on WT presynaptic ultrastructures (C1). The two other distribution profiles, with more vesicles in reserve populations, are less represented (C2, C3).

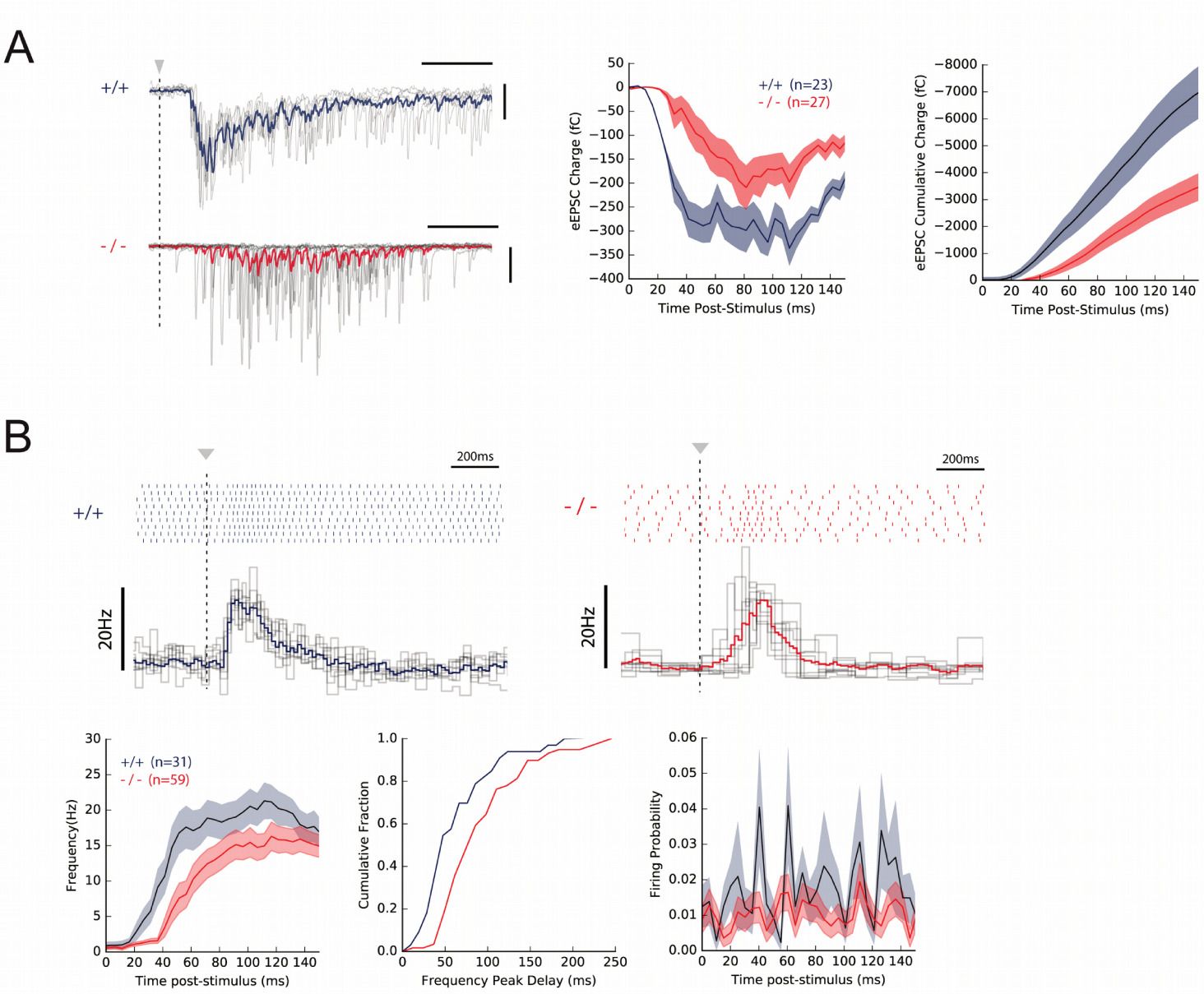

Figure 8. Synapsin2 controls firing acceleration during MLI excitation by GC terminals.

A. Single GC photostimulation evoked different patterns of eEPSC bursts in WT and SYN2-/- unitary terminals. Two representative examples of evoked eEPSC bursts in WT (blue) and SYN2-/- condition (red). In average, SYN2-/- traces are facilitating and delayed while WT traces are more phasic and depressing (right panels).

B. Using the same terminals in the same conditions, the associated loose-patch experiments displayed distinct spike output firing patterns in WT and SYN2-/- neurons. There is a significant delay of evoked bursting activity (~20ms) in mice lacking Synapsin2 (left and central panel). Post-stimulus histogram (right histogram) shows that the delay and synchronicity of temporal coding is significantly impaired in SYN2-/- animals (red) while WT MLIs present a very high spiking regularity.

SUPPLEMENTARY DATA

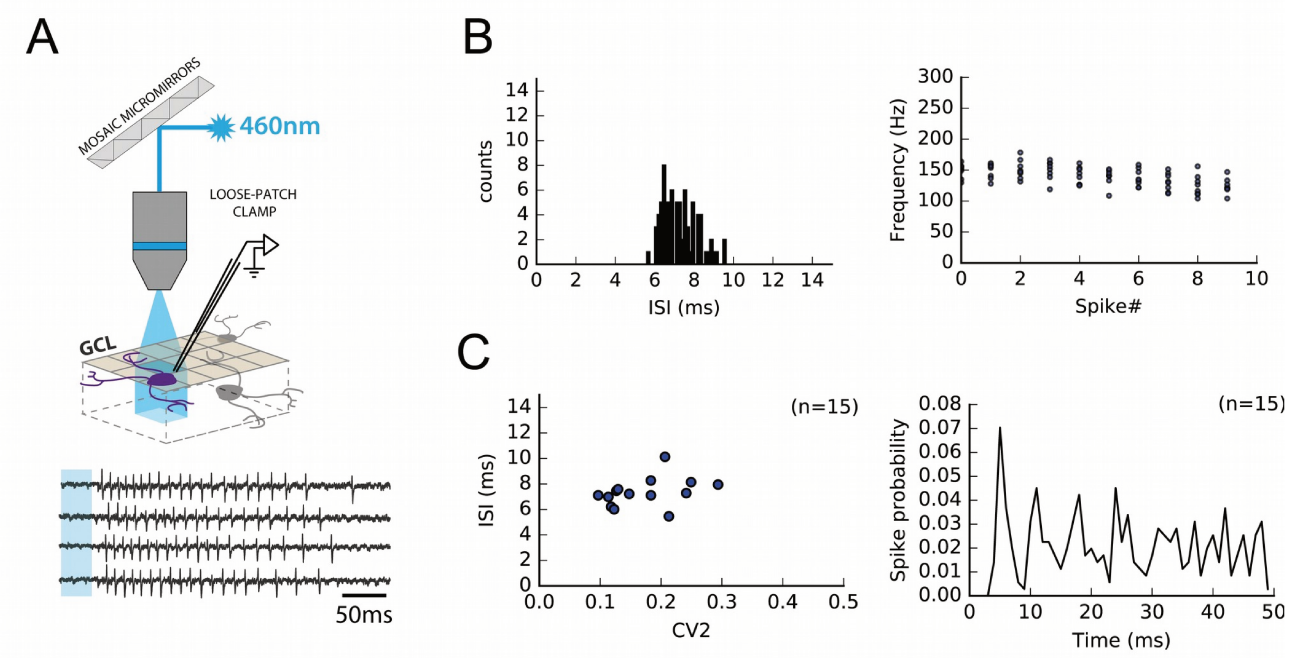

Supplementary figure 1. Robust high frequency GC bursting activity after RubiGlutamate uncaging.

A. Experiment schematics showing an activated GC following RubiGlutamate photo-dissociation by GC layer illumination. Loose-patch clamp recordings from GCs show that RubiGlutamate uncaging induces high frequency and reproducible bursts of action potentials.
B. Example showing the very high fidelity of the inter-spike interval (ISI) during the 10 firsts spikes of glutamate-uncaging evoked GC bursting acivity (left). The firing frequency is highly stable during the burst (right) and very robust between trials.
C. Group data showing no global differences of firing frequency (ISI) and firing variability (CV2) between different cells (n=15) (left). Post-stimulus histogram of the different spikes from all trials of 15 different cells aligned on spike#1. Inter-cellular variability of evoked bursting activity is weak (right).

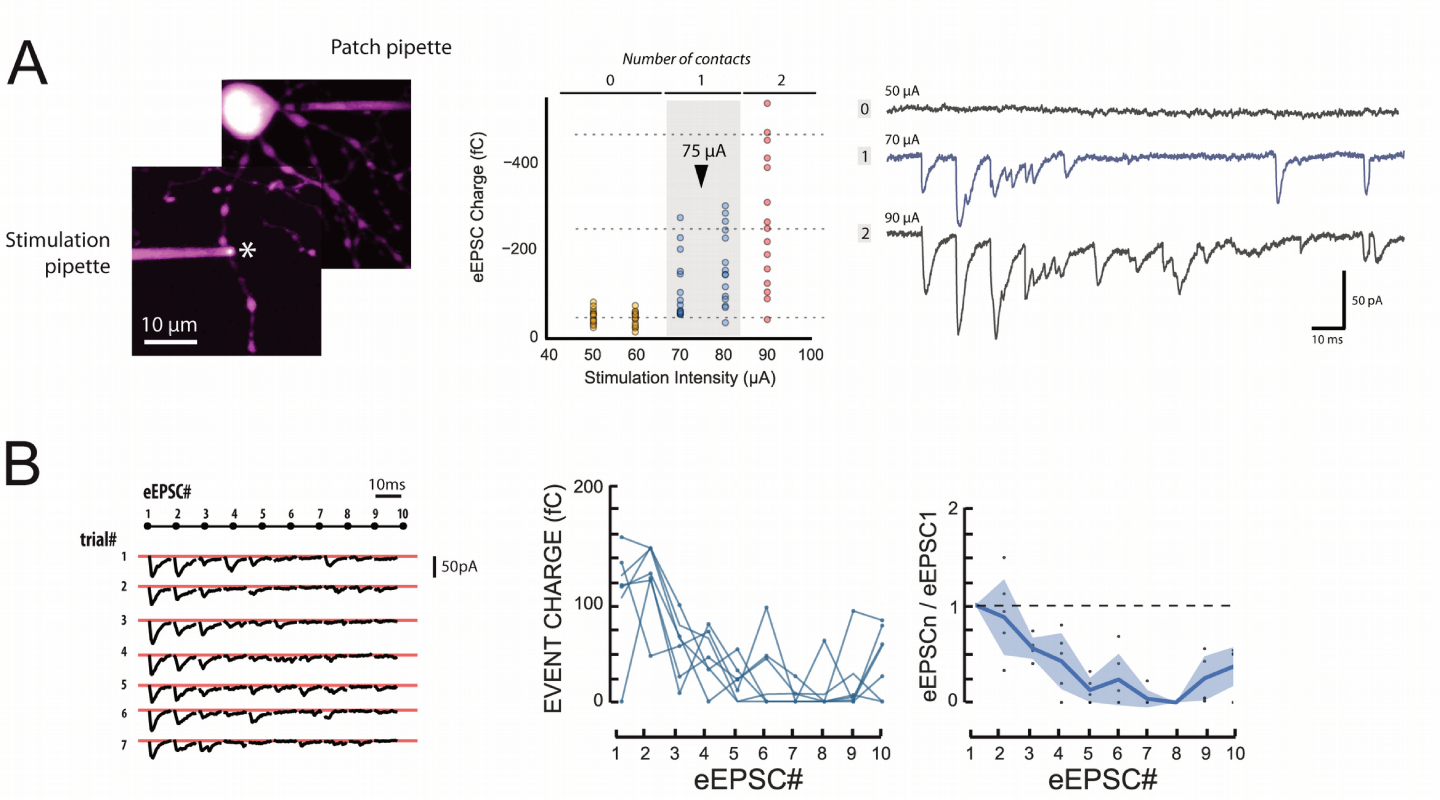

Supplementary figure 2. Inter-synaptic heterogeneity of GC synaptic terminals during high frequency activation of single presynaptic contacts.

A. Two-photon experiment showing a patched MLI filled with Atto-594. The stimulation pipette is also filled with Atto-594 to position the tip next to isolated dendrites (left). Minimal configuration is used to stimulate unitary GC contacts. Increasing the intensity of electrical stimulation evoked multiple levels of multivesicular release, the intensity of stimulation was choosen between the suprathreshold value for noise (zero eovked currents), and subthreshold value for a double-contact stimulation.
B. High-frequency eEPSC bursts (10 pulses at 100Hz) are evoked with electrical pulses under minimal configuration (middle). We extracted the eEPSC charge for each event from different trials. Isolated synapses endowed very specific patterns of short term plasticity which are robust over trials. Example of a depressing synapse with absolute charge values and normalisation on eEPSC1 (right).

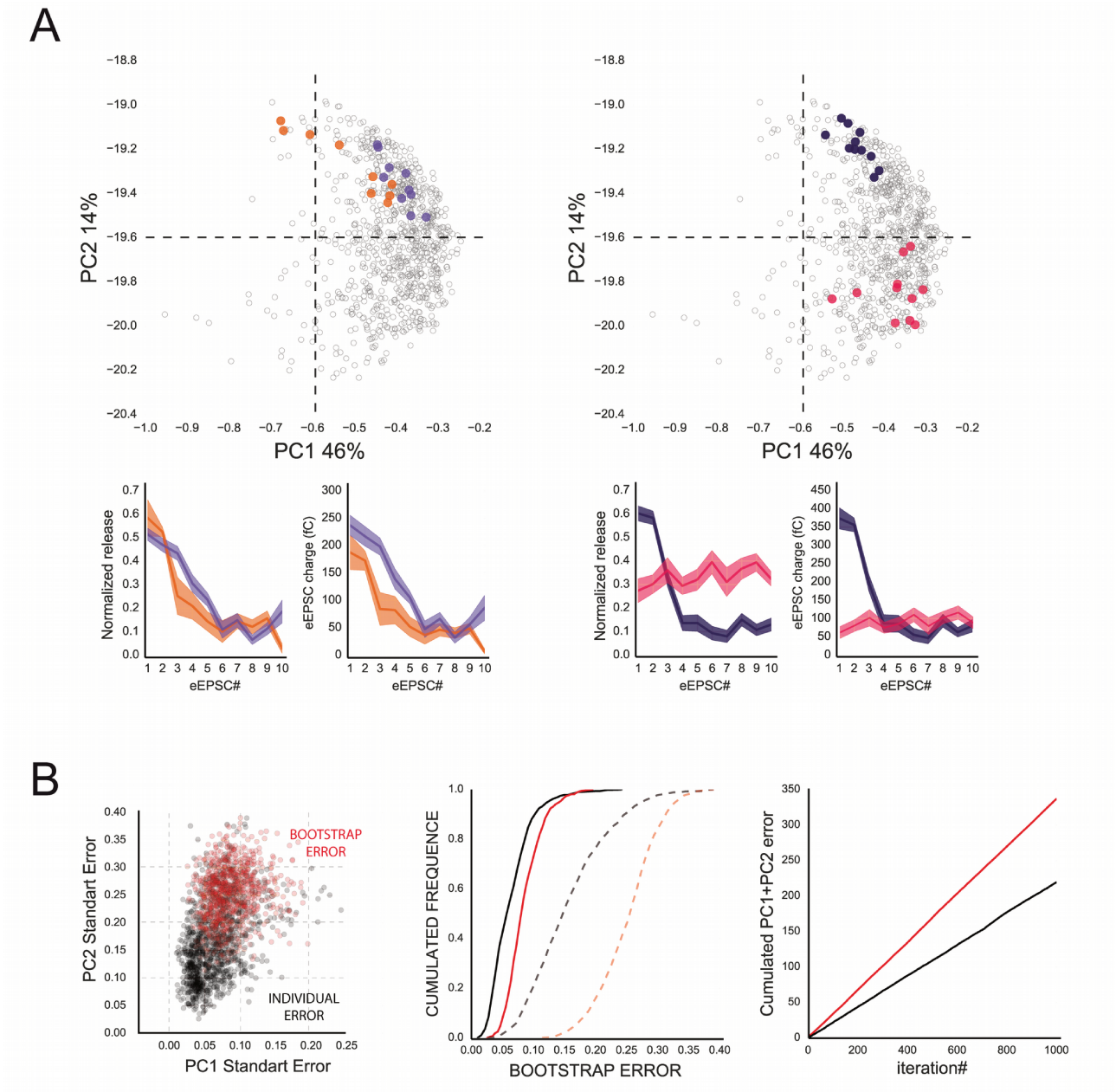

Supplementary figure 3. Robustness of the functional identity of single GC terminals within all the population of GC synapses.

A. Functional mapping of each eEPSC train recorded for 100 neurons. PCA is computed independently for each eEPSC train. Recordings originating fro the same synaptic terminals are located in a very specific position inside the cloud of points showing an internal reproducibility of short term plasticity phenotypes. eEPSC trains from two synapses with the same functional identity are clustered nearby inside the PCA transform (left panel, example of two depressing synapses) while two functionally distinct contacts are distant one from another (right panel, one depressing and one sustaining synapse).
B. Scatter-plot of the bootstrap error for the two first principal components based on randomly-picked eEPSC trains (red) and individual errors within single synapse observations show that unitary synapses have a robust functional identity far from randomness (left panel). Error is highly reduced in both principal components (middle panel : PC1; filled lines, PC2; dashed lines) and the cumulative error slope of population bootstrap is higher than the intra-synaptic error (right panel).

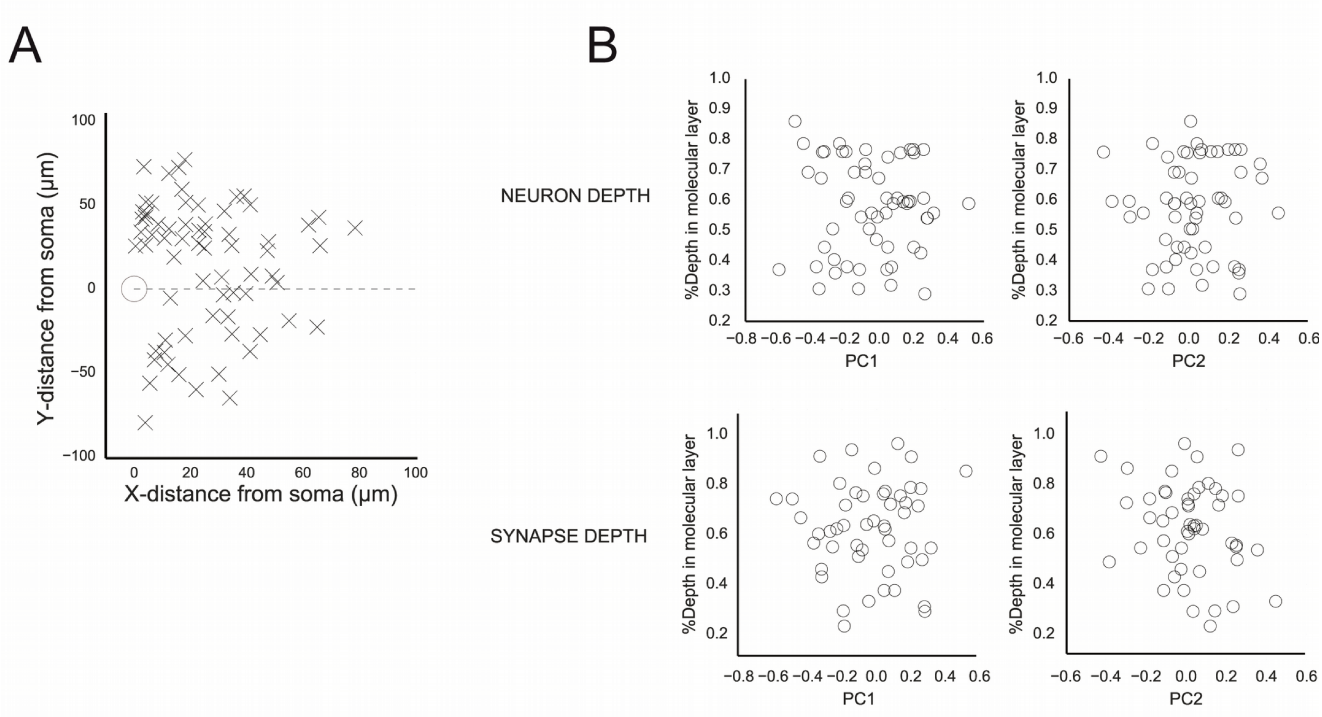

Supplementary figure 4. Lack of physiological correlations between the short term plasticity of GC presynaptic inputs and the nature of post-synaptic targets.

A. The XY position of the stimulation pipette tip is plotted into a 2D space where position (0,0) represents the somatic center of MLIs. Stimulated synapses were at somatic distances >20µm By choosing such distances, we were able to discard post-synaptic non-linearities linked to variations of compartmental volume of MLI dendrites that could affect short term plasticity (Abrahamsson, Cathala, Matsui, Shigemoto, & DiGregorio, 2012).

B. We found no relations between interneuron positions inside the molecular layer and the short term plasticity of their GC inputs illustrated by PC1 and PC2 (see Figure 3 for the related principal component). The position of the stimulated synapses was neither related to short term functional behaviours.

Docked Vesicles

	Mean Svs#	+/- SEM	Variance	Median Svs#	MedianDeviation
All	6,833	0,356	13,379	6	2,965
Cat1 [LowRRP]	**4,916**	**0,398**	**3,659**	**5**	**1,482**
Cat2 [NoReserve]	7,446	0,561	14,502	7	2,965
Cat3 [BigReserve]	7,297	0,64	15,181	6	4,447

Synaptic Parameters

	Mean Synapse Surface (µm²)	+/- SEM	Mean SV Density (count/µm²)	+/- SEM
All	1,311	0,041	22,46	1,214
Cat1 [LowRRP]	1,318	0,059	17,182	1,358
Cat2 [NoReserve]	1,249	0,06	17,943	1,495
Cat3 [BigReserve]	1,384	0,083	**31,63**	**2,2**

150nm Vesicles

	Mean Svs#	+/- SEM	Variance	Median Svs#	MedianDeviation
All	4,583	0,267	7,65	4	2,965
Cat1 [LowRRP]	5,958	0,405	3,789	5,5	2,223
Cat2 [NoReserve]	**3,042**	**0,27**	**3,359**	**3**	**1,482**
Cat3 [BigReserve]	5,648	0,533	10,22	5	1,482

Reserve Vesicles

	Mean Svs#	+/- SEM	Variance	Median Svs#	MedianDeviation
All	2,597	0,133	7,731	2	2,965
Cat1 [LowRRP]	1,375	0,14	1,88	1	1,482
Cat2 [NoReserve]	1,281	0,11	2,287	1	1,482
Cat3 [BigReserve]	**5,06**	**0,25**	**9,205**	**5**	**2,96**

Supplementary table 1. Heterogeneous distributions of synaptic vesicules within a population of GC-to-MLI synapses.

Article 1. *"Ultrastructural molecular and functional heterogeneities of granule cell presynaptic terminals"*

GENERAL DISCUSSION

Multidimensional heterogeneity at facilitating granule cell terminals

During my PhD, I have described several levels of heterogeneity at granule cell presynaptic terminals:

i) Heterogeneity of the presynaptic machinery (Appendix #1): We have shown that releasable synaptic vesicles are segregated in two pools at granule cell-to-Purkinje cell synapses. A fully releasable pool that can be released by single action potential but that can be fully silenced under baseline activity (~2Hz), and a reluctant that can be recruited in tens of milliseconds by high-frequency activities. The fast recruitment of reluctant vesicle underlies part of the large facilitation of glutamate release during high-frequency stimulation. Heterogeneous populations of synaptic vesicles provide a dynamic filtering of information transfer giving significance to high-frequency information while filtering low frequencies.

ii) At the level of a population of unitary synapses: The profile of short-term plasticity is heterogeneous at individual granule cell synapses. Notably, facilitation during repetitive activity is observed in a subset of granule cell terminals. The heterogeneous functioning of induvidual granule-cell to molecular-layer interneuron synaptic terminals underlie intrinsic heterogeneities in different aspects: the ultrastructural organization of vesicular populations and the molecular composition of individual synapses.

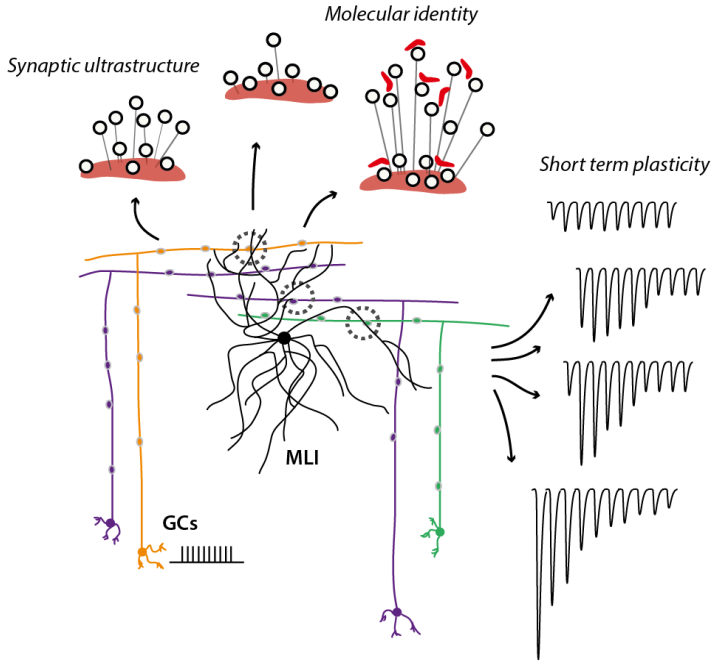

Multidimensional heterogeneity at granule cell presynaptic terminals.
We shed light on the elements explaining inter-synaptic heterogeneity of granule cell presynaptic terminals. The synapse-specific expression of a molecule can diversify the short term plasticity behaviors at granule cell boutons.

iii) At the network level: There is a heterogeneous drive of single molecular-layer interneuron by unitary granule cell synaptic terminals that relies on heterogeneous profiles of short term plasticity.

Finally, the expression of presynaptic molecules has consequences at the network level. The heterogeneous expression of a presynaptic molecule diversifies information coding at the network level. The generation of hypervariable presynaptic terminals enhance the temporal precision of information coding.

However, further experiments should require robust correlative methods in order to link ultrastructural, molecular and functional properties of individual synapses. For example, viral injections targeting granule cells could be used to invalidate SynapsinII transcripts at individual neurons and provide a specific somatic labeling (with a fluorescent marker for example) of the same neurons and/or tagging individual presynaptic vesicles. It would be of great interest to associate these parameters at the level of unitary connections, however, this requires to develop new tools for integrated analysis.

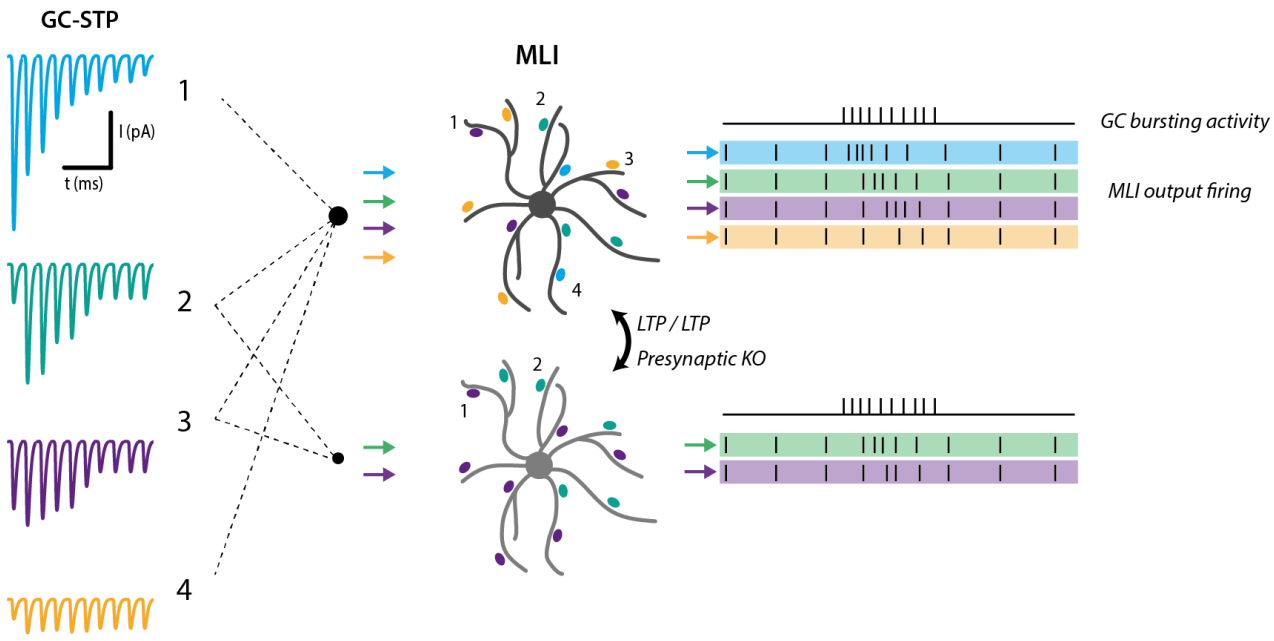

Hypervariable granule cell presynaptic terminals diversifies molecular layer interneuron output firing pattern. Different presynaptic terminals with different short term presynaptic plasticities can contact the same post-synaptic neuron. In the mouse model lacking SynapsinII, short term plasticities tend to homogeneity.

Presynaptic heterogeneity expands the coding abilities of the feedforward network

My experiments show that MLI are differentially entrained by specific short term plasticity during high-frequency stimulations. As the population of GC synapses display a wide range of short term plasticity behaviours, the output firing pattern of MLI relies on the nature of activated GC inputs.

Temporal coding of the feedforward network is determined at the level of unitary GC presynaptic terminals that introduce contact-specific delays into the feedforward network activation. Considering the importance of time delays for internal models of motor adjustments (Kistler, van Hemmen, & De Zeeuw, 2000; Mauk & Buonomano, 2004; Wolpert, Miall, & Kawato, 1998) synapse-specific diversification of short term plasticities has strong consequences onto learning and predictive functions of the cerebellum. Indeed, heterosynaptic long term plasticities between the different PC inputs are triggered within very short time windows (<100ms) (D'Angelo & De Zeeuw, 2009; Rahmati et al., 2014; Suvrathan, Payne, & Raymond, 2016). Also, the inhibitory control of PCs by molecular layer interneurons is essential for motor adjustments (Dizon & Khodakhah, 2011; Jelitai, Puggioni, Ishikawa, Rinaldi, & Duguid, 2016).

A similar mechanism of temporal coding has been characterized at the input stage of cerebellar cortex. GCs respond to multimodal sensorimotor inputs provided by different MFs displaying a modality-specific short term plasticity profile (Chabrol, Arenz, Wiechert, Margrie, & DiGregorio, 2015). The coincident activation of specific MF inputs provides input-dependent time delays of GC firing.

While direct inhibition between MLIs and PCs is time-invariant (Blot et al., 2016), we have shown that the "hypervariable" GC-MLI connection provides a potential source of information filtering and temporal adjustments for sensorimotor integration. Both MF-GC and GC-MLI terminals are critical elements in the computation of sensorimotor information by cerebellar cortex.

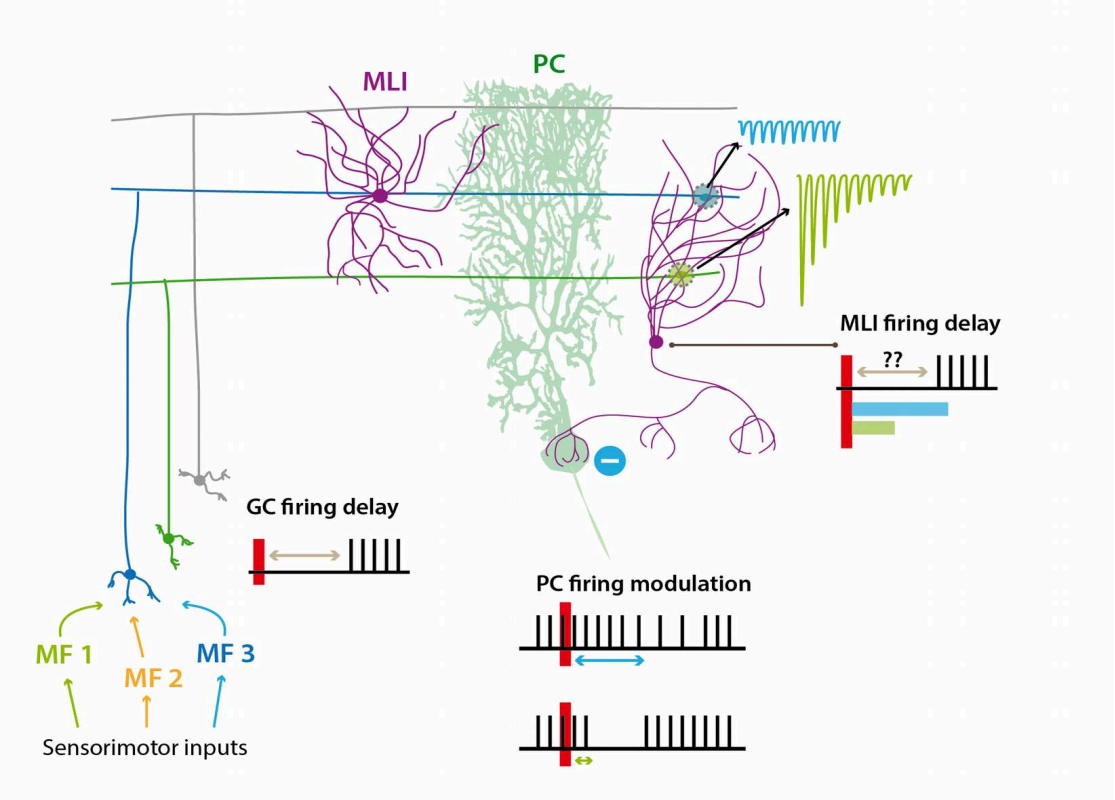

Presynaptic GC heterogeneity expands the coding abilities of the feedforward network.
Modality-specific coincident activation of MF inputs generate specific GC firing delays (Chabrol et al., 2015). Our results show that MLI firing delay depends on the unitary GC input which is being activated. Altogether, these results testify that STP sets temporal coding rules in the computation of sensorimotor information by cerebellar networks.

Metaplasticity of granule cell presynaptic terminals

We characterized functional diversity of short term plasticity at a population of GC-MLI synapses and identified SynapsinII as a candidate for molecular, ultrastructural and functional variability. Such a result was obtained with experimental conditions that prohibited the expression of various forms of post-synaptic and trans-synaptic long-term plasticities. In this condition, single synapses displayed a strong functional identity persisting for long periods of time. Since we observed a high variety of STP behaviours expressed at the level of unitary synapses, we could wonder to what extent experience can reshape presynaptic plasticity at the level of unitary contacts by affecting the proteome of unitary synapses.

Do single GC synaptic terminals display intrinsic long-lived short term plasticity behaviours?

Can single-synapse experience lead to different short term plasticity profiles depending on the environment and network activity?

In the cerebellar cortex, experience is prone to modify the properties of neurotransmitter release through persistent adjustments of synaptic weight. These mechanisms are often homeostatic compensations resulting from network adaptations (Marcaggi & Attwell, 2005; Soler-Llavina & Sabatini, 2006) or depend on the firing pattern experienced by a given terminal (Tran-Van-Minh, Abrahamsson, Cathala, & DiGregorio, 2016).

i) Influence of spatiotemporal integration onto GC neurotransmission.

Spatial segregation and temporal coincidence have much importance for network adjustments of synaptic weight as it has been shown at the granule cell presynaptic terminals where the mechanisms of long term adjustments of neurotransmission are often trans-synaptic. For example, spillover activates endocannabinoid retrograde signalling mediating long term depression of neurotransmitter release (Marcaggi & Attwell, 2005) and this phenomenon occurs if the activated GCs form beams of adjacent fibres while scattered synaptic contacts onto PC dendritic trees have no effect. Thus, the spatial pattern of GC activation will shape long term adjustments of synaptic weight (Wilms & Häusser, 2015).

ii) Rate-coding and temporal coding are critical parameters for GC presynaptic adjustments

GC synapses are also highly sensitive to the timing of the input stimuli. Indeed, presynaptic activation of NMDA receptors trigger synaptic potentiation in a frequency-dependant manner (Bouvier et al., 2016); bursts of action potentials at high frequencies (>33Hz) potentiate the synapse while low frequencies (10Hz) have no effect. In the case of heterosynaptic plasticity, the timing delay between PF and climbing fiber activation will determine the directionality of the protocol effect (potentiation or depression) (Suvrathan et al., 2016). In the same study, the authors have shown that a same induction protocol can elicit different long term modifications depending on the location of the GCs in the cerebellar cortex. Such an an inter-synaptic

variability in the sensitivity to induction protocols could be explained by differences in the molecular composition of unitary synapses.

iii) Control of LTP induction at GC-PC terminals by a sub-category of GC-MLI synapses [Hypothesis].

In a recent paper from the team (Appendix #3), we demonstrated that feedforward inhibition is essential for the induction of long term plasticities at GC-PC terminals (Binda et al., 2016). Ionotropic GABA receptors onto PC dendritic shaft cooperate with $CaV_{3.1}$ channels and $mGluR_1$ receptors onto PC spines in the induction of synaptic potentiation. Burst stimulations at 100Hz were used to induce synaptic potentiation through the activation of inhibitory MLI. Interestingly, LTP induction protocols are not efficient when the induction frequency is lower than 30~50Hz (unpublished personal observations).

Knowing the very high functional heterogeneity of STP profiles at the GC-MLI connections during similar bursts of evoked activity (100Hz), the time delay between MLI activation and direct PF excitation might vary depending on the STP profile of the GCs that are activated during the induction protocol. The effect of specific delays between MLI-PC inhibition and GC-PC excitation onto LTP induction are currently tested in the lab. In the case extremely short lags (<10~50ms) are mandatory for LTP induction, GC-PC LTP induction would be restricted to specific GC-MLI connections with specific STPs.

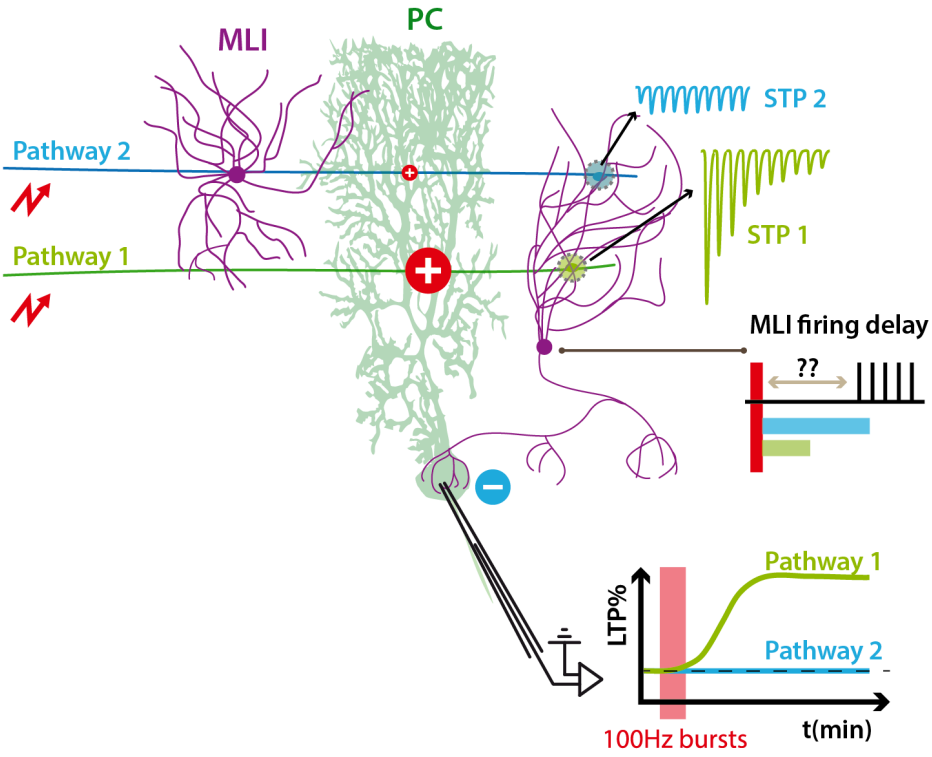

Possible interactions between GC-PC LTP induction and GC-MLI functional STP heterogeneity.
LTP induction following GC bursting activity requires he recruitment of feedforward inhibition (Binda et al., 2016). The induction of GC-PC LTP might require very precise time delays of MLI activation. Knowing that GC specific inputs induce various delays of MLI activation, we can expect that GC-PC potentiation is determined by the nature of GC-MLI presynaptic terminals.

Functional heterogeneity is shaped by the molecular machinery of presynaptic terminals

The adjustment of synaptic weight and STP properties is determined by an incredible number of interactions from different natures; homosynaptic, heterosynaptic and homeostatic and affect both presynaptic and post synaptic compartments (Sanes & Lichtman, 1999).

Presynaptic release parameters are tuned by physical or soluble signals provided by the post-synaptic neuron (Regehr, Carey, & Best, 2009). For example, the post-synaptic integrity can modulate presynaptic release probability through a trans-synaptic interaction of neuroligin/neurexin complexes (Futai et al., 2007). Interestingly, even if presynaptic terminals display an apparent inter-synaptic diversity of release probability, post-synaptic neurons tend to homogenize presynaptic parameters in a branch-specific manner (Branco, Staras, Darcy, & Goda, 2008). In this study, the activation of post-synaptic neurons normalizes release probability of the input synapses showing that presynaptic release parameters are under the control of network activity.

Because they contain the release sites of synaptic vesicles, active zones are a hot spot for neurotransmitter release adjustments. Indeed, in studies from the neuromuscular junction of Drosophilia and hippocampal cultures, experience can remodel the active zone by changing its size and molecular composition (Graf, Daniels, Burgess, Schwarz, & DiAntonio, 2009; Kittel & Heckmann, 2016; Matz, Gilyan, Kolar, McCarvill, & Krueger, 2010; Weyhersmüller, Hallermann, Wagner, & Eilers, 2011). involving several molecules such as Bassoon, Piccolo, RIM-BP. As the number of release sites is associated to an enhanced release probability (Branco, Marra, & Staras, 2010; Weyhersmüller et al., 2011), synaptic enhancement has been observed with a concomitant increase of the number of (N) and active zone size (Kittel & Heckmann, 2016; Matz et al., 2010; Weyhersmüller et al., 2011). Synaptic enhancement and depression can induce fast morphological modifications that are maintained over time by acting onto the number of neurotransmitter release sites (Doussau, Humeau, Benfenati, & Poulain, 2010; Goda & Stevens, 1998).

Presynaptic terminals are also subject to dynamical rearrangements of their molecular composition. Even if some molecules form stable components of the presynaptic machinery, others can diffuse from one synaptic varicosity to another inside the same axonal branch (Kalla et al., 2006; Star, Newton, & Murthy, 2005; Tsuriel et al., 2009). For example, the exchange rate of Bassoon from one synapse to another is very low (Tsuriel et al., 2009). While Bassoon and various elements from the cytomatrix are considered as stable elements, other molecules have more important rate of inter-synaptic diffusion. Rab3 and Munc13-1 (Kalla et al., 2006; Star et al., 2005) can be shuffled between presynaptic varicosities and the kinetics of exchange are enhanced by neuronal activity.

Following the same idea, populations of presynaptic vesicles can shift from one synapse to another (Staras & Branco, 2010) and contribute in a "superpool" of presynaptic vesicles both *in-vitro* (Staras et al., 2010) and *in-vivo* (Herzog et al., 2011) taking part in neurotransmission. As these mechanisms provide a synapse-to-synapse diffusion of vesicles accompanied by associated molecular interactors, these mechanisms might contribute to inter-synaptic heterogeneity through a redistribution of vesicle populations. Sharing vesicles between synapses might be the consequence of an homeostatic equalization of neurotransmission (Branco & Staras, 2009; Padamsey & Jeans, 2012) through pre/post-synaptic cross-talks and induce reallocations of synaptic vesicles depending on local molecular partners during neuronal activity (Fornasiero et al., 2012). In the latter study, the authors have characterized the importance of Synapsins in the activity-dependent shuffling of synaptic vesicles between synaptic varicosities. In the absence of Synapsin I,II,III genes; synaptic vesicles are dispersed inside the axonal compartment meaning that Synapsins are essential elements in the regulation of vesicular dynamics during neuronal activity.

SynapsinII tunes STP heterogeneity at GC terminals

Even if synaptic efficiency is highly related to the structural arrangement of the active zone, the number of release sites and release probability do not explain the time course of short term synaptic plasticity during repetitive activity especially during synaptic facilitation (Miki et al., 2016; Valera, Doussau, Poulain, Barbour, & Isope, 2012). Actin and Myosin dependant mechanisms provide the supply of replacement synaptic vesicles during sustained activation of granule cell terminals which promotes in-fine synaptic facilitation of glutamate release (Miki et al., 2016). Synapsins are presynaptic phosphoproteins involved in actin polymerization (Shupliakov, Haucke, & Pechstein, 2011), vesicular clustering (Hilfiker et al., 1999) and short term synaptic plasticity (Feliciano, Matos, Andrade, & Bykhovskaia, 2017; Medrihan et al., 2013). Therefore, they form very good candidates for the segregation of functional pools of synaptic vesicles and the regulation of short term synaptic plasticity.

Synapse-specific expression of Synapsin isoforms has already been characterized in other brain structures. The expression of various Synapsin isoforms is associated to heterogeneous behaviours of neurotransmitter release machinery at different neuronal systems, such as tectopulvinar, thalamic and cortical synaptic connections (Feliciano et al., 2017; Kielland, Erisir, Walaas, & Heggelund, 2006; Sudhof et al., 1989; Wei, Masterson, Petry, & Bickford, 2011). While SynapsinI is generally considered as a widespread isoform, SynapsinII tends to be synapse-specific (Feliciano et al., 2017; Sudhof et al., 1989). For now, synapse-specific expression of protein isoforms has always been associated to a precise category of presynaptic terminals (i.e. excitatory versus inhibitory terminals) (Gitler et al., 2004).

Here, I show that SynapsinII expression is not uniform within a unique category of synapses from the cerebellar cortex. SynapsinII is expressed at a fraction of GC presynaptic terminals generating functional inter-synaptic heterogeneity. Synapse-specific expression of SynapsinII modifies the cycle of synaptic vesicles and shapes short term synaptic plasticity exclusively at a subset of GC terminals by increasing the number of release-ready vesicles at the active zone and limiting exocytosis during short bursts of high-frequency eEPSCs. By studying short term plasticity of unitary synapses in a mouse model lacking SynapsinII, we observed a huge reduction of inter-synaptic heterogeneity both in ultrastructural and functional aspects.

Alternative spicing of SynapsinII generates different variants; SynapsinIIa and IIb. Our functional and ultrastructural data was not specific as the deletion of SynapsinII impaired the expression of both IIa and IIb variants. Also, we used pan-Syn2 antibodies for our immunohistochemistry and electron microscopy assays. SynapsinII variants show distinct patterns of spatial and developmental expression of their respective mRNA (Zurmöhle, Herms, Schlingensiepen, Brysch, & Schlingensiepen, 1996) and distinct functional contributions to STP (Gitler, Cheng, Greengard, & Augustine, 2008), further experiments need to assess the expression of both SynapsinII variants in the physiology of cerebellar cortex.

Is inter-synaptic heterogeneity of molecular markers such as SynapsinII the expression of long term plasticities, or is it the privilege of a subcategory of synapses expressing neurotransmitter release behaviours in a hard-wired fashion? Further studies need to take in account the interactions between short term and long term plasticity. SynapsinII transcription is promoted and regulated by activity (Chin, Li, & Greengard, 1994; Skoblenick et al., 2010), heterogeneously expressed proteins such as SynapsinII could play a central function in the modulation of short term plasticity over specific periods of time depending on network activity and brain experience.

Questioning the functional organization of granule cell presynaptic inputs in the cerebellar cortex

My work shows that single MLI are contacted by different GC terminals displaying a large panel of STP behaviours. This is in total contradiction with previous works showing that target dependence rules functional connectivity at GC presynaptic terminals (Bao, Reim, & Sakaba, 2010). For now, the reasons of these surprising differences remain unknown. However, based on personal results, I deducted that experimental protocols can bias observations towards target-dependence.

i) Compound stimulation of PF beams (5~10 contacts) connecting post-synaptic neurons displayed beam-to-beam variability. In most of the cases, the post synaptic cell received both facilitating and depressing signals. This was independent from their morphological identity (Basket or stellate) neither from their position in the depth of molecular layer. The latter result is fundamental because it shows that presynaptic STP is not biased by fiber conductivity issues (Wyatt, Tanapat, & Wang, 2005).

ii) Target-dependence appears when GCs (and not PFs) are stimulated at high intensities (~10 simultaneous contacts) and when GCs are in the same microzone than the recorded neuron. In that case only, interneurons recorded next to the pia mater received facilitating inputs and the ones next to PCs endowed a lower facilitation.
Even in these conditions, STP of presynaptic inputs was not associated with the presence of Basket connections onto Purkinje cell soma (seen under 2-Photon microscopy).
Thus, I suggest that target-dependence is an exceptional case favoured by extreme experimental conditions.

iii) It is true that in the same experimental conditions (beam stimulation of parallel fibers), PCs receive presynaptic contacts characterized by a stronger facilitation sustainability than GC-MLI synapses. I have also observed STP variations during sequential beam stimulation and double-patch recordings at the GC-PC. In these conditions, I was able to modify STP of GC terminals with high-frequency stimuli. Thus, I supposed that STP might be influenced by post-synaptic targets but can be easily tuned by experience.

Previously in the team, we have shown that a stereotyped pattern of inter-modular GC connections (Valera et al., 2016) meaning that the active contacts onto a given neuron (Interneurons or PCs) come from very specific microzones from the same lobule. Even if this pattern is *hard-wired* between animals, it is

possible to switch connections on with reactivation protocols.

The next step is to link the functional connectivity map with inter-synaptic heterogeneity of GC terminals.

Is there a stereotyped mapping for GC STP?

Further experiments will be needed to test the mutual relationships between individual granule cells and individual molecular layer interneurons.

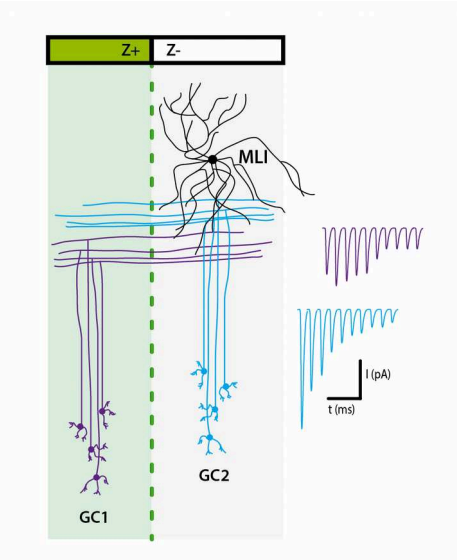

Inter-modular short term plasticity
Hypothetic case of figure here the presynaptic plasticity of granule cell presynaptic terminals rely on the mutual position of the presynaptic granule cell, and the post synaptic interneuron replaced inside the ZebrinII band pattern.

Z+: ZebrinII positive band
Z-: ZebrinII negative band

References

Abrahamsson, T., Cathala, L., Matsui, K., Shigemoto, R., and DiGregorio, D.A. (2012). Thin Dendrites of Cerebellar Interneurons Confer Sublinear Synaptic Integration and a Gradient of Short-Term Plasticity. Neuron *73*, 1159–1172.

Albus, J.S. (1971). A theory of cerebellar function. Math. Biosci. *10*, 25–61.

Alcami, P., and Marty, A. (2013). Estimating functional connectivity in an electrically coupled interneuron network. Proc. Natl. Acad. Sci. U. S. A. *110*, E4798-807.

Anderson, D., Engbers, J.D.T., Heath, N.C., Bartoletti, T.M., Mehaffey, W.H., Zamponi, G.W., and Turner, R.W. (2013). The Cav3–Kv4 Complex Acts as a Calcium Sensor to Maintain Inhibitory Charge Transfer during Extracellular Calcium Fluctuations. J. Neurosci. *33*.

Apps, R., and Hawkes, R. (2009). Cerebellar cortical organization: a one-map hypothesis. Nat. Rev. Neurosci. *10*, 670–681.

Arenz, A., Bracey, E.F., and Margrie, T.W. (2009). Sensory representations in cerebellar granule cells. Curr. Opin. Neurobiol. *19*, 445–451.

Atluri, P.P., and Regehr, W.G. (1996). Determinants of the Time Course of Facilitation at the Granule Cell to Purkinje Cell Synapse. J. Neurosci. *16*.

Atwood, H.L., and Karunanithi, S. (2002). Diversification of synaptic strength: presynaptic elements. Nat. Rev. Neurosci. *3*, 497–516.

Bähler, M., and Greengard, P. (1987). Synapsin I bundles F-actin in a phosphorylation-dependent manner. Nature *326*, 704–707.

Bao, J., Reim, K., and Sakaba, T. (2010). Target-dependent feedforward inhibition mediated by short-term synaptic plasticity in the cerebellum. J. Neurosci. *30*, 8171–8179.

Bastian, A.J. (2006). Learning to predict the future: the cerebellum adapts feedforward movement control. Curr. Opin. Neurobiol. *16*, 645–649.

Bastianelli, E. (2003). Distribution of calcium-binding proteins in the cerebellum. The Cerebellum *2*, 242–262.

Bender, V.A., Pugh, J.R., and Jahr, C.E. (2009). Presynaptically expressed long-term potentiation increases multivesicular release at parallel fiber synapses. J. Neurosci. *29*, 10974–10978.

Binda, F., Dorgans, K., Reibel, S., Sakimura, K., Kano, M., Poulain, B., and Isope, P. (2016). Inhibition promotes long-Term potentiation at cerebellar excitatory synapses. Sci. Rep. *6*.

Blackman, A. V., Abrahamsson, T., Costa, R.P., Lalanne, T., and Sjöström, P.J. (2013). Target-cell-specific short-term plasticity in local circuits. Front. Synaptic Neurosci. *5*, 11.

Blot, A., and Barbour, B. (2014). Ultra-rapid axon-axon ephaptic inhibition of cerebellar Purkinje cells by the pinceau. Nat. Neurosci. *17*, 289–295.

Blot, A., de Solages, C., Ostojic, S., Szapiro, G., Hakim, V., and Léna, C. (2016). Time-invariant feed-forward

inhibition of Purkinje cells in the cerebellar cortex *in vivo*. J. Physiol. *594*, 2729–2749.

Bornschein, G., Arendt, O., Hallermann, S., Brachtendorf, S., Eilers, J., and Schmidt, H. (2013). Paired-pulse facilitation at recurrent Purkinje neuron synapses is independent of calbindin and parvalbumin during high-frequency activation. J. Physiol. *591*, 3355–3370.

Bouvier, G., Higgins, D., Spolidoro, M., Carrel, D., Mathieu, B., Léna, C., Dieudonné, S., Barbour, B., Brunel, N., and Casado, M. (2016). Burst-Dependent Bidirectional Plasticity in the Cerebellum Is Driven by Presynaptic NMDA Receptors. Cell Rep. *15*, 104–116.

Brachtendorf, S., Eilers, J., and Schmidt, H. (2015). A use-dependent increase in release sites drives facilitation at calretinin-deficient cerebellar parallel-fiber synapses. Front. Cell. Neurosci. *9*, 27.

Branco, T., and Staras, K. (2009). The probability of neurotransmitter release: variability and feedback control at single synapses. Nat. Rev. Neurosci. *10*, 373–383.

Branco, T., Staras, K., Darcy, K.J., and Goda, Y. (2008). Local dendritic activity sets release probability at hippocampal synapses. Neuron *59*, 475–485.

Branco, T., Marra, V., and Staras, K. (2010). Examining size–strength relationships at hippocampal synapses using an ultrastructural measurement of synaptic release probability. J. Struct. Biol. *172*, 203–210.

Brenowitz, S.D., and Regehr, W.G. (2007). Reliability and heterogeneity of calcium signaling at single presynaptic boutons of cerebellar granule cells. J. Neurosci. *27*, 7888–7898.

Brunel, N., Hakim, V., Isope, P., Nadal, J.-P., Barbour, B., Wenthold, R.J., and Malinow, R. (2004). Optimal information storage and the distribution of synaptic weights: perceptron versus Purkinje cell. Neuron *43*, 745–757.

Bykhovskaia, M. (2011). Synapsin regulation of vesicle organization and functional pools. Semin. Cell Dev. Biol. *22*, 387–392.

Candiani, S., Moronti, L., Pennati, R., De Bernardi, F., Benfenati, F., and Pestarino, M. (2010). The synapsin gene family in basal chordates: evolutionary perspectives in metazoans. BMC Evol. Biol. *10*, 32.

Carter, A.G., and Regehr, W.G. (2002). Quantal events shape cerebellar interneuron firing. Nat. Neurosci. *5*, 1309–1318.

Cesca, F., Baldelli, P., Valtorta, F., and Benfenati, F. (2010). The synapsins: key actors of synapse function and plasticity. Prog. Neurobiol. *91*, 313–348.

Chabrol, F.P., Arenz, A., Wiechert, M.T., Margrie, T.W., and DiGregorio, D.A. (2015). Synaptic diversity enables temporal coding of coincident multisensory inputs in single neurons. Nat. Neurosci. *18*, 718–727.

Chadderton, P., Margrie, T.W., and Häusser, M. (2004). Integration of quanta in cerebellar granule cells during sensory processing. Nature *428*, 856–860.

Chamberland, S., and Tóth, K. (2016). Functionally heterogeneous synaptic vesicle pools support diverse synaptic signalling. J. Physiol. *594*, 825–835.

Chan-Palay, V., and Palay, S.L. (1972). The stellate cells of the rat's cerebellar cortex. Zeitschrift Anat. Und Entwicklungsgeschichte *136*, 224–248.

Chen, C., Arai, I., Satterfield, R., Young, S.M., and Jonas, P. (2017). Synaptotagmin 2 Is the Fast Ca(2+) Sensor at a Central Inhibitory Synapse. Cell Rep. *18*, 723–736.

Chen, S., Augustine, G.J., and Chadderton, P. (2016). The cerebellum linearly encodes whisker position during voluntary movement. Elife *5*, e10509.

Chilcote, T.J., Siow, Y.L., Schaeffer, E., Greengard, P., and Thiel, G. (1994). Synapsin IIa bundles actin filaments. J. Neurochem. *63*, 1568–1571.

Chin, L.S., Li, L., and Greengard, P. (1994). Neuron-specific expression of the synapsin II gene is directed by a specific core promoter and upstream regulatory elements. J. Biol. Chem. *269*, 18507–18513.

Chu, C.-P., Bing, Y.-H., and Qiu, D.-L. (2011). Sensory stimulus evokes inhibition rather than excitation in cerebellar Purkinje cells in vivo in mice. Neurosci. Lett. *487*, 182–186.

Chu, C.-P., Bing, Y.-H., Liu, H., and Qiu, D.-L. (2012). Roles of Molecular Layer Interneurons in Sensory Information Processing in Mouse Cerebellar Cortex Crus II In Vivo. PLoS One *7*, e37031.

Collin, T., Chat, M., Lucas, M.G., Moreno, H., Racay, P., Schwaller, B., Marty, A., and Llano, I. (2005). Developmental Changes in Parvalbumin Regulate Presynaptic Ca2+ Signaling. J. Neurosci. *25*, 96–107.

Crowley, J.J., Carter, A.G., and Regehr, W.G. (2007). Fast Vesicle Replenishment and Rapid Recovery from Desensitization at a Single Synaptic Release Site. J. Neurosci. *27*, 5448–5460.

D'Angelo, E., and De Zeeuw, C.I. (2009). Timing and plasticity in the cerebellum: focus on the granular layer. Trends Neurosci. *32*, 30–40.

Debanne, D., Guérineau, N.C., Gähwiler, B.H., and Thompson, S.M. (1996). Paired-pulse facilitation and depression at unitary synapses in rat hippocampus: quantal fluctuation affects subsequent release. J. Physiol. *491 (Pt 1)*, 163–176.

Delvendahl, I., Straub, I., and Hallermann, S. (2015). Dendritic patch-clamp recordings from cerebellar granule cells demonstrate electrotonic compactness. Front. Cell. Neurosci. *9*, 93.

DiGregorio, D.A., Nusser, Z., and Silver, R.A. (2002). Spillover of glutamate onto synaptic AMPA receptors enhances fast transmission at a cerebellar synapse. Neuron *35*, 521–533.

Dittman, J.S., Kreitzer, a C., and Regehr, W.G. (2000). Interplay between facilitation, depression, and residual calcium at three presynaptic terminals. J. Neurosci. *20*, 1374–1385.

Dizon, M.J., and Khodakhah, K. (2011). The Role of Interneurons in Shaping Purkinje Cell Responses in the Cerebellar Cortex. J. Neurosci. *31*.

Dolphin, A.C., and Greengard, P. (1981). Presence of protein I, a phosphoprotein associated with synaptic vesicles, in cerebellar granule cells. J. Neurochem. *36*, 1627–1631.

Doussau, F., Humeau, Y., Benfenati, F., and Poulain, B. (2010). A novel form of presynaptic plasticity based on the fast reactivation of release sites switched off during low-frequency depression. J. Neurosci. *30*, 16679–16691.

Dugue, G.P. (2005). Target-Dependent Use of Coreleased Inhibitory Transmitters at Central Synapses. J. Neurosci. *25*, 6490–6498.

Dulubova, I., Lou, X., Lu, J., Huryeva, I., Alam, A., Schneggenburger, R., Südhof, T.C., and Rizo, J. (2005). A Munc13/RIM/Rab3 tripartite complex: from priming to plasticity? EMBO J. *24*, 2839–2850.

Dykstra, S., Engbers, J.D.T., Bartoletti, T.M., and Turner, R.W. (2016). Determinants of rebound burst responses in rat cerebellar nuclear neurons to physiological stimuli. J. Physiol. *594*, 985–1003.

Eccles, J.C., Llinàs, R., and Sasaki, K. (1966a). Parallel fibre stimulation and the responses induced thereby in the Purkinje cells of the cerebellum. Exp. Brain Res. *1*.

Eccles, J.C., Llinàs, R., and Sasaki, K. (1966b). The inhibitory interneurones within the cerebellar cortex. Exp. Brain Res. *1*.

Eccles, J.C., Ito, M., and Szentágothai, J. (1967). The Cerebellum as a Neuronal Machine (Springer Berlin Heidelberg).

Eggermann, E., Bucurenciu, I., Goswami, S.P., and Jonas, P. (2012). Nanodomain coupling between Ca^{2+} channels and sensors of exocytosis at fast mammalian synapses. Nat. Rev. Neurosci. *13*, 7–21.

Espinosa, J.S., and Luo, L. (2008). Timing neurogenesis and differentiation: insights from quantitative clonal analyses of cerebellar granule cells. J. Neurosci. *28*, 2301–2312.

Feliciano, P., Matos, H., Andrade, R., and Bykhovskaia, M. (2017). Synapsin II Regulation of GABAergic Synaptic Transmission Is Dependent on Interneuron Subtype. J. Neurosci. *37*, 1757–1771.

Fogelson, A.L., and Zucker, R.S. (1985). Presynaptic calcium diffusion from various arrays of single channels. Implications for transmitter release and synaptic facilitation. Biophys. J. *48*, 1003–1017.

Fornasiero, E.F., Raimondi, A., Guarnieri, F.C., Orlando, M., Fesce, R., Benfenati, F., and Valtorta, F. (2012). Synapsins contribute to the dynamic spatial organization of synaptic vesicles in an activity-dependent manner. J. Neurosci. *32*, 12214–12227.

Foster, K.A., Crowley, J.J., and Regehr, W.G. (2005). The influence of multivesicular release and postsynaptic receptor saturation on transmission at granule cell to Purkinje cell synapses. J. Neurosci. *25*, 11655–11665.

Franconville, R., Revet, G., Astorga, G., Schwaller, B., and Llano, I. (2011). Somatic calcium level reports integrated spiking activity of cerebellar interneurons in vitro and in vivo. J. Neurophysiol. *106*, 1793–1805.

Fujita, M. (1982). Adaptive filter model of the cerebellum. Biol. Cybern. *45*, 195–206.

Futai, K., Kim, M.J., Hashikawa, T., Scheiffele, P., Sheng, M., and Hayashi, Y. (2007). Retrograde modulation of presynaptic release probability through signaling mediated by PSD-95-neuroligin. Nat. Neurosci. *10*, 186–195.

Gabbiani, F., Midtgaard, J., and Knöpfel, T. (1994). Synaptic integration in a model of cerebellar granule cells. J. Neurophysiol. *72*, 999–1009.

Garner, C.C., Kindler, S., and Gundelfinger, E.D. (2000). Molecular determinants of presynaptic active zones. Curr. Opin. Neurobiol. *10*, 321–327.

Gelman, S. (2011). Heterogeneous release probabilities and activity-dependent short-term synaptic depression. Commun. Integr. Biol. *4*, 603–605.

Giovannucci, A., Badura, A., Deverett, B., Najafi, F., Pereira, T.D., Gao, Z., Ozden, I., Kloth, A.D., Pnevmatikakis,

E., Paninski, L., et al. (2017). Cerebellar granule cells acquire a widespread predictive feedback signal during motor learning. Nat. Neurosci. *20*, 727–734.

Gitler, D., Xu, Y., Kao, H.-T., Lin, D., Lim, S., Feng, J., Greengard, P., and Augustine, G.J. (2004a). Molecular determinants of synapsin targeting to presynaptic terminals. J. Neurosci. *24*, 3711–3720.

Gitler, D., Takagishi, Y., Feng, J., Ren, Y., Rodriguiz, R.M., Wetsel, W.C., Greengard, P., and Augustine, G.J. (2004b). Different presynaptic roles of synapsins at excitatory and inhibitory synapses. J. Neurosci. *24*, 11368–11380.

Gitler, D., Cheng, Q., Greengard, P., and Augustine, G.J. (2008). Synapsin IIa controls the reserve pool of glutamatergic synaptic vesicles. J. Neurosci. *28*, 10835–10843.

Goda, Y., and Stevens, C.F. (1998). Readily releasable pool size changes associated with long term depression. Neurobiology *95*, 1283–1288.

Goodsell, D.S. (2009). Neuromuscular synapse. Biochem. Mol. Biol. Educ. *37*, 204–210.

Goussakov, I. V, Fink, K., Elger, C.E., and Beck, H. (2000). Metaplasticity of mossy fiber synaptic transmission involves altered release probability. J. Neurosci. *20*, 3434–3441.

Graf, E.R., Daniels, R.W., Burgess, R.W., Schwarz, T.L., and DiAntonio, A. (2009). Rab3 Dynamically Controls Protein Composition at Active Zones. Neuron *64*, 663–677.

Gundappa-Sulur, G., De Schutter, E., and Bower, J.M. (1999). Ascending granule cell axon: an important component of cerebellar cortical circuitry. J. Comp. Neurol. *408*, 580–596.

Hallermann, S., and Silver, R.A. (2013). Sustaining rapid vesicular release at active zones: potential roles for vesicle tethering. Trends Neurosci. *36*, 185–194.

Hallermann, S., Fejtova, A., Schmidt, H., Weyhersmüller, A., Silver, R.A., Gundelfinger, E.D., and Eilers, J. (2010). Bassoon speeds vesicle reloading at a central excitatory synapse. Neuron *68*, 710–723.

Hamori, J. (1975). Cerebellar cortex, cytology and organization. Electroencephalogr. Clin. Neurophysiol. *38*, 222.

Hanse, E., and Gustafsson, B. (2001a). Vesicle release probability and pre-primed pool at glutamatergic synapses in area CA1 of the rat neonatal hippocampus. J. Physiol. *531*, 481–493.

Hanse, E., and Gustafsson, B. (2001b). Factors explaining heterogeneity in short-term synaptic dynamics of hippocampal glutamatergic synapses in the neonatal rat. J. Physiol. *537*, 141–149.

Hanse, E., and Gustafsson, B. (2001c). Quantal variability at glutamatergic synapses in area CA1 of the rat neonatal hippocampus. J. Physiol. *531*, 467–480.

Harvey, R.J., and Napper, R.M.A. (1988). Quantitative study of granule and Purkinje cells in the cerebellar cortex of the rat. J. Comp. Neurol. *274*, 151–157.

Häusser, M., Clark, B.A., Price, M.T., Olney, J.W., Steinbach, J.H., Seal, A.J., Henley, J.M., Jane, D.E., Watkins, J.C., and Collingridge, G.L. (1997). Tonic synaptic inhibition modulates neuronal output pattern and spatiotemporal synaptic integration. Neuron *19*, 665–678.

Herzog, E., Nadrigny, F., Silm, K., Biesemann, C., Helling, I., Bersot, T., Steffens, H., Schwartzmann, R., Nagerl, U.

V., El Mestikawy, S., et al. (2011). In Vivo Imaging of Intersynaptic Vesicle Exchange Using VGLUT1Venus Knock-In Mice. J. Neurosci. *31*, 15544–15559.

Hilfiker, S., Pieribone, V.A., Czernik, A.J., Kao, H.T., Augustine, G.J., and Greengard, P. (1999). Synapsins as regulators of neurotransmitter release. Philos. Trans. R. Soc. Lond. B. Biol. Sci. *354*, 269–279.

Hioki, H., Fujiyama, F., Taki, K., Tomioka, R., Furuta, T., Tamamaki, N., and Kaneko, T. (2003). Differential distribution of vesicular glutamate transporters in the rat cerebellar cortex. Neuroscience *117*, 1–6.

Huang, C., Wang, L., and Huang, R.H. (2006). Cerebellar granule cell: ascending axon and parallel fiber. Eur. J. Neurosci. *23*, 1731–1737.

Huang, C.-C., Sugino, K., Shima, Y., Guo, C., Bai, S., Mensh, B.D., Nelson, S.B., and Hantman, A.W. (2013). Convergence of pontine and proprioceptive streams onto multimodal cerebellar granule cells. Elife *2*.

Huang, Z.J., Di Cristo, G., and Ango, F. (2007). Development of GABA innervation in the cerebral and cerebellar cortices. Nat. Rev. Neurosci. *8*, 673–686.

Humeau, Y., Doussau, F., Vitiello, F., Greengard, P., Benfenati, F., and Poulain, B. (2001). Synapsin Controls Both Reserve and Releasable Synaptic Vesicle Pools during Neuronal Activity and Short-Term Plasticity in Aplysia. J. Neurosci. *21*, 4195–4206.

Hunter, J.D., and Milton, J.G. (2001). Synaptic heterogeneity and stimulus-induced modulation of depression in central synapses. J. Neurosci. *21*, 5781–5793.

Isaacson, J.S., and Scanziani, M. (2011). How inhibition shapes cortical activity. Neuron *72*, 231–243.

Ishikawa, T., Shimuta, M., and Hä Usser, M. (2015). Multimodal sensory integration in single cerebellar granule cells in vivo.

Ishiyama, S., Schmidt, H., Cooper, B.H., Brose, N., and Eilers, J. (2014). Munc13-3 Superprimes Synaptic Vesicles at Granule Cell-to-Basket Cell Synapses in the Mouse Cerebellum. J. Neurosci. *34*, 14687–14696.

Isope, P., and Barbour, B. (2002). Properties of unitary granule cell-Purkinje cell synapses in adult rat cerebellar slices. J. Neurosci. *22*, 9668–9678.

Ito, M. Cerebellar circuitry as a neuronal machine. Prog. Neurobiol. *78*, 272–303.

Iwasaki, S., Momiyama, A., Uchitel, O.D., and Takahashi, T. (2000). Developmental changes in calcium channel types mediating central synaptic transmission. J. Neurosci. *20*, 59–65.

Jackman, S.L., and Regehr, W.G. (2017). The Mechanisms and Functions of Synaptic Facilitation. Neuron *94*, 447–464.

Jelitai, M., Puggioni, P., Ishikawa, T., Rinaldi, A., and Duguid, I. (2016). Dendritic excitation-inhibition balance shapes cerebellar output during motor behaviour. Nat. Commun. *7*, 13722.

Jörntell, H., and Ekerot, C.-F. (2006). Properties of somatosensory synaptic integration in cerebellar granule cells in vivo. J. Neurosci. *26*, 11786–11797.

Jung, J.H., Szule, J.A., Marshall, R.M., and McMahan, U.J. (2016). Variable priming of a docked synaptic vesicle. Proc. Natl. Acad. Sci. *113*, E1098–E1107.

Kaeser, P.S., Deng, L., Wang, Y., Dulubova, I., Liu, X., Rizo, J., and Südhof, T.C. (2011). RIM proteins tether Ca2+

channels to presynaptic active zones via a direct PDZ-domain interaction. Cell *144*, 282–295.

Kalla, S., Stern, M., Basu, J., Varoqueaux, F., Reim, K., Rosenmund, C., Ziv, N.E., and Brose, N. (2006). Molecular Dynamics of a Presynaptic Active Zone Protein Studied in Munc13-1-Enhanced Yellow Fluorescent Protein Knock-In Mutant Mice. J. Neurosci. *26*, 13054–13066.

Kao, H.T., Porton, B., Hilfiker, S., Stefani, G., Pieribone, V.A., DeSalle, R., and Greengard, P. (1999). Molecular evolution of the synapsin gene family. J. Exp. Zool. *285*, 360–377.

Kielland, A., Erisir, A., Walaas, S.I., and Heggelund, P. (2006). Synapsin utilization differs among functional classes of synapses on thalamocortical cells. J. Neurosci. *26*, 5786–5793.

Kistler, W.M., van Hemmen, J.L., and De Zeeuw, C.I. (2000). Time window control: a model for cerebellar function based on synchronization, reverberation, and time slicing. Prog. Brain Res. *124*, 275–297.

Kittel, R.J., and Heckmann, M. (2016). Synaptic Vesicle Proteins and Active Zone Plasticity. Front. Synaptic Neurosci. *8*, 8.

Koester, H.J., and Johnston, D. (2005). Target cell-dependent normalization of transmitter release at neocortical synapses. Science *308*, 863–866.

Koester, H.J., and Sakmann, B. (2000). Calcium dynamics associated with action potentials in single nerve terminals of pyramidal cells in layer 2/3 of the young rat neocortex. J. Physiol. *529 Pt 3*, 625–646.

Korogod, N., Petersen, C.C.H., and Knott, G.W. (2015). Ultrastructural analysis of adult mouse neocortex comparing aldehyde perfusion with cryo fixation. Elife *4*.

Kreitzer, A.C., Carter, A.G., Regehr, W.G., Herkenham, M., Bonner, T.I., Deutsch, D.G., Walker, J.M., Imperato, A., Pedrazzini, T., Roques, B.P., et al. (2002). Inhibition of interneuron firing extends the spread of endocannabinoid signaling in the cerebellum. Neuron *34*, 787–796.

Kulik, A., Nakadate, K., Hagiwara, A., Fukazawa, Y., Lujan, R., Saito, H., Suzuki, N., Futatsugi, A., Mikoshiba, K., Frotscher, M., et al. (2004). Immunocytochemical localization of the alpha1A subunit of the P/Q-type calcium channel in the rat cerebellum. Eur. J. Neurosci. *19*, 2169–2178.

Larsen, R.S., and Sjöström, P.J. (2015). Synapse-type-specific plasticity in local circuits. Curr. Opin. Neurobiol. *35*, 127–135.

Laßek, M., Weingarten, J., and Volknandt, W. (2014). The Proteome of the Murine Presynaptic Active Zone. Proteomes *2*, 243–257.

Li, L., Chin, L.-S., Greengard, P., Copeland, N.G., Gilbert, D.J., and Jenkins, N.A. (1995). Localization of the Synapsin II (SYN2) Gene to Human Chromosome 3 and Mouse Chromosome 6. Genomics *28*, 365–366.

Li, L., Tasic, B., Micheva, K.D., Ivanov, V.M., Spletter, M.L., Smith, S.J., and Luo, L. (2010). Visualizing the distribution of synapses from individual neurons in the mouse brain. PLoS One *5*, e11503.

Liao, D., Hessler, N.A., and Malinow, R. (1995). Activation of postsynaptically silent synapses during pairing-induced LTP in CA1 region of hippocampal slice. Nature *375*, 400–404.

Limbach, C., Laue, M.M., Wang, X., Hu, B., Thiede, N., Hultqvist, G., and Kilimann, M.W. (2011). Molecular in situ topology of Aczonin/Piccolo and associated proteins at the mammalian neurotransmitter release site. Proc. Natl. Acad. Sci. *108*, E392–E401.

Liu, Q.A., and Shio, H. (2008). Mitochondrial Morphogenesis, Dendrite Development, and Synapse Formation in Cerebellum Require both Bcl-w and the Glutamate Receptor δ2. PLoS Genet. *4*, e1000097.

Llano, I., and Gerschenfeld, H.M. (1993). Inhibitory synaptic currents in stellate cells of rat cerebellar slices. J. Physiol. *468*, 177–200.

Llano, I., Tan, Y.P., and Caputo, C. (1997). Spatial heterogeneity of intracellular Ca2+ signals in axons of basket cells from rat cerebellar slices. J. Physiol. 509–519.

Longair, M.H., Baker, D.A., and Armstrong, J.D. (2011). Simple Neurite Tracer: open source software for reconstruction, visualization and analysis of neuronal processes. Bioinformatics *27*, 2453–2454.

Malagon, G., Miki, T., Llano, I., Neher, E., and Marty, A. (2016). Counting Vesicular Release Events Reveals Binomial Release Statistics at Single Glutamatergic Synapses. J. Neurosci. *36*, 4010–4025.

Mann-Metzer, P., and Yarom, Y. (1999). Electrotonic Coupling Interacts with Intrinsic Properties to Generate Synchronized Activity in Cerebellar Networks of Inhibitory Interneurons. J. Neurosci. *19*.

Marcaggi, P., and Attwell, D. (2005). Endocannabinoid signaling depends on the spatial pattern of synapse activation. Nat. Neurosci. *8*, 776–781.

Marcaggi, P., and Attwell, D. (2007). Short- and long-term depression of rat cerebellar parallel fibre synaptic transmission mediated by synaptic crosstalk. J. Physiol. *578*, 545–550.

Markram, H., and Tsodyks, M. (1996a). Redistribution of synaptic efficacy between neocortical pyramidal neurons. Nature *382*, 807–810.

Markram, H., and Tsodyks, M. (1996b). Redistribution of synaptic efficacy: A mechanism to generate infinite synaptic input diversity from a homogenous population of neurons without changing absolute synaptic efficacies. J. Physiol. *90*, 229–232.

Markram, H., Wang, Y., and Tsodyks, M. (1998). Differential signaling via the same axon of neocortical pyramidal neurons. Proc. Natl. Acad. Sci. U. S. A. *95*, 5323–5328.

Marr, D. (1969). A theory of cerebellar cortex. J. Physiol. *202*, 437–470.

Maschi, D., and Klyachko, V.A. (2017). Spatiotemporal Regulation of Synaptic Vesicle Fusion Sites in Central Synapses. Neuron *94*.

Matz, J., Gilyan, A., Kolar, A., McCarvill, T., and Krueger, S.R. (2010). Rapid structural alterations of the active zone lead to sustained changes in neurotransmitter release. Proc. Natl. Acad. Sci. U. S. A. *107*, 8836–8841.

Mauk, M.D., and Buonomano, D. V. (2004). The neuronal basis of temporal processing. Annu. Rev. Neurosci. *27*, 307–340.

Medrihan, L., Cesca, F., Raimondi, A., Lignani, G., Baldelli, P., and Benfenati, F. (2013). Synapsin II desynchronizes neurotransmitter release at inhibitory synapses by interacting with presynaptic calcium channels. Nat. Commun. *4*, 1512.

Medrihan, L., Ferrea, E., Greco, B., Baldelli, P., and Benfenati, F. (2014). Asynchronous GABA Release Is a Key Determinant of Tonic Inhibition and Controls Neuronal Excitability: A Study in the Synapsin II-/- Mouse. Cereb. Cortex bhu141-.

Mejia-Gervacio, S., Collin, T., Pouzat, C., Tan, Y.P., Llano, I., and Marty, A. (2007). Axonal Speeding: Shaping Synaptic Potentials in Small Neurons by the Axonal Membrane Compartment. Neuron *53*, 843–855.

Midtgaard, J. (1992). Membrane properties and synaptic responses of Golgi cells and stellate cells in the turtle cerebellum in vitro. J. Physiol. *457*, 329–354.

Miki, T., Malagon, G., Pulido, C., Llano, I., Neher, E., and Marty, A. (2016). Actin- and Myosin-Dependent Vesicle Loading of Presynaptic Docking Sites Prior to Exocytosis. Neuron *91*, 808–823.

Miki, T., Kaufmann, W.A., Malagon, G., Gomez, L., Tabuchi, K., Watanabe, M., Shigemoto, R., and Marty, A. (2017). Numbers of presynaptic Ca^{2+} channel clusters match those of functionally defined vesicular docking sites in single central synapses. Proc. Natl. Acad. Sci. 201704470.

Mintz, I.M., Sabatini, B.L., and Regehr, W.G. (1995). Calcium control of transmitter release at a cerebellar synapse. Neuron *15*, 675–688.

Mittmann, W., Koch, U., and Häusser, M. (2005). Feed-forward inhibition shapes the spike output of cerebellar Purkinje cells. J. Physiol. *563*, 369–378.

Molineux, M.L., Fernandez, F.R., Mehaffey, W.H., and Turner, R.W. (2005). A-Type and T-Type Currents Interact to Produce a Novel Spike Latency-Voltage Relationship in Cerebellar Stellate Cells. J. Neurosci. *25*.

Moulder, K.L., and Mennerick, S. (2006). Synaptic vesicles: turning reluctance into action. Neuroscientist *12*, 11–15.

Mukherjee, K., Yang, X., Gerber, S.H., Kwon, H.-B., Ho, A., Castillo, P.E., Liu, X., and Südhof, T.C. (2010). Piccolo and bassoon maintain synaptic vesicle clustering without directly participating in vesicle exocytosis. Proc. Natl. Acad. Sci. U. S. A. *107*, 6504–6509.

Nahir, B., and Jahr, C.E. (2013). Activation of extrasynaptic NMDARs at individual parallel fiber-molecular layer interneuron synapses in cerebellum. J. Neurosci. *33*, 16323–16333.

Napper, R.M.A., and Harvey, R.J. (1988). Number of parallel fiber synapses on an individual Purkinje cell in the cerebellum of the rat. J. Comp. Neurol. *274*, 168–177.

Navone, F., Greengard, P., and De Camilli, P. (1984). Synapsin I in nerve terminals: selective association with small synaptic vesicles. Science *226*, 1209–1211.

Obata, K., Ito, M., Ochi, R., and Sato, N. (1967). Pharmacological properties of the postsynaptic inhibition by Purkinje cell axons and the action of ?-aminobutyric acid on Deiters neurones. Exp. Brain Res. *4*.

Orenbuch, A., Shalev, L., Marra, V., Sinai, I., Lavy, Y., Kahn, J., Burden, J.J., Staras, K., and Gitler, D. (2012). Synapsin selectively controls the mobility of resting pool vesicles at hippocampal terminals. J. Neurosci. *32*, 3969–3980.

Pachoud, B., Sharma, P., Bergerot, A., Knöpfel, T., and Marcaggi, P. (2014). Quantification of the density of cooperative neighboring synapses required to evoke endocannabinoid signaling. Neuroscience *256*, 412–425.

Padamsey, Z., and Jeans, A. (2012). Imaging synaptic vesicles using VGLUT1-venus knock-in mice: insights into the dynamic nature of intersynaptic vesicle exchange. J. Neurosci. *32*, 3284–3286.

Palay, S.L., and Chan-Palay, V. (1974). Cerebellar cortex: cytology and organization (Berlin,;Heidelberg,;New York,: Springer).

Pan, B., and Zucker, R.S. (2009). A general model of synaptic transmission and short-term plasticity. Neuron *62*, 539–554.

Paula-Barbosa, M.M., Tavares, M.A., Ruela, C., and Barroca, H. (1983). The distribution of stellate cell descending axons in the rat cerebellum: a Golgi and a combined Golgi-electron microscopical study. J. Anat. 757–764.

Pichitpornchai, C., Rawson, J.A., and Rees, S. (1994). Morphology of parallel fibres in the cerebellar cortex of the rat: an experimental light and electron microscopic study with biocytin. J. Comp. Neurol. *342*, 206–220.

Porton, B., Wetsel, W.C., and Kao, H.-T. (2011). Synapsin III: role in neuronal plasticity and disease. Semin. Cell Dev. Biol. *22*, 416–424.

Powell, K., Mathy, A., Duguid, I., and Häusser, M. (2015). Synaptic representation of locomotion in single cerebellar granule cells. Elife *4*.

Rahmati, N., Owens, C.B., Bosman, L.W.J., Spanke, J.K., Lindeman, S., Gong, W., Potters, J.-W., Romano, V., Voges, K., Moscato, L., et al. (2014). Cerebellar Potentiation and Learning a Whisker-Based Object Localization Task with a Time Response Window. J. Neurosci. *34*.

Rancz, E.A., Ishikawa, T., Duguid, I., Chadderton, P., Mahon, S., and Häusser, M. (2007). High-fidelity transmission of sensory information by single cerebellar mossy fibre boutons. Nature *450*, 1245–1248.

Regehr, W.G., Carey, M.R., and Best, A.R. (2009). Activity-dependent regulation of synapses by retrograde messengers. Neuron *63*, 154–170.

Rieubland, S., Roth, A., and Häusser, M. (2014). Structured connectivity in cerebellar inhibitory networks. Neuron *81*, 913–929.

Ritzau-Jost, A., Delvendahl, I., Rings, A., Byczkowicz, N., Harada, H., Shigemoto, R., Hirrlinger, J., Eilers, J., and Hallermann, S. (2014). Ultrafast action potentials mediate kilohertz signaling at a central synapse. Neuron *84*, 152–163.

Rizo, J., and Xu, J. (2015). The Synaptic Vesicle Release Machinery. Annu. Rev. Biophys. *44*, 339–367.

Rothman, J.S., Kocsis, L., Herzog, E., Nusser, Z., and Silver, R.A. (2016). Physical determinants of vesicle mobility and supply at a central synapse. Elife *5*.

Rowan, M.J.M., Tranquil, E., and Christie, J.M. (2014). Distinct Kv channel subtypes contribute to differences in spike signaling properties in the axon initial segment and presynaptic boutons of cerebellar interneurons. J. Neurosci. *34*, 6611–6623.

Rozov, A., Burnashev, N., Sakmann, B., and Neher, E. (2001). Transmitter release modulation by intracellular Ca2+ buffers in facilitating and depressing nerve terminals of pyramidal cells in layer 2/3 of the rat neocortex indicates a target cell-specific difference in presynaptic calcium dynamics. J. Physiol. *531*, 807–826.

Ryan, T.A., Li, L., Chin, L.S., Greengard, P., and Smith, S.J. (1996). Synaptic vesicle recycling in synapsin I knock-out mice. J. Cell Biol. *134*, 1219–1227.

Salton, G., Wong, A., and Yang, C.S. (1975). A vector space model for automatic indexing. Commun. ACM *18*, 613–620.

Sanes, J.R., and Lichtman, J.W. (1999). Can molecules explain long-term potentiation? Nat. Neurosci. *2*, 597–

604.

Satake, S., and Imoto, K. (2014). Cav2.1 channels control multivesicular release by relying on their distance from exocytotic Ca2+ sensors at rat cerebellar granule cells. J. Neurosci. *34*, 1462–1474.

Satake, S., Inoue, T., and Imoto, K. (2016). Synaptic Multivesicular Release in the Cerebellar Cortex: Its Mechanism and Role in Neural Encoding and Processing. The Cerebellum *15*, 201–207.

Scheuber, A., Miles, R., and Poncer, J.C. (2004). Presynaptic Cav2.1 and Cav2.2 differentially influence release dynamics at hippocampal excitatory synapses. J. Neurosci. *24*, 10402–10409.

Schiebler, W., Jahn, R., Doucet, J.P., Rothlein, J., and Greengard, P. (1986). Characterization of synapsin I binding to small synaptic vesicles. J. Biol. Chem. *261*, 8383–8390.

Schikorski, T., and Stevens, C.F. (2001). Morphological correlates of functionally defined synaptic vesicle populations. Nat. Neurosci. *4*, 391–395.

Schilling, K., and Oberdick, J. (2009). The Treasury of the Commons: Making Use of Public Gene Expression Resources to Better Characterize the Molecular Diversity of Inhibitory Interneurons in the Cerebellar Cortex. The Cerebellum *8*, 477–489.

Schmidt, H., Brachtendorf, S., Arendt, O., Hallermann, S., Ishiyama, S., Bornschein, G., Gall, D., Schiffmann, S.N., Heckmann, M., and Eilers, J. (2013). Nanodomain coupling at an excitatory cortical synapse. Curr. Biol. *23*, 244–249.

Schneggenburger, R., Han, Y., and Kochubey, O. (2012). Ca 2+ channels and transmitter release at the active zone. Cell Calcium *52*, 199–207.

Schwartz, E.J., Rothman, J.S., Dugue, G.P., Diana, M., Rousseau, C., Silver, R.A., and Dieudonne, S. (2012). NMDA Receptors with Incomplete Mg2+ Block Enable Low-Frequency Transmission through the Cerebellar Cortex. J. Neurosci. *32*, 6878–6893.

Shupliakov, O., and Brodin, L. (2010). Recent insights into the building and cycling of synaptic vesicles. Exp. Cell Res. *316*, 1344–1350.

Shupliakov, O., Haucke, V., and Pechstein, A. (2011). How synapsin I may cluster synaptic vesicles. Semin. Cell Dev. Biol. *22*, 393–399.

Siksou, L., Rostaing, P., Lechaire, J.-P., Boudier, T., Ohtsuka, T., Fejtová, A., Kao, H.-T., Greengard, P., Gundelfinger, E.D., Triller, A., et al. (2007). Three-dimensional architecture of presynaptic terminal cytomatrix. J. Neurosci. *27*, 6868–6877.

Siksou, L., Silm, K., Biesemann, C., Nehring, R.B., Wojcik, S.M., Triller, A., El Mestikawy, S., Marty, S., and Herzog, E. (2013). A role for vesicular glutamate transporter 1 in synaptic vesicle clustering and mobility. Eur. J. Neurosci. *37*, 1631–1642.

Sims, R.E., and Hartell, N. a (2005). Differences in transmission properties and susceptibility to long-term depression reveal functional specialization of ascending axon and parallel fiber synapses to Purkinje cells. J. Neurosci. *25*, 3246–3257.

Sims, R.E., and Hartell, N. a (2006). Differential susceptibility to synaptic plasticity reveals a functional specialization of ascending axon and parallel fiber synapses to cerebellar Purkinje cells. J. Neurosci. *26*, 5153–

5159.

Skoblenick, K.J., Argintaru, N., Xu, Y., Dyck, B.A., Basu, D., Tan, M.L., Mazurek, M.F., and Mishra, R.K. (2010). Role of AP-2α Transcription Factor in the Regulation of Synapsin II Gene Expression by Dopamine D1 and D2 Receptors. J. Mol. Neurosci. *41*, 267–277.

Soler-Llavina, G.J., and Sabatini, B.L. (2006). Synapse-specific plasticity and compartmentalized signaling in cerebellar stellate cells. Nat. Neurosci. *9*, 798–806.

Sotelo, C. (2015). Molecular Layer Interneurons of the Cerebellum: Developmental and Morphological Aspects. The Cerebellum *14*, 534–556.

Spanne, A., and Jörntell, H. (2015). Questioning the role of sparse coding in the brain. Trends Neurosci. *38*, 417–427.

Star, E.N., Newton, A.J., and Murthy, V.N. (2005). Real-time imaging of Rab3a and Rab5a reveals differential roles in presynaptic function. J. Physiol. *569*, 103–117.

Staras, K., and Branco, T. (2010). Sharing vesicles between central presynaptic terminals: implications for synaptic function. Front. Synaptic Neurosci. *2*, 20.

Staras, K., Branco, T., Burden, J.J., Pozo, K., Darcy, K., Marra, V., Ratnayaka, A., and Goda, Y. (2010). A vesicle superpool spans multiple presynaptic terminals in hippocampal neurons. Neuron *66*, 37–44.

Sudhakar, S.K., Torben-Nielsen, B., and De Schutter, E. (2015). Cerebellar Nuclear Neurons Use Time and Rate Coding to Transmit Purkinje Neuron Pauses. PLOS Comput. Biol. *11*, e1004641.

Sudhof, T., Czernik, A., Kao, H., Takei, K., Johnston, P., Horiuchi, A., Kanazir, S., Wagner, M., Perin, M., De Camilli, P., et al. (1989). Synapsins: mosaics of shared and individual domains in a family of synaptic vesicle phosphoproteins. Science (80-.). *245*, 1474–1480.

Südhof, T.C. (2012). The presynaptic active zone. Neuron *75*, 11–25.

Sultan, F., and Bower, J.M. (1998). Quantitative Golgi study of the rat cerebellar molecular layer interneurons using principal component analysis. J. Comp. Neurol. *393*, 353–373.

Suvrathan, A., Payne, H.L., and Raymond, J.L. (2016). Timing Rules for Synaptic Plasticity Matched to Behavioral Function. Neuron *92*, 959–967.

Szule, J.A., Harlow, M.L., Jung, J.H., De-Miguel, F.F., Marshall, R.M., and McMahan, U.J. (2012). Regulation of Synaptic Vesicle Docking by Different Classes of Macromolecules in Active Zone Material. PLoS One *7*, e33333.

Takamori, S. (2016). Presynaptic Molecular Determinants of Quantal Size. Front. Synaptic Neurosci. *8*, 2.

Takamori, S., Holt, M., Stenius, K., Lemke, E. a, Grønborg, M., Riedel, D., Urlaub, H., Schenck, S., Brügger, B., Ringler, P., et al. (2006). Molecular anatomy of a trafficking organelle. Cell *127*, 831–846.

Tan, Y.P., and Llano, I. (1999). Modulation by K+ channels of action potential-evoked intracellular Ca2+ concentration rises in rat cerebellar basket cell axons. J. Physiol. *520 Pt 1*, 65–78.

Taschenberger, H., Woehler, A., and Neher, E. (2016). Superpriming of synaptic vesicles as a common basis for intersynapse variability and modulation of synaptic strength. Proc. Natl. Acad. Sci. U. S. A. *113*, E4548-57.

Teyler, T.J., and Discenna, P. (1984). Long-term potentiation as a candidate mnemonic device. Brain Res. *319*, 15–28.

Thach, W.T., Goodkin, H.P., and Keating, J.G. (1992). The Cerebellum and the Adaptive Coordination of Movement. Annu. Rev. Neurosci. *15*, 403–442.

Tran-Van-Minh, A., Cazé, R.D., Abrahamsson, T., Cathala, L., Gutkin, B.S., and DiGregorio, D.A. (2015). Contribution of sublinear and supralinear dendritic integration to neuronal computations. Front. Cell. Neurosci. *9*, 67.

Tran-Van-Minh, A., Abrahamsson, T., Cathala, L., and DiGregorio, D.A. (2016). Differential Dendritic Integration of Synaptic Potentials and Calcium in Cerebellar Interneurons. Neuron *91*, 837–850.

Trommershauser, J., Schneggenburger, R., Zippelius, A., and Neher, E. (2003). Heterogeneous Presynaptic Release Probabilities: Functional Relevance for Short-Term Plasticity. Biophys. J. *84*, 1563–1579.

Tsodyks, M. V, and Markram, H. (1997). The neural code between neocortical pyramidal neurons depends on neurotransmitter release probability. Proc. Natl. Acad. Sci. U. S. A. *94*, 719–723.

Tsuriel, S., Fisher, A., Wittenmayer, N., Dresbach, T., Garner, C.C., and Ziv, N.E. (2009). Exchange and redistribution dynamics of the cytoskeleton of the active zone molecule bassoon. J. Neurosci. *29*, 351–358.

Valera, A.M., Doussau, F., Poulain, B., Barbour, B., and Isope, P. (2012). Adaptation of granule cell to Purkinje cell synapses to high-frequency transmission. J. Neurosci. *32*, 3267–3280.

Valera, A.M., Binda, F., Pawlowski, S.A., Dupont, J.-L., Casella, J.-F., Rothstein, J.D., Poulain, B., and Isope, P. (2016). Stereotyped spatial patterns of functional synaptic connectivity in the cerebellar cortex. Elife *5*.

Vervaeke, K., Lőrincz, A., Gleeson, P., Farinella, M., Nusser, Z., and Silver, R.A. (2010). Rapid Desynchronization of an Electrically Coupled Interneuron Network with Sparse Excitatory Synaptic Input. Neuron *67*, 435–451.

Watanabe, J., Rozov, A., and Wollmuth, L.P. (2005). Target-Specific Regulation of Synaptic Amplitudes in the Neocortex. J. Neurosci. *25*, 1024–1033.

Weber, A.M., Wong, F.K., Tufford, A.R., Schlichter, L.C., Matveev, V., and Stanley, E.F. (2010). N-type Ca2+ channels carry the largest current: implications for nanodomains and transmitter release. Nat. Neurosci. *13*, 1348–1350.

Weber, T., Zemelman, B. V, McNew, J.A., Westermann, B., Gmachl, M., Parlati, F., Söllner, T.H., and Rothman, J.E. (1998). SNAREpins: minimal machinery for membrane fusion. Cell *92*, 759–772.

Wei, H., Masterson, S.P., Petry, H.M., and Bickford, M.E. (2011). Diffuse and Specific Tectopulvinar Terminals in the Tree Shrew: Synapses, Synapsins, and Synaptic Potentials. PLoS One *6*, e23781.

van Welie, I., Smith, I.T., and Watt, A.J. (2011). The metamorphosis of the developing cerebellar microcircuit. Curr. Opin. Neurobiol. *21*, 245–253.

Weyhersmüller, A., Hallermann, S., Wagner, N., and Eilers, J. (2011). Rapid Active Zone Remodeling during Synaptic Plasticity. J. Neurosci. *31*.

Wilhelm, B.G., Mandad, S., Truckenbrodt, S., Kröhnert, K., Schäfer, C., Rammner, B., Koo, S.J., Claßen, G.A., Krauss, M., Haucke, V., et al. (2014). Composition of isolated synaptic boutons reveals the amounts of vesicle trafficking proteins. Science (80-.). *344*.

Williams, M.E., de Wit, J., and Ghosh, A. (2010). Molecular Mechanisms of Synaptic Specificity in Developing Neural Circuits. Neuron *68*, 9–18.

Wilms, C.D., and Häusser, M. (2015). Reading out a spatiotemporal population code by imaging neighbouring parallel fibre axons in vivo. Nat. Commun. *6*, 6464.

Wolpert, D.M., Miall, R.C., and Kawato, M. (1998). Internal models in the cerebellum. Trends Cogn. Sci. *2*, 338–347.

Wu, L.-G., Westenbroek, R.E., Borst, J.G.G., Catterall, W.A., and Sakmann, B. (1999). Calcium Channel Types with Distinct Presynaptic Localization Couple Differentially to Transmitter Release in Single Calyx-Type Synapses. J. Neurosci. *19*.

Wyatt, K.D., Tanapat, P., and Wang, S.S.-H. (2005). Speed limits in the cerebellum: constraints from myelinated and unmyelinated parallel fibers. Eur. J. Neurosci. *21*, 2285–2290.

Xie, Z., Long, J., Liu, J., Chai, Z., Kang, X., and Wang, C. (2017). Molecular Mechanisms for the Coupling of Endocytosis to Exocytosis in Neurons. Front. Mol. Neurosci. *10*, 47.

Xu-Friedman, M.A., and Regehr, W.G. (2003). Ultrastructural contributions to desensitization at cerebellar mossy fiber to granule cell synapses. J. Neurosci. *23*, 2182–2192.

Xu-Friedman, M. a, and Regehr, W.G. (2004). Structural contributions to short-term synaptic plasticity. Physiol. Rev. *84*, 69–85.

Xu-Friedman, M.A., Harris, K.M., and Regehr, W.G. (2001). Three-Dimensional Comparison of Ultrastructural Characteristics at Depressing and Facilitating Synapses onto Cerebellar Purkinje Cells. J. Neurosci. *21*.

Yang, Y., and Calakos, N. (2013). Presynaptic long-term plasticity. Front. Synaptic Neurosci. *5*, 8.

Zampighi, G.A., Fain, N., Zampighi, L.M., Cantele, F., Lanzavecchia, S., and Wright, E.M. (2008). Conical Electron Tomography of a Chemical Synapse: Polyhedral Cages Dock Vesicles to the Active Zone. J. Neurosci. *28*, 4151–4160.

Zhang, W., and Linden, D.J. (2009). Neuromodulation at single presynaptic boutons of cerebellar parallel fibers is determined by bouton size and basal action potential-evoked Ca transient amplitude. J. Neurosci. *29*, 15586–15594.

Zhang, W., and Linden, D.J. (2012a). Calcium influx measured at single presynaptic boutons of cerebellar granule cell ascending axons and parallel fibers. Cerebellum *11*, 121–131.

Zhang, W., and Linden, D.J. (2012b). Calcium Influx Measured at Single Presynaptic Boutons of Cerebellar Granule Cell Ascending Axons and Parallel Fibers. The Cerebellum *11*, 121–131.

Zucker, R.S., and Regehr, W.G. (2002). Short-term synaptic plasticity. Annu. Rev. Physiol. *64*, 355–405.

Zurmöhle, U., Herms, J., Schlingensiepen, R., Brysch, W., and Schlingensiepen, K.H. (1996). Changes in the expression of synapsin I and II messenger RNA during postnatal rat brain development. Exp. Brain Res. *108*, 441–449.

APPENDIX

I had the opportunity to contribute to other research projects in the team and also in collaboration with other labs. For (1), I performed patch-clamp acquisitions to assess the two-pool model under different calcium conditions and using synapse-permeant exogenous calcium buffer EGTA-AM. I also designed experimental protocols that perform realistic patterns of synaptic activity (pseudo-random stimuli) and in a physiological range. For (2), I characterized *in-vitro* network and synaptic abnormalities in cerebellar cortices from mutant mice expressing Episodic Ataxia type2. In (3), I tested the induction of a Long-Term Potentiation protocol *in-vitro* with the presence of inhibition blockers or not. For (4), I provided methodological and technical assistance in the labeling, acquisition and analysis of presynaptic terminals from dentate gyrus of aged rats.

(1) A frequency-dependent mobilization of heterogeneous pools of synaptic vesicles shapes presynaptic plasticity

F. Doussau [1,], H. Schmidt [2], K. Dorgans [1], A. M. Valera [1], B. Poulain [1] and P. Isope [1].*

[1] Institute of Cellular and Integrative Neurosciences, CNRS, 5 Rue Blaise Pascal 67084 Strasbourg, France.

[2] Carl-Ludwig institute for Physiology, University of Leipzig, Germany

(2) Characterization of the dominant inheritance mechanism of Episodic Ataxia type 2

K. Dorgans [b,1], J. Salvi [c,1], F. Bertaso [c], L. Bernard [c], P. Lory [c,], F. Doussau [b], A. Mezghrani [a,*]*

[a] Institut des Neurosciences de Montpellier, INSERM U1051, Hôpital Saint Eloi - Bâtiment INM, 80 rue Augustin Fliche, 34091 Montpellier, France

[b] Institut des Neurosciences Cellulaires et Intégratives-INCI CNRS-UPR 3212, 5 rue Blaise Pascal, 67084 Strasbourg, France

[c] Institut de Génomique Fonctionnelle, CNRS UMR 5203, INSERM U1191, Université de Montpellier, LabEx 'Ion Channel Science and Therapeutics', 141 rue de la Cardonille, 34094 Montpellier, France

(3) Inhibition promotes long-term potentiation at cerebellar excitatory synapses

F. Binda [1], K. Dorgans [1], S. Reibel [2], K. Sakimura [3], M. Kano [4], B. Poulain [1] & P. Isope [1,5]

[1] Institute of Cellular and Integrative Neurosciences, CNRS, 5 Rue Blaise Pascal 67084 Strasbourg, France.

[2] Chronobiotron UMS 3415, 5 Rue Blaise Pascal 67084 Strasbourg, France.

[3] Department of Cellular Neurobiology,
Brain Research Institute, Niigata University, Niigata 951-8585, Japan.

[4] Department of Neurophysiology, Graduate School of Medicine, The University of Tokyo, Tokyo 113-0033, Japan.

[5] University of Strasbourg, 5 Rue Blaise Pascal 67084 Strasbourg, France.

(4) Late-life environmental enrichment induces acetylation events and nuclear factor κB-dependent regulations in the hippocampus of aged rats showing improved plasticity and learning

R. Neidl,[1,2] A. Schneider,[1,2*] O. Bousiges,[1,2,3] M. Majchrzak,[1,2] A. Barbelivien[1,2] A. Pereira de Vasconcelos,[1,2] K. Dorgans,[4] F. Doussau,[4] JP. Loeffler,[5] JC. Cassel,[1,2] and AL. Boutillier[1,2]*

[1] Laboratoire de Neurosciences Cognitives et Adaptatives, Université de Strasbourg, F-67000 Strasbourg, France,

[2] Laboratoire de Neurosciences Cognitives
et Adaptatives, Centre National de la Recherche Scientifique, UMR 7364, F-67000 Strasbourg, France,

[3] Hôpitaux Universitaires de Strasbourg, F-67000 Strasbourg, France,

[4] Institut des Neurosciences Cellulaires et Intégratives, Centre National de la Recherche Scientifique, Unité Propre de Recherche 3212,
F-67084 Strasbourg, France,

[5] Institut National de la Santé et de la Recherche Médicale U1118, Mécanismes centraux et périphériques de la neurodégénérescence, Université de Strasbourg, F-67085 Strasbourg, France

eLIFE elifesciences.org

RESEARCH ARTICLE

Frequency-dependent mobilization of heterogeneous pools of synaptic vesicles shapes presynaptic plasticity

Frédéric Doussau[1]*, Hartmut Schmidt[2], Kevin Dorgans[1], Antoine M Valera[1†], Bernard Poulain[1], Philippe Isope[1]

[1]Institut des Neurosciences Cellulaires et Intégratives, CNRS, Université de Strasbourg, Strasbourg, France; [2]Carl-Ludwig Institute for Physiology, University of Leipzig, Leipzig, Germany

Abstract The segregation of the readily releasable pool of synaptic vesicles (RRP) in sub-pools that are differentially poised for exocytosis shapes short-term plasticity. However, the frequency-dependent mobilization of these sub-pools is poorly understood. Using slice recordings and modeling of synaptic activity at cerebellar granule cell to Purkinje cell synapses of mice, we describe two sub-pools in the RRP that can be differentially recruited upon ultrafast changes in the stimulation frequency. We show that at low-frequency stimulations, a first sub-pool is gradually silenced, leading to full blockage of synaptic transmission. Conversely, a second pool of synaptic vesicles that cannot be released by a single stimulus is recruited within milliseconds by high-frequency stimulation and support an ultrafast recovery of neurotransmitter release after low-frequency depression. This frequency-dependent mobilization or silencing of sub-pools in the RRP in terminals of granule cells may play a role in the filtering of sensorimotor information in the cerebellum.

DOI: https://doi.org/10.7554/eLife.28935.001

***For correspondence:** doussau@inci-cnrs.unistra.fr

Present address: †Department of Neuroscience, Physiology and Pharmacology, University College London, London, United Kingdom

Competing interests: The authors declare that no competing interests exist.

Funding: See page 20

Received: 30 May 2017
Accepted: 06 October 2017
Published: 09 October 2017

Reviewing editor: Inna Slutsky, Tel Aviv University, Israel

Introduction

In neuronal networks, transfer of information largely relies on the ability of presynaptic terminals to convert changes in the firing rate of action potential (AP) into corresponding changes of neurotransmitter release. During trains of APs, the immediate tuning of synaptic efficacy is determined by the combination of multiple parameters including AP frequency, past firing activity, number of release-competent synaptic vesicles (SVs), also referred as the readily-releasable pool (RRP), vesicular release probability (p_r), and number of release sites (N). To date, the deciphering of cellular mechanisms underlying synaptic efficacy has been challenged by the contentious definition of the RRP (***Neher, 2015***). Depending on studies, the RRP either corresponds to a large population of docked SVs releasable by hyperosmotic stimulation or to SVs releasable by a single AP (***Moulder and Mennerick, 2005***; ***Pan and Zucker, 2009***; ***Neher, 2015***). Besides, there is increasing evidence that the RRP comprises heterogeneous populations of SVs that are differently poised for exocytosis and sequentially recruited for exocytosis. In the calyx of Held, for example, the RRP can be separated into a fast-releasing pool (FRP) and a slowly releasing one (SRP) (***Sakaba and Neher, 2001***; ***Sakaba, 2006***; ***Schneggenburger et al., 2012***). During a train of APs, SRP vesicles are first converted into FRP vesicles and then mature to a fully-releasable state (***Lee et al., 2012***, ***2013***). In the cerebellar cortex, at synapses between granule cells (GCs) and molecular layer interneurons (MLIs), two subsets of the RRP have been described that are also mobilized by a two-step process, although the transition is faster than at the Calyx of Held (***Ishiyama et al., 2014***; ***Miki et al., 2016***). Together, these studies suggest that short-term plasticity during high-frequency trains is shaped by the

differential mobilization of sub-pools of SVs in the RRP (**Pan and Zucker, 2009**; **Miki et al., 2016**). However, the mechanisms controlling these pools/steps upon a broad bandwidth of stimulation frequencies are still unknown.

Counter-intuitively, the size of the RRP does not determine the direction of presynaptic plasticity during high-frequency stimulation; at the calyx of Held with a very large RRP (700 to 5000 SVs; **Borst and Soria van Hoeve, 2012**) synaptic transmission quickly depresses, whereas at the GC to Purkinje cell (PC) synapse, synaptic transmission facilitates during tens of APs (**Kreitzer and Regehr, 2000**; **Valera et al., 2012**; **Schmidt et al., 2013**) despite a small RRP (4–8 SVs, **Xu-Friedman et al., 2001**) and a relatively high p_r (**Schmidt et al., 2013**; **Sims and Hartell, 2005**; **Valera et al., 2012** - but see **Atluri and Regehr, 1996**). Using computer simulations combined with variance-mean analysis of postsynaptic responses, we previously showed that this striking facilitation is mediated by an increase in the number of release sites within milliseconds upon a Ca^{2+}-dependent process (**Valera et al., 2012**; **Brachtendorf et al., 2015**). Here, we investigated the cellular mechanisms underlying presynaptic short-term plasticity at GC-PC synapses not only during burst of activity but also upon fast changes in the stimulation frequency, as observed during in vivo recordings (**Chadderton et al., 2004**; **Jörntell and Ekerot, 2006**; **Rancz et al., 2007**; **Arenz et al., 2008**; **van Beugen et al., 2013**). We describe two subsets of SVs in the RRP with distinct properties: a fully-releasable pool that can be released by a single AP and a reluctant pool that is available for fusion within milliseconds at high stimulation frequencies. Moreover, we show that the fully-releasable pool can be specifically and almost completely silenced by low-frequency stimulation. The ultrafast recruitment of reluctant SVs enables the large facilitation of glutamate release at high frequencies and the rapid recovery of neurotransmitter release following the near complete inactivation of fully-releasable SVs. We finally designed a model demonstrating how two pools of SVs can account for the low-frequency depression of glutamate release and its ultrafast recovery at high frequencies. These results support the idea that the distinct composition of the RRP in presynaptic terminals of GCs implements a dynamic filter of neuronal activity. This may explain how sensory inputs covering a wide range of firing rates are processed within the cerebellar cortex.

Results

Low-frequency depression at the granule cell-Purkinje cell synapse

In order to better understand the mechanisms underlying the strong facilitation of glutamate release during repetitive stimulations of the GC-PC synapse, we first measured synaptic transmission over a broad range of frequencies using transverse cerebellar slices prepared from young mice (P18 to P25). To focus on presynaptic mechanisms and to rule out postsynaptic contributions, we pharmacologically blocked the induction of postsynaptic long-term plasticity (LTP and LTD), NMDA-dependent plasticity (**Bidoret et al., 2009**; **Bouvier et al., 2016**), and endocannabinoid signaling (**Marcaggi and Attwell, 2005**; **Beierlein et al., 2007**). We stimulated parallel fibers (PFs) with trains of stimuli (50 pulses) elicited at different frequencies (2, 50 and 100 Hz) and at near-physiological temperature (34°C) (**Figure 1A**). As already reported in rodent cerebellar slices (**Kreitzer and Regehr, 2000**), a sustained facilitation of synaptic transmission was observed up to the 25^{th}-30^{th} stimulus at frequencies above 50 Hz, indicating that the number of SVs released increased with stimulation frequency. The paired-pulse facilitation at the first interval increased with frequency (paired-pulse facilitation $EPSC_2/EPSC_1$: 171.15% ± 10.03 at 50 Hz, n = 9, 215.96% ± 6.90 at 100 Hz, n = 27, **Figure 1A**). After 30 to 40 stimuli, a depression ($EPSC_n/EPSC_1 < 1$) was observed.

At many synapses, asynchronous release of quanta can be triggered by repeated stimulation (**Rudolph et al., 2011**; **Kaeser and Regehr, 2014**). Since asynchronous release can be detected by changes in the charge/amplitude ratio, we measured the charge and peak amplitude of EPSC during 50 Hz and 2 Hz stimulation. The perfect superimposition of normalized charges and amplitudes at any stimulus number during 50 Hz and 2 Hz trains suggested that our stimulation protocol did not evoke asynchronous release (**Figure 1A**). We then estimated the number of quanta released during stimulation. Values of quantal parameters described at unitary GC-PC synapses of mice (**Schmidt et al., 2013**) were used to estimate the number of quanta released at GC-PC synapse during stimulation at 2 Hz, 50 Hz and 100 Hz. The number of PFs stimulated in each experiment was estimated by dividing the mean value of EPSC amplitude at 0.033 Hz by the median EPSC amplitude

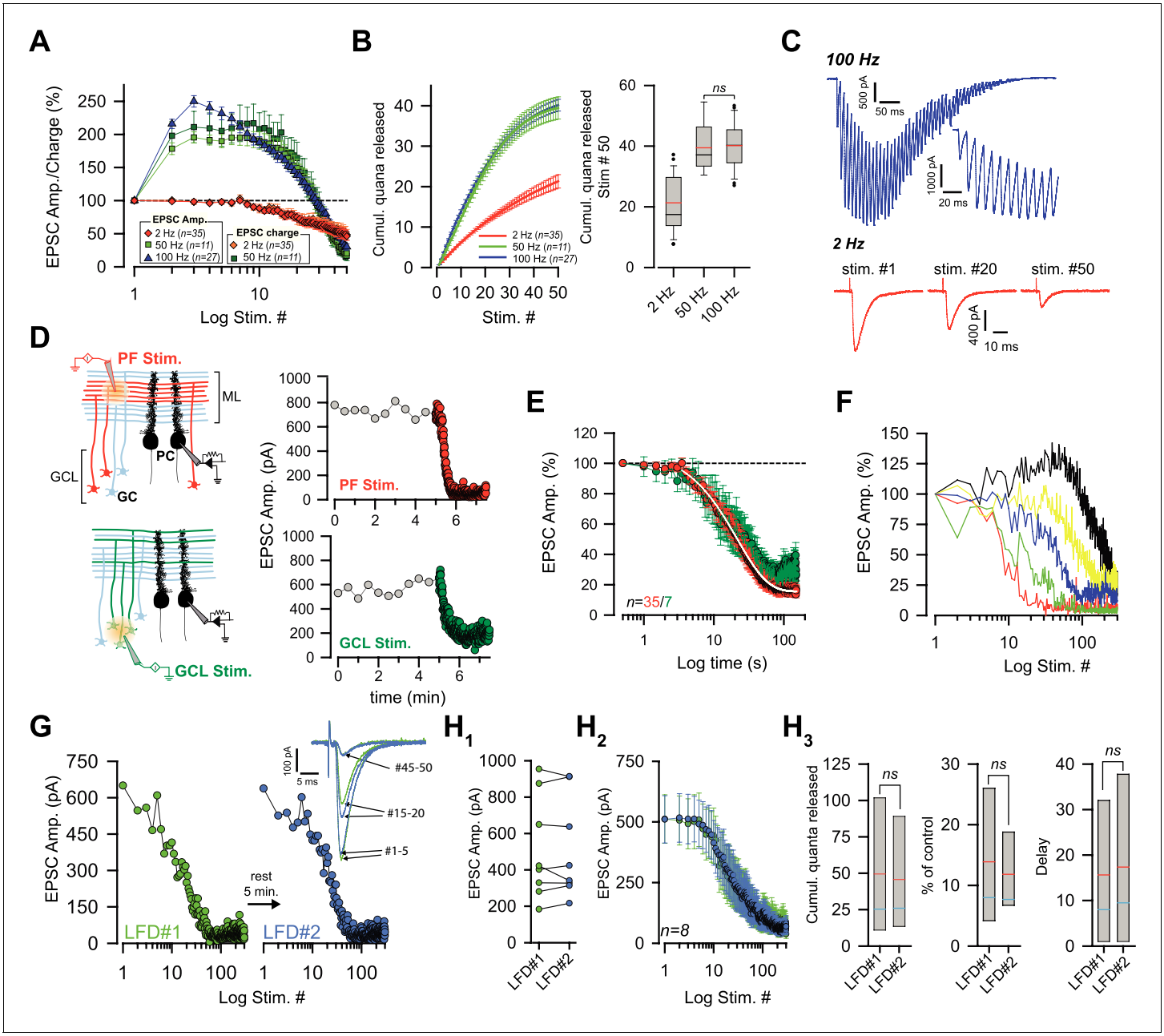

Figure 1. Low-frequency depression at GC-PC synapses. (**A**) Averaged EPSC amplitude and charge versus stimulus number during train of stimuli at 2, 50 and 100 Hz. At 50 Hz EPSC amplitude and EPSC charge are represented by light and dark green squares, respectively. At 2 Hz, EPSC amplitudes and EPSC charge are represented with red diamonds and orange diamonds, respectively. Note strong facilitation at 50 and 100 Hz, no facilitation at 2 Hz. (**B**) *Left* and *right panels* represent the number of quanta released during trains of 50 stimuli at 2, 50 and 100 Hz. *Left panel:* Cumulative number of quanta release versus stimulus number at 2 Hz (red line), 50 Hz (green line) and 100 Hz (blue line). Note that the superposition of values at 50 Hz and 100 Hz mask the values at 100 Hz. *Right panel:* Box-plots showing the corresponding cumulative number of quanta released at the 50th stimulus. No difference was observed between 50 and 100 Hz (*t*-test, p=0.82). Mean and median values are indicated in red and black, respectively. (**C**) Representative recording traces of EPSCs evoked at 100 Hz and 2 Hz. *Inset*: The first EPSCs observed during 100 Hz train. The stimulus artifacts have been subtracted for the 100 Hz train. (**D**) *left*, schematics showing the two modes of stimulation. Extracellular stimulations in the molecular layer (ML) (*upper panel*) activated beams of PFs (in red) whereas stimulations of the granule cell layer (GCL) (*lower panel*) led to sparse activations of PFs (in green) Non-stimulated GCs are represented in light blue. Stimulated areas are represented by concentric orange circles. *Right*, two examples of the time course of EPSC amplitudes following stimulation of PFs (*upper panel*) or of GC somata (*lower panel*) at 0.033 Hz (gray points) and 2 Hz (red or green points respectively). (**E**) Mean normalized EPSC amplitude during sustained 2 Hz stimulations of PFs or GC somata (red and green points respectively). Note the delay before the actual induction of LFD. The depression was fitted by a monoexponential function (tau = 21.7 s, white line). (**F**) Selected time course of LFD recorded in 5 PCs showing differences in the onset and the plateau of depression. (**G, H**) LFDs elicited in the same cell share the same

Figure 1 continued on next page

Figure 1 continued

profile of depression. (**G**) Time courses of two successive LFDs elicited in the same cell. The second LFD protocol (LFD#2, blue points) was performed after a resting period of 5 min (LFD#1, green points). *inset,* traces correspond to averaged EPSCs recorded during LFD#1 and LFD#2 (green and blue traces, respectively) at the indicated stimulus numbers. (H_1) EPSC amplitudes recorded at the first stimulus of LFD#1 (green points) and LFD#2 (blue points). The similar sizes of EPSC amplitudes in LFD#1 and LFD#2 indicates full recovery from depression during the resting period (paired *t*-test performed on EPSCs#1 of LFD#1 and LFD#2, p=0.94, *n* = 8). (H_2) Superimposition of mean EPSC amplitudes recorded during LFD#1 (green points) and LFD#2 (blue points). Same set of experiment as in H_1. (H_3) Box-plots showing the cumulative number of quanta released during LFD#1 and LFD#2 (number of quanta released during LFD: 49.5 quanta ± 18.8 quanta for LFD#1 versus 45.6 quanta ±, 14.5 quanta for LFD#2, paired *t*-test, p=0.47, *n* = 8), the plateau of LFD#1 and LFD#2 (mean percentage of initial response for LFD: 13.9 ± 5.2% for LFD#1 versus 11.8% ±, 3.2 for LFD#2, paired *t*-test, p=0.39, n = 8) and the delay before the onset of depression (15.6 stimuli ± 6.6 stimuli for LFD#1 versus 17.4 stimuli ± 7.2 for LFD#2. paired *t*-test, p=0.13, *n* = 8). Since none of these parameters were statistically different between the two conditions, LFD#1 and LFD#2 were considered identical. Blue and red lines indicate median and mean values respectively. Same set of experiments as in H_1, H_2.

DOI: https://doi.org/10.7554/eLife.28935.002

The following figure supplement is available for figure 1:

Figure supplement 1. LFD can be elicited by a broad range of frequencies.

DOI: https://doi.org/10.7554/eLife.28935.003

obtained at unitary GC-PC synapses (5.3 pA, including release failure, ***Schmidt et al., 2013***). The number of quanta released at any synaptic terminal during each protocol was estimated by dividing the cumulative EPSC amplitude by the number of PFs stimulated and by the mean value of the quantal content obtained at unitary GC-PC synapse (8 pA, ***Schmidt et al., 2013***). Our estimation does not take in account the ~10% of GC boutons that contain two active zones and make contact on two dendritic spines (***Xu-Friedman et al., 2001***). Therefore, the estimation of the number of quanta released at individual GC terminals have been underestimated through overestimations of the number of PFs recruited by external stimulation. Nevertheless, these errors should be constant in all the stimulation paradigms and we believe that the comparison between cumulative values of quanta released at individual GC terminals are relevant information. Cumulative EPSC amplitude plots demonstrate that the total number of quanta released is proportional to the stimulation frequency. However, although initial facilitation during the first two or three pulses is higher at 10 ms than at 20 ms intervals (***Valera et al., 2012***) no difference was observed in the maximal recruitment of releasable SVs between 50 Hz and 100 Hz (number of quanta released per bouton at 50 Hz = 39.47 ± 2.75, *n = 9* compared to 40.14 ± 7.50 at 100 Hz, *n = 27*, p=0.82, *t*-test, ***Figure 1B***).

Conversely, at 2 Hz, the synaptic responses did not facilitate during the first stimuli (***Figure 1A,C***) and depressed rapidly after a mean delay of 7 stimuli ± 5 stimuli (*n* = 35) (***Figure 1D,E***). We named this rapid blockage of synaptic transmission 'low frequency depression' (LFD). Strikingly, the EPSC amplitudes decreased mono-exponentially in the majority of cells recorded (*n* = 32) with a mean time constant of 15.9 s ± 1.2 s. A lack of LFD was observed for ~12% of PCs recorded in the vermis (5 cells out of 39 cells). These cells were excluded from the statistical analysis.

APs are reliably initiated and transmitted along PFs at high frequencies and at physiologic temperature (35˚C) (***Kreitzer and Regehr, 2000***; ***Isope and Barbour, 2002***; ***Baginskas et al., 2009***). Nevertheless, repetitive extracellular stimulations of PFs can decrease the excitability of fibers excitability due to K^+ accumulation in the extracellular space (***Kocsis et al., 1983***). To test, whether LFD was caused by decreased excitability of PFs, we placed the stimulation electrode in the granule cell layer (GCL) to stimulate clusters of GC somata rather than beams of PFs (***Figure 1D***). The lack of any significant change in the onset and the kinetics of depression after stimulating GC somata (***Figure 1D,E***) suggested that impaired PF excitability did not cause LFD.

While the onset and the plateau of LFD varied among PCs (***Figure 1F***), the depression could be reliably induced in a given PC as long as the recording of EPSCs could be maintained. In a series of 8 experiments, two LFD (LFD#1 and LFD#2) separated by a resting period of 5 to 10 min were successively induced. EPSC amplitudes fully recovered after the resting period following the end of LFD#1 protocol and the time courses of EPSCs amplitude of LFD#1 LFD#2 were identical (***Figure 1G,H***). Our findings reveal for a first time that a sustained stimulation at low frequency can almost completely silence the release apparatus of GC terminals.

In vivo recordings have shown that GCs fire spontaneously in a range of 0.4 to 10 Hz (***Chadderton et al., 2004***; ***Jörntell and Ekerot, 2006***). Therefore, we applied successively at the

same synapse low-frequency stimulations in a range of 0.5 to 10 Hz (stimulations with random frequencies, ***Figure 1—figure supplement 1A***) or at a fix low frequency (0.5 Hz, 2 Hz or 5 Hz, ***Figure 1—figure supplement 1B,C***). No change in the properties of LFD were observed after a shift in the firing frequency (***Figure 1—figure supplement 1D,E***) indicating that presynaptic terminals of GCs can filter a broad range of low-frequency activities of GCs.

Immediate recovery from LFD by high-frequency trains

High-frequency stimulations can induce rapid refilling of release sites and the recruitment of new ones (***Saviane and Silver, 2006***; ***Hallermann et al., 2010***; ***Valera et al., 2012***; ***Chamberland et al., 2014***). Therefore, we tested whether an increase of stimulation frequency could fully restore release from presynaptic terminals after LFD induction. Alternatively, LFD may result from an activity-dependent blockage of presynaptic voltage-dependent calcium channels (***Xu and Wu, 2005***). In this latter case, accelerating the refilling of the RRP or increasing the number of release sites *N* should not restore glutamate release after LFD. LFD was induced by 300 stimuli at 2 Hz, and a train of 50 stimuli at 100 Hz was applied immediately after the last stimulus (***Figure 2A***). Strikingly, after a full blockage of synaptic transmission, the glutamate release capacity recovered to 70.7 ± 7.6% within 10 ms, reached a peak of amplitude after 5 to 8, and then declined progressively (***Figure 2B–D***). After the 7^{th} stimuli, EPSC amplitudes evoked by the 100 Hz recovery train reached values that were not significantly different from values observed at the same stimulus number in a control train elicited before LFD induction (***Figure 2C,D***). This suggests that a full recovery from LFD was achieved within 70 ms.

We then studied how the frequency of stimulation in the train influenced the ability of depressed synapses to recover a full capacity of release. Accordingly, 50 Hz and 20 Hz trains were applied after LFD and compared to 50 Hz and 20 Hz trains applied in control conditions. Mean amplitudes of EPSCs recorded during train at 50 Hz applied in control condition were not statistically different from those recorded after LFD induction (***Figure 2E***) within approximately 50 ms (5 stimuli). With 20 Hz applied after LFD, the recovery was limited, and EPSC amplitudes were smaller than the ones recorded in control condition (***Figure 2F***).

Recovery from LFD relies on the fast recruitment of reluctant SVs by a high-frequency train

In principle, the ultrafast recovery of synaptic transmission following LFD could be mediated by (1) a frequency-dependent ultrafast replenishment of the RRP and/or by (2) the recruitment of a reluctant pool of SVs that cannot be mobilized at low frequency as suggested in ***Valera et al., 2012***. To test the latter mechanism, we studied whether the recovery from LFD by a 100 Hz train was affected by previous exhaustion of the reluctant pool. Our results suggested that the reluctant pool can be recruited by short bursts at high frequency (paired-pulse/triplet stimulation at 50 or 100 Hz, ***Valera et al., 2012***). Therefore, we modified the stimulation paradigm for LFD and used 100 triplets of stimuli repeated at 2 Hz ($LFD_{triplet}$) instead of the 300 single pulses at 2 Hz (LFD). The total number of stimuli was the same in $LFD_{triplet}$ and LFD. The triplet frequency was changed from 10 Hz to 200 Hz during the experiment. Since LFD protocols can be repeated several times after a recovery time (***Figure 1G***), we systematically applied the LFD and $LFD_{triplet}$ protocols to each PC recorded. Strikingly, the level of recovery after $LFD_{triplet}$ was inversely proportional to the frequency of triplet stimulation (***Figure 3B,C***). For example, when triplets frequency was set at 200 Hz during $LFD_{triplet}$, synaptic transmission hardly recovered (maximal recovery 38.9%±7.19 n = 6, compared to 196.7%± 8.7, after LFD, n = 27, ***Figure 3C***). This finding suggested that $LFD_{triplet}$ stimulation depleted or disabled the population of SVs that support the recovery from LFD. If SVs released only during $LFD_{triplet}$ (that is, at the second and third pulse of triplet stimulation) and during recovery by 100 Hz train belong to the same pool (the reluctant pool), then the number of quanta released during LFD and recovery train or during $LFD_{triplet}$ and recovery train should be the same. We next applied LFD and $LFD_{triplet}$ (triplet at 100 Hz) successively in the same cells followed by the application of a 100 Hz recovery train (***Figure 4A,B***). Cumulative EPSC amplitudes were determined, and the approximate number of quanta released for the whole protocol (LFD or $LFD_{triplet}$ +recovery train) was estimated (***Figure 4C***). The normalized cumulative EPSC amplitude was higher during $LFD_{triplet}$ than during LFD (6440.9 ± 945% for LFD compared to 9353.5 ± 1199.9% for $LFD_{triplet}$, $p<0.001$, paired t test,

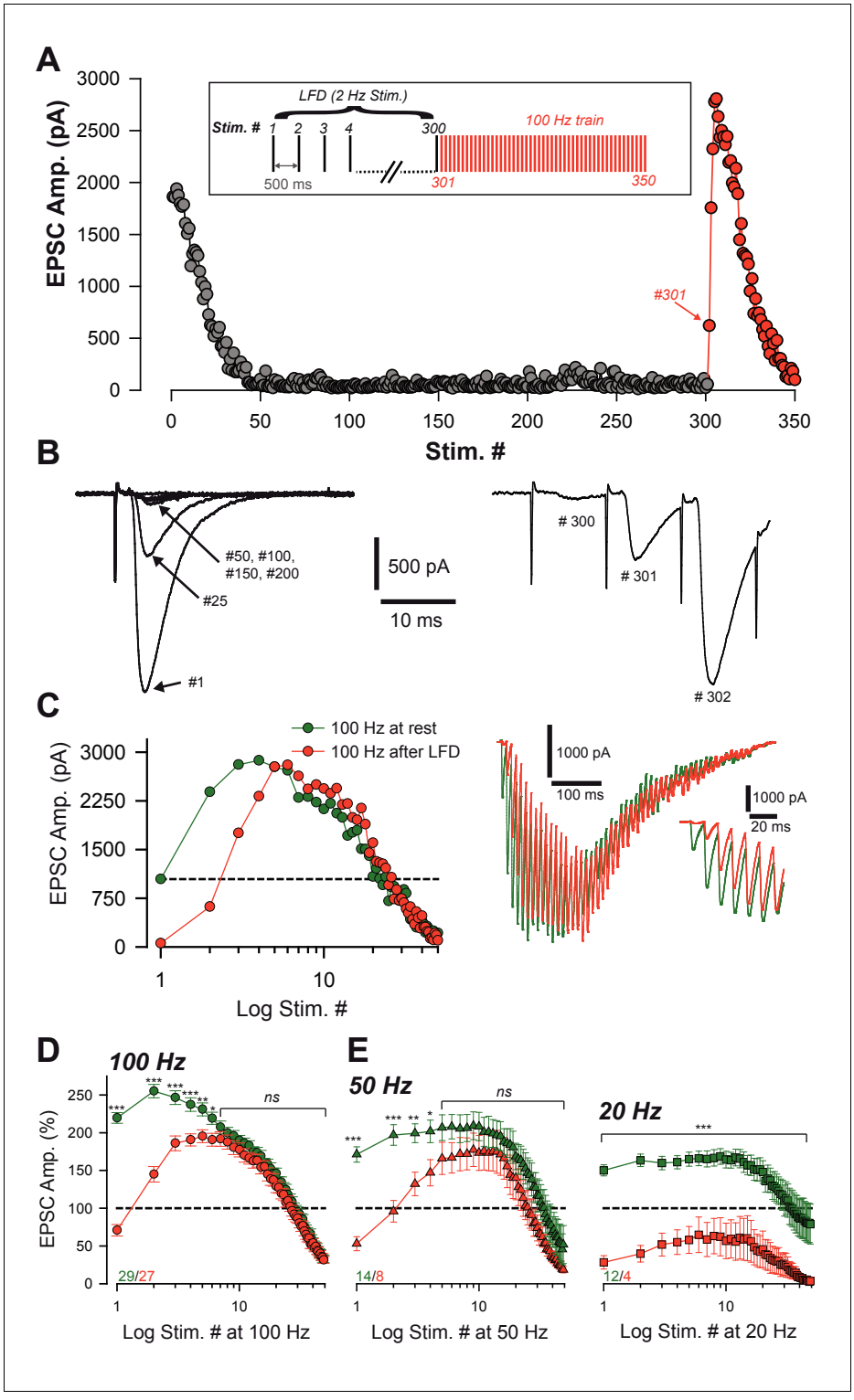

Figure 2. Ultrafast recovery from LFD by high-frequency trains. (**A**) Typical experiment illustrating the time course of EPSC amplitude during LFD (gray points, stimulation at 2 Hz) and the fast recovery from LFD via high-frequency trains (red points, stimulation 100 Hz). *Inset*: protocol of stimulation. Stimulus #1 corresponds to the beginning of the 2 Hz stimulation. (**B**) Recording traces of superimposed EPSCs recorded during 2 Hz stimulation (*left*) and during the following 100 Hz train (*right*) at the indicated stimulus number from (**A**). Note the ultrafast recovery from depression at 100 Hz (stimulus # 301). (**C**) *Left*, Representative EPSC amplitudes evoked by a 100 Hz train applied before (green), and 10 ms after 300 stimuli at 2 Hz. The dashed line corresponds to the baseline amplitude

Figure 2 continued on next page

Figure 2 continued

defined as mean amplitude at 0.033 Hz. Note the similar size of EPSCs after the fourth stimulus at 100 Hz. *Right*, Corresponding traces recorded during these 100 Hz trains. *Inset*: The first EPSCs observed during train application. (**D**) Mean values of normalized EPSC amplitude elicited by trains of stimulation at 100 Hz at baseline (0.033 Hz, green) or after LFD induction (2 Hz, red). EPSC amplitudes were not significantly different after the seventh stimuli (MWRST, p=0.181, *n* = 27). (**E**) Mean values of normalized EPSC amplitude elicited by trains of stimulation at 50 Hz and 20 Hz at baseline (0.033 Hz, green) or after LFD induction (2 Hz, red). EPSC amplitudes were not significantly different after the after the fifth stimuli for 50 Hz trains (*t*-test, p=0.137, *n* = 13). EPSC amplitudes in 20 Hz trains elicited after LFDnever reached amplitudes of EPSCs of 20 Hz trains elicited at rest. Numbers at the bottom of the graphs indicate the number of cells recorded under each condition.

DOI: https://doi.org/10.7554/eLife.28935.004

n = 18, ***Figure 4C,D***). This suggests that reluctant SVs were recruited by the triplet stimulation. When the cumulative EPSC amplitude measured during the recovery train was added, no significant differences were observed between the two protocols (11696.3 ± 1163.6% for LFD and recovery train compared to 11379.0 ± 1349.6% for $LFD_{triplet}$ and recovery train, p=0.61, paired *t* test, *n* = 18, ***Figure 4C,D***). This suggests that SVs recruited only during $LFD_{triplet}$ or only during recovery train belong to the same reluctant pool. Accordingly, the calculated number of quanta released during LFD was statistically lower than during $LFD_{triplet}$ (42.7 ± 6.2 quanta for LFD compared to 60.8 ± 8.0 quanta for $LFD_{triplet}$, p<0.01, paired t-test, n = 18, ***Figure 4E***) and the total number of quanta released during LFD and recovery train or $LFD_{triplet}$ and recovery train were not significantly different (77.5 ± 7.7 quanta released for LFD and recovery train compared to 74.8 ± 8.9 quanta released for $LFD_{triplet}$ and recovery, p=0.51, paired *t*-test, *n* = 18, ***Figure 4E***). Moreover, the number of quanta released during LFD and solely during recovery train (that is, at stimuli #301 to stimuli #350) were not significantly different (42.7 ± 6.2 quanta released for LFD compared to 32.1 ± 2.3 quanta released for recovery train, p=0.1, paired *t*-test, *n* = 18, ***Figure 4E***). These results suggest that releasable SVs in GC boutons segregate in two distinct pools: the fully-releasable pool that can be released by a single AP and a reluctant pool that can only be recruited during bursts of APs reaching frequencies $\geq$ 20 Hz.

Physiologically, the duration of spontaneous activity of GCs preceding high-frequency bursts is variable. Therefore, the recruitment of the reluctant pool may occur regardless of the status of the fully-releasable pool. This latter pool may be fully available, partially silenced or fully silenced. Since strong paired-pulse facilitation indicates recruitment of the reluctant pool (***Valera et al., 2012***; ***Miki et al., 2016***, this study), we studied how high-frequency paired-pulse stimulations randomly applied during the course of LFD influenced paired-pulse facilitation. Paired-pulse stimulation at high frequencies applied during LFD induced strikingly high PPR values (***Figure 4—figure supplement 1A,C***). These strikingly high PPR values were observed whatever was the percentage of inhibition and regardless of the timing of LFD (***Figure 4—figure supplement 1D***). These findings strongly suggest that the status of the fully-releasable pool does not influence the mobilization of the reluctant pool.

A two-pool model accounts for basic experimental findings

Our data suggest a segregation of SVs into different pools at GC terminals, which is in line with several previous studies (***Valera et al., 2012***; ***Ishiyama et al., 2014***; ***Brachtendorf et al., 2015***; ***Miki et al., 2016***). They further suggest that SVs can be recruited from a reluctant pool into a fully-releasable pool on a millisecond timescale. Several models can account for these findings (***Figure 5***), including a single-pool model with Ca^{2+}-independent replenishment, a sequential two-pool model with Ca^{2+}-dependent recruitment (***Millar et al., 2005***; ***Sakaba, 2008***), and a parallel two-pool model with intrinsically different SVs in which both pools are restored independent of Ca^{2+} (***Wölfel et al., 2007***; ***Schneggenburger et al., 2012***). An important demand on such models is that it needs to integrate the observed high-frequency facilitation and LFD.

First, we analyzed a sequential two-pool model, where release is triggered via a Ca^{2+}-driven, five-site sensor from a fraction of releasable SVs (***Millar et al., 2005***; ***Sakaba, 2008***) (***Figure 6A***, see Materials and methods). These SVs become replenished in two steps. The first step corresponds to a Ca^{2+}-dependent priming step ($R_0 \rightarrow R_1$) and the second one to a Ca^{2+}-independent filling step

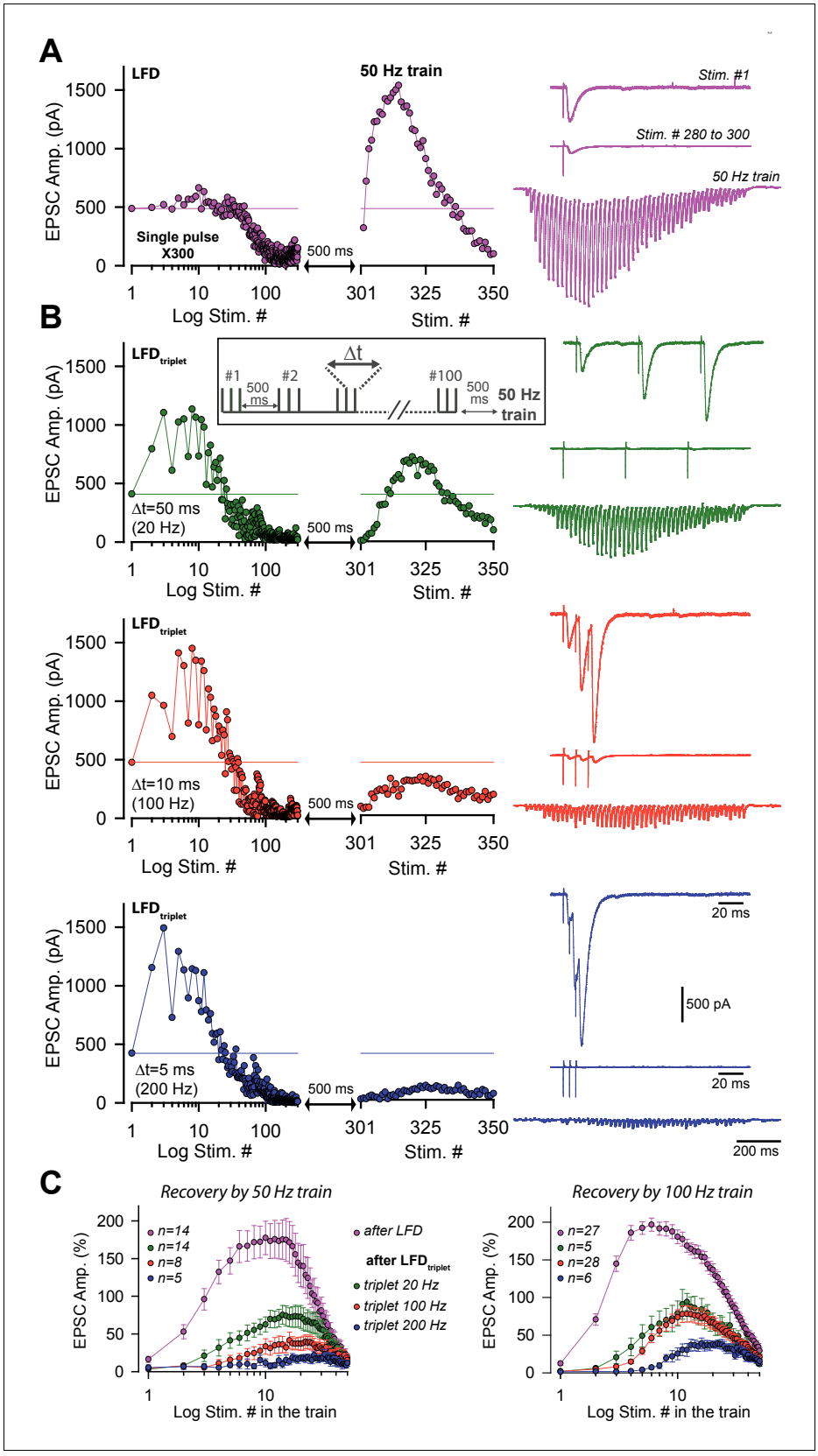

Figure 3. Short-term facilitation during triple-pulse stimulation at high frequency impedes recovery from LFD via high-frequency trains. (**A**) *Left panels* an example of EPSC amplitudes during LFD followed by a 50 Hz train of

Figure 3 continued on next page

Figure 3 continued

stimulation. *Right panel, upper trace*, EPSCs elicited by the first stimulation at 2 Hz, *middle traces*, averaged EPSCs recorded during the LFD plateau (stimuli #280 to #300), *bottom traces*, EPSC recorded during the 50 Hz train applied 500 ms after the 2 Hz stimulation (artifacts subtracted). (**B**) *left panels*, time courses of EPSC amplitudes induced by triples pulse at different frequencies ($LFD_{triplet}$, see inset for protocol) as indicated and by a subsequent 50 Hz train. *Right panel, upper trace*, EPSCs elicited by the first triplet at 2 Hz, *middle traces*, averaged EPSCs recorded during the LFD plateau (stimuli #80 to #100), *bottom traces*, EPSC recorded during the 50 Hz train applied 500 ms after the 2 Hz stimulation (artifacts subtracted). For *A* and *B*, all data and traces were obtained in the same PC, and LFDs or $LFDs_{triplet}$ were elicited after a resting period of 5 min after the end of each protocol. (**C**) Mean values of normalized EPSC amplitudes evoked by 50 Hz train (*left*) and 100 Hz train (*right*) applied 500 ms after LFD induction (300 single stimuli at 2 Hz or 100 triple pulses at 2 Hz). Same color code than in *A* and *B*.

DOI: https://doi.org/10.7554/eLife.28935.005

($R_1 \rightarrow V$). In this case, R_0+R_1 and V correspond to the reluctant and the fully-releasable pool, respectively, as observed in our experiments. In the simulations, release was triggered by Gaussian-shaped Ca^{2+} signals with amplitudes of ~22 µM (***Schmidt et al., 2013***). Ca^{2+}-dependent recruitment was assumed to be driven by residual Ca^{2+} (***Figure 6B***) with an initial amplitude of 520 nM and a decay constant of 42 ms (***Brenowitz and Regehr, 2007***). During high-frequency stimulation (100 Hz), this residual Ca^{2+} sums linearly during 50 stimuli (***Brenowitz and Regehr, 2007***), building up to a steady state amplitude of ~2 µM. This high concentration of residual Ca^{2+} drove rapid recruitment of SVs from the reluctant pool into the fully-releasable pool causing a transient increase of the latter pool (***Figure 6C***; ***Valera et al., 2012***). Acting in concert with slow Ca^{2+} unbinding from the release sensor, which generates a moderate facilitation on the ms timescale (***Bornschein et al., 2013***), SV recruitment resulted in prolonged and facilitated release consistent with our experimental observations (***Figure 6D,E***, compared with ***Figure 1***). On the other hand, during low-frequency stimulation (2 Hz), residual Ca^{2+} dropped back to its resting level between pulses and recruited SVs returned to the reluctant pool between stimuli. This resulted in the progressive depletion of fully-releasable SVs, leading to LFD. Renewed driving of the depressed model at high-frequency reproduced a rapid recovery from LFD and was followed by facilitation (***Figure 6D*** compared with ***Figure 2***), thus illustrating the recruitment of the reluctant pool.

Next, we simulated release using two alternative models. The single pool model incorporates an 'allosteric' release sensor (***Lou et al., 2005***) and a replenishment step at a fixed, Ca^{2+}-independent rate (one-pool model, ***Wölfel et al., 2007***). The parallel pool model postulates two pools of releasable SVs (SRP and FRP, see introduction) with fast and slow intrinsic release rates (parallel two-pool model, ***Wölfel et al., 2007***). In both models, the pools are replenished at a fixed rate independent of Ca^{2+}. Both models predict a depression of release during high-frequency stimulation and a strong facilitation during sustained low-frequency stimulation (***Figure 6F,G***). This is in stark contrast to our experimental results that show the opposite behavior of GC synapses. The latter two models successfully described several aspects of release at the depressing calyx of Held synapse that operates with a very large RRP (***Sätzler et al., 2002***) but cannot explain the release mechanisms at GC-PC synapses, which are based on a small number of releasable SVs and a rapid Ca^{2+} driven recruitment of SVs.

Taken together, these findings show that several aspects of our experimental findings, in particular high-frequency facilitation and LFD, can be reproduced by a simple sequential two-pool model with Ca^{2+}-dependent recruitment. This does not exclude a contribution of more sophisticated mechanisms like activity- dependent 'a posteriori' modifications (***Wölfel et al., 2007***) or a separate facilitation sensor (***Atluri and Regehr, 1996***; ***Jackman et al., 2016***) but hints towards the minimal requirements for sustained release from a small terminal operating with a small number of releasable SVs.

Recovery from LFD depends on the size of both pools

The two-pool sequential model predicts that the kinetics of refilling of the fully-releasable pool after LFD depends on the state of the reluctant pool. For example, when both the fully-releasable pool and the reluctant pool have been depleted by high-frequency stimulation, the replenishment should

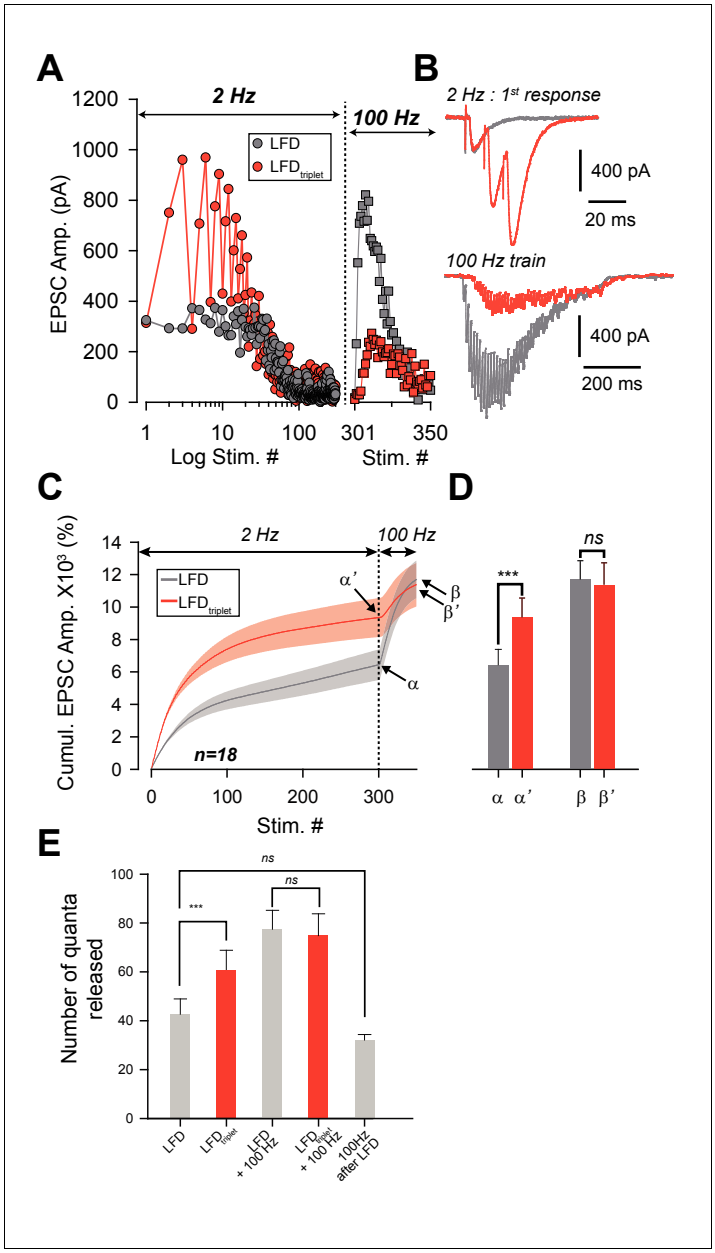

Figure 4. Recruitment of reluctant vesicles by high-frequency trains underpins recovery from LFD. (**A**) Superimposition of ESPC amplitudes elicited during LFD (2 Hz, gray circles) or $LFD_{triplet}$ (2 Hz with triplet stimulation at 100 Hz, red circles) in the same PC, and during the recovery from LFD via application of a 100 Hz train (gray squares for a 100 Hz train applied 500 ms after LFD, and red squares for a 100 Hz train applied 500 ms after $LFD_{triplet}$). (**B**) *upper traces*, superimposition of the first EPSCs recorded at stimulus #1 for LFD (gray trace) and $LFD_{triplet}$ (red trace). *Lower traces*, EPSCs recorded during the 100 Hz trains applied 500 ms after LFD (gray trace) or 500 ms after $LFD_{triplet}$. (**C**) Mean values of cumulative EPSC amplitudes during LFD and $LFD_{triplet}$ followed by a recovery train at 100 Hz (n = 18 cells). LFD and $LFD_{triplet}$ were elicited successively in the same PCs. The dashed line indicates the beginning of the 100 Hz trains. α and α' correspond to the cumulative value at the end of LFD protocols, β and β' are values obtained following the recovery trains. (**D**) Mean values of a, a', b and β' (same y axis as in *C*). (**E**) Estimation of the number of quanta released at GC-PC synapse during LFD, $LFD_{triplet}$ and during the recovery via 100 Hz train (same set of experiments as in *D*). For the panels *D* and *E*, data were compared by using paired *t*-test.

DOI: https://doi.org/10.7554/eLife.28935.006

The following figure supplement is available for figure 4:

Figure 4 continued on next page

Figure 4 continued

Figure supplement 1. The status of the fully-releasable pool does not influence the mobilization of the reluctant pool.

DOI: https://doi.org/10.7554/eLife.28935.007

start first in the reluctant pool, and then the fully-releasable pool can be reloaded. To test this hypothesis, we determined the recovery kinetics of the fully-releasable pool after LFD (***Figure 7A***, red points) and $LFD_{triplet}$ (triplet at 200 Hz; ***Figure 7A***, blue points) by applying low-frequency stimulation at 0.033 Hz starting 30 s after the end of the LFD protocol. As shown in ***Figure 7A***, full recovery after LFD was described by a single exponential function (tau = 153.8 s, R^2 = 0.93), indicating a single-step process. Recovery following $LFD_{triplet}$ also followed a single exponential time course (tau = 212.8 s, ***Figure 7A***) but started with a long delay. Averaged time courses show that simple 90 s shift led to an identical monoexponential recovery in both LFD (mean tau = 156.3 s, R^2 = 0.98, *n* = 8) and $LFD_{triplet}$ (mean tau = 149.3 s, R^2 = 0.96, *n* = 6) (***Figure 7B,C***). The delay preceding the exponential recovery from depression after $LFD_{triplet}$ (~90 s) may reflect the time required to reconstitute the reluctant pool. To test this possibility, the following paradigm was designed: SVs from both the reluctant and fully-releasable pools were depleted by $LFD_{triplet}$ (triplets at 100 Hz), then a 100 Hz test train was applied after a variable resting period (500 ms, 10 s or 1 min of rest after the end of LFD, ***Figure 7D***). As shown in ***Figure 7D***, amplitudes of EPSCs during the test trains increased proportionally to the length of the resting period. More interestingly, after 1 min of rest, the first responses in the test train were still fully blocked (***Figure 7E***) whereas the amplitudes of the late responses reflecting the recruitment of the releasable pool (after stimuli # 11–12 in the test train) were similar to the corresponding responses in the control train (***Figure 7F***). This demonstrates that even after 1 min of rest, no SVs from the fully-releasable pool were ready to be released, despite partial reconstitution of the reluctant pool.

Reluctant SVs can be recruited by increasing Ca^{2+} entry

Finally, we investigated whether SVs in the reluctant pool are maintained in a state of low release probability. In this case, the reluctant pool could be affected by modifications of p_r. First, we studied the properties of LFD and recovery by 100 Hz train upon an increase in p_r. Based on our previous studies, we estimated that an increase of $[Ca^{2+}]_e$ from 2.5 mM to 4 mM can increase p_r from 0.25 to 0.67 for SVs in the fully-releasable pool (***Valera et al., 2012***). In the presence of 4 mM $[Ca^{2+}]_e$, the number of quanta released during LFD almost doubled as compared to LFD elicited in 2.5 mM $[Ca^{2+}]_e$ (***Figure 8A–C***). However, the time course of normalized amplitudes of EPSCs during LFD was barely affected in high $[Ca^{2+}]_e$; neither the delay, nor the plateau of LFD or the decay time constant were statistically different in low and high Ca^{2+} conditions (***Figure 8D,E***). This suggests that similar

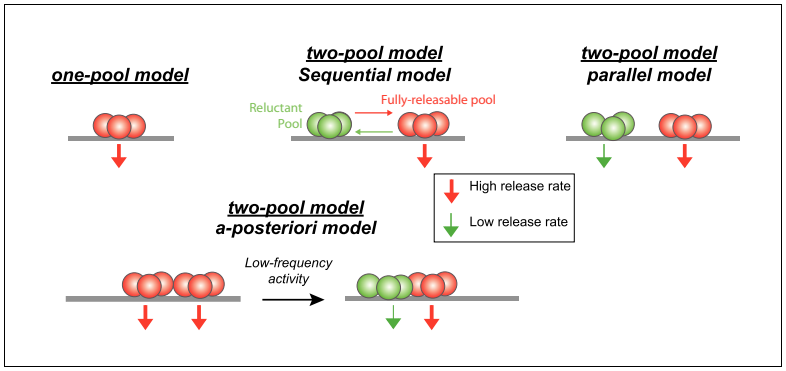

Figure 5. Schematics showing different models of SV release at GC-PC synapses. Based on hypothesis proposed in other synapses, presynaptic release could be mediated by a homogeneous pool of release-ready SVs (one-pool model) or through a two-pool model with alternative stages of transition between the two pools. For the two-pool model, releasable SVs are separated in a fully-releasable pool (red SVs) or a reluctant one (green SVs).

DOI: https://doi.org/10.7554/eLife.28935.008

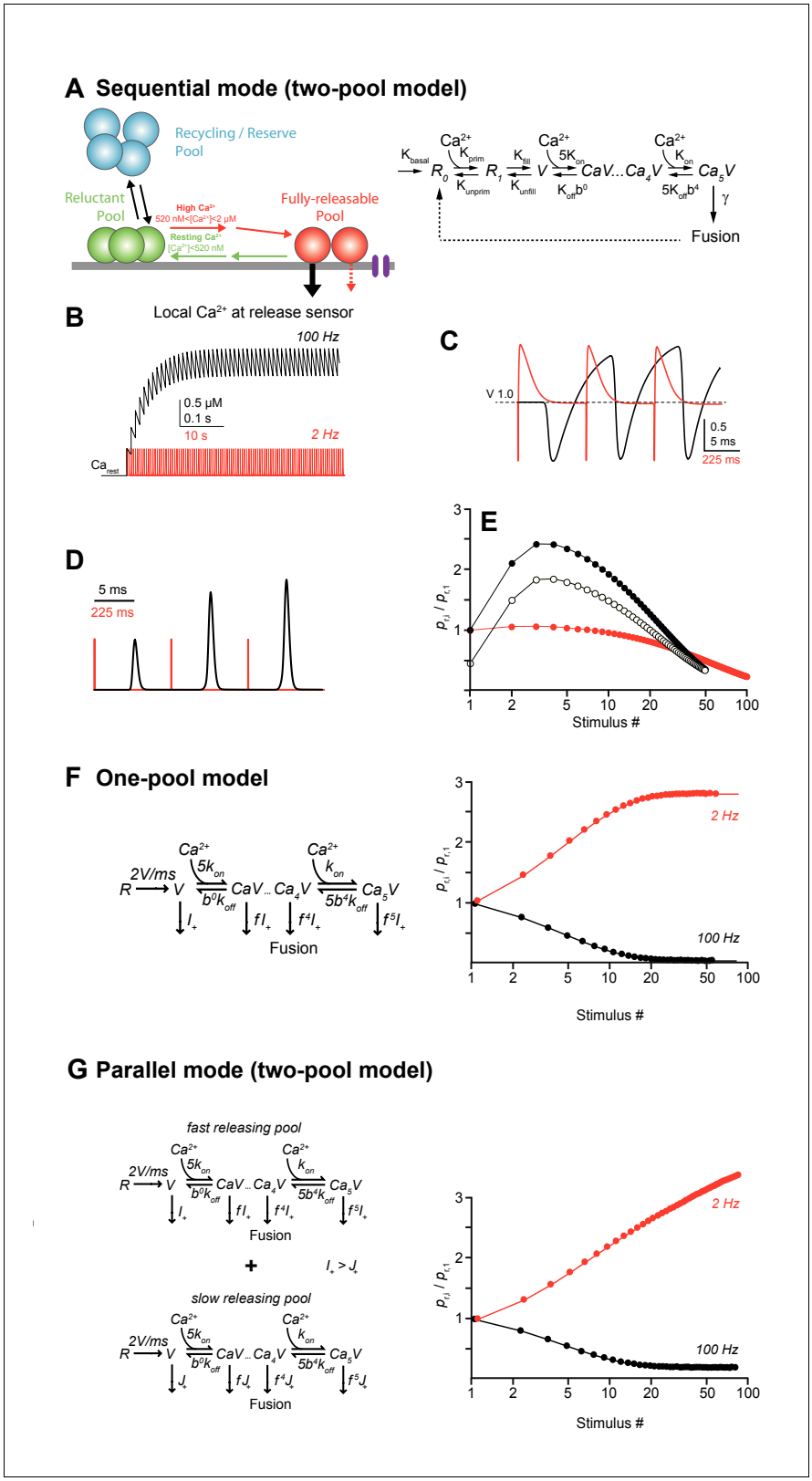

Figure 6. Models of LFD and short-term facilitation. (**A**) *Left*, scheme illustrating the sequential model of Ca^{2+} binding and release at the PF-PC synapse. Voltage-dependent calcium channels are represented in purple. *Right*, in the corresponding mathematical model the recycling/reserve pool is contained only implicitly by restoration of the reluctant pool (R_0+R_1) from fused SVs (dashed arrow) and via a basal refilling rate (k_{basal}). Therefore, this model

Figure 6 continued on next page

Figure 6 continued

is referred to as sequential 'two-pool' model. During high-frequency stimulation, the residual Ca^{2+} increases, resulting in recruitment of SVs from the reluctant pool into the fully-releasable pool, that is, a temporal increase in the fully-releasable pool that enables short-term facilitation (red arrow). The residual Ca^{2+} generates an additional moderate, short-lasting facilitation due to slow unbinding from the release sensor (dashed red arrow). During low-frequency activation at 2 Hz, the residual Ca^{2+} drops back to resting level between stimuli and SVs recruited to the fully-releasable pool return to the reluctant pool (green arrow). (**B**) Simulated amplitudes of residual Ca^{2+} during high- (100 Hz, black) or low-frequency (2 Hz, red) activation starting from a resting Ca^{2+} (Ca_{rest}) level of 50 nM. (**C**) Fraction of Ca^{2+} unoccupied SVs in the fully-releasable pool (V) of the release sensor during the initial three activations of a 100 Hz (black) or 2 Hz (red) activation train. Note that during the first three stimuli at low frequency, the fully-releasable pool relaxes to its initial (V = 1, i.e. 100%) from a transient overfilling (V > 1) prior to the next pulse. The fully-releasable pool continues to increase in size during high-frequency activation due to the build-up of residual Ca^{2+} and continuous recruitment of reluctant vesicles (cf. **B**). (**D**) Transmitter release rates during three stimuli at high (black) or low frequencies (red), normalized to the first release event (**E**) Paired-pulse ratios (PPRs) calculated as the ratio of release probabilities in the i-th ($p_{r,i}$) and the first pulse ($p_{r,1}$) during 100 Hz (filled black) or 2 Hz (red) stimulation. Open circles show PPRs during 100 Hz activations started in a previously depressed state. (**F**) *Left*, one-pool model of Ca^{2+} binding and release according to ***Wölfel et al., 2007*** consisting of the 'allosteric' sensor model (***Lou et al., 2005***) supplemented with a reloading step of 2 SVs/ms. *Right*, in contrast to our experimental findings, this model generates low-frequency facilitation and high-frequency depression. (**G**) *Left*, as in *F* but for two parallel, non-interacting pools of SVs differing in their release rate constants thereby generating a 'fast releasing pool of SVs' (release rate I_+ as in *F*) and a 'slowly releasing pool of SVs' (release rate $J_+<I_+$ as in *F*, Wölfel et al., 2007). Both models are restored via Ca^{2+} independent reloading steps of 2 SVs/ms. *Right*, note that similar to the model in *F*, this simulation generates a high-frequency depression and a low-frequency facilitation. Models in F and G fail to reproduce our experimental findings.

DOI: https://doi.org/10.7554/eLife.28935.009

mechanisms underlying LFD occur at low and high p_r conditions. On the other hand, the recovery from LFD was strongly reduced (maximal recovery 85.5%±11.6 *n* = 5, ***Figure 8D***) with high $[Ca^{2+}]_e$. This indicates that the reluctant pool was partially exhausted after LFD in high $[Ca^{2+}]_e$. Hence, the increase in the number of quanta released during LFD in high $[Ca^{2+}]_e$ probably arises from the recruitment of SVs in reluctant pool.

Next, we tested whether recruitment of the reluctant pool could be affected by impairing the spatiotemporal profile of $[Ca^{2+}]$. EGTA is a slow Ca^{2+} chelator that does not affect $[Ca^{2+}]$ in the nanodomain during single AP but dampens the building-up of $[Ca^{2+}]$ during high-frequency trains (***Schmidt et al., 2013***). Accordingly, LFD and the recovery from LFD by 100 Hz train were monitored before and after application of 10 µM EGTA-AM. Bath application of 10 µM EGTA-AM did not affect the basal release of glutamate (***Figure 8F***, ***Schmidt et al., 2013***) and the time course of LFD (***Figure 8F–H***) whereas the recovery from LFD was slowed-down and reduced during the first responses of the 100 Hz train. Statistically significant differences were detected only at stimulus #4 and #5 of the train (p=0.031 for both stimuli, signed rank test, n = 6) (***Figure 8G***). The reduction in the number of reluctant SVs recruited by a 100 Hz recovery train following an alteration of the spatiotemporal profile of Ca^{2+} confirms our simulation that suggests that one transition step from the reluctant state to the fully-releasable is Ca^{2+}-dependent.

Discussion

The present work demonstrates that the release of glutamate and the presynaptic short-term plasticity at GC-PC synapses are shaped by two pools of releasable SVs, namely fully-releasable SVs and reluctant SVs, which are differentially poised for exocytosis. Whether both pools constitute sub-pools of the RRP is still a matter of debate (***Pan and Zucker, 2009***; ***Neher, 2015***). Here, we propose that the RRP is restricted to the fully-releasable pool, that is, to the only SVs that can be released by a single AP (see also ***Miki et al., 2016***).

Mechanism underlying the recruitment of reluctant SVs

We cannot exclude that GC boutons are heterogeneous and divided in subsets equipped only with the fully-releasable pool, only with the reluctant pool or with both pools. Nevertheless, we previously

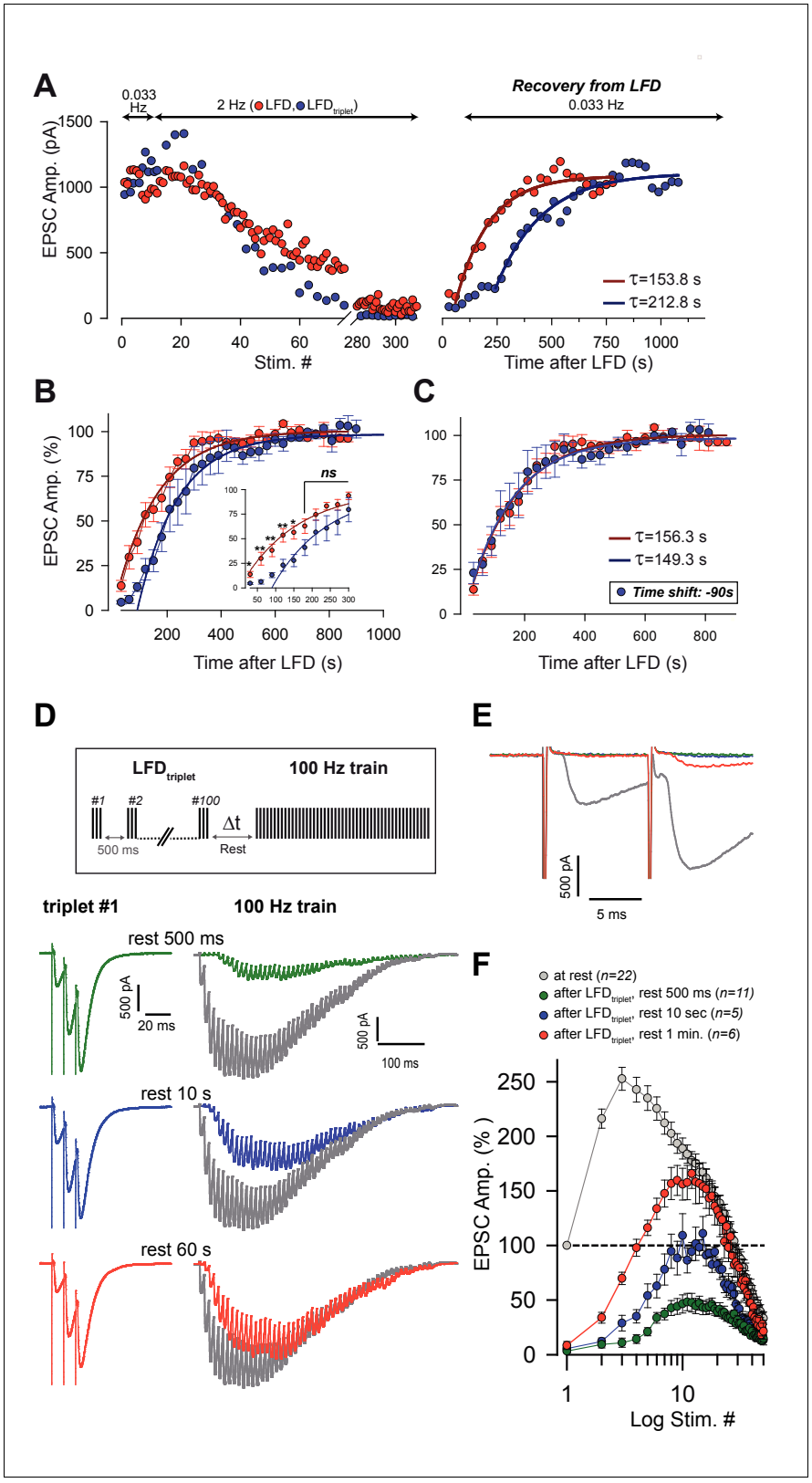

Figure 7. Kinetics of recovery from LFD and LFD$_{triplet}$. (**A**) *Left*, superimposition of the time course of LFD and LFD$_{triplet}$ (triplet stimulation at 200 Hz) elicited successively in the same cell after establishing a baseline of at least 10 successive stimuli at 0.033 Hz. *Right*, recovery from depression probed 30 s after the end of both LFD and LFD$_{triplet}$ by a 0.033 Hz stimulation. For clarity, EPSC amplitudes were plotted against stimulus number in the *left*

Figure 7 continued on next page

Figure 7 continued

graph and against time in the *right* graph. The thick red and blue lines on the *right* graph show monoexponential fits. Note the delay of recovery after $LFD_{triplet}$, stimulation. (**B**) Normalized mean amplitudes of EPSCs evoked by 0.033 Hz stimulation 30 s after LFD (red points, $n = 8$) and after $LFD_{triplet}$ (triplet stimulation at 200 Hz, blue points, $n = 6$). EPSC amplitudes were normalized to the mean value of EPSCs recorded during a baseline established by stimulation at 0.033 Hz. Thick red and blue lines represent monoexponential fits. (**C**) same values as in *B*, except that the time axis was shifted by 90 s for experimental values obtained during the recovery train applied after $LFD_{triplet}$ (blue points). (**D**) Recovery from $LFD_{triplet}$ probed by 100 Hz as indicated by the stimulation paradigm. *Left*, EPSC traces recorded during the 1st triplet stimulation at 2 Hz. *Right*, EPSC traces recorded during 100 Hz trains applied 500 ms, 10 s or 60 s after LFD protocol ended. Traces are superimposed with EPSCs recorded during a 100 Hz train applied before LFD induction (gray traces). (**E**) Superimposition of the first responses to the trains recorded in *D*. The color code is the same as in *D*. (**F**) Mean values of EPSC amplitudes recorded during 100 Hz trains applied 500 ms, 10 s or 60 s after the LFD protocol ended.

DOI: https://doi.org/10.7554/eLife.28935.010

showed that stimulations of unitary GC-PC synapses and stimulations of beam of PFs gave similar values of the PPR (***Valera et al., 2012***; ***Brachtendorf et al., 2015***). Since the ultrafast recruitment of the reluctant pool underlies part of the strong paired-pulse facilitation observed at GC-PC synapses, we believe that most of GC terminals are equipped with both pools. Our simulation and experimental findings show that the recruitment of reluctant SVs is achieved via both Ca^{2+}-dependent and Ca^{2+}-independent steps. Several presynaptic proteins involved in priming stages bear C2-domains that mediate their actions in Ca^{2+}-dependent and Ca^{2+}-independent priming processes (***Pinheiro et al., 2016***). Notably, two C2-domain-containing proteins have been implicated in short-term facilitation, synaptotagmin 7 (***Jackman et al., 2016***; ***Jackman and Regehr, 2017***) and Munc13s (***Betz et al., 1998***; ***Augustin et al., 2001***; ***Basu et al., 2007***; ***Shin et al., 2010***; ***Zhou et al., 2013***). Synaptotagmin 7 is unlikely to play a role in the ultrafast recruitment of SVs from the reluctant pool because of the slow kinetics of its C2A domain (***Hui et al., 2005***; ***Brandt et al., 2012*** but see ***Jackman and Regehr, 2017***). Alternatively, Munc13s can mediate short-term facilitation through the calmodulin-binding domain (***Junge et al., 2004***; ***Zikich et al., 2008***) and/or via heterodimerization of the C2A-domain with the Rab3-binding protein RIM (***Camacho et al., 2017***). Interestingly, Munc13s are required in a superpriming step that may be analogous to the transition process described in this study (***Lee et al., 2013***; ***Lipstein et al., 2013***; ***Ishiyama et al., 2014***). At present, it is not known whether these interactions are fast enough to mediate the transition from the reluctant pool to the fully-releasable one.

In other cerebellar synapses, strong short-term facilitation relies on an ultrafast reloading of release sites (***Saviane and Silver, 2006***; ***Miki et al., 2013***). Future experiments will determine whether these fast reloading processes are analogous to the fast recruitment of reluctant SVs at GC to PC synapses. Several scaffolding proteins of the cytomatrix at the active zone such as Bassoon or actin filaments tether SVs in the close vicinity of release sites (***Schoch and Gundelfinger, 2006***; ***Siksou et al., 2007***, ***2011***; ***Gundelfinger et al., 2015***; ***Kittel and Heckmann, 2016***) and are required to speed-up the refilling of emptied release sites during high-frequency stimulations (***Hallermann et al., 2010***; ***Lee et al., 2012***; ***Hallermann and Silver, 2013***; ***Miki et al., 2016***). At GC-PC synapses, these filamentous proteins may serve as tracks or molecular motors driving reluctant SVs up to the fusion sites (***Hallermann and Silver, 2013***). Anyhow, both experimental data (***Figure 7***) and simulations (***Figure 6***) suggest that SVs can revert from the fully-releasable status back to the reluctant one, but it remains unclear why the equilibrium shifts toward the reluctant state at low frequencies. The step back to the reluctant state may correspond to an 'a posteriori' mechanism impeding the functioning of active release sites in the low-frequency range (***Wölfel et al., 2007***; ***Schneggenburger et al., 2012***). After SV fusion, release sites have to be purged of SV membranes and the time course of this clearance by endocytosis may act as a limiting factor for exocytosis during repetitive activities (***Hosoi et al., 2009***; ***Hua et al., 2013***). On the other hand, as proposed for invertebrate synapses (***Silverman-Gavrila et al., 2005***; ***Doussau et al., 2010***), LFD may arise from an imbalance in the activation of presynaptic kinases and phosphatases and as such the kinase/phosphatase balance would act as a frequency sensor regulating the equilibrium between the two pools.

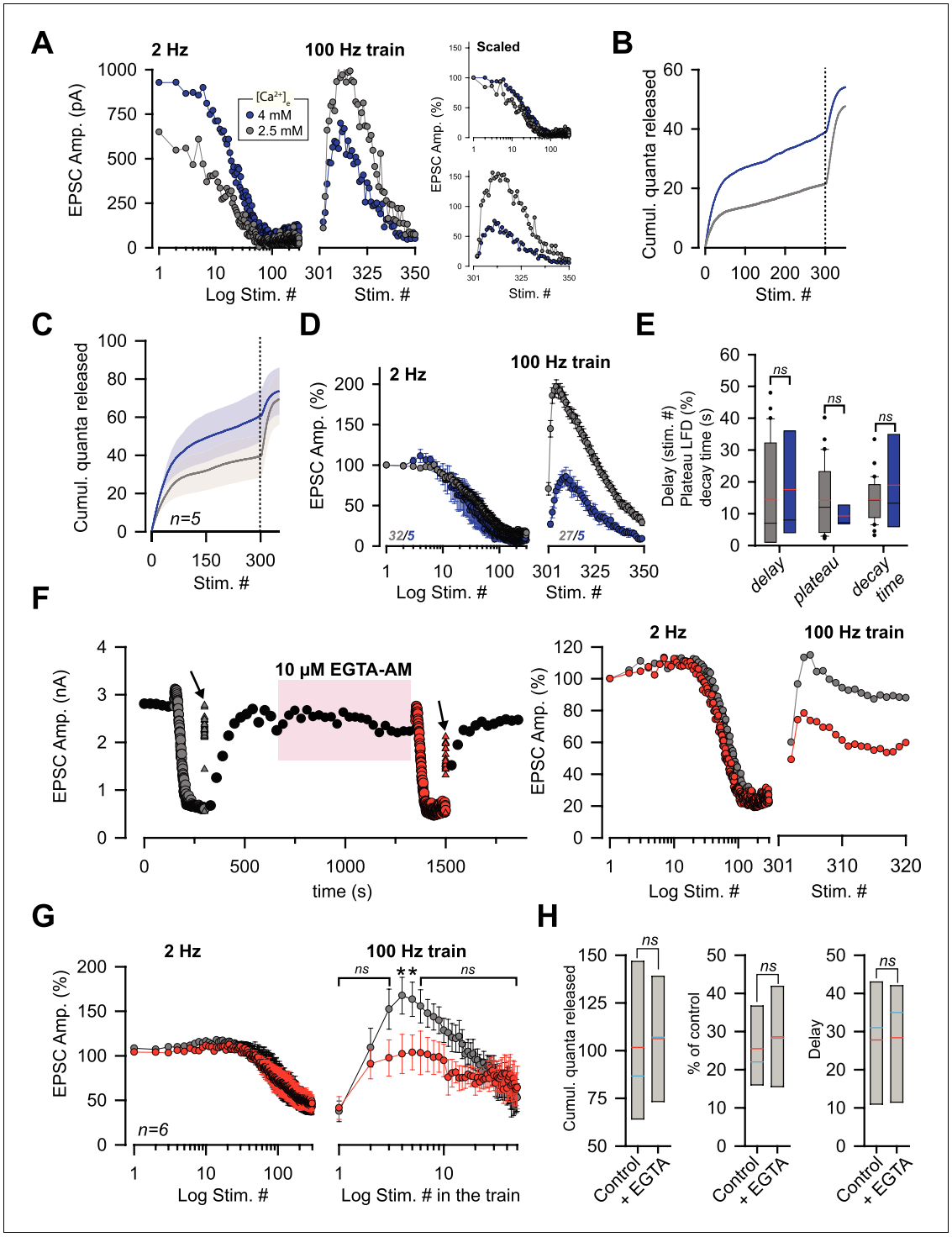

Figure 8. The reluctant pool can be recruited by increasing p_r. (**A**) Amplitude of ESPCs in the same PC during LFD (*left panel*) and during the recovery from LFD (*middle panel*) by a 100 Hz train before and after an increase in $[Ca^{2+}]_e$ from 2.5 mM (gray points) to 4 mM (blue point). The right panels show the same experiment with EPSC amplitudes normalized with respect to the first response of LFD (**B**) Corresponding cumulative number of quanta release during LFD (stimuli #1 to #300) and during the recovery train (stimuli #301 to #350) in low and high $[Ca^{2+}]_e$. (same color code than in *A*). (**C**), Mean values of the cumulative number of quanta release during LFD (stimuli #1 to #300) and during recovery train at 100 Hz (stimuli #301 to #350) in low and high $[Ca^{2+}]_e$. The dashed line represents the end of the LFD protocol (same color code than in *A*). LFD and recovery trains were recorded in the same PCs. (**D**), Mean values of normalized EPSC amplitudes during LFD (*left panel*) and during the recovery via a

Figure 8 continued on next page

Figure 8 continued

100 Hz train (*right panel*) in presence of 2.5 mM (gray points, same set of data than in ***Figure 1E*** for LFD and same set of data than in ***Figure 2D*** for recovery trains) and 4 mM $[Ca^{2+}]_e$ (blue points). EPSC amplitudes were normalized with respect to the first response of LFD. (**E**) Box-plots showing the delay (mean number of stimuli before the onset of LFD: 14.5 ± 2.8, *n* = 30 at $[Ca^{2+}]_e$ = 2.5 mM compared to 17.6 ± 8.0, *n* = 5, at $[Ca^{2+}]_e$=4 mM, MWRST, p=0.60), plateau of LFD (mean percentage of initial responses: 14.2 ± 2.0%, *n* = 30 at $[Ca^{2+}]_e$ = 2.5 mM compared to 9.3 ± 1.4%, *n* = 5, at $[Ca^{2+}]_e$=4 mM, p=0.69, MWRST) and decay time (tau: 14.3 s ± 1.3 s, *n* = 30 at $[Ca^{2+}]_e$ = 2.5 mM compared to 18.9 s ± 6.8 s, *n* = 5, at $[Ca^{2+}]_e$=4 mM, p=0.87, MWRST) in presence of 2.5 mM (gray boxes, same set of data than in ***Figure 1E*** for LFD and same set of data than in ***Figure 2D*** for recovery trains) and 4 mM $[Ca^{2+}]_e$ (blue boxes). Black and red lines indicate median and mean values, respectively. (**F**) *left*, typical experiment showing the time course of EPSC amplitudes before and after application of 10 µM EGTA-AM. Black points correspond to EPSCs recorded during 0.033 Hz stimulation. Gray and red symbols correspond to EPSCs recorded during LFD (circles) and during the recovery trains at 100 Hz (triangles) before and after the bath application of 10 µM EGTA-AM respectively. Arrows indicate the application of a recovery train at 100 Hz. The pink box represents the bath application of 10 µM EGTA-AM. *Right*, corresponding ESPC amplitudes normalized with respect to the first response of LFD. (**G**) Mean EPSC amplitudes recorded during LFD (*left panel*) and during recovery trains (*right panel*) before (gray points) and after (red points) application of EGTA-AM. Note the difference in EPSC amplitudes evoked during the first stimuli at 100 Hz. Numbers at the *bottom* of the graphs indicate the number of cells recorded. (**H**) Box-plots showing the cumulative number of quanta released during LFD, the plateau of LFD and the delay before the onset of LFD before and after application of 10 µM EGTA-AM (same set of experiment as in *G*). None of these three parameters were statistically different between the two conditions (paired *t*-test, p=0.65, for the cumulative number of quanta released, paired *t*-test, p=0.39 for the plateau of LFD and paired *t*-test, p=0.89, for the delay, *n* = 6). Blue and red lines indicate median and mean values respectively.

DOI: https://doi.org/10.7554/eLife.28935.011

Our calculations indicate that the number of SVs that can be released during high-frequency trains after a full depletion of fully-releasable SVs corresponds to the size of the reluctant pool (***Figure 4***). Since the number of SVs released per bouton (30–40 SVs, ***Figures 1*** and ***4***) during 50/100 Hz trains, LFD, $LFD_{triplet}$ or during recovery trains far exceeds the number of docked SVs counted in one varicosity at GC-PC synapses (4–8 SVs, ***Xu-Friedman et al., 2001***), we postulate that the two releasable pools are refilled by other pools (recycling pool, reserve pool) during LFD, $LFD_{triplet}$ and during the late phase of high-frequency trains.

The segregation of releasable SVs in two pools shapes short-term plasticity

Neuronal networks in the cerebellar cortex have to process sensory information coded at ultra-high frequencies (up to 1 kilohertz, ***van Kan et al., 1993***; ***Arenz et al., 2008***, ***Arenz et al., 2009***). Most of this information is conveyed to the granular layer, the input stage of the cerebellar cortex, via the mossy fiber (MF) pathway. Strikingly, MF-GC synapses can sustain high frequency trains of input by using a specific arrangement of the presynaptic machinery to achieve ultra-fast reloading of SVs (***Saviane and Silver, 2006***; ***Rancz et al., 2007***; ***Hallermann et al., 2010***; ***Ritzau-Jost et al., 2014***). However, it is not clear how these high- frequency inputs are integrated at the GC-PC synapses, the major site for information storage in the cerebellum (***Thach et al., 1992***; ***Ito, 2006***; ***D'Angelo and De Zeeuw, 2009***). We previously showed that none of the classical mechanisms for facilitation (including the buffer saturation model and residual Ca^{2+}, ***Pan and Zucker, 2009***; ***Regehr, 2012***) involving only an increase in p_r can account for the high paired-pulse facilitation at GC-PC synapses and for its unusual ability to sustain glutamate release at high-frequency trains. During a train of APs at high frequency, the local $[Ca^{2+}]$ at release sites increases (***Schmidt et al., 2013***) leading to an immediate increase in the number of release sites *N* that underlies high values of paired-pulse facilitation (***Valera et al., 2012***; ***Brachtendorf et al., 2015***). Here, we show that this increase in *N* arises from the fast recruitment of reluctant SVs into a fully-releasable pool. A fast and sequential recruitment of a 'replacement pool' in 'a docked pool' accounting for paired-pulse facilitation has been recently described at GC-MLI synapses (***Miki et al., 2016***). The GC-PC synapse is unique, because it allows for inactivation of the fully-releasable pool by low-frequency stimulation. The combination of both mechanisms endows these synapses with the striking ability to filter repetitive activities around

2 Hz and to invert the orientation of presynaptic plasticity (full depression versus strong facilitation) depending on the stimulation frequency (***Figure 2***). Finally, during high-frequency inputs, GC-PC synapses are able to set the release glutamate independently of the state of the synapse (synapse at rest or depressed synapse) (***Figure 2***).

Physiological implications

Our results provide new hypotheses about information processing in the MF-GC-PC pathway. In vivo experiments have shown that in lobules IV and V, GCs responding to joint rotation fire spontaneously at 2–10 Hz due to sustained synaptic inputs from MFs. Upon joint movement, their firing rate shifts instantaneously into burst mode with frequencies ranging from ~50 Hz to 300 Hz (***Jörntell and Ekerot, 2006***). Based on our work, we propose that GC-PC synapses filter GC activity. In the absence of sensory activity, GC inputs to PCs are silenced as most SVs are in the reluctant state. During joint movement, the efficient transmission of high-frequency activity from MF to GC (***Saviane and Silver, 2006***; ***Rancz et al., 2007***; ***Hallermann et al., 2010***) and from GC to PC (***Valera et al., 2012***) is enabled by the recruitment of the reluctant pool at GC-PC terminals. The efficient filtering of low-frequency activity would enhance the signal to noise ratio and enable PCs to discern sensory signals from spontaneous activity in GCs. Future in vivo studies will reveal whether this model correspond to a realistic process of information in the cerebellar cortex.

Materials and methods

All experimental protocols are in accordance with European and French guidelines for animal experimentation and have been approved by the Bas-Rhin veterinary office, Strasbourg, France (authorization number A 67–311 to FD).

Slice preparation

Acute horizontal cerebellar slices were prepared from male C57Bl/6 mice aged 18–25 days. Mice were anesthetized by isoflurane inhalation and decapitated. The cerebellum was dissected out in ice-cold ACSF bubbled with carbogen (95% O_2, 5% CO_2) and containing (in mM) 120 NaCl, 3 KCl, 26 $NaHCO_3$, 1.25 NaH_2PO_4, 2.5 $CaCl_2$, 2 $MgCl_2$, 10 glucose and 0.05 minocyclin. Slices were then prepared (Microm HM650V, Germany) in an ice-cold solution containing (in mM) 93 *N*-Methyl-D-Glucamine, 2.5 KCl, 0.5 $CaCl_2$, 10 $MgSO_4$, 1.2 NaH_2PO_4, 30 $NaHCO_3$, 20 HEPES, 3 Na-Pyruvate, 2 Thiourea, 5 Na-ascorbate, 25 D-Glucose and 1 Kynurenic acid (***Millar et al., 2005***; ***Wölfel et al., 2007***; ***Sakaba, 2008***). Slices 300 µm thick were briefly soaked in a sucrose-based solution at 34°C bubbled with carbogen and containing (in mM) 230 sucrose, 2.5 KCl, 26 $NaHCO_3$, 1.25 NaH_2PO_4, 25 glucose, 0.8 $CaCl_2$ and 8 $MgCl_2$ before being maintained in bubbled ASCF medium (see above) at 34°C until further use.

Electrophysiology

After at least 1 hr of recovery at 34°C, a slice was transferred to a recording chamber. In order to block inhibitory transmission, postsynaptic plasticity and retrograde signaling, $GABA_B$ and endocannabinoid signaling, slices were continuously perfused with bubbled ACSF containing the following $GABA_A$, $GABA_B$, NMDA, CB1 and mGluR1 receptor antagonists: 100 µM picrotoxin, 10 µm CGP52432 (3-[[(3,4-Dichlorophenyl)-methyl]amino]propyl(diethoxymethyl)phosphinic acid), 100 µM D-AP5 (D-(-)−2-Amino-5-phosphonopentanoic acid) and 1 µM AM251 (1-(2,4-Dichlorophenyl)−5-(4-iodophenyl)−4-methyl-N-(piperidin-1-yl)−1H-pyrazole-3-carboxamide) and 2 µM JNJ16259685 ((3,4-Dihydro-2H-pyrano[2,3-b]quinolin-7-yl)-(cis-4-methoxycyclohexyl)-methanone). Recordings were made at 34°C in PCs located in the vermis. PCs were visualized using infrared contrast optics on an Olympus BX51WI upright microscope. Whole-cell patch-clamp recordings were obtained using a Multiclamp 700A amplifier (Molecular Devices, USA). Pipette (2.5–3 MΩresistance) capacitance was cancelled and series resistance (R_s) between 5 and 8 mΩ was compensated at 80%. R_s was monitored regularly during the experiment and the recording was stopped when R_s changed significantly (>20%). The membrane potential was held at −60 mV. The intracellular solution for voltage-clamp recording contained (in mM): 140 $CsCH_3SO_3$, 10 Phosphocreatine, 10 HEPES, 5 QX314-Cl, 10 BAPTA, 4 Na-ATP and 0.3 Na-GTP. Parallel fibers were stimulated extracellularly using a monopolar glass electrode filled with ACSF, positioned at least 100 µm away from the PC to ensure a clear

separation between the stimulus artifact and EPSCs. Pulse train and low-frequency stimulation were generated using an Isostim A320 isolated constant current stimulator (World Precision Instruments, UK) controlled by WinWCP freeware (John Dempster, Strathclyde Institute of Pharmacy and Biomedical Sciences, University of Strathclyde, UK). The synaptic currents evoked in PCs were low-pass filtered at 2 KHz and sampled at 20 to 50 KHz (National Instruments, Austin, Texas).

Simulation of transmitter release and Ca^{2+}dynamics

Models for Ca^{2+}-dependent SV fusion and replenishment (***Sakaba, 2008***) were transformed into the corresponding ordinary differential equations and numerically solved using Mathematica 10.0 (Wolfram Research). Release rates were obtained by differentiation of the fused state. Paired-pulse ratios were calculated from the ratios of release probabilities obtained by the integration of release rates. Parameters for the release sensor part of the sequential two-pool model (***Figure 7A,V***, corresponding to fully-releasable SVs) were similar to those used by Sakaba (***Schmidt et al., 2013***) with forward rate k_{on} = 1*10^8 $M^{-1}s^{-1}$, backward rate k_{off} = 3000 s^{-1}, cooperativity b = 0.25, and release rate γ = 5000 s^{-1}. Parameters for the replenishment part of this model (R_0, R_1 representing the reluctant pool) were similar to those given by ***Millar et al., 2005*** for a phasic synapse and defined empirically. The forward and backward rate constants of Ca^{2+}-dependent priming and unpriming were k_{prim} = 8*10^8 $M^{-1}s^{-1}$ and k_{unprim} = 120 s^{-1}, respectively. Ca^{2+}-independent filling and unfilling rates were k_{fill} = 200 s^{-1} and k_{unfil} = 150 s^{-1}, respectively. Ninety percent of released SVs were recycled into the unprimed pool, supported by a slow Ca^{2+}-independent filling rate of k_{basal} = 0.002 s^{-1}, reflecting filling from a reserve pool. Recovery from low-frequency depression (LFD, see results section) was simulated by restarting the model at high frequency with the size of the releasable pool set to the value at the end of the 2 Hz train, and the unprimed pool (R_0) fully recovered. The one-pool model (***Figure 7F***) and the parallel two-pool model (***Figure 7G***) and their parameters were taken from ***Wölfel et al. (2007)***.

Release-triggering Ca^{2+} signals were simulated as repeated Gaussian curves spaced by interstimulus intervals and adjusted to match the amplitude (22.5 µM) and half-width (5 µs) of the estimated action potential-mediated Ca^{2+} signal at the release sensor of PF synapses (***Schmidt et al., 2013***). In the sequential two-pool model (***Figure 7A***), SV replenishment was driven by residual Ca^{2+} with an amplitude of 520 nM per pulse, dropping exponentially with a time constant of 42 ms and summing linearly depending on the length of the interstimulus interval (***Brenowitz and Regehr, 2007***). For the two other models (***Figure 7G,F***) SV replenishment occurred at a constant rate of 2 SV/ms (***Wölfel et al., 2007***). Resting Ca^{2+} was assumed to be 50 nM.

Data and statistical analysis

Data were acquired using WinWCP 4.2.x freeware (John Dempster, SIPBS, University of Strathclyde, UK). Analyses were performed using PClamp9 (Molecular Devices, USA), Igor (6.22A) graphing and analysis environment (Wavemetrics, USA). Error bars in figures show SEMs. Student's *t* test or paired *t*-test were performed when data were normally distributed; the Mann-Whitney Rank Sum Test (MWRST) or the signed rank test were used in all other cases. Statistical tests were performed using SigmaPlot 11 (Systat Software). The levels of significance are indicated as *ns* (not significant) when $p>0.05$, * when $p\leq0.05$, ** when $p\leq0.01$ and *** when $p\leq0.001$.

Acknowledgements

This work was supported by the Centre National pour la Recherche Scientifique, the Université de Strasbourg, the Agence Nationale pour la Recherche Grant (ANR-15-CE37-0001-01 CeMod) and by the Fondation pour la Recherche Médicale to PI (# DEQ20140329514). We thank the TIGER project funded by INTERREG IV Rhin Supérieur program and European Funds for Regional Development (FEDER, # A31). This work was also supported by a DFG grant to HS (SCHM1838). AMV and KD were funded by a fellowship from the Ministère de la Recherche. AMV was also funded by a fellowship from the Fondation pour la Recherche Médicale. We thank Sophie Reibel-Foisset and the animal facility Chronobiotron (UMS 3415 CNRS and Strasbourg University) for technical assistance. We thank Dr. Frank Pfrieger, Dr. Matilde Cordero-Erausquin and Joanna Lignot (Munro Language Services) for proofreading.

Additional information

Funding

Funder	Grant reference number	Author
Agence Nationale de la Recherche	ANR-2010-JCJC-1403-1 MicroCer	Philippe Isope
Fondation pour la Recherche Médicale	DEQ20140329514	Philippe Isope
Centre National de la Recherche Scientifique		Philippe Isope
Université de Strasbourg		Philippe Isope
INTERREG IV Rhin superieur	FEDER # A31	Philippe Isope
Deutsche Forschungsgemeinschaft	SCHM1838	Hartmut Schmidt
Agence Nationale de la Recherche	ANR15-37-CE37-0001-01 CeModR	Philippe Isope

The funders had no role in study design, data collection and interpretation, or the decision to submit the work for publication.

Author contributions

Frédéric Doussau, Conceptualization, Resources, Data curation, Formal analysis, Supervision, Validation, Investigation, Visualization, Methodology, Writing—original draft, Project administration, Writing—review and editing; Hartmut Schmidt, Resources, Software, Formal analysis, Funding acquisition, Investigation, Methodology, Writing—review and editing; Kevin Dorgans, Data curation, Software, Formal analysis, Investigation, Methodology; Antoine M Valera, Software, Formal analysis; Bernard Poulain, Conceptualization, Writing—review and editing; Philippe Isope, Conceptualization, Formal analysis, Supervision, Funding acquisition, Validation, Investigation, Visualization, Methodology, Project administration, Writing—review and editing

Author ORCIDs

Frédéric Doussau, http://orcid.org/0000-0002-3769-1402
Hartmut Schmidt, https://orcid.org/0000-0002-9516-423X
Kevin Dorgans, http://orcid.org/0000-0003-1724-6384
Antoine M Valera, https://orcid.org/0000-0002-0230-9752
Bernard Poulain, http://orcid.org/0000-0002-2601-5310
Philippe Isope, https://orcid.org/0000-0002-0630-5935

Ethics

Animal experimentation: All experimental protocols are in accordance with European and French guidelines for animal experimentation and have been approved by the Bas-Rhin veterinary office, Strasbourg, France (authorization number A 67-311 to FD)

Decision letter and Author response

Decision letter https://doi.org/10.7554/eLife.28935.013
Author response https://doi.org/10.7554/eLife.28935.014

Additional files

Supplementary files

- Transparent reporting form

DOI: https://doi.org/10.7554/eLife.28935.012

References

Arenz A, Bracey EF, Margrie TW. 2009. Sensory representations in cerebellar granule cells. *Current Opinion in Neurobiology* **19**:445–451. DOI: https://doi.org/10.1016/j.conb.2009.07.003, PMID: 19651506

Arenz A, Silver RA, Schaefer AT, Margrie TW. 2008. The contribution of single synapses to sensory representation in vivo. *Science* **321**:977–980 . DOI: https://doi.org/10.1126/science.1158391, PMID: 18703744

Atluri PP, Regehr WG. 1996. Determinants of the time course of facilitation at the granule cell to Purkinje cell synapse. *Journal of Neuroscience* **16**:5661–5671. PMID: 8795622

Augustin I, Korte S, Rickmann M, Kretzschmar HA, Südhof TC, Herms JW, Brose N. 2001. The cerebellum-specific Munc13 isoform Munc13-3 regulates cerebellar synaptic transmission and motor learning in mice. *Journal of Neuroscience* **21**:10–17. PMID: 11150314

Baginskas A, Palani D, Chiu K, Raastad M. 2009. The H-current secures action potential transmission at high frequencies in rat cerebellar parallel fibers. *European Journal of Neuroscience* **29**:87–96 . DOI: https://doi.org/10.1111/j.1460-9568.2008.06566.x, PMID: 19087162

Basu J, Betz A, Brose N, Rosenmund C. 2007. Munc13-1 C1 domain activation lowers the energy barrier for synaptic vesicle fusion. *Journal of Neuroscience* **27**:1200–1210 . DOI: https://doi.org/10.1523/JNEUROSCI.4908-06.2007, PMID: 17267576

Beierlein M, Fioravante D, Regehr WG. 2007. Differential expression of posttetanic potentiation and retrograde signaling mediate target-dependent short-term synaptic plasticity. *Neuron* **54**:949–959 . DOI: https://doi.org/10.1016/j.neuron.2007.06.002, PMID: 17582334

Betz A, Ashery U, Rickmann M, Augustin I, Neher E, Südhof TC, Rettig J, Brose N. 1998. Munc13-1 is a presynaptic phorbol ester receptor that enhances neurotransmitter release. *Neuron* **21**:123–136. PMID: 9697857

Bidoret C, Ayon A, Barbour B, Casado M. 2009. Presynaptic NR2A-containing NMDA receptors implement a high-pass filter synaptic plasticity rule. *PNAS* **106**:14126–14131 . DOI: https://doi.org/10.1073/pnas.0904284106, PMID: 19666514

Bornschein G, Arendt O, Hallermann S, Brachtendorf S, Eilers J, Schmidt H. 2013. Paired-pulse facilitation at recurrent Purkinje neuron synapses is independent of calbindin and parvalbumin during high-frequency activation. *The Journal of Physiology* **591**:3355–3370. DOI: https://doi.org/10.1113/jphysiol.2013.254128, PMID: 23671160

Borst JG, Soria van Hoeve J. 2012. The calyx of Held synapse: from model synapse to auditory relay. *Annual Review of Physiology* **74**:199–224. DOI: https://doi.org/10.1146/annurev-physiol-020911-153236, PMID: 22035348

Bouvier G, Higgins D, Spolidoro M, Carrel D, Mathieu B, Léna C, Dieudonné S, Barbour B, Brunel N, Casado M. 2016. Burst-Dependent Bidirectional Plasticity in the Cerebellum Is Driven by Presynaptic NMDA Receptors. *Cell Reports* **15**:104–116 . DOI: https://doi.org/10.1016/j.celrep.2016.03.004, PMID: 27052175

Brachtendorf S, Eilers J, Schmidt H. 2015. A use-dependent increase in release sites drives facilitation at calretinin-deficient cerebellar parallel-fiber synapses. *Frontiers in Cellular Neuroscience* **9**:27. DOI: https://doi.org/10.3389/fncel.2015.00027, PMID: 25691858

Brandt DS, Coffman MD, Falke JJ, Knight JD. 2012. Hydrophobic contributions to the membrane docking of synaptotagmin 7 C2A domain: mechanistic contrast between isoforms 1 and 7. *Biochemistry* **51**:7654–7664. DOI: https://doi.org/10.1021/bi3007115, PMID: 22966849

Brenowitz SD, Regehr WG. 2007. Reliability and heterogeneity of calcium signaling at single presynaptic boutons of cerebellar granule cells. *Journal of Neuroscience* **27**:7888–7898 . DOI: https://doi.org/10.1523/JNEUROSCI.1064-07.2007, PMID: 17652580

Camacho M, Basu J, Trimbuch T, Chang S, Pulido-Lozano C, Chang SS, Duluvova I, Abo-Rady M, Rizo J, Rosenmund C. 2017. Heterodimerization of Munc13 C2A domain with RIM regulates synaptic vesicle docking and priming. *Nature Communications* **8**:15293 . DOI: https://doi.org/10.1038/ncomms15293, PMID: 28489077

Chadderton P, Margrie TW, Häusser M. 2004. Integration of quanta in cerebellar granule cells during sensory processing. *Nature* **428**:856–860 . DOI: https://doi.org/10.1038/nature02442, PMID: 15103377

Chamberland S, Evstratova A, Tóth K. 2014. Interplay between synchronization of multivesicular release and recruitment of additional release sites support short-term facilitation at hippocampal mossy fiber to CA3 pyramidal cells synapses. *Journal of Neuroscience* **34**:11032–11047. DOI: https://doi.org/10.1523/JNEUROSCI.0847-14.2014, PMID: 25122902

D'Angelo E, De Zeeuw CI. 2009. Timing and plasticity in the cerebellum: focus on the granular layer. *Trends in neurosciences* **32**:30–40 . DOI: https://doi.org/10.1016/j.tins.2008.09.007, PMID: 18977038

Doussau F, Humeau Y, Benfenati F, Poulain B. 2010. A novel form of presynaptic plasticity based on the fast reactivation of release sites switched off during low-frequency depression. *Journal of Neuroscience* **30**:16679–16691. DOI: https://doi.org/10.1523/JNEUROSCI.3644-09.2010, PMID: 21148007

Gundelfinger ED, Reissner C, Garner CC. 2015. Role of Bassoon and Piccolo in Assembly and Molecular Organization of the Active Zone. *Frontiers in Synaptic Neuroscience* **7**:e19.

Hallermann S, Fejtova A, Schmidt H, Weyhersmüller A, Silver RA, Gundelfinger ED, Eilers J. 2010. Bassoon speeds vesicle reloading at a central excitatory synapse. *Neuron* **68**:710–723 . DOI: https://doi.org/10.1016/j.neuron.2010.10.026, PMID: 21092860

Hallermann S, Silver RA. 2013. Sustaining rapid vesicular release at active zones: potential roles for vesicle tethering. *Trends in Neurosciences* **36**:185–194. DOI: https://doi.org/10.1016/j.tins.2012.10.001, PMID: 23164531

Hosoi N, Holt M, Sakaba T. 2009. Calcium dependence of exo- and endocytotic coupling at a glutamatergic synapse. *Neuron* **63**:216–229. DOI: https://doi.org/10.1016/j.neuron.2009.06.010, PMID: 19640480

Hua Y, Woehler A, Kahms M, Haucke V, Neher E, Klingauf J. 2013. Blocking endocytosis enhances short-term synaptic depression under conditions of normal availability of vesicles. *Neuron* **80**:343–349 . DOI: https://doi.org/10.1016/j.neuron.2013.08.010, PMID: 24139039

Hui E, Bai J, Wang P, Sugimori M, Llinas RR, Chapman ER. 2005. Three distinct kinetic groupings of the synaptotagmin family: candidate sensors for rapid and delayed exocytosis. *PNAS* **102**:5210–5214 . DOI: https://doi.org/10.1073/pnas.0500941102, PMID: 15793006

Ishiyama S, Schmidt H, Cooper BH, Brose N, Eilers J. 2014. Munc13-3 superprimes synaptic vesicles at granule cell-to-basket cell synapses in the mouse cerebellum. *Journal of Neuroscience* **34**:14687–14696. DOI: https://doi.org/10.1523/JNEUROSCI.2060-14.2014, PMID: 25355221

Isope P, Barbour B. 2002. Properties of unitary granule cell–>Purkinje cell synapses in adult rat cerebellar slices. *Journal of Neuroscience* **22**:9668–9678. PMID: 12427822

Ito M. 2006. Cerebellar circuitry as a neuronal machine. *Progress in Neurobiology* **78**:272–303. DOI: https://doi.org/10.1016/j.pneurobio.2006.02.006, PMID: 16759785

Jackman SL, Regehr WG. 2017. The Mechanisms and Functions of Synaptic Facilitation. *Neuron* **94**:447–464 . DOI: https://doi.org/10.1016/j.neuron.2017.02.047, PMID: 28472650

Jackman SL, Turecek J, Belinsky JE, Regehr WG. 2016. The calcium sensor synaptotagmin 7 is required for synaptic facilitation. *Nature* **529**:88–91 . DOI: https://doi.org/10.1038/nature16507, PMID: 26738595

Junge HJ, Rhee JS, Jahn O, Varoqueaux F, Spiess J, Waxham MN, Rosenmund C, Brose N. 2004. Calmodulin and Munc13 form a Ca2+ sensor/effector complex that controls short-term synaptic plasticity. *Cell* **118**:389–401. DOI: https://doi.org/10.1016/j.cell.2004.06.029, PMID: 15294163

Jörntell H, Ekerot CF. 2006. Properties of somatosensory synaptic integration in cerebellar granule cells in vivo. *Journal of Neuroscience* **26**:11786–11797. DOI: https://doi.org/10.1523/JNEUROSCI.2939-06.2006, PMID: 17093099

Kaeser PS, Regehr WG. 2014. Molecular mechanisms for synchronous, asynchronous, and spontaneous neurotransmitter release. *Annual Review of Physiology* **76**:333–363. DOI: https://doi.org/10.1146/annurev-physiol-021113-170338, PMID: 24274737

Kittel RJ, Heckmann M. 2016. Synaptic vesicle proteins and active zone plasticity. *Frontiers in Synaptic Neuroscience* **8**:8. DOI: https://doi.org/10.3389/fnsyn.2016.00008, PMID: 27148040

Kocsis JD, Malenka RC, Waxman SG. 1983. Effects of extracellular potassium concentration on the excitability of the parallel fibres of the rat cerebellum. *The Journal of Physiology* **334**:225–244. DOI: https://doi.org/10.1113/jphysiol.1983.sp014491, PMID: 6864558

Kreitzer AC, Regehr WG. 2000. Modulation of transmission during trains at a cerebellar synapse. *Journal of Neuroscience* **20**:1348–1357. PMID: 10662825

Lee JS, Ho WK, Lee SH. 2012. Actin-dependent rapid recruitment of reluctant synaptic vesicles into a fast-releasing vesicle pool. *PNAS* **109**:E765–E774 . DOI: https://doi.org/10.1073/pnas.1114072109, PMID: 22393020

Lee JS, Ho WK, Neher E, Lee SH. 2013. Superpriming of synaptic vesicles after their recruitment to the readily releasable pool. *PNAS* **110**:15079–15084 . DOI: https://doi.org/10.1073/pnas.1314427110, PMID: 23980146

Lipstein N, Sakaba T, Cooper BH, Lin KH, Strenzke N, Ashery U, Rhee JS, Taschenberger H, Neher E, Brose N. 2013. Dynamic control of synaptic vesicle replenishment and short-term plasticity by Ca(2+)-calmodulin-Munc13-1 signaling. *Neuron* **79**:82–96 . DOI: https://doi.org/10.1016/j.neuron.2013.05.011, PMID: 23770256

Lou X, Scheuss V, Schneggenburger R. 2005. Allosteric modulation of the presynaptic Ca2+ sensor for vesicle fusion. *Nature* **435**:497–501. DOI: https://doi.org/10.1038/nature03568, PMID: 15917809

Marcaggi P, Attwell D. 2005. Endocannabinoid signaling depends on the spatial pattern of synapse activation. *Nature Neuroscience* **8**:776–781. DOI: https://doi.org/10.1038/nn1458, PMID: 15864304

Miki T, Hirai H, Takahashi T. 2013. Activity-dependent neurotrophin signaling underlies developmental switch of Ca2+ channel subtypes mediating neurotransmitter release. *Journal of Neuroscience* **33**:18755–18763. DOI: https://doi.org/10.1523/JNEUROSCI.3161-13.2013, PMID: 24285882

Miki T, Malagon G, Pulido C, Llano I, Neher E, Marty A. 2016. Actin- and myosin-dependent vesicle loading of presynaptic docking sites prior to exocytosis. *Neuron* **91**:808–823 . DOI: https://doi.org/10.1016/j.neuron.2016.07.033, PMID: 27537485

Millar AG, Zucker RS, Ellis-Davies GC, Charlton MP, Atwood HL. 2005. Calcium sensitivity of neurotransmitter release differs at phasic and tonic synapses. *Journal of Neuroscience* **25**:3113–3125 . DOI: https://doi.org/10.1523/JNEUROSCI.4717-04.2005, PMID: 15788768

Moulder KL, Mennerick S. 2005. Reluctant vesicles contribute to the total readily releasable pool in glutamatergic hippocampal neurons. *Journal of Neuroscience* **25**:3842–3850 . DOI: https://doi.org/10.1523/JNEUROSCI.5231-04.2005, PMID: 15829636

Neher E. 2015. Merits and limitations of vesicle pool models in view of heterogeneous populations of synaptic vesicles. *Neuron* **87**:1131–1142. DOI: https://doi.org/10.1016/j.neuron.2015.08.038, PMID: 26402599

Pan B, Zucker RS. 2009. A general model of synaptic transmission and short-term plasticity. *Neuron* **62**:539–554. DOI: https://doi.org/10.1016/j.neuron.2009.03.025, PMID: 19477155

Pinheiro PS, Houy S, Sørensen JB. 2016. C2-domain containing calcium sensors in neuroendocrine secretion. *Journal of Neurochemistry* **139**:943–958. DOI: https://doi.org/10.1111/jnc.13865, PMID: 27731902

Rancz EA, Ishikawa T, Duguid I, Chadderton P, Mahon S, Häusser M. 2007. High-fidelity transmission of sensory information by single cerebellar mossy fibre boutons. *Nature* **450**:1245–1248 . DOI: https://doi.org/10.1038/nature05995, PMID: 18097412

Regehr WG. 2012. Short-term presynaptic plasticity. *Cold Spring Harbor Perspectives in Biology* **4**:a005702. DOI: https://doi.org/10.1101/cshperspect.a005702, PMID: 22751149

Ritzau-Jost A, Delvendahl I, Rings A, Byczkowicz N, Harada H, Shigemoto R, Hirrlinger J, Eilers J, Hallermann S. 2014. Ultrafast action potentials mediate kilohertz signaling at a central synapse. *Neuron* **84**:152–163 . DOI: https://doi.org/10.1016/j.neuron.2014.08.036, PMID: 25220814

Rudolph S, Overstreet-Wadiche L, Wadiche JI. 2011. Desynchronization of multivesicular release enhances Purkinje cell output. *Neuron* **70**:991–1004 . DOI: https://doi.org/10.1016/j.neuron.2011.03.029, PMID: 21658590

Sakaba T, Neher E. 2001. Preferential potentiation of fast-releasing synaptic vesicles by cAMP at the calyx of Held. *PNAS* **98**:331–336 . DOI: https://doi.org/10.1073/pnas.021541098, PMID: 11134533

Sakaba T. 2006. Roles of the fast-releasing and the slowly releasing vesicles in synaptic transmission at the calyx of Held. *Journal of Neuroscience* **26**:5863–5871. DOI: https://doi.org/10.1523/JNEUROSCI.0182-06.2006, PMID: 16738227

Sakaba T. 2008. Two Ca(2+)-dependent steps controlling synaptic vesicle fusion and replenishment at the cerebellar basket cell terminal. *Neuron* **57**:406–419 . DOI: https://doi.org/10.1016/j.neuron.2007.11.029, PMID: 18255033

Saviane C, Silver RA. 2006. Fast vesicle reloading and a large pool sustain high bandwidth transmission at a central synapse. *Nature* **439**:983–987 . DOI: https://doi.org/10.1038/nature04509, PMID: 16496000

Schmidt H, Brachtendorf S, Arendt O, Hallermann S, Ishiyama S, Bornschein G, Gall D, Schiffmann SN, Heckmann M, Eilers J. 2013. Nanodomain coupling at an excitatory cortical synapse. *Current Biology* **23**:244–249. DOI: https://doi.org/10.1016/j.cub.2012.12.007, PMID: 23273895

Schneggenburger R, Han Y, Kochubey O. 2012. Ca(2+) channels and transmitter release at the active zone. *Cell Calcium* **52**:199–207. DOI: https://doi.org/10.1016/j.ceca.2012.04.011, PMID: 22682961

Schoch S, Gundelfinger ED. 2006. Molecular organization of the presynaptic active zone. *Cell and Tissue Research* **326**:379–391. DOI: https://doi.org/10.1007/s00441-006-0244-y, PMID: 16865347

Shin OH, Lu J, Rhee JS, Tomchick DR, Pang ZP, Wojcik SM, Camacho-Perez M, Brose N, Machius M, Rizo J, Rosenmund C, Südhof TC. 2010. Munc13 C2B domain is an activity-dependent Ca2+ regulator of synaptic exocytosis. *Nature Structural & Molecular Biology* **17**:280–288. DOI: https://doi.org/10.1038/nsmb.1758, PMID: 20154707

Siksou L, Rostaing P, Lechaire JP, Boudier T, Ohtsuka T, Fejtová A, Kao HT, Greengard P, Gundelfinger ED, Triller A, Marty S. 2007. Three-dimensional architecture of presynaptic terminal cytomatrix. *Journal of Neuroscience* **27**:6868–6877. DOI: https://doi.org/10.1523/JNEUROSCI.1773-07.2007, PMID: 17596435

Siksou L, Triller A, Marty S. 2011. Ultrastructural organization of presynaptic terminals. *Current Opinion in Neurobiology* **21**:261–268. DOI: https://doi.org/10.1016/j.conb.2010.12.003, PMID: 21247753

Silverman-Gavrila LB, Orth PM, Charlton MP. 2005. Phosphorylation-dependent low-frequency depression at phasic synapses of a crayfish motoneuron. *Journal of Neuroscience* **25**:3168–3180. DOI: https://doi.org/10.1523/JNEUROSCI.4908-04.2005, PMID: 15788774

Sims RE, Hartell NA. 2005. Differences in transmission properties and susceptibility to long-term depression reveal functional specialization of ascending axon and parallel fiber synapses to Purkinje cells. *Journal of Neuroscience* **25**:3246–3257. DOI: https://doi.org/10.1523/JNEUROSCI.0073-05.2005, PMID: 15788782

Sätzler K, Söhl LF, Bollmann JH, Borst JG, Frotscher M, Sakmann B, Lübke JH. 2002. Three-dimensional reconstruction of a calyx of Held and its postsynaptic principal neuron in the medial nucleus of the trapezoid body. *Journal of Neuroscience* **22**:10567–10579 . PMID: 12486149

Thach WT, Goodkin HP, Keating JG. 1992. The cerebellum and the adaptive coordination of movement. *Annual Review of Neuroscience* **15**:403–442. DOI: https://doi.org/10.1146/annurev.ne.15.030192.002155, PMID: 1575449

Valera AM, Doussau F, Poulain B, Barbour B, Isope P. 2012. Adaptation of granule cell to Purkinje cell synapses to high-frequency transmission. *Journal of Neuroscience* **32**:3267–3280. DOI: https://doi.org/10.1523/JNEUROSCI.3175-11.2012, PMID: 22378898

van Beugen BJ, Gao Z, Boele HJ, Hoebeek F, De Zeeuw CI. 2013. High frequency burst firing of granule cells ensures transmission at the parallel fiber to purkinje cell synapse at the cost of temporal coding. *Frontiers in Neural Circuits* **7**:95. DOI: https://doi.org/10.3389/fncir.2013.00095, PMID: 23734102

van Kan PL, Gibson AR, Houk JC. 1993. Movement-related inputs to intermediate cerebellum of the monkey. *Journal of Neurophysiology* **69**:74–94. PMID: 8433135

Wölfel M, Lou X, Schneggenburger R. 2007. A mechanism intrinsic to the vesicle fusion machinery determines fast and slow transmitter release at a large CNS synapse. *Journal of Neuroscience* **27**:3198–3210. DOI: https://doi.org/10.1523/JNEUROSCI.4471-06.2007, PMID: 17376981

Xu J, Wu LG. 2005. The decrease in the presynaptic calcium current is a major cause of short-term depression at a calyx-type synapse. *Neuron* **46**:633–645. DOI: https://doi.org/10.1016/j.neuron.2005.03.024, PMID: 15944131

Xu-Friedman MA, Harris KM, Regehr WG. 2001. Three-dimensional comparison of ultrastructural characteristics at depressing and facilitating synapses onto cerebellar Purkinje cells. *Journal of Neuroscience* **21**:6666–6672. PMID: 11517256

Zhou K, Stawicki TM, Goncharov A, Jin Y. 2013. Position of UNC-13 in the active zone regulates synaptic vesicle release probability and release kinetics. *eLife* **2**:e01180. DOI: https://doi.org/10.7554/eLife.01180

Zikich D, Mezer A, Varoqueaux F, Sheinin A, Junge HJ, Nachliel E, Melamed R, Brose N, Gutman M, Ashery U. 2008. Vesicle priming and recruitment by ubMunc13-2 are differentially regulated by calcium and calmodulin. *Journal of Neuroscience* **28**:1949–1960. DOI: https://doi.org/10.1523/JNEUROSCI.5096-07.2008, PMID: 18287511

Neurobiology of Disease 106 (2017) 110–123

Contents lists available at ScienceDirect

Neurobiology of Disease

journal homepage: www.elsevier.com/locate/ynbdi

Characterization of the dominant inheritance mechanism of Episodic Ataxia type 2

Kevin Dorgans [b,1], Julie Salvi [c,1], Federica Bertaso [c], Ludivine Bernard [c], Philippe Lory [c,*], Frederic Doussau [b], Alexandre Mezghrani [a,*]

[a] Institut des Neurosciences de Montpellier, INSERM U1051, Hôpital Saint Eloi - Bâtiment INM, 80 rue Augustin Fliche, 34091 Montpellier, France
[b] Institut des Neurosciences Cellulaires et Intégratives-INCI CNRS-UPR 3212, 5 rue Blaise Pascal, 67084 Strasbourg, France
[c] Institut de Génomique Fonctionnelle, CNRS UMR 5203, INSERM U1191, Université de Montpellier, LabEx 'Ion Channel Science and Therapeutics', 141 rue de la Cardonille, 34094 Montpellier, France

ARTICLE INFO

Article history:
Received 21 November 2016
Revised 30 June 2017
Accepted 4 July 2017
Available online 05 July 2017

Keywords:
Episodic ataxia
Cerebellum
Voltage activated calcium channel
Neurotransmission
P/Q-type calcium channel
Pathogenic mechanisms
Protein trafficking
Dominant negative effect

ABSTRACT

Episodic Ataxia type 2 (EA2) is an autosomal dominant neuronal disorder linked to mutations in the $Ca_v2.1$ subunit of P/Q-type calcium channels. In vitro studies have established that EA2 mutations induce loss of channel activity and that EA2 mutants can exert a dominant negative effect, suppressing normal $Ca_v2.1$ activity through protein misfolding and trafficking defects. To date, the role of this mechanism in the disease pathogenesis is unknown because no animal model exists. To address this issue, we have generated a mouse bearing the R1497X nonsense mutation in $Ca_v2.1$ ($Ca_v2.1^{R1497X}$). Phenotypic analysis of heterozygous $Ca_v2.1^{R1497X}$ mice revealed ataxia associated with muscle weakness and generalized absence epilepsy. Electrophysiological studies of the cerebellar circuits in heterozygous $Ca_v2.1^{R1497X}$ mice highlighted severe dysregulations in synaptic transmission of the two major excitatory inputs as well as alteration of the spontaneous activity of Purkinje cells. Moreover, these neuronal dysfunctions were associated with a strong suppression of $Ca_v2.1$ channel expression in the cerebellum of heterozygous $Ca_v2.1^{R1497X}$ mice. Finally, the presence of $Ca_v2.1$ in cerebellar lipid raft microdomains was strongly impaired in heterozygous $Ca_v2.1^{R1497X}$ mice. Altogether, these results reveal a pathogenic mechanism for EA2 based on a dominant negative activity of mutant channels.

1. Introduction

Episodic Ataxia type 2 (EA2) is an autosomal dominant neurological disorder linked to mutations in the *CACNA1A* gene (Ophoff et al., 1996). EA2 is characterized by sudden attacks of ataxia that are often associated with permanent ataxia, nystagmus, muscle weakness and hemiplegic migraine (Strupp et al., 2007; Baloh, 2012). In some cases, other neurologic symptoms such as dystonia, epilepsy and cognitive impairments are also present (Jouvenceau et al., 2001; Maselli et al., 2003; Jung et al., 2010; Rajakulendran et al., 2010). The *CACNA1A* gene codes for the $Ca_v2.1$ pore forming subunit of the neuronal P/Q-type calcium (Ca^{2+}) channel, a member of the voltage-dependent calcium channel (VDCC) family. $Ca_v2.1$ channels are tightly associated with two auxiliary subunits, β and α2δ, essential for channel trafficking and functional regulation in neurons (Zamponi et al., 2015). Presynaptic $Ca_v2.1$ channels are involved in neurotransmitter release of most excitatory and inhibitory synapses in the central nervous system (Zamponi et al., 2015). In the cerebellum, $Ca_v2.1$ channels are expressed in cerebellar granule cells (GCs) and in Purkinje cells (PCs) (Jun et al., 1999). Cerebellar sensory-motor information is conveyed by two main excitatory inputs, composed of the mossy fibers (MFs) and the climbing fibers (CFs). MFs contact GCs via the parallel fibers (PFs) up to the PCs, the sole output of the cerebellum. Each PC also receives a single CF axon coming from the inferior olive. In GCs, $Ca_v2.1$ channels are essential for PF-PC synaptic transmission (Jun et al., 1999; Galliano et al., 2013). During early postnatal development, postsynaptic $Ca_v2.1$ channels in PCs are implicated in the homosynaptic competition between multiple CFs (Miyazaki et al., 2004; Hashimoto et al., 2011). Furthermore, somatodendritic $Ca_v2.1$ channels in PC are implicated in the activation of Ca^{2+} activated potassium channels (BK and SK2) (Edgerton and Reinhart, 2003; Womack and Khodakhah, 2004; Hosy et al., 2011). Irregularity of spontaneous PC firing due to insufficient activation of BK and SK2 channels is found in several $Ca_v2.1$ loss of function mouse strains such as the PC-specific $Ca_v2.1$ knock out (*Purky*) as well as in tottering (*tg*) and leaner (tg^{la}) strains (Walter et al., 2006; Alvina and Khodakhah, 2010; Mark et al., 2011; Stahl and Thumser, 2014).

* Corresponding authors.
E-mail addresses: philippe.lory@igf.cnrs.fr (P. Lory), alexandre.mezghrani@inserm.fr (A. Mezghrani).
[1] Equal contribution.
Available online on ScienceDirect (www.sciencedirect.com).

http://dx.doi.org/10.1016/j.nbd.2017.07.004
0969-9961/

To date, the molecular mechanism underlying EA2 is poorly known. On the basis of the identified mutations, EA2 appears to be due to a loss of channel function. More than 80 different mutations have been characterized until now and the majority result in a premature stop codon (Rajakulendran et al., 2012). In vitro, these truncated proteins have a dominant negative effect, inhibiting wild type (wt) $Ca_v2.1$ channel activity (Jouvenceau et al., 2001; Raghib et al., 2001; Jeng et al., 2006; Raike et al., 2007; Jeng et al., 2008). This dominant negative effect appears to involve defects in protein folding that promotes $Ca_v2.1$ degradation and cellular stress (Page et al., 2004; Wan et al., 2005; Mezghrani et al., 2008; Fu et al., 2017). Interestingly, the induction of channel misfolding is due to an ectopic interaction between the N-terminal part of the EA2 mutant and the full-length form (Page et al., 2004; Mezghrani et al., 2008). Moreover, the dominant suppression of $Ca_v2.1$ in vitro can be relieved by the co-expression of a free N-terminal peptide (Dahimene et al., 2016). However, it is not known whether this dominant-negative mechanism is involved in the in vivo pathology of EA2.

In this study, we generated the *$Ca_v2.1^{R1497X}$* mouse strain, in which a well described EA2 nonsense mutation (Jen et al., 1999) was inserted into the *cacna1a* gene. Heterozygous *$Ca_v2.1^{R1497X}$* mice exhibited defective motor coordination and gait abnormalities. Furthermore, muscle weakness and generalized epileptic seizures were also present. Morphological and functional analyses of the cerebellar circuit of heterozygous *$Ca_v2.1^{R1497X}$* mice revealed several synaptic dysfunctions such as decrease in PF-PC connectivity and increase of CF-PC synaptic transmission. These synaptic defaults were associated with a severe decrease in cerebellar $Ca_v2.1$ channel expression and trafficking defects, strongly suggesting a dominant-negative effect of the $Ca_v2.1^{R1497X}$ mutation. These results highlight a new pathophysiological mechanism for EA2.

2. Materials and methods

2.1. Animal handling and generation of *$Ca_v2.1^{R1497X}$* mouse

Procedures for the care and treatment of animals were carried out according to CNRS guidelines, and the experimental protocol was approved by the institutional animal care committee of the IGF in accordance with directives of the French Ministry of Agriculture (agreement number: D34-172-13). C57BL/6J mice were purchased from Charles River (L'Arbresle, France). The $Ca_v2.1^{R1497X}$ knock-in mouse line was generated at the "Genetic Engineering and Mouse Transgenesis" (GEMTis) facility at Centre of Immunophenomic-CIPHE INSERM US12 (Marseille, France). Briefly, point mutations (AGG codon at position 4489 d in TGA) in exon 29 of the CACNA1A gene were inserted in the genomic fragment BACRP23-282G1 (Fig. 1). The construct was electroporated in ES cells and positive clones were selected by antibiotic resistance. ES cells (derived from C57BL6) were then injected in blastocysts to generate the F1 germline. The mouse strain was maintained in a C57BL6/J background.

2.2. Functional exploration of motor mouse behavior

Locomotor activity was recorded using circular corridors (Imetronic, France). The circular corridor is composed of 4 infrared sensors (every quadrant) at ground level allowing recording of walking activities. Another detector is positioned at a height of 7.5 cm to follow mouse rearing activity. Horizontal activity is the number of quadrants that the mouse has traversed every 5 min while vertical activity corresponds to the number of rearing movements in a 5 min time frame. Motor coordination was evaluated using rotarod (Ugo Basile, Italy) and beam

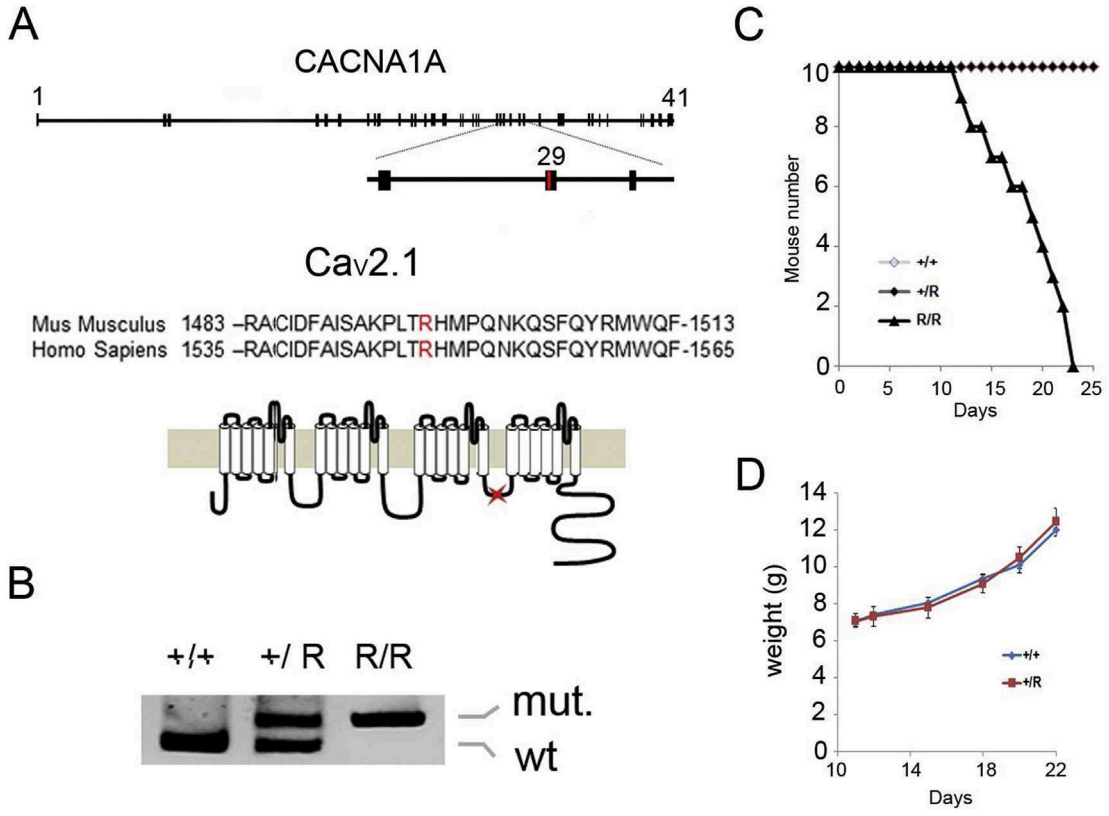

Fig. 1. Generation of the $Ca_v2.1^{R1497X}$ knock-in mouse. A. Schematic representation of the nonsense mutation inserted in the mouse *CACNA1A* gene (upper panel). Homology between the mouse and human proteins in the region around the mutated amino acid (middle panel). Position of the premature stop codon (R1497X) in the $Ca_v2.1$ channel as a function of its multipass transmembrane structure (lower panel). B. Visualization of wt (322 bp) and mutated (407 bp) alleles by PCR. C. Survival curves of homozygous $Ca_v2.1^{R1497X}$ (R/R), heterozygous (+/R) and wt (+/+) mice showing lethality of homozygous $Ca_v2.1^{R1497X}$ mice ($n = 10$). D. Weight curves showing the growth of wt (+/+) and heterozygous $Ca_v2.1^{R1497X}$ (+/R) mice.

tests. Rotarod experiments were performed in accelerating mode (from 4 to 40 rpm) during four constitutive days. Data correspond to the mean time (three trials) before the mouse falls off the rod. A fixed rod velocity (24 rpm for 60 s) was used to evaluate the effect of isoproterenol treatment on motor activity. For beam tests, two 12 mm and 24 mm-square beams were used. The ability of the mouse to cross a beam (time, number of footslips) was evaluated by video tracking. Number of footslips and time were recorded for three independent crossings. Forced running on a treadmill (LE8706, Bioseb, France) was used to analyze dynamic motor dysfunctions (gait abnormalities, muscle weakness and motor incoordination). For habituation, mice were placed on the treadmill at a low speed (5 cm/s) before performing the test at a higher velocity (20 cm/s) for 20 min. For muscle strength monitoring, grip, grid and inverted grid tests were used. A grip test (Bioseb, France) was used to evaluate muscle strength in the front limbs as well as in the rear limbs. Five trials were performed for each and data are expressed in force unit (g). The loaded grid test was used to evaluate static motor functions, assessing the ability of the mouse to hold grids with four different weights (10, 20, 30 and 40 g) for 30 s. Data were calculated as follows: Grid score (Arbitrary unit) = 40 * t1 + 30 * t2 + 20 * t3 + 10 * t4 (max = 3000). For the inverted grid test, mice were suspended by the tail and allowed to hold the loaded grid by the front limbs for a maximum 5 min. Three non-consecutive trials were performed.

2.3. Surgery and electroencephalography (EEG) recordings

Wild-type (wt) and heterozygous $Ca_v2.1^{R1497X}$ male mice were anesthetized with 2 ml/kg of a saline solution containing 40% (v/v) ketamine (Imalgene 500) and 20% (v/v) xylazine (Rompun 2%) and placed in a stereotaxic frame using the David Kopf mouse adaptor. A male microconnector (Pinnacle Technology Inc., Lawrence, KS) was fixed by four extradural screws, two on each parietal bone. The microconnector was then fixed with dental acrylic cement. After surgery, animals were individually housed and maintained in a 12 h light/dark cycle with food and water ad libitum for 1 week of recovery. For recordings, animals were put into individual Plexiglas boxes, and their microconnectors connected to an EEG preamplifier circuit and to the EEG amplifier. The electrical activity recorded by extradural electrodes was filtered and recorded by a computer equipped with Sirenia® software (Pinnacle Technology Inc.). EEG recordings were performed together with video monitoring of animal behavior.

2.4. Biochemistry and Immunochemistry

2.4.1. Antibodies

Antibodies against indicated proteins were obtained as follows: $Ca_v2.1$ (against the intracellular loop II–III), $Ca_v2.2$, $Ca_v1.2$, α2δ2, SERCA2, BK and SK2 from Alomone (Israel); $Ca_v2.1$ for IHCs from Synaptic Systems (against the loop I-II, Germany); Calbindin from Swant (Switzerland); VGluT1 and VGluT2 from Millipore (France); Flotillin and tubulin from Sigma-Aldrich (France); Calreticulin from Enzo life science (France); Alexa conjugated secondary antibodies were purchased from Life Technologies (France).

2.4.2. Western blots

WBs were performed as previously described (Mezghrani et al., 2008). Briefly, tissue and cell lysis were performed in NP40 buffer (1% NP40, 150 mM NaCl, 50 mM Tris-HCl pH = 7.8 and protease inhibitor cocktail (Roche, France)) and clarified by microcentrifugation. Protein concentration was determined with a BCA kit (Thermofisher Scientific, France). Protein extracts (50 μg) were run on SDS-PAGE gels, transferred to nitrocellulose (0.2 μM, Biorad, France) and processed for immunodetection. Proteins were detected using Enhanced Chemiluminescent reagent (Supersignal West Femto, Thermofisher Scientific, France) with a Chemidoc apparatus (Biorad). Quantifications were performed using Image Lab 4.0.1 software.

2.4.3. Lipid raft isolation

The protocol for raft purification was performed essentially as described by Davies et al. (2006). Briefly, two to three cerebella were used for each condition. Tissue extracts were prepared in MES-Triton buffer (2% Triton; 25 mM MES, pH = 6.5; 150 mM NaCl) and homogenized at 4 °C with a potter-Eveljhem homogenizer. After clearing at 10000 g, supernatants were loaded on a discontinued sucrose gradient (5, 30 and 45% sucrose in MES buffer (150 mM NaCl; 25 mM MES pH = 6.5)) and ultracentrifuged for 18 h at 140,000*g* at 4 °C. 1 ml fractions were collected and analyzed by WB. Typically, the Triton-insoluble upper fractions (4 to 6) contain lipid raft microdomains. 40 μl of each fraction were used for WB.

2.4.4. Immunohistochemistry (IHC) and hematoxylin/eosin staining

Mice were anesthetized using pentobarbital and transcardially perfused with either 4% paraformaldehyde (PFA) or phosphate buffer saline (PBS) alone followed by 4% PFA post-fixation. Cerebellar slices (50 μM) were processed from fixed tissue using a vibratome (Leica, Germany). Slices were incubated in PBS-T (0.5% Triton) with goat serum for 2 h and with primary antibodies (Calbindin: 1/1000°, VGluT1: 1/2000°, VGluT2: 1/2000°) for 12 h. Slices were then incubated for 4 h with secondary Alexa-conjugated antibodies and DAPI. IHCs were imaged using a Leica SP8 confocal microscope (MRI, Montpellier, France). For hematoxylin/eosin (H/E) staining, brains were hemisected after fixation and dehydrated in graded ethanol solutions, cleared in xylene, and embedded in paraffin. Brains were cut on a microtome and sections were stained with H/E (RHEM, Montpellier, France). Cell quantification in different cerebellar layers was performed with NDP software (Hamamatsu, Japan) for at least 10 cerebellar slices (2 mice for each condition).

2.5. Electrophysiological recordings

For this part, the experimenters were blinded to the genotype. Mice (18–25 days) were anesthetized by isoflurane inhalation and decapitated. Cerebella were extracted in ice-cold ACSF bubbled with carbogen (95% O_2, 5% CO_2) containing 120 mM NaCl, 3 mM KCl, 2 mM $NaHCO_3$, 1.25 NaH_2PO_4, 2.5 mM $CaCl_2$, 2 mM $MgCl_2$, 10 mM glucose and 0.05 mM minocyclin. Cerebellar slices (300 μm) were prepared using a vibratome (Microm HM650V) in dissociation buffer (93 mM *N*-Methyl-D-Glucamine, 2.5 mM KCl, 0.5 mM $CaCl_2$, 10 mM $MgSO_4$, 1.2 mM NaH_2PO_4, 30 mM $NaHCO_3$, 20 mM HEPES, 3 mM Na-Pyruvate, 2 mM Thiourea, 5 mM Na-ascorbate, 25 mM D-Glucose and 1 mM Kynurenic acid). Slices were maintained in a bubbled ACSF medium at 34 °C for 1 h. Slices were then transferred to the recording chamber at 34 °C and continuously perfused with ACSF (100 μM picrotoxin, 10 μM CGP52432; 100 μM D-AP5; 1 μM AM251 and 2 μM JNJ16259685). Whole-cell patch experiments and recordings were performed using infrared contrast with a Multiclamp 700A amplifier (Molecular Devices) on an Olympus microscope (BX51WI). Recordings were made at 34 °C in PCs located in the vermis. Whole-cell patch-clamp recordings were obtained using a Multiclamp 700A amplifier (Molecular Devices). Pipette (2.5–3 MΩ resistance) capacitance was cancelled and series resistance (R_s) between 5 and 8 mΩ was compensated at 80%. R_s was monitored regularly during the experiment and the recording was stopped when R_s d significantly (>20%). Internal solution used for PC patch-clamp contained 140 mM $CsCH_3SO_3$, 10 mM Phosphocreatine, 10 mM HEPES, 5 mM QX-314-Cl, 10 mM BAPTA, 4 mM Na-ATP and 0.3 mM Na-GTP, 1 mM Neurobiotin. To evoke glutamate release from PFs, a monopolar glass electrode (5 MΩ) filled with ACSF was used. Electrical stimuli were applied in the molecular layer of horizontal slices at a clear distance from the patched PCs (>100 μm). The amplitude and length of electrical pulses was adjusted with an isolated electrical stimulator (Digitimer DS3) triggered by WinWCP software (John Dempster, Strathclyde Institute of Pharmacy and Biomedical Sciences, University of Strathclyde, UK). All evoked synaptic currents (eEPSCs) were low-pass filtered at 2 kHz and sampled at 20 KHz (National Instruments). Various

PC holding voltages (Vh) were performed according to the experimental protocol (Paired-pulses Vh = −60 mV, Input-output Vh = −10 mV). For CF-PC eEPSC recordings, stimulations were performed in the GCL at short distances (20–50 μm) from the PC (Vh = −10 mV) on sagittal slices. Electrical stimuli intensities were adjusted and the pipette was moved to find the all-or-none CF fiber evoked response. Intrinsic firing of PC was recorded on horizontal slices in juxtacellular configuration using high-resistance borosilicate pipettes (>10 MΩ) filled with high NaCl medium. Data were acquired using WinWCP 4.2× freeware (John Dempster, SIPBS, University of Strathclyde, UK) and analyzed with WinPython freeware, Igor 6.22A (Wavemetrics, USA). Data are expressed as Mean +/− SEM. For statistical analysis, Student's *t*-test and Mann-Whitney Rank Sum Test (MWRST) were used ($p > 0.05$, $^{*}p \le 0.05$, $^{**}p \le 0.005$ and $^{***}p \le 0.001$).

2.6. Data analysis for extracellular recordings

Action potentials were detected with custom Python scripts (WinPython) and firing frequency was calculated cell-by-cell using the median value of the ISIs. The irregularity of discharge was assessed with the coefficient of variation (CV) and the coefficient of variation of two consecutive spikes (CV2).

$$CV = \frac{\mathrm{std(ISI)}}{<\mathrm{ISI}>}$$

$$CV_2 = 2\frac{|\mathrm{ISI_{n+1}} - \mathrm{ISI}_n|}{(\mathrm{ISI_{n+1}} + \mathrm{ISI_n})}$$

As PCs undergo frequency variations, we calculated for each cell a local variation parameter based on spike refractory period (*LvR*; Shinomoto et al., 2009) known as a frequency independent parameter.

$$L_{vR} = \frac{3}{n-1}\sum_{i=1}^{n-1}\left(1 - \frac{4\mathrm{ISI_i ISI}_{i+1}}{(\mathrm{ISI_i} + \mathrm{ISI}_{i+1})^2}\right)\left(1 + \frac{4R}{\mathrm{ISI_i} + \mathrm{ISI}_{i+1}}\right)$$

3. Results

3.1. Phenotypic characterization of $Ca_v2.1^{R1497X}$ knock-in mice

The majority of *CACNA1A* mutations in EA2 are nonsense, producing truncated polypeptides. Numerous EA2 truncated mutants have been described, offering a large choice for the generation of new mouse models of this disorder (Rajakulendran et al., 2012). Of note, the longest EA2 mutant protein with dominant negative activity is truncated at position 1820 deleting the C-terminus part of the $Ca_v2.1$ channel (Jouvenceau et al., 2001). Here we generated a new EA2 knock-in mouse model, named $Ca_v2.1^{R1497X}$, by inserting a nonsense mutation that was originally identified in a large family (Jen et al., 1999). This mutation is located in exon 29 at positions 4489-91 of the *CACNA1A* gene (Fig. 1A) (Jen et al., 1999). The mutated codon leads to a premature stop at position 1497 in the mouse and 1549 in humans (Fig. 1A). The truncated channel lacks the fourth domain and the C-terminus, likely inducing a strong loss-of-function (Fig. 1A). Patients harboring this mutation generally display episodic and basal ataxia associated with hemiplegic migraine (Jen et al., 1999). Phenotypic variability is remarkably high in this family ranging from mild to severe neurologic disorders (Jen et al., 1999). Furthermore, muscle weakness due to abnormal neuromuscular transmission was found in some of these patients (Jen et al., 2001; Maselli et al., 2003). The mutation was inserted in the C57BL/6 mouse genome by homologous recombination and efficient transmission of the mutated allele to the F1 generation was obtained (Fig. 1B). $Ca_v2.1^{R1497X}$ mouse breeding was normal with a Mendelian distribution. Homozygous mice ($Ca_v2.1^{R1497X/R1497X}$; R/R) died postnatally at less than three weeks of age (Fig. 1C) and were not further investigated in behavioral tests. Heterozygous mice ($Ca_v2.1^{+/R1497X}$; +/R) did not show premature lethality. They displayed normal growth and were indistinguishable from wt (+/+) mice (Fig. 1D). Motor activity was analyzed in an automatic circular corridor, allowing horizontal motor activity and vertical activity (rearing movements) to be recorded (Fig. 2A–B). Whereas horizontal activity appeared normal in heterozygous $Ca_v2.1^{+/R1497X}$ mice at 12 weeks of age, a modest hypoactivity was observed at 36 weeks as compared to wt littermates (Fig. 2A). However, vertical activity that reflects the frequency of rearing movements was significantly lower in $Ca_v2.1^{+/R1497X}$ mice for both 12 and 36 week old animals (Fig. 2B). Next, we investigated a possible alteration in basal motor function, as assessed by the rotarod test where animals are forced to move to avoid falling off the rod, at 3 to 12 weeks of age (Fig. 2C). $Ca_v2.1^{+/R1497X}$ mice spent significantly less time on the rod as compared to wt mice at all ages tested (Fig. 2C). This motor abnormality appeared early (3 weeks) and was stable with age as 36 weeks old mice had a similar level of impairment (Fig. 2D). Coordination impairment in young $Ca_v2.1^{+/R1497X}$ mice was identical from the first to the last rotarod trials suggesting a normal motor learning in $Ca_v2.1^{+/R1497X}$ mice (Fig. 2D). Gait and coordination functions were also analyzed using the beam test. The numbers of splits corresponding to gait abnormalities were significantly higher in $Ca_v2.1^{+/R1497X}$ mice on two different beams (12 and 24 mm width) (Fig. 2E). These results demonstrate the presence of a basal ataxia in $Ca_v2.1^{+/R1497X}$ mice as defined by the presence of motor coordination and gait disorders (Fig. 2C–E). Episodic ataxia is rarely observed in mice but has been described for EA1 and $Ca_v2.1$ knock-down mouse models (Herson et al., 2003; Salvi et al., 2014). Of importance, $Ca_v2.1^{+/R1497X}$ mice did not show signs of attacks of dyskinesia during cage handling or behavioral tests, in contrast to loss-of-function $Ca_v2.1$ mouse models such as *tg* and *purky* where recurrent attacks of dyskinesia are triggered by mild stressors (Shirley et al., 2008; Mark et al., 2011).

As it has previously been shown that noradrenergic activation can induce episodic ataxia in a $Ca_v2.1$ deficient mouse model (Salvi et al., 2014), we explored the effects of isoproterenol (ISO) treatment in $Ca_v2.1^{+/R1497X}$ mice. Using the rotarod test at a constant velocity (24 rpm), we found that isoproterenol treatment increased motor dysfunction in $Ca_v2.1^{+/R1497X}$ mice for several hours (Fig. 2F) with no sign of dyskinesia. These results indicate that $Ca_v2.1^{+/R1497X}$ mice exhibit a basal ataxia which is reinforced by a stress inducer. Altogether, these findings support a dominant mode of transmission of the cerebellar motor dysfunction in the $Ca_v2.1^{R1497X}$ mouse model.

Next, we assessed whether other behavioral defects associated with EA2 were also present in $Ca_v2.1^{+/R1497X}$ mice. To assess dynamic motor functions, we first analyzed the ability of $Ca_v2.1^{+/R1497X}$ mice to run on a treadmill at a sustained velocity (Fig. 3A). Following delivery of electric shocks, the ability of mice to remain on the rolling belts during running was evaluated. We observed a tendency toward an increase in the number of shocks for $Ca_v2.1^{+/R1497X}$ mice compared to wt littermates suggesting the presence of motor disability (Fig. 3A). Motor dysfunctions can also be tested using a more static test, the inverted grid. This test revealed the presence of muscular deficits in the $Ca_v2.1^{+/R1497X}$ mice, as illustrated by their lower ability to hold onto the grid (Fig. 3B). To determine whether there was any possible muscle weakness, muscle strength was monitored by grip tests for front limbs and four limbs (Fig. 3C–D). At two different ages (12 and 36 weeks), muscle strength was lower in the front limbs and as well as for the four limbs of $Ca_v2.1^{+/R1497X}$ mice (Fig. 3C–D), with the level of muscle weakness being equivalent (data not shown). To further confirm these results, we used the grid test, a more sensitive test to analyze muscle strength (Fig. 3E). $Ca_v2.1^{+/R1497X}$ mice showed a lower aptitude to support the weight of calibrated grids than wt mice (Fig. 3E). Taken together, these data reveal muscle weakness in $Ca_v2.1^{+/R1497X}$ mice, mimicking human EA2 disease.

As EA2 patients often suffer from generalized absence epileptic seizures, we assessed this paroxistic brain activity in $Ca_v2.1^{+/R1497X}$ mice

by cortical electroencephalogram (EEG) recordings in awake mice (Rajakulendran et al., 2010). EEGs revealed the presence of bilateral generalized abnormal spike-wave discharges in $Ca_v2.1^{+/R1497X}$ mice that were not presented in wt littermates (Fig. 3F). These spontaneous seizures (1–2 s) had an intrinsic frequency of 6–8 Hz and appeared >4 times per hour (Fig. 3G). The presence of non-convulsive generalized seizures in $Ca_v2.1^{+/R1497X}$ mice is in good agreement with a loss of $Ca_v2.1$ activity causing alterations in the corticothalamic rhythmicity (Bomben et al., 2016). Importantly, one should note that such generalized seizures were never observed in other heterozygous $Ca_v2.1$ mutant

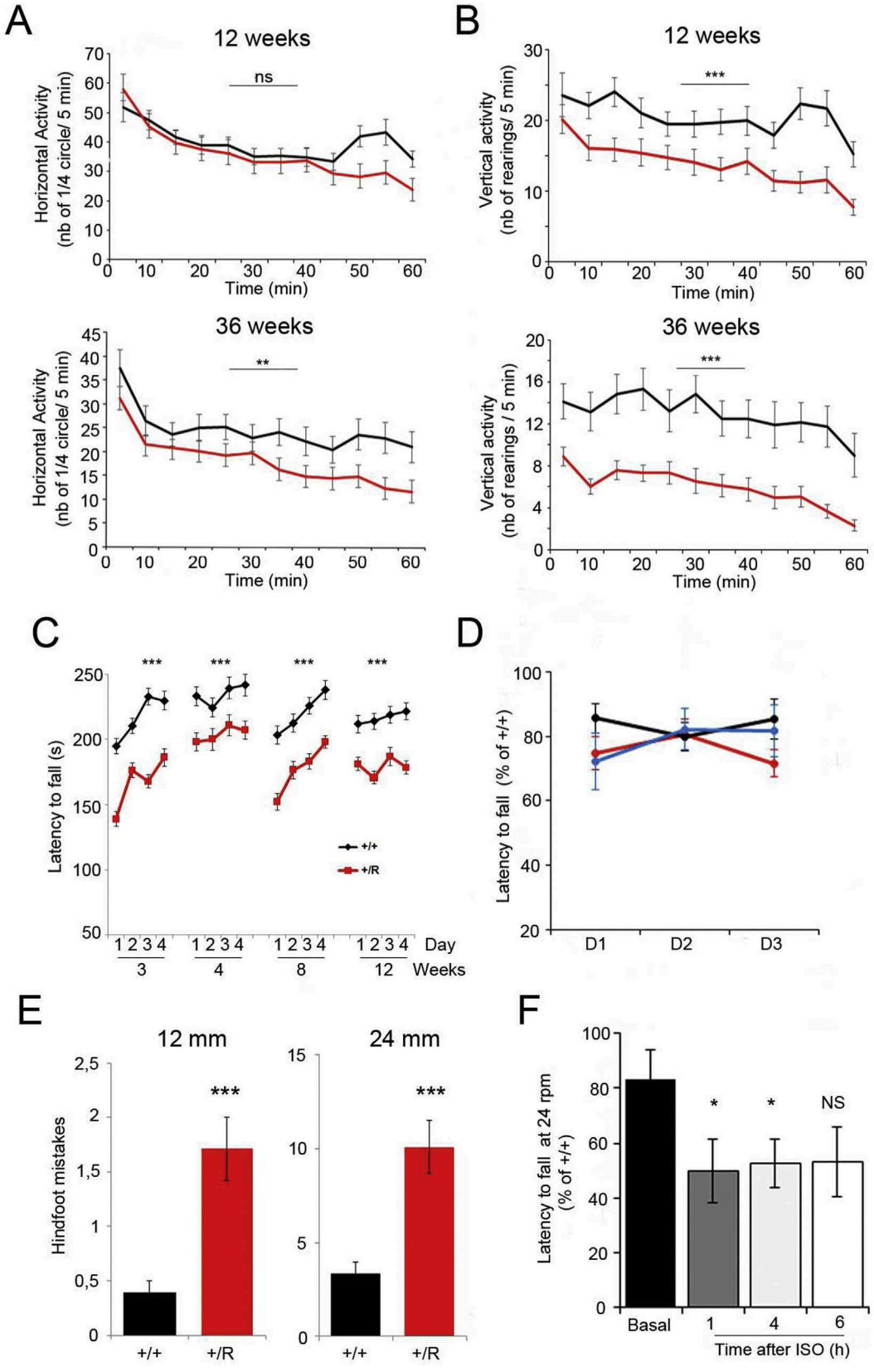

mouse models (Pietrobon, 2010). The existence of all these neurological defects in $Ca_v2.1^{+/R1497X}$ mice clearly demonstrates the dominant mode of transmission of the disease and validates this new $Ca_v2.1^{R1497X}$ mouse strain as a suitable model to study EA2.

3.2. Developmental alterations in cerebellar synaptic microcircuits in $Ca_v2.1^{+/R1497X}$ mice

As the prominent phenotype in $Ca_v2.1^{+/R1497X}$ mice is the presence of basal ataxia, cerebellar morphology and synaptic connectivity were analyzed. Immunohistochemistry (IHC) of cerebellar sagittal sections stained with calbindin revealed a normal size and morphology of the cerebellum in $Ca_v2.1^{+/R1497X}$ mice (Fig. 4A, left). No cellular signs of PC degeneration were observed in the cerebellar lobes of $Ca_v2.1^{+/R1497X}$ mice (Fig. 4A, left). Furthermore, hematoxylin and eosin (H/E) staining confirmed the absence of cell death in $Ca_v2.1^{+/R1497X}$ mice cerebellum (Fig. 4A, right; Fig. 4B, upper panel). Cellular quantification of H/E staining was undertaken to estimate any subtle cell loss in each cerebellar layer of $Ca_v2.1^{+/R1497X}$ mice (Fig. 4B). Similarly to the calbindin staining data, no apparent loss of PCs was observed in either young (3w) or adult (45w) $Ca_v2.1^{+/R1497X}$ mice (Fig. 4B, upper panel). We found an slight increase in cell number in the molecular layer (ML) as well as in the GC layer (GCL) of $Ca_v2.1^{+/R1497X}$ mouse cerebellum as compared to wt cerebellum (Fig. 4B, middle and lower panels). This excess of cells in the ML was observed at two different ages (3 and 45 weeks) (Fig. 4B). Thus, the motor abnormalities are not due to loss of cerebellar cells such as PCs or GCs. These data suggest however an alteration of GC development due to cellular dysfunction induced by $Ca_v2.1$ mutation. GCs are connected to PCs via the PFs that can be specifically labelled with VGluT1. IHCs of cerebellar slices with a VGluT1 antibody revealed a lower intensity in $Ca_v2.1^{+/R1497X}$ mice, compared to wt, suggesting the presence of defects in PF/PC connectivity (Fig. 4C). In contrast, VGluT2 labelling was higher in $Ca_v2.1^{+/R1497X}$ mice as compared to wt littermates, with more intense immunoreactivity in the proximal part of PCs dendrites (Fig. 4D). However, the CF territory, as reflected by the area of VGlut2 staining, was not significantly expanded in the upper part of the ML. These data suggest the presence of synaptic abnormalities in both PFs and CFs excitatory inputs. Due to interconnected developmental processes, VGluT1 territory expansion correlates with the size of the PC dendrites corresponding to the ML. The area of VGluT1 territory was identical between $Ca_v2.1^{+/R1497X}$ and wt mice suggesting a normal development of PCs (Fig. 4C). Direct visualization of PC morphology following intracellular neurobiotin injections revealed no major change in PC dendritic trees in the $Ca_v2.1^{+/R1497X}$ mouse cerebellum (Fig. 4E, left). However, fine defects in PC dendrite morphology were present in heterozygous mice such as the abundance and forms of PCs spines (Fig. 4E). Quantifications revealed a significant decrease of spine number in PCs of $Ca_v2.1^{+/R1497X}$ mice as compared to wt (Fig. 4F). Taken together, these results reveal no profound cerebellar abnormality but rather subtle changes in cerebellar circuitry that might be due to alterations in the synaptic connectivity between PF-PC and CF-PC.

Alterations in presynaptic excitatory inputs as well as in PC postsynaptic compartments might have major consequences for cerebellum activity. In PFs, $Ca_v2.1$ channels control >80% of evoked glutamate release (Mintz et al., 1995). Therefore, we studied the properties of glutamate release at PF-PC synapses in cerebellar slices of $Ca_v2.1^{+/R1497X}$ mice and wt littermates. To focus our study on presynaptic mechanisms and to rule out a postsynaptic contribution, we pharmacologically blocked the induction of postsynaptic long term plasticity (LTP and LTD), NMDA-dependent plasticity and endocannabinoid signaling (Marcaggi and Attwell, 2005; Beierlein et al., 2007). Following electrical stimulations of PFs with pulses of increasing intensities (see schematic, Fig. 5A), we found that the mean amplitudes of evoked excitatory postsynaptic currents (eEPSCs) were strongly affected at PF-PC synapses at all intensities in $Ca_v2.1^{+/R1497X}$ mice (mean eEPSC values for stimulations at 30 μA: 3033.02 pA ± 1005.96 pA, $n = 9$ for wt mice compared to 223.97 pA ± 36.51 pA, $n = 4$ for $Ca_v2.1^{+/R1497X}$ mice, MWRST, $p = 0.006$) (Fig. 5B). Strikingly, even though synaptic transmission was impaired in $Ca_v2.1^{+/R1497X}$ mice, short-term plasticity probed by paired-pulse stimulation at 3 different frequencies (10, 50 and 100 Hz) or high-frequency trains at 50 Hz was identical in both genotypes (Fig. 5C). This indicates that in active PF boutons of $Ca_v2.1^{+/R1497X}$ mice, the probability of Ca^{2+} entry and release is not affected. In line with the IHC experiments, these results suggest that defects in $Ca_v2.1$ channels in the cerebellar cortex lead to a developmental decrease in the number of functional PF synaptic contacts rather than an impairment of presynaptic mechanisms in active boutons.

Since our IHCs experiments showed that the density of innervations of CFs on PCs is abnormally increased in $Ca_v2.1^{+/R1497X}$ mice, we checked whether the synaptic properties were altered at CF-PC synapses. CFs were stimulated and the properties of synaptic transmission were studied by eEPSC recordings on PCs in acute slices (Fig. 5D). In $Ca_v2.1^{+/R1497X}$ mice, the mean eEPSC amplitude at a CF-PC synapse was larger than in wt mice (mean eEPSC: 2.24 nA ± 0.24 nA, $n = 8$ for wt mice compared to 4.27 nA ± 0.58 nA, $n = 7$ for $Ca_v2.1^{+/R1497X}$ mice, $p = 0.005$) (Fig. 5E). This effect was not associated with a modification in the paired-pulse ratio (PPR) (PPR: 0.67 ± 0.05, $n = 8$ for wt mice compared to 0.61 ± 0.04, $n = 7$, for $Ca_v2.1^{+/R1497X}$ mice, $p = 0.39$) (Fig. 5E–F) indicating that the increase in the synaptic strength was the result of an anomalous number of release sites in $Ca_v2.1^{+/R1497X}$ mice rather than in an increase in the probability of release at each synaptic site.

These data are highly reminiscent of the phenomenon of CF multi-innervation observed in PC specific $Ca_v2.1$ KO mice (Miyazaki et al., 2012). In the absence of synaptic input, PCs fire spontaneously and the precision of their intrinsic pacemaking plays a fundamental role in cerebellar physiology (Walter et al., 2006). The neuronal excitability and the shape of action potentials are under the control of BK and SK2 potassium channels that are exclusively activated by $Ca_v2.1$ channels (Womack et al., 2004; Womack and Khodakhah, 2004). Using juxtacellular recordings of PCs in acute slices, we monitored the intrinsic activity of PCs in $Ca_v2.1^{+/R1497X}$ and wt littermate mice (Fig. 6A). Extracellular recordings revealed that spontaneous activity of PCs was affected in $Ca_v2.1^{+/R1497X}$ mice as compared to wt (Fig. 6B). The mean interspike interval (ISI) of spontaneous action potentials was clearly longer in PCs from $Ca_v2.1^{+/R1497X}$ mice (median ISI: 40 ± 13 ms for +/R compared to 32 ± 10 ms for +/+) (Fig. 6C). This effect was associated with a significant increase in the coefficient of variation of the ISI (median CV: 0.37 ± 0.15 for +/R compared to 0.24 ± 0.2 for +/+) (Fig. 6C) and also for two consecutive ISIs (CV2: 0.37 ± 0.12 for +/R compared to 0.2 ± 0.14 for +/+) (Fig. 6C). Furthermore, irregularities of spontaneous firing in $Ca_v2.1^{+/R1497X}$ mutants are better described by using the firing local variations parameters (LvR: 0.23 ± 0.14 for +/R compared to 0.11 ± 0.168 for +/+) (Kumbhare and Baron, 2015; Shinomoto et al., 2009). Taken together, our results highlight several

Fig. 2. Motor coordination and gait abnormalities in heterozygous $Ca_v2.1^{R1497X}$ mice. A–B. Spontaneous motor activity of heterozygous $Ca_v2.1^{R1497X}$ mice ($n_{+/R} = 12$; red) and wt littermates ($n_{+/+} = 10$, black) analyzed on a circular corridor: Horizontal activity (A) corresponds to the number of quadrants executed in 5 min. Vertical activity (B) represents the number of rearing movements executed in 5 min. Data for each mouse is the mean of 3 independent trials. C. Rotarod tests of heterozygous $Ca_v2.1^{R497X}$ ($n_{+/R} = 20$) and wt ($n_{+/+} = 24$) mice. Data are the means of 3 trials per day. D. Progression of motor dysfunction in heterozygous $Ca_v2.1^{R1497X}$ mice was evaluated by the Rotarod performance test. Data are expressed in percent (normalized to wt) for 3 week old (red; $n_{+/R} = 20$ and $n_{+/+} = 24$); 12 week old (black; $n_{+/R} = 20$ and $n_{+/+} = 24$) and 36 week old mice (blue; $n_{+/R} = 13$ and $n_{+/+} = 8$). E. Beam tests were performed with 12 and 24 mm-square beams for heterozygous $Ca_v2.1^{R497X}$, ($n_{+/R} = 14$) and wt ($n_{+/+} = 11$) mice. The number of footslips was measured during beam crossing (means of 3 independent trials). F. Increased motor dysfunction in heterozygous $Ca_v2.1^{R1497X}$ mice after isoproterenol treatment. Rotarod tests (normalized to wt; $n_{+/R} = 13$; $n_{+/+} = 12$) were performed at a fixed rod velocity (24 rpm; 60 s) both before (basal) and after isoproterenol treatment (ISO; 20 mg/kg) at the indicated time points. Data represent means +/− SEM with non-parametric *t*-test ($p < 0.05$ = *; $p < 0.01$ = **; $p < 0.001$ = ***).

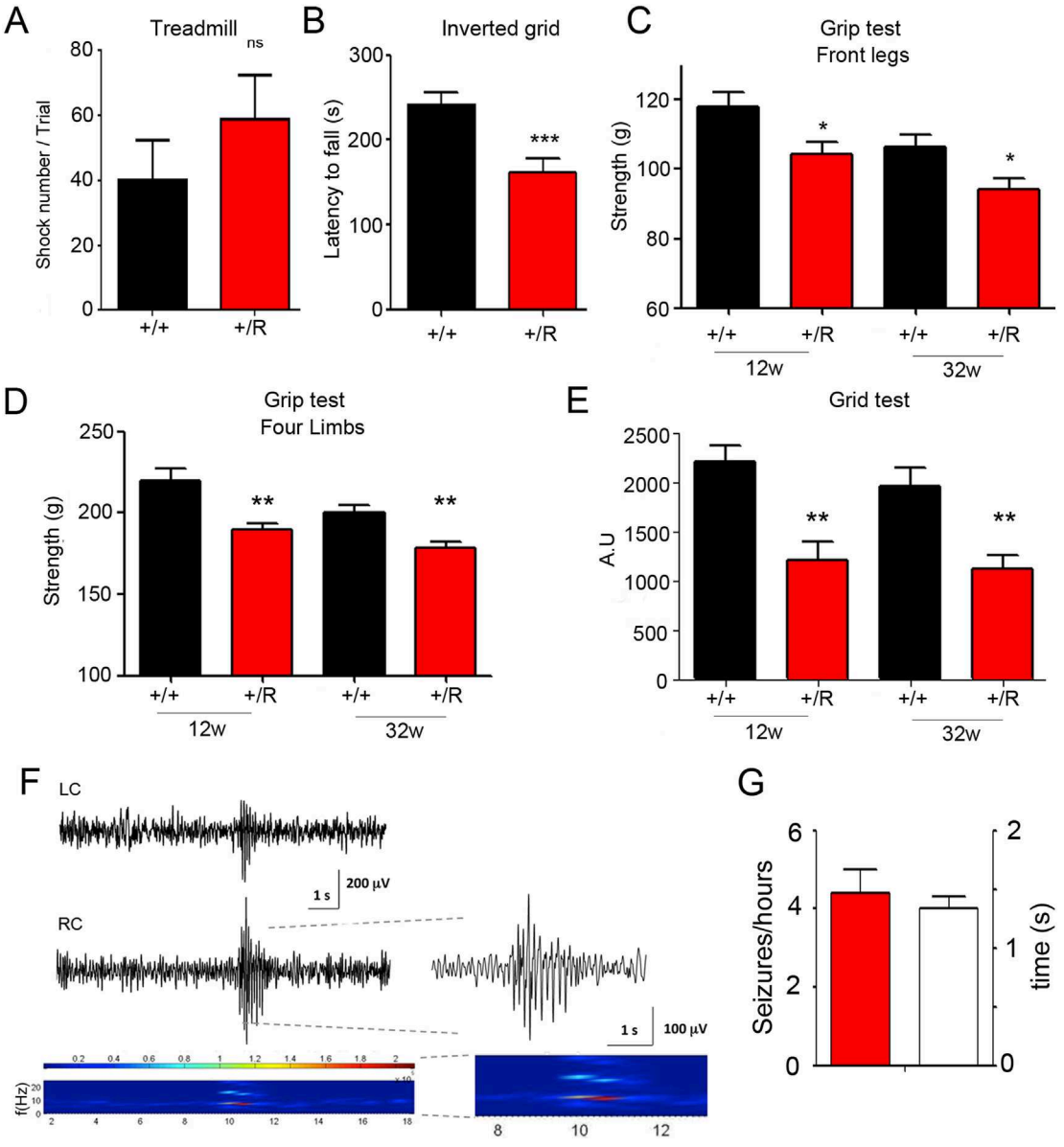

Fig. 3. Muscle weakness and spontaneous spike-wave seizures in heterozygous $Ca_v2.1^{R1497X}$ mice. A. Dynamic motor performances of heterozygous $Ca_v2.1^{R1497X}$ ($n_{+/R} = 13$) and wt ($n_{+/+} = 12$) mice were analyzed on a treadmill (30 min at 20 cm/s). Data presented are the means of electric shocks endured in 3 non-consecutive trials (mean + SEM, *t*-test, $p < 0{,}05$). B. The time before mice fell off an inverted grid was recorded for the two genotypes ($n_{+/+} = 36$; $n_{+R} = 34$). Data are the mean of 3 trials (mean + SEM, *t*-test with $p < 0{,}05$). C–E. Presence of muscle weakness in heterozygous $Ca_v2.1^{R1497X}$ mice. Muscle strength was evaluated by grip (C, D) and grid (E) tests ($n_{+/+} = 12$, $n_{+/R} = 12$). For grip tests, data are the means of 5 trials (mean + SEM, see methods for score calculation). F. Representative EEG traces from left and right cortices showing bilateral synchronous paroxystic activity, with enlargement of the spike-wave discharge (SWD) on the right (upper). Corresponding short-time Fourier transform representation (frequency over time) and frequency band raw power (lower part). G. The average number of SWD (left) and the duration of single SWD (right) recorded per hour for heterozygous $Ca_v2.1^{R1497X}$ mice ($n = 3$) are shown.

dysfunctions in the cerebellar microcircuits in $Ca_v2.1^{+/R1497X}$ mice suggesting that the computing of sensorimotor information by the cerebellar cortex is impaired. The abnormal number of synaptic contacts leading to synaptic strength dysfunctions at both PF-PC and CF-PC synapses indicate that a deficiency in $Ca_v2.1$ expression induces cellular disturbances during the early postnatal development of the cerebellum.

3.3. Suppression of protein expression and traffic defects of $Ca_v2.1$ channels in $Ca_v2.1^{+/R1497X}$ mice

In order to characterize the $Ca_v2.1$ channel defects associated with neuronal dysfunctions in our EA2 model, we analyzed the expression of $Ca_v2.1$ channels in cerebellar protein extracts of juvenile (18 day) and adult (90 day) $Ca_v2.1^{R1497X}$ mice by Western blot (WB) analyses (Fig. 7A). Protein profiles of $Ca_v2.1$ channels in mouse cerebellum revealed the presence of typical multiple isoforms (245, 190, 170 kDa) with two predominant forms of 190 and 170 kDa (Fig. 7A). $Ca_v2.1^{+/R1497X}$ mice displayed a similar protein profile (Fig. 7A). While the 170 kDa band could potentially correspond to the $Ca_v2.1$-R1497X truncated channel (Fig. 7A, right panel), it was also present in wt samples, precluding its formal identification. Nonetheless, expression levels of $Ca_v2.1$ channel was strongly decreased in $Ca_v2.1^{+/R1497X}$ mice, irrespective of age (Fig. 7B–C; 77% and 65% decreases in 18 day old and adult mice, respectively). The very low level of $Ca_v2.1$ protein in $Ca_v2.1^{+/R1497X}$ cerebellum cannot be explained solely by the lack of a single allele, clearly indicating a dominant negative effect of the EA2 mutant protein on expression of the wt form. We therefore assessed whether other related ion channels might also be downregulated in $Ca_v2.1^{+/R1497X}$ mice. Notably though, neither the cerebellar expression of $Ca_v2.2$ of $Ca_v1.2$ VDCCs was affected in $Ca_v2.1^{+/R1497X}$ mice (+/R; Fig.

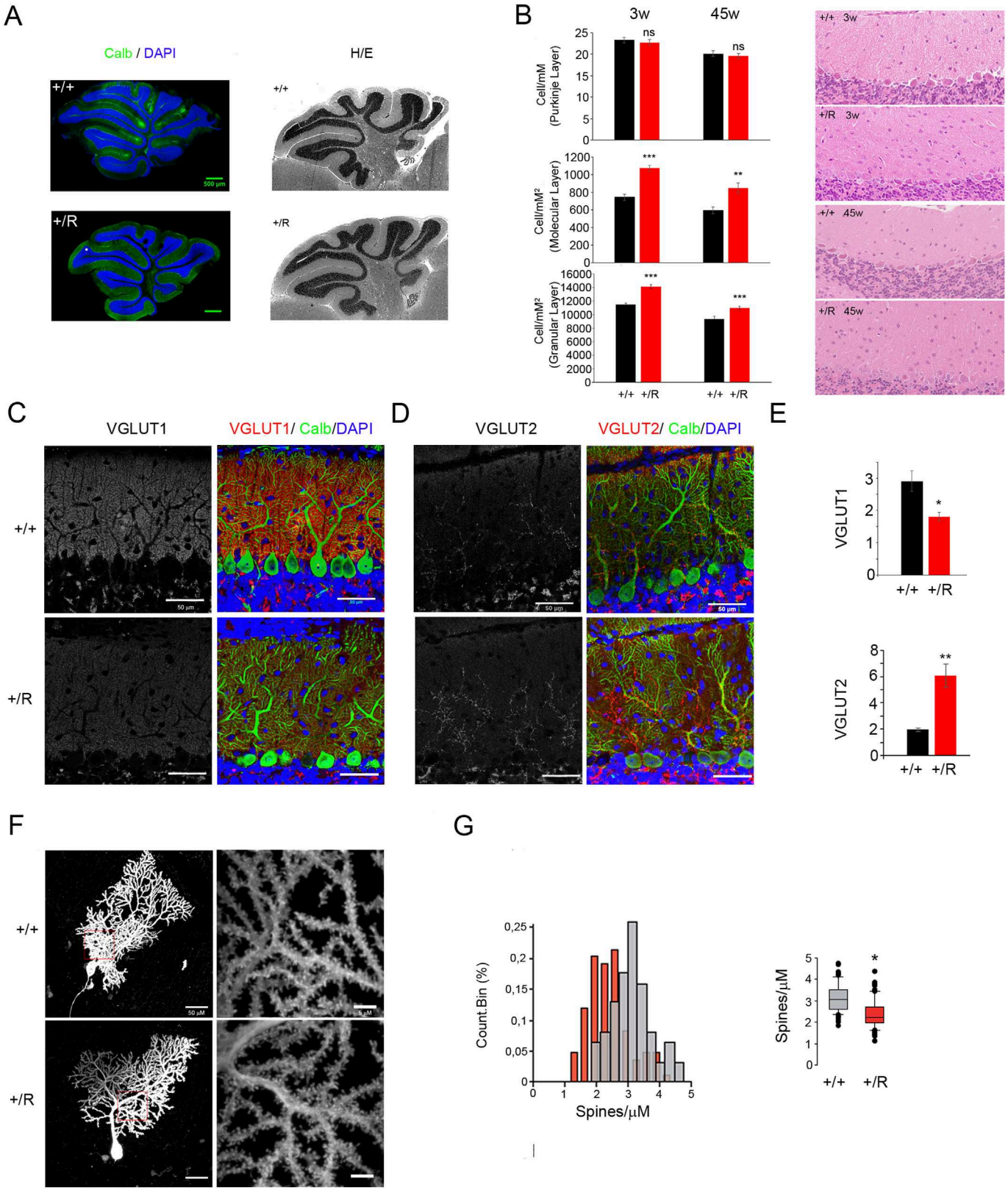

Fig. 4. Cellular and synaptic abnormalities in cerebellum of heterozygous $Ca_v2.1^{R1497X}$ mice. A. The cerebellar structure of $Ca_v2.1^{R1497X}$ mice (+/R: heterozygous; +/+: wt) was analyzed by immunohistochemistry (Calbindin/DAPI) (left) and hematoxilin/eosin staining (H/E) (right). B. The numbers of cell in PCs (PCL), molecular (ML) and GCs (GCL) layers were determined by H/E staining at 3 weeks ($n = 10$) and 45 weeks ($n = 8$). Statistics: Mean + SEM, t-test <0,05. C. PF synapses labelled with anti-VGluT1 (left part) and co-stained with anti-Calbindin (Calb) and DAPI are presented (merge, right part). D. CF synapses labelled with anti-VGluT2 (left) and co-stained with anti-Calbindin (Calb) and DAPI (merge, right) are shown. E. Morphological analysis of PCs were monitored by neurobiotin staining. F. Analysis of PC spin density detected with neurobiotin ($n_{+/+} = 72$; $n_{+/R} = 93$). Statistics: Mean + SEM, t-test <0,05.

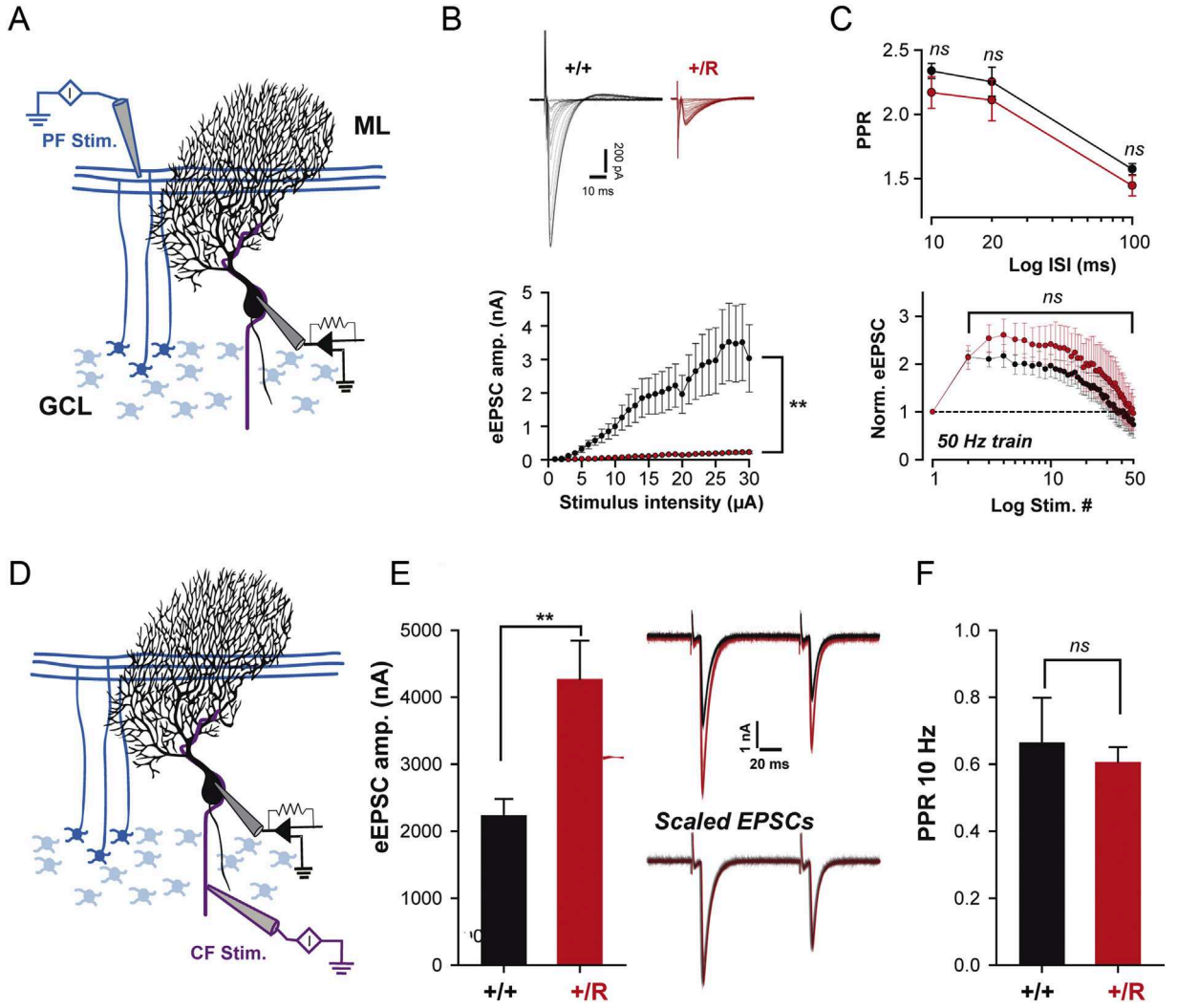

Fig. 5. Heterozygous $Ca_v2.1^{R1497X}$ mice exhibit decreased synaptic strength of PF excitatory inputs on PCs. A. Schematic showing the position of the recording (right, on PC) and stimulating electrodes (left, on PFs) in acute cerebellar slices. GCs are represented in blue, PC in black and CF in purple. ML: molecular layer, GCL: granule cell layer B. Upper traces: superimposed eEPSCs recorded at GC-PC synapses in wt (black) and heterozygous $Ca_v2.1^{R1497X}$ (red) mice during stimuli of increasing intensities (from 10 to 100 μA). Lower panel: Means values of eEPSCs amplitude to stimuli of increasing intensities obtained in wt (black) and heterozygous $Ca_v2.1^{R1497X}$ (red) mice. C. Upper panel: Mean values of the paired-pulse ratio (PPR) obtained at GC-PC synapses using 3 different frequency (10, 50 and 100 Hz) in wt (black) and heterozygous $Ca_v2.1^{R1497X}$ (red) mice. ISI: inter-stimulus interval. PPR values were statistically identical between wt and heterozygous $Ca_v2.1^{R1497X}$ (*t*-test; $p = 0.149$, $p = 0.461$ and $p = 0.182$ for PPR at10 Hz, 50 Hz and 100 Hz respectively). Lower panel: averaged eEPSCs amplitude versus stimulus number obtained in wt (black) and heterozygous $Ca_v2.1^{R1497X}$ (red) mice during 50 Hz trains. The lack of statistical difference between mean normalized eEPSC amplitude ($eEPSC_{stim,n}/eEPSC_{stim,1}$) obtained in wt and heterozygous $Ca_v2.1^{R1497X}$ mice and tested at any stimulus number (*t*-test, $p > 0.2$) suggests that mechanisms underlying short-term facilitation during high-frequency train were not affected in heterozygous $Ca_v2.1^{R1497X}$ mice. D. Same as in A with the difference that the stimulating electrode (purple) is positioned closed to CF. E. Mean eEPSC amplitude obtained in wt (black) and heterozygous $Ca_v2.1^{R1497X}$ (red) mice at CF-PC synapse. Traces correspond to representative eEPSCs recorded at the CF-PC synapses in wt (black) and heterozygous $Ca_v2.1^{R1497X}$ (red) mice after a paired-pulse stimulation of CFs at 10 Hz. F. Mean values of PPR at 10 Hz obtained in wt (black) and heterozygous $Ca_v2.1^{R1497X}$ (red) mice at CF-PC synapses. Black and red numbers above symbols or histograms indicate the number of cells for wt and heterozygous $Ca_v2.1^{R1497X}$ mice respectively.

7D) and furthermore, expression of the calcium-sensitive BK and SK channels (functionally linked to $Ca_v2.1$) was also unchanged (Fig. 7D). These results reveal a severe suppression of $Ca_v2.1$ expression in the cerebellum of $Ca_v2.1^{+/R1497X}$ mice without major changes in the cerebellar expression of other ion channels.

We hypothesized that the presence of misfolded truncated channels in $Ca_v2.1^{+/R1497X}$ mice might affect the assembly and trafficking of wt $Ca_v2.1$ channels in the ER. In order to address this hypothesis, we studied the localization of $Ca_v2.1$ channels to lipid raft microdomains (Davies et al., 2006). Indeed, protein insertion into lipid rafts takes place in post-ER compartments that reflects the sorting of $Ca_v2.1$ channels from the ER. First, we analyzed the presence of protein markers and $Ca_v2.1$ channels in lipid rafts from cerebella of wt mice (Fig. 8A). As expected, the lipid raft marker flotillin was mainly found in the upper fractions (4–6) of the sucrose gradient. The absence of both calreticulin and SERCA2 proteins in flotillin-positive fractions excluded a possible contamination of lipid rafts by ER resident proteins (Fig. 8A). $Ca_v2.1$ channels were detected in the same fractions as flotillin, confirming its presence in lipid raft microdomains (Fig. 8A). However, while $Ca_v2.1$ channels were easily detectable in lipid raft fractions from wt cerebellum, the presence of $Ca_v2.1$ protein in the upper fractions for $Ca_v2.1^{+/R1497X}$ mice was minimal (Fig. 8B–D). Indeed, the proportion ((Protein in flotillin positive fractions / protein in all fractions) × 100) of $Ca_v2.1$ channels in lipid rafts from $Ca_v2.1^{+/R1497X}$ mice was drastically lower than in wt mice (2% for +/R compared to 26% for wt) (Fig. 8D). This was specific to $Ca_v2.1$ as general protein trafficking in lipid rafts was normal, as monitored as a function of flotillin distribution (Fig. 8C–D). Furthermore, the Glycophosphatidyl Inositol (GPI) anchored α2δ2 auxiliary subunit, required for the targeting of $Ca_v2.1$ channels to lipid rafts (Davies et al., 2006), remained correctly targeted in $Ca_v2.1^{+/R1497X}$ mice (81% for wt mice, 96% for $Ca_v2.1^{+/R1497X}$ mice). In the cerebellum and particularly in PCs, $Ca_v2.1$ channels are present in large protein clusters

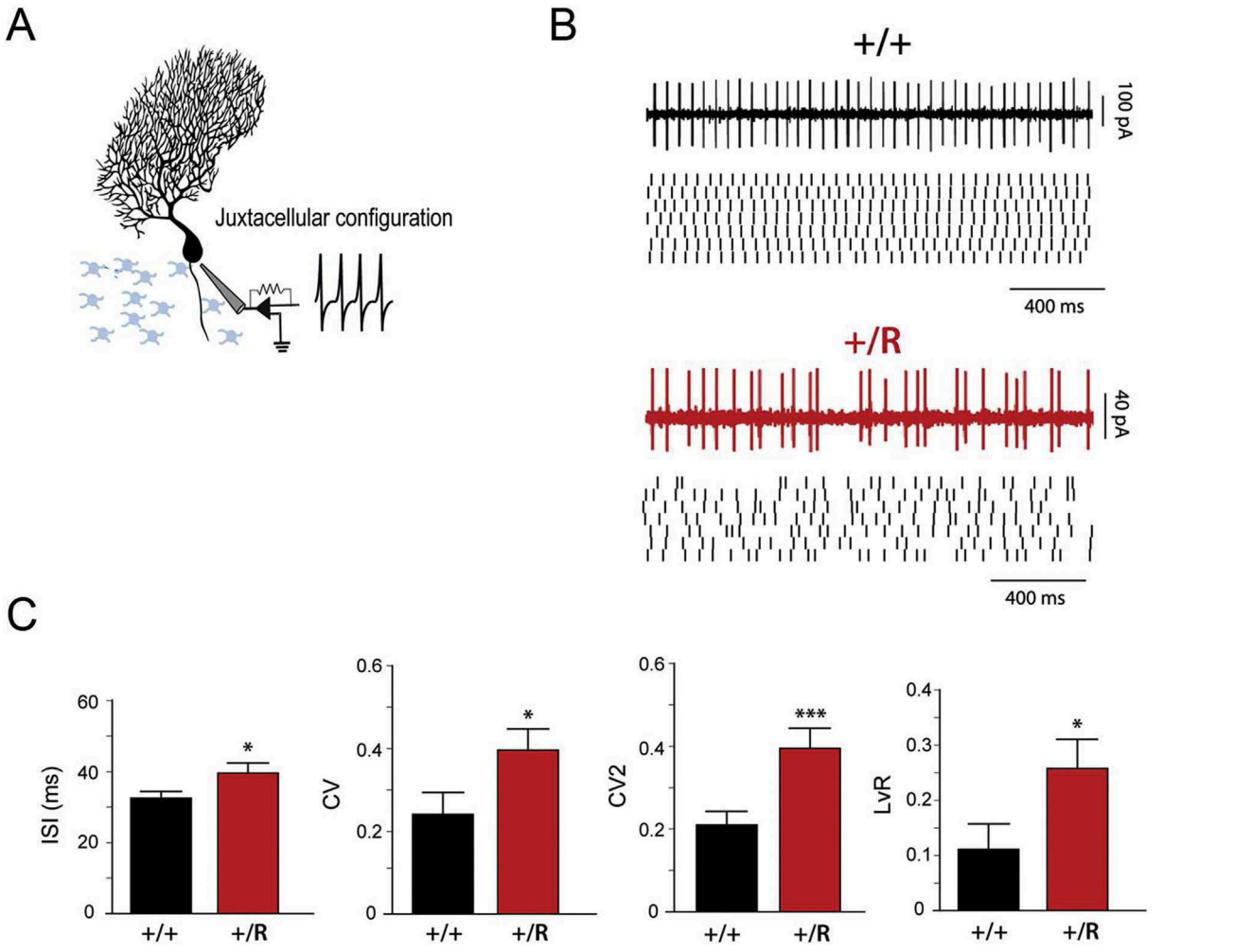

Fig. 6. Alteration of intrinsic PC neuronal activity in heterozygous $Ca_v2.1^{R1497X}$ mice. A. Schematic of juxtacellular recordings of PC activity in cerebellar acute slices. B. Representative traces of spontaneous firing in PCs from wt (+/+, in black) and heterozygous $Ca_v2.1^{R1497X}$ (+/R, in red) mice. C. Mean values of the interspike (ISI), coefficient of variation (CV), coefficient of variation of two consecutives spikes (CV2) and local variation parameter (Lvr) in wt (black) and heterozygous $Ca_v2.1^{R1497X}$ (red) PCs ($n_{(+/+)} = 48$, $n_{(+/R)} = 58$). For statistical analysis, Student's *t*-test and Mann-Whitney Rank Sum Test (MWRST) were used. ($p > 0.05$, $^{*}p \le 0.05$, $^{**}p \le 0.005$ and $^{***}p \le 0.001$).

containing BK and SK2 channels (Indriati et al., 2013). Intriguingly, SK2, but not BK, was present in lipid raft microdomains in the cerebellum of wt mice (Fig. 8C) and SK2 localization to lipid rafts was defective in $Ca_v2.1^{+/R1497X}$ mice (+/R)(56% for wt and 31% for $Ca_v2.1^{+/R1497X}$) (Fig. 8C–D). Taken together, these results show that trafficking of $Ca_v2.1$ as well as SK2 channels is affected in $Ca_v2.1^{+/R1497X}$ mice suggesting a physical interaction between these two channels in post-ER compartments. Overall, these data demonstrate the dominant negative effect of an EA2 mutant in the cerebellar neurons of $Ca_v2.1^{+/R1497X}$ mice. The EA2 mutant suppresses expression of the wt $Ca_v2.1$ channel and disrupts $Ca_v2.1$ trafficking to lipid raft microdomains.

4. Discussion

In this study, we demonstrate that the pathophysiology of EA2 proceeds via a dominant negative mechanism, supporting the dominant inheritance in this disease. We developed a novel mouse model carrying a human nonsense mutation in the *$Ca_v2.1$* gene ($Ca_v2.1^{R1497X}$). This mouse model recapitulates human EA2, exhibiting key behavioral, electrophysiological and biochemical properties of the human disease. Our model clearly contrasts with a recently described missense EA2 mutation mouse model which did not display an abnormal motor phenotype (Rose et al., 2014). Importantly, while heterozygous mutations have been shown to result in the dominant suppression of $Ca_v2.1$ in vitro, this is the first in vivo demonstration of the pathophysiological relevance of the dominant negative mechanism in EA2.

In this novel $Ca_v2.1^{+/R1497X}$ mouse model, the onset of the disease occurs in young animals, similarly to human EA2 where the ataxic phenotype manifests at a young age. In most neuronal tissues, the onset of $Ca_v2.1$ channel expression occurs postnatally, approximately one week after birth (Rosato-Siri et al., 2002; Fedchyshyn and Wang, 2005). Indeed, cerebellum development occurs postnatally and $Ca_v2.1$ channel expression is induced concomitantly with PF-PC and CF-PC synaptic maturation. $Ca_v2.1^{+/R1497X}$ mice displayed developmental defects including abnormally high numbers of GCs in ML and GL, as well as signs of CF multi-innervation. Furthermore, eEPSCs at the PF-PC synapses were strongly diminished in $Ca_v2.1^{+/R1497X}$ mice. This defect is likely due either to an increase in silent PF-PC synapses and/or to a general decrease in the number of synapses. Specific invalidation of $Ca_v2.1$ in GCs has been found to result in profound transmission defects without affecting motor performance (Galliano et al., 2013). However, ablation of $Ca_v2.1$ in both GCs and MFs leads to a heterogeneous phenotype with both mildly and severely ataxic mice (Maejima et al., 2013). Thus, the defect in PF-PC synaptic transmission is probably not the principal cause of motor disturbances observed in $Ca_v2.1^{+/R1497X}$ mice. Indeed, CF-PC synaptic transmission is abnormally elevated in $Ca_v2.1^{+/R1497X}$ mice due to an increase of synaptic contacts. While suppression of $Ca_v2.1$ channels in PCs leads to the persistence of multiple CF innervations that induce an increase in CF-PC eEPSCs (Kano et al., 2013), we did

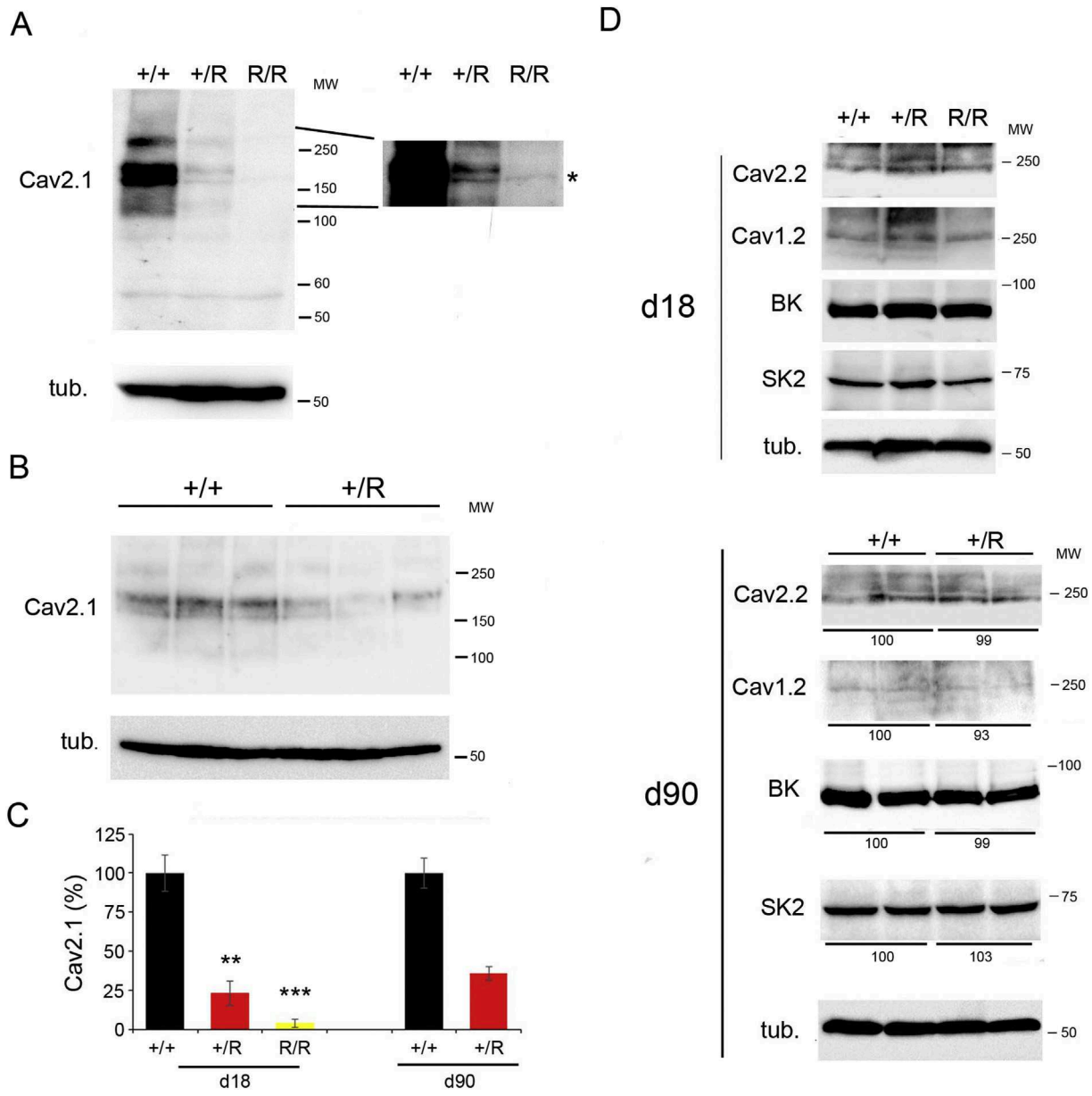

Fig. 7. Suppression of $Ca_v2.1$ channel expression in the cerebellum of $Ca_v2.1^{+/R1497X}$ mice. A, B. Western blots were performed to assess $Ca_v2.1$ channel expression in cerebellar protein lysates of young (18 days) (A) and adult (90 days) (B) $Ca_v2.1^{R1497X}$ mice (short (left panel) and long (right panel) exposures are shown). *indicated the $Ca_v2.1$-R1497X protein. Tubulin was used as loading control. C. Densitometric quantifications of $Ca_v2.1$ channels in the cerebellum of heterozygous and homozygous $Ca_v2.1^{R1497X}$ mice. Tubulin was used for normalization. Data ($n = 3$) represent means +/− SEM with non-parametric *t*-test (; $p < 0.01$ = **; $p < 0.001$ = ***). D. Expression of the indicated ion channels were monitored in cerebellar protein lysates of young (18 days) and adult (90 days) $Ca_v2.1^{R1497X}$ mice by WB.

not detect abnormal heterosynaptic competition between PFs and CFs in $Ca_v2.1^{+/R1497X}$ mice. These data strongly suggest that only complete elimination of $Ca_v2.1$ channels in PCs gives rise to this type of developmental defect (Miyazaki et al., 2012). Notably, there was also important differences in other defects detected in these two mice models. Indeed, hyperspiny transformation of PC dendrites was observed in the $Ca_v2.1$ KO mice (Miyazaki et al., 2012). In contrast, hypospiny transformation was present in the $Ca_v2.1^{+/R1497X}$ mouse arguing for the existence of distinct developmental defects in the two strains. Alterations in the regularity of spontaneous PC spiking linked to somato-dendritic functions has been proposed to reflect ataxia severity (Walter et al., 2006; Stahl and Thumser, 2014). We observed a decrease in the regularity of spontaneous PC spiking, likely reflecting ataxia in heterozygous $Ca_v2.1^{+/R1497X}$ mice as observed in homozygous *tg* mouse. The ataxic phenotype in $Ca_v2.1^{+/R1497X}$ mice is probably due to the neuronal dysfunctions of both the GCs and the PCs. Thus, our data reveal a dominant negative activity of EA2 mutants in GCs as well as in PCs during postnatal cerebellar development.

$Ca_v2.1^{+/R1497X}$ mice, similarly to human EA2, show generalized epileptic seizures with the typical spike-wave discharge patterns of absence epilepsy. The epileptic phenotype in our heterozygous mice provides another argument in favor of a dominant negative role of the $Ca_v2.1^{R1497X}$ mutant. This is notable as no epileptic phenotype has been detected in the currently used ataxia mouse models (tg^{la}, *tg* and *$Ca_v2.1$ KO* heterozygous animals). The origin of absence epilepsy has been proposed to be due to changes in the inhibition/excitation balance in the thalamocortical loop in which presynaptic $Ca_v2.1$ channels sustain synaptic transmission in several different neurons (Maheshwari and Noebels, 2014). Cortical interneurons appear to play a pivotal role as $Ca_v2.1$ inactivation in these cells is sufficient to induce both absence and generalized convulsive seizures (Rossignol et al., 2013). The epileptic phenotype in $Ca_v2.1^{+/R1497X}$ mice suggests a possible failure in

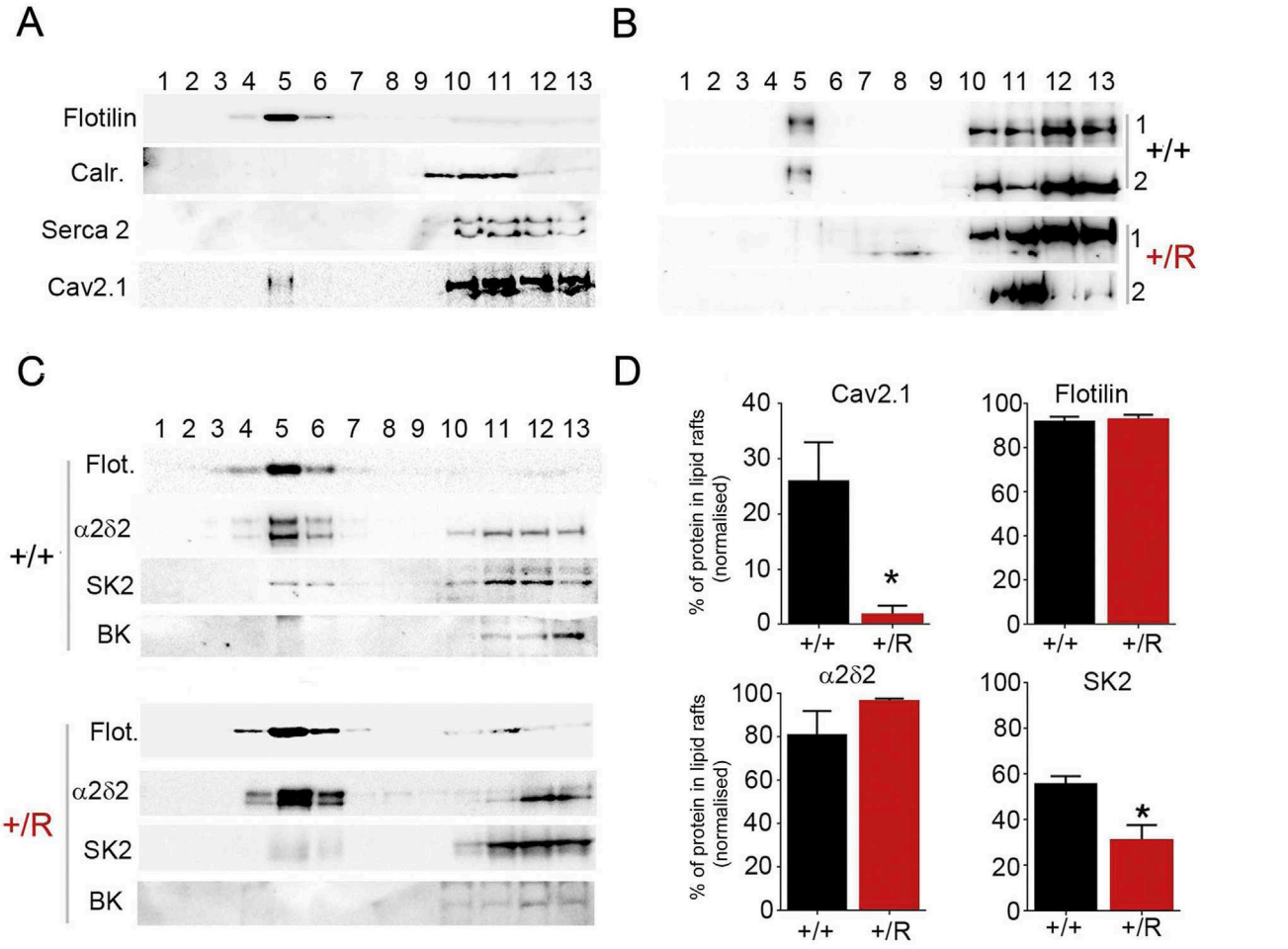

Fig. 8. Disruption of $Ca_v2.1$ channel trafficking to lipid raft microdomains in $Ca_v2.1^{+/R1497X}$ mice. A. The presence of $Ca_v2.1$ channels in cerebellar lipid raft microdomains of cerebella from wt mice was monitored in sucrose gradient fractions by WB. Flotillin, calreticulin (Calr) and SERCA2 were monitored as controls. B. $Ca_v2.1$ protein distribution in gradient fractions from cerebellum of wt (+/+) and heterozygous $Ca_v2.1^{R1497X}$ (+/R) mice were monitored by WB. C. WBs for flotillin (Flot), α2δ2 auxiliary subunit, SK2 and BK channels in cerebellar fractions from wt (+/+) and heterozygous $Ca_v2.1^{R1497X}$ (+/R) mice are shown. D. Densitometric quantification of the percentage of the indicated proteins in the lipid rafts of heterozygous $Ca_v2.1^{R1497X}$ (+/R) and wt (+/+) mice ($n = 4$, mean + SEM with non-parametric t-test ($p < 0.05 = *$; $p < 0.01 = **$)).

synaptic transmission in this subset of neurons. However, dysfunctions in cerebellar output might be sufficient to generate aberrant thalamocortical rhythmicity as observed in different $Ca_v2.1$ loss-of-function mice models (Maejima et al., 2013). Future studies will be necessary to determine whether spike-wave discharges in $Ca_v2.1^{+/R1497X}$ mice are specifically due to cortical interneuron defects or rather to more generalized neuronal defects.

Similar to EA2 patients carrying the $Ca_v2.1^{R1532X}$ mutation, $Ca_v2.1^{+/R1497X}$ mice exhibited muscle weakness. These data suggest that the NMJ is functionally affected in $Ca_v2.1^{+/R1497X}$ mice but not in *tg* and $Ca_v2.1$ KO mice where the phenotype was not observed. At the NMJ, other VDCCs such as $Ca_v2.2$ and $Ca_v2.3$ channels may be able to functionally replace presynaptic $Ca_v2.1$ channels (Plomp et al., 2003; Urbano et al., 2003; Kaja et al., 2006). The deficiency in NMJ in $Ca_v2.1^{+/R1497X}$ mice together with electrophysiology findings in tg^{la} mice support also the presence of dominant activity of EA2 mutants in motoneuron (Kaja et al., 2008).

Several studies on the dominant negative activity of EA2 mutants showed that impaired channel trafficking contributes to the pathogenic mechanism (Raghib et al., 2001; Wan et al., 2005; Jeng et al., 2006; Raike et al., 2007; Jeng et al., 2008). In addition, intracellular retention of $Ca_v2.1$ channels induced by misfolded EA2 mutants leads to almost complete $Ca_v2.1$ suppression (Page et al., 2004; Mezghrani et al., 2008). In agreement with these in vitro studies, we find that the amount of $Ca_v2.1$ protein is markedly reduced in the cerebellum of $Ca_v2.1^{+/R1497X}$ mice. Indeed, our biochemical data demonstrate a dominant-negative effect of the $Ca_v2.1^{R1497X}$ protein in vivo. Also, these experiments reveal very low levels of EA2 mutant protein, probably due to an extensive proteolysis as observed in vitro (Mezghrani et al., 2008; Fu et al., 2017). Interestingly, the low level of $Ca_v2.1$ protein in the $Ca_v2.1^{+/R1497X}$ mouse cerebellum suggests that there is no accumulation of misfolded channels in $Ca_v2.1^{+/R1497X}$ animals. This downregulation of $Ca_v2.1$ channels in the cerebellum of $Ca_v2.1^{+/R1497X}$ mice likely contributes to their neurodevelopmental defects. This occurs despite an absence of alterations in the expression of other ion channels, e.g. $Ca_v2.2$, $Ca_v1.2$, BK and SK2 channels in $Ca_v2.1^{+/R1497X}$ mouse cerebellum. This observation does not rule out a possible functional alteration of other ion channels that might occur at the cellular level in $Ca_v2.1^{+/R1497X}$ mice cerebellum.

Collectively, these data indicate that the sustained unfolding protein response (UPR), previously hypothesized to contribute to the EA2 pathogenic mechanism (Page et al., 2004), is absent in an animal model of EA2.

The targeting of $Ca_v2.1$ channel to lipid rafts is driven by the α2δ auxiliary subunits, especially the α2δ2 isoform (Davies et al., 2006). In $Ca_v2.1^{+/R1497X}$ mice, the defective targeting of $Ca_v2.1$ channels to lipid raft microdomains reveals the failure of these channels to properly traffic in the mouse cerebellum. Notably though, the α2δ2 subunit was appropriately targeted to the raft microdomains in these mice (Fig. 8), strongly suggesting that the interaction between these two proteins is

impaired in the context of the R1497X mutation. Furthermore, we found a significantly decreased level of SK2 channels in lipid rafts in $Ca_v2.1^{+/R1497X}$ mice. We actually ignore if SK2 membrane expression in non-raft compartments is also decreasing in $Ca_v2.1^{+/R1497X}$ mice. Our data therefore add new evidence of a physical link between $Ca_v2.1$ and SK2 channels, a conclusion which is supported by the co-clustering of these channels in somato-dendritic nanodomains in PCs (Indriati et al., 2013). Together, our results point to the targeting of pre-assembled clusters of α2δ2, $Ca_v2.1$ and SK2 proteins to lipid rafts in cerebellar neurons.

In conclusion, our study demonstrates that the functional defects in $Ca_v2.1^{+/R1497X}$ mice are due to the dominant-negative suppression of $Ca_v2.1$ channels and attests to the importance of the $Ca_v2.1^{+/R1497X}$ mouse model for studies of EA2 pathophysiology as well as the development of therapeutic strategies for this disease.

Conflict of interest

The authors declare no conflict of interest.

Acknowledgments

This work was supported by grants from the Agence Nationale pour la Recherche (Grant 2010JCJC11020) and the Association Française contre les Myopathies (AFM, Grant 13550 and 14352). We are indebted to Drs E. Valjent and C. Raoul for help with behavioral experiments and for discussions. We acknowledge Dr. P. Isope, Dr. F. Ango and Dr. N. Taylor for logistic assistance and suggestions on the manuscript. We also thank Montpellier Rio Imaging (MRI) and the animal facilities of Montpellier (Réseau des Animaleries de Montpellier).

References

Alvina, K., Khodakhah, K., 2010. The therapeutic mode of action of 4-aminopyridine in cerebellar ataxia. J. Neurosci. 30, 7258–7268.
Baloh, R.W., 2012. Episodic ataxias 1 and 2. Handb. Clin. Neurol. 103, 595–602.
Beierlein, M., Fioravante, D., Regehr, W.G., 2007. Differential expression of posttetanic potentiation and retrograde signaling mediate target-dependent short-term synaptic plasticity. Neuron 54, 949–959.
Bomben, V.C., Aiba, I., Qian, J., Mark, M.D., Herlitze, S., Noebels, J.L., 2016. Isolated P/Q calcium channel deletion in layer VI corticothalamic neurons generates absence epilepsy. J. Neurosci. 36, 405–418.
Dahimene, S., Page, K.M., Nieto-Rostro, M., Pratt, W.S., D'Arco, M., Dolphin, A.C., 2016. A CaV2.1 N-terminal fragment relieves the dominant-negative inhibition by an episodic ataxia 2 mutant. Neurobiol. Dis. 93, 243–256.
Davies, A., Douglas, L., Hendrich, J., Wratten, J., Tran Van Minh, A., Foucault, I., Koch, D., Pratt, W.S., Saibil, H.R., Dolphin, A.C., 2006. The calcium channel alpha2delta-2 subunit partitions with CaV2.1 into lipid rafts in cerebellum: implications for localization and function. J. Neurosci. 26, 8748–8757.
Edgerton, J.R., Reinhart, P.H., 2003. Distinct contributions of small and large conductance Ca^{2+}-activated K^+ channels to rat Purkinje neuron function. J. Physiol. 548, 53–69.
Fedchyshyn, M.J., Wang, L.Y., 2005. Developmental transformation of the release modality at the calyx of held synapse. J. Neurosci. 25, 4131–4140.
Fu, S.J., Jeng, C.J., Ma, C.H., Peng, Y.J., Lee, C.M., Fang, Y.C., Lee, Y.C., Tang, S.C., Hu, M.C., Tang, C.Y., 2017. Ubiquitin ligase RNF138 promotes episodic ataxia type 2-associated aberrant degradation of human Cav2.1 (P/Q-type) calcium channels. J. Neurosci. 1 37 (9), 2485–2503.
Galliano, E., Gao, Z., Schonewille, M., Todorov, B., Simons, E., Pop, A.S., D'Angelo, E., van den Maagdenberg, A.M., Hoebeek, F.E., De Zeeuw, C.I., 2013. Silencing the majority of cerebellar granule cells uncovers their essential role in motor learning and consolidation. Cell Rep. 3, 1239–1251.
Hashimoto, K., Tsujita, M., Miyazaki, T., Kitamura, K., Yamazaki, M., Shin, H.S., Watanabe, M., Sakimura, K., Kano, M., 2011. Postsynaptic P/Q-type Ca^{2+} channel in Purkinje cell mediates synaptic competition and elimination in developing cerebellum. Proc. Natl. Acad. Sci. U. S. A. 108, 9987–9992.
Herson, P.S., Virk, M., Rustay, N.R., Bond, C.T., Crabbe, J.C., Adelman, J.P., Maylie, J., 2003. A mouse model of episodic ataxia type-1. Nat. Neurosci. 6, 378–383.
Hosy, E., Piochon, C., Teuling, E., Rinaldo, L., Hansel, C., 2011. SK2 channel expression and function in cerebellar Purkinje cells. J. Physiol. 589, 3433–3440.
Indriati, D.W., Kamasawa, N., Matsui, K., Meredith, A.L., Watanabe, M., Shigemoto, R., 2013. Quantitative localization of Cav2.1 (P/Q-type) voltage-dependent calcium channels in Purkinje cells: somatodendritic gradient and distinct somatic coclustering with calcium-activated potassium channels. J. Neurosci. 33, 3668–3678.
Jen, J., Yue, Q., Nelson, S.F., Yu, H., Litt, M., Nutt, J., Baloh, R.W., 1999. A novel nonsense mutation in CACNA1A causes episodic ataxia and hemiplegia. Neurology 53, 34–37.
Jen, J., Wan, J., Graves, M., Yu, H., Mock, A.F., Coulin, C.J., Kim, G., Yue, Q., Papazian, D.M., Baloh, R.W., 2001. Loss-of-function EA2 mutations are associated with impaired neuromuscular transmission. Neurology 57, 1843–1848.
Jeng, C.J., Chen, Y.T., Chen, Y.W., Tang, C.Y., 2006. Dominant-negative effects of human P/Q-type Ca^{2+} channel mutations associated with episodic ataxia type 2. Am. J. Phys. Cell Physiol. 290, C1209–C1220.
Jeng, C.J., Sun, M.C., Chen, Y.W., Tang, C.Y., 2008. Dominant-negative effects of episodic ataxia type 2 mutations involve disruption of membrane trafficking of human P/Q-type Ca^{2+} channels. J. Cell. Physiol. 214, 422–433.
Jouvenceau, A., Eunson, L.H., Spauschus, A., Ramesh, V., Zuberi, S.M., Kullmann, D.M., Hanna, M.G., 2001. Human epilepsy associated with dysfunction of the brain P/Q-type calcium channel. Lancet 358, 801–807.
Jun, K., Piedras-Renteria, E.S., Smith, S.M., Wheeler, D.B., Lee, S.B., Lee, T.G., Chin, H., Adams, M.E., Scheller, R.H., Tsien, R.W., Shin, H.S., 1999. Ablation of P/Q-type Ca(2+) channel currents, altered synaptic transmission, and progressive ataxia in mice lacking the alpha(1A)-subunit. Proc. Natl. Acad. Sci. U. S. A. 96, 15245–15250.
Jung, J., Testard, H., Tournier-Lasserve, E., Riant, F., Vallet, A.E., Berroir, S., Broussolle, E., 2010. Phenotypic variability of episodic ataxia type 2 mutations: a family study. Eur. Neurol. 64, 114–116.
Kaja, S., Van de Ven, R.C., Ferrari, M.D., Frants, R.R., Van den Maagdenberg, A.M., Plomp, J.J., 2006. Compensatory contribution of Cav2.3 channels to acetylcholine release at the neuromuscular junction of tottering mice. J. Neurophysiol. 95, 2698–2704.
Kaja, S., Van De Ven, R.C., Frants, R.R., Ferrari, M.D., Van Den Maagdenberg, A.M., Plomp, J.J., 2008. Reduced ACh release at neuromuscular synapses of heterozygous leaner Ca(v)2.1-mutant mice. Synapse 62, 337–344.
Kano, M., Nakayama, H., Hashimoto, K., Kitamura, K., Sakimura, K., Watanabe, M., 2013. Calcium-dependent regulation of climbing fibre synapse elimination during postnatal cerebellar development. J. Physiol. 591, 3151–3158.
Kumbhare, D., Baron, M.S., 2015. A novel tri-component scheme for classifying neuronal discharge patterns. J. Neurosci. Methods 239, 148–161.
Maejima, T., Wollenweber, P., Teusner, L.U., Noebels, J.L., Herlitze, S., Mark, M.D., 2013. Postnatal loss of P/Q-type channels confined to rhombic-lip-derived neurons alters synaptic transmission at the parallel fiber to purkinje cell synapse and replicates genomic Cacna1a mutation phenotype of ataxia and seizures in mice. J. Neurosci. 33, 5162–5174.
Maheshwari, A., Noebels, J.L., 2014. Monogenic models of absence epilepsy: windows into the complex balance between inhibition and excitation in thalamocortical microcircuits. Prog. Brain Res. 213, 223–252.
Marcaggi, P., Attwell, D., 2005. Endocannabinoid signaling depends on the spatial pattern of synapse activation. Nat. Neurosci. 8, 776–781.
Mark, M.D., Maejima, T., Kuckelsberg, D., Yoo, J.W., Hyde, R.A., Shah, V., Gutierrez, D., Moreno, R.L., Kruse, W., Noebels, J.L., Herlitze, S., 2011. Delayed postnatal loss of P/Q-type calcium channels recapitulates the absence epilepsy, dyskinesia, and ataxia phenotypes of genomic Cacna1a mutations. J. Neurosci. 31, 4311–4326.
Maselli, R.A., Wan, J., Dunne, V., Graves, M., Baloh, R.W., Wollmann, R.L., Jen, J., 2003. Presynaptic failure of neuromuscular transmission and synaptic remodeling in EA2. Neurology 61, 1743–1748.
Mezghrani, A., Monteil, A., Watschinger, K., Sinnegger-Brauns, M.J., Barrere, C., Bourinet, E., Nargeot, J., Striessnig, J., Lory, P., 2008. A destructive interaction mechanism accounts for dominant-negative effects of misfolded mutants of voltage-gated calcium channels. J. Neurosci. 28, 4501–4511.
Mintz, I.M., Sabatini, B.L., Regehr, W.G., 1995. Calcium control of transmitter release at a cerebellar synapse. Neuron 15, 675–688.
Miyazaki, T., Hashimoto, K., Shin, H.S., Kano, M., Watanabe, M., 2004. P/Q-type Ca^{2+} channel alpha1A regulates synaptic competition on developing cerebellar Purkinje cells. J. Neurosci. 24, 1734–1743.
Miyazaki, T., Yamasaki, M., Hashimoto, K., Yamazaki, M., Abe, M., Usui, H., Kano, M., Sakimura, K., Watanabe, M., 2012. Cav2.1 in cerebellar Purkinje cells regulates competitive excitatory synaptic wiring, cell survival, and cerebellar biochemical compartmentalization. J. Neurosci. 32, 1311–1328.
Ophoff, R.A., Terwindt, G.M., Vergouwe, M.N., van Eijk, R., Oefner, P.J., Hoffman, S.M., Lamerdin, J.E., Mohrenweiser, H.W., Bulman, D.E., Ferrari, M., Haan, J., Lindhout, D., van Ommen, G.J., Hofker, M.H., Ferrari, M.D., Frants, R.R., 1996. Familial hemiplegic migraine and episodic ataxia type-2 are caused by mutations in the Ca^{2+} channel gene CACNL1A4. Cell 87, 543–552.
Page, K.M., Heblich, F., Davies, A., Butcher, A.J., Leroy, J., Bertaso, F., Pratt, W.S., Dolphin, A.C., 2004. Dominant-negative calcium channel suppression by truncated constructs involves a kinase implicated in the unfolded protein response. J. Neurosci. 24, 5400–5409.
Pietrobon, D., 2010. CaV2.1 channelopathies. Pflugers Arch. 460, 375–393.
Plomp, J.J., van den Maagdenberg, A.M., Ferrari, M.D., Frants, R.R., Molenaar, P.C., 2003. Transmitter release deficits at the neuromuscular synapse of mice with mutations in the Cav2.1 (alpha1A) subunit of the P/Q-type Ca^{2+} channel. Ann. N. Y. Acad. Sci. 998, 29–32.
Raghib, A., Bertaso, F., Davies, A., Page, K.M., Meir, A., Bogdanov, Y., Dolphin, A.C., 2001. Dominant-negative synthesis suppression of voltage-gated calcium channel Cav2.2 induced by truncated constructs. J. Neurosci. 21, 8495–8504.
Raike, R.S., Kordasiewicz, H.B., Thompson, R.M., Gomez, C.M., 2007. Dominant-negative suppression of Cav2.1 currents by alpha(1)2.1 truncations requires the conserved interaction domain for beta subunits. Mol. Cell. Neurosci. 34, 168–177.
Rajakulendran, S., Graves, T.D., Labrum, R.W., Kotzadimitriou, D., Eunson, L., Davis, M.B., Davies, R., Wood, N.W., Kullmann, D.M., Hanna, M.G., Schorge, S., 2010. Genetic and functional characterisation of the P/Q calcium channel in episodic ataxia with epilepsy. J. Physiol. 588, 1905–1913.
Rajakulendran, S., Kaski, D., Hanna, M.G., 2012. Neuronal P/Q-type calcium channel dysfunction in inherited disorders of the CNS. Nat. Rev. Neurol. 8, 86–96.

Rosato-Siri, M.D., Piriz, J., Tropper, B.A., Uchitel, O.D., 2002. Differential Ca^{2+}-dependence of transmitter release mediated by P/Q- and N-type calcium channels at neonatal rat neuromuscular junctions. Eur. J. Neurosci. 15, 1874–1880.

Rose, S.J., Kriener, L.H., Heinzer, A.K., Fan, X., Raike, R.S., van den Maagdenberg, A.M., Hess, E.J., 2014. The first knockin mouse model of episodic ataxia type 2. Exp. Neurol. 261, 553–562.

Rossignol, E., Kruglikov, I., van den Maagdenberg, A.M., Rudy, B., Fishell, G., 2013. CaV 2.1 ablation in cortical interneurons selectively impairs fast-spiking basket cells and causes generalized seizures. Ann. Neurol. 74, 209–222.

Salvi, J., Bertaso, F., Mausset-Bonnefont, A.L., Metz, A., Lemmers, C., Ango, F., Fagni, L., Lory, P., Mezghrani, A., 2014. RNAi silencing of P/Q-type calcium channels in Purkinje neurons of adult mouse leads to episodic ataxia type 2. Neurobiol. Dis. 68, 47–56.

Shinomoto, S., Kim, H., Shimokawa, T., Matsuno, N., Funahashi, S., Shima, K., Fujita, I., Tamura, H., Doi, T., Kawano, K., Inaba, N., Fukushima, K., Kurkin, S., Kurata, K., Taira, M., Tsutsui, K., Komatsu, H., Ogawa, T., Koida, K., Tanji, J., Toyama, K., 2009. Relating neuronal firing patterns to functional differentiation of cerebral cortex. PLoS Comput. Biol. 5 (7), e1000433.

Shirley, T.L., Rao, L.M., Hess, E.J., Jinnah, H.A., 2008. Paroxysmal dyskinesias in mice. Mov. Disord. 23, 259–264.

Stahl, J.S., Thumser, Z.C., 2014. Flocculus Purkinje cell signals in mouse Cacna1a calcium channel mutants of escalating severity: an investigation of the role of firing irregularity in ataxia. J. Neurophysiol. 112, 2647–2663.

Strupp, M., Zwergal, A., Brandt, T., 2007. Episodic ataxia type 2. Neurotherapeutics 4, 267–273.

Urbano, F.J., Piedras-Renteria, E.S., Jun, K., Shin, H.S., Uchitel, O.D., Tsien, R.W., 2003. Altered properties of quantal neurotransmitter release at endplates of mice lacking P/Q-type Ca^{2+} channels. Proc. Natl. Acad. Sci. U. S. A. 100, 3491–3496.

Walter, J.T., Alvina, K., Womack, M.D., Chevez, C., Khodakhah, K., 2006. Decreases in the precision of Purkinje cell pacemaking cause cerebellar dysfunction and ataxia. Nat. Neurosci. 9, 389–397.

Wan, J., Khanna, R., Sandusky, M., Papazian, D.M., Jen, J.C., Baloh, R.W., 2005. CACNA1A mutations causing episodic and progressive ataxia alter channel trafficking and kinetics. Neurology 64, 2090–2097.

Womack, M.D., Khodakhah, K., 2004. Dendritic control of spontaneous bursting in cerebellar Purkinje cells. J. Neurosci. 24, 3511–3521.

Womack, M.D., Chevez, C., Khodakhah, K., 2004. Calcium-activated potassium channels are selectively coupled to P/Q-type calcium channels in cerebellar Purkinje neurons. J. Neurosci. 24, 8818–8822.

Zamponi, G.W., Striessnig, J., Koschak, A., Dolphin, A.C., 2015. The physiology, pathology, and pharmacology of voltage-gated calcium channels and their future therapeutic potential. Pharmacol. Rev. 67, 821–870.

SCIENTIFIC REPORTS

OPEN

Inhibition promotes long-term potentiation at cerebellar excitatory synapses

Received: 25 April 2016
Accepted: 30 August 2016
Published: 19 September 2016

F. Binda[1], K. Dorgans[1], S. Reibel[2], K. Sakimura[3], M. Kano[4], B. Poulain[1] & P. Isope[1,5]

The ability of the cerebellar cortex to learn from experience ensures the accuracy of movements and reflex adaptation, processes which require long-term plasticity at granule cell (GC) to Purkinje neuron (PN) excitatory synapses. PNs also receive GABAergic inhibitory inputs via GCs activation of interneurons; despite the involvement of inhibition in motor learning, its role in long-term plasticity is poorly characterized. Here we reveal a functional coupling between ionotropic $GABA_A$ receptors and low threshold Ca_V3 calcium channels in PNs that sustains calcium influx and promotes long-term potentiation (LTP) at GC to PN synapses. High frequency stimulation induces LTP at GC to PN synapses and Ca_V3-mediated calcium influx provided that inhibition is intact; LTP is mGluR1, intracellular calcium store and Ca_V3 dependent. LTP is impaired in $Ca_V3.1$ knockout mice but it is nevertheless recovered by strengthening inhibitory transmission onto PNs; promoting a stronger hyperpolarization via $GABA_A$ receptor activation leads to an enhanced availability of an alternative Purkinje-expressed Ca_V3 isoform compensating for the lack of $Ca_V3.1$ and restoring LTP. Accordingly, a stronger hyperpolarization also restores Ca_V3-mediated calcium influx in PNs from $Ca_V3.1$ knockout mice. We conclude that by favoring Ca_V3 channels availability inhibition promotes LTP at cerebellar excitatory synapses.

In everyday life, we all benefit from the fine work performed by the cerebellum which allows us to fine tune our movements during daily actions in response to environmental changes and while executing complicate tasks such as walking or playing the violin. In line with its role in adaptive control of skilled movements and motor learning[1–4] the cerebellum receives vestibular, sensory and motor information which are conveyed from the entire body to the cerebellar cortex where they converge to Purkinje neurons (PNs). PNs are the sole output of the cerebellar cortex and they receive two main excitatory inputs, parallel fibers (PFs) and climbing fibers (CFs). PFs are the axons of granule cells (GCs) which relay proprioceptive, somatosensory and vestibular information reaching the cerebellum via mossy fibers (MFs) originating from several pre-cerebellar nuclei in the brainstem and spinal cord (Fig. 1a).

Long-term plasticity has been described at GC to PN synapses with long-term depression (LTD) caused by co-activation of PFs and CF[5] while the sole PFs stimulation leads to long-term potentiation (LTP)[6–10]. Furthermore, long lasting alterations in the strength of transmission at these excitatory synapses have been proposed as the molecular basis of cerebellar motor learning[1,11]. Indeed, mouse models lacking key molecules for LTD and LTP induction also show impairment in adaptation of the vestibulo-ocular reflex (VOR), a well- established model for cerebellum-mediated motor learning[10,12–15].

The same bundle of PFs which excites PNs also drives molecular layer interneurons (MLIs: basket and stellate cells, Fig. 1a) which provide feedforward inhibition (FFI) through GABAergic inhibitory synapses on the same PN. PFs-mediated excitation in PNs is therefore balanced by inhibition which ultimately influences the final output of the cerebellum. Indeed, a precise time window for PFs excitatory inputs summation and spike generation in PNs is defined by FFI[16]. Sustained PFs activation also promotes repetitive MLIs stimulation and therefore FFI-mediated influence on long-term plasticity is also expected. Accordingly, the block of inhibition promotes LTD[17] and LTP is

[1]Institute of Cellular and Integrative Neurosciences, CNRS, 5 Rue Blaise Pascal 67084 Strasbourg, France. [2]Chronobiotron UMS 3415, 5 Rue Blaise Pascal 67084 Strasbourg, France. [3]Department of Cellular Neurobiology, Brain Research Institute, Niigata University, Niigata 951-8585, Japan. [4]Department of Neurophysiology, Graduate School of Medicine, The University of Tokyo, Tokyo 113-0033, Japan. [5]University of Strasbourg, 5 Rue Blaise Pascal 67084 Strasbourg, France. Correspondence and requests for materials should be addressed to F.B. (email: binda@inci-cnrs.unistra.fr)

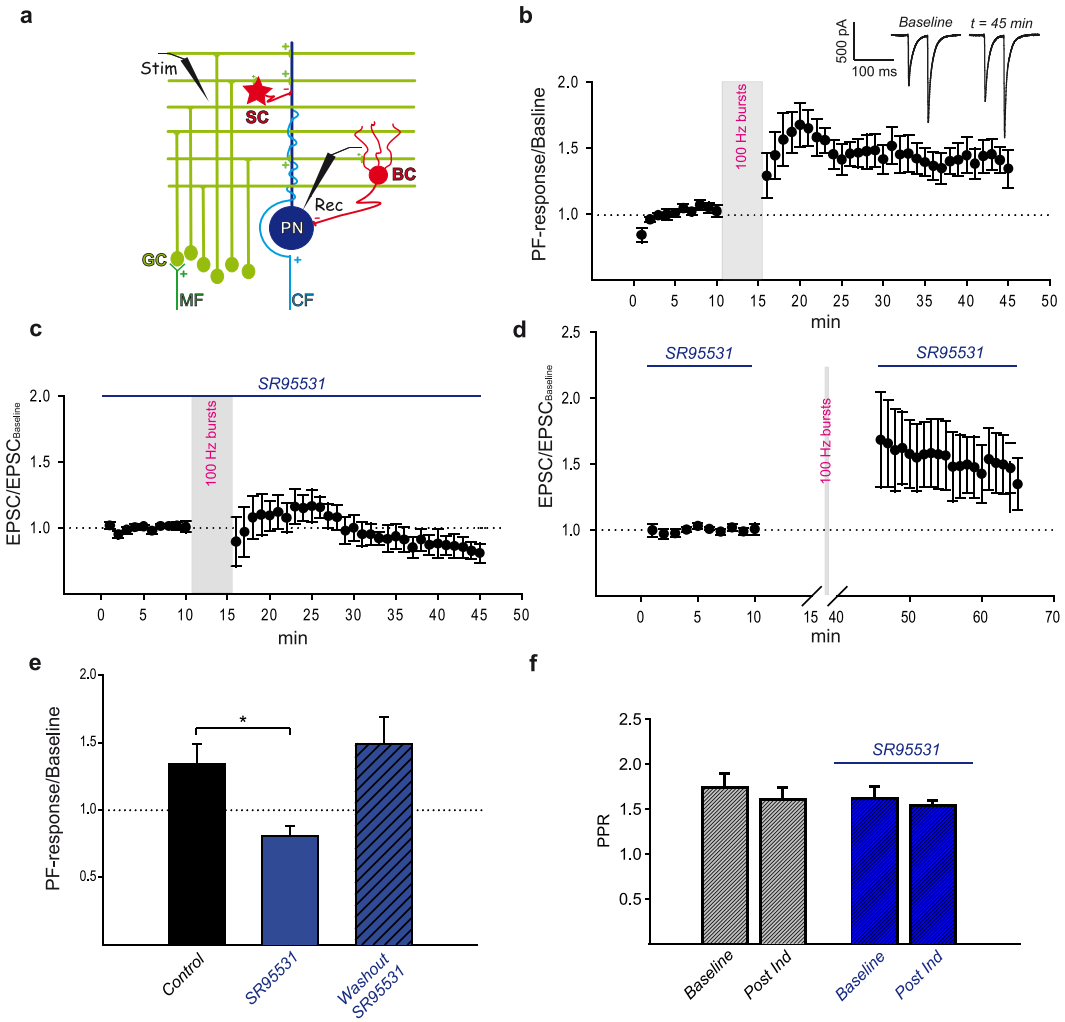

Figure 1. High frequency PFs stimulation induces $GABA_A$ receptor dependent LTP at PF to PN synapses. A schematic representation of the cerebellar microcircuit and experimental setting is shown in panel **a**. Purkinje neurons (PN) receive excitatory inputs from climbing fibers (CF) and mossy fibers (MF) via granule cells (GC) activation. Parallel fibers excitatory synapses (green+) drive PNs and inhibitory (red −) molecular layer interneurons stellate (SC) and basket (BC) cells. Traces elicited by paired-pulses PFs stimulation (Stim, **a**) in a voltage-clamped PN (Rec, **a**) at different time points are showed in the inset of panel **b**. The *Baseline* trace was obtained from averaging of all recordings during baseline while the *t = 45 min* trace is the average of three consecutive PF-mediated responses recorded every 20 seconds at the indicated time point. High frequency PFs stimulation induced a long lasting increase in PNs response (MLI_{dep}-LTP, **b**: mean ± SEM, N = 5, RM ANOVA $P < 0.001$). Bath application of the $GABA_A$ receptor antagonist SR95531 prevented MLI_{dep}-LTP (**c**, mean ± SEM, N = 5, RM ANOVA $P < 0.001$). A summary graph for SR95531-mediated effect on MLI_{dep}-LTP is shown in panel **e** (bar represents normalized PF-Rsp at t = 45 min, mean ± SEM, data from panel b and c), *indicates a statistically significant difference among values (t-test, P = 0.011). Keeping GABAergic transmission intact only during high frequency PFs stimulation was sufficient to induce MLI_{dep}-LTP (**d**). For these experiments, a 10 minutes baseline was established with SR95531 and the antagonist was washed out for at least 15 minutes before the induction protocol was applied; SR95531 was added back to the recording chamber immediately or 15 minutes after high frequency stimulation (**d**, mean ± SEM, N = 7, RM ANOVA $P < 0.001$; **e**, bar represents normalized PF-Rsp at t = 65 min, mean ± SEM, data from panel d). PPRs value (mean ± SEM) for the baseline (t = 10) and the post induction phase (t = 45) with or without bath application of SR95531 are shown in panel **f**.

modulated by activation of the ionotropic $GABA_A$ receptor *in vivo*[18]. In addition, mice selectively lacking synaptic $GABA_A$ receptors in PNs show impairment of consolidation of the vestibulo-cerebellar motor learning[19].

How inhibition modulates long-term plasticity at PF to PN synapses is nevertheless still unknown. PNs express low threshold voltage-gated T-type calcium channels (Ca_V3) which have been recently linked to calcium signaling, LTP at PF to PN synapses and to some aspects of motor learning[15,20,21]. Ca_V3 channels are opened by small depolarization of the cell membrane and they generate a transient current which rapidly inactivates[22]. Recovery from inactivation requires cell membrane re-hyperpolarization and therefore Ca_V3 channels can be influenced by inhibitory inputs as shown in thalamic neurons where GABAergic transmission promotes T-type

channels-mediated low threshold calcium spikes[23,24]. By investigating the molecular pathway leading to LTP in PNs, we demonstrate a tight cooperation between ionotropic GABA receptors and low threshold voltage-gated T-type calcium channels (Ca_V3) which promotes LTP at PF to PN synapses. We show that potentiation of transmission at PF to PN synapses following high frequency PFs stimulation requires calcium influx via Ca_V3 channels and $GABA_A$ receptor activation. Also, we provide evidence supporting Ca_V3 modulation by inhibitory inputs leading to an increase in channels availability. We then conclude that FFI can control LTP at PF to PN synapses.

Results

LTP at PF to PN synapses is $GABA_A$ receptor-dependent. The role played by inhibition in LTP induction at PF to PN synapses was investigated in acute cerebellar slices. In voltage clamped PNs ($V_h = -60$ mV), molecular layer electrical paired-pulses stimulation (20 Hz) induced PF-mediated fast inward currents with facilitation at the second response (Fig. 1b inset, Baseline). The induced response (PF-Rsp) was stable within 10 minutes from the beginning of the recording (Fig. 1b, average baseline value: -781.31 ± 25.77 pA, mean ± SEM, N = 5). Once baseline was established, PFs were stimulated at high frequency (burst of 15 pulses at 100 Hz repeated every 3 seconds for a period of 5 minutes) while PNs were switched to current clamp mode. This induction protocol was chosen to mimic GCs physiological activity[25–27] and to ensure reliable PF to MLI transmission whose failure rate has been shown to decrease at high frequency rate[28]. Train of PFs bursts stimulation caused a long lasting potentiation of the PFs-induced response (Fig. 1b). Higher values were reached at an early phase (Fig. 1b, normalized PF-$Rsp_{t20} = 1.68 \pm 0.18$, mean ± SEM, N = 5) with a later stable lower level maintained until the end of the recording (steady state) (Fig. 1b inset, t = 45 min; Fig. 1b, normalized PF-$Rsp_{t45} = 1.34 \pm 0.14$, mean ± SEM, N = 5). Since LTP can be expressed at presynaptic and/or postsynaptic site[29], the paired-pulse ratio (PPR) was investigated to discriminate between these possibilities. PPRs at steady state showed no statistically significant difference when compared to baseline (Fig. 1f, $PPR_{t10} = 1.74 \pm 0.15$, $PPR_{t45} = 1.6 \pm 0.13$, mean ± SEM; PPR_{t10} vs PPR_{t45}: one-way repeated measures (RM) ANOVA, Tukey's post hoc test, $P > 0.05$, N = 5) indicating that a change in the presynaptic probability of release was unlikely.

The role of GABAergic transmission in LTP induction was then pharmacologically investigated by bath application of the selective $GABA_A$ receptor antagonist SR95531 (5 μM). PNs holding current ($I_{holding}$) and baseline PF-mediated response decay time constant (τ_{off}) displayed no statistically significant difference in the presence of the antagonist ($I_{holding}$ SR95531: -346.74 ± 44.44 pA, mean ± SEM, $I_{holding}$ control: -241.63 ± 55.46, mean ± SEM, P = 0.177, t test, N = 5; τ_{off} SR95531: 7.14 ± 0.8 ms, mean ± SEM, τ_{off} control: 5.49 ± 2 ms, mean ± SEM, P = 0.467, t-test, N = 5) suggesting that, under our experimental conditions, PNs were clamped at a membrane potential ($V_h = -60$ mV) close to the equilibrium potential of $GABA_A$ receptor-mediated currents (calculated $E_{Cl} = -63$ mV) and that the PF-mediated response was mostly mediated by AMPA receptors.

Blocking the $GABA_A$ receptor had a profound effect on LTP (Fig. 1e) which was completely abolished by SR95531 (Fig. 1c, t = 45, normalized EPSC = 0.81 ± 0.07, mean ± SEM, N = 5; Fig. 1e, mean ± SEM, t-test, P = 0.011) with no statistically significant change in PPRs (Fig. 1f, $PPR_{t10} = 1.61 \pm 0.13$, $PPR_{t45} = 1.53 \pm 0.06$, mean ± SEM; PPR_{t10} vs PPR_{t45}: one-way repeated measures (RM) ANOVA, Tukey's post hoc test, $P > 0.05$, N = 5).

LTP at PF to PN synapses could therefore be induced by high frequency PFs stimulation provided that the ionotropic GABAergic transmission was intact, supporting a role of MLIs in long-term potentiation at PF to PN synapses; for simplicity we will refer to LTP established under our experimental condition as MLI dependent LTP (MLI_{dep}-LTP) in the later part of the text.

PF to MLI synapses and the MLIs network can also be affected by long-term plasticity that could ultimately influence our recordings[30–34]. We therefore isolated the effect of high frequency PFs stimulation on EPSCs by applying SR95531 during the baseline and the post induction phase while maintaining inhibition active during the induction protocol. Keeping inhibitory transmission intact while applying PFs bursts stimulation was necessary and sufficient to establish MLI_{dep}-LTP at PF to PN synapses (Fig. 1d) with no statistically significant change in PPRs ($PPR_{t10} = 1.78 \pm 0.08$, $PPR_{t65} = 1.58 \pm 0.1$, mean ± SEM; PPR_{t10} vs, PPR_{t65}, RM ANOVA, Tukey's post hoc test, P = 0.054, N = 7). Furthermore, EPSC increase was comparable to the potentiation obtained with intact GABAergic transmission (Fig. 1e,d: normalized $EPSC_{t65} = 1.49 \pm 0.2$; Fig. 1e,b: normalized PF-$response_{t45} = 1.34 \pm 0.14$, P = 0.593, t-test).

Taken together our data support the requirement of $GABA_A$ receptor activation in MLI_{dep}-LTP; MLI_{dep}-LTP is likely postsynaptic and it is expressed at PF to PN synapses.

Molecular pathway to MLI_{dep}-LTP. Low threshold voltage-gated Ca_V3 channels have recently been linked to postsynaptic LTP at PF to PN synapses[15] and they are influenced by inhibitory inputs as shown in thalamic and deep cerebellar nuclei (DCN) neurons[23,24,35–37]. We therefore investigated their possible role in MLI_{dep}-LTP by pharmacologically blocking their activation with the highly specific T-type calcium channels antagonist TTA-P2[38] (Merck; 500 nM). In the presence of the Ca_V3 channels antagonist, high frequency PFs stimulation failed to induce MLI_{dep}-LTP with the induced responses slightly decreasing below baseline level after the first transient increment (Fig. 2a, t = 45, normalized PF-Rsp = 0.9 ± 0.09 mean ± SEM, N = 5); PPRs showed no statistically significant difference from baseline (Fig. 2a inset, $PPR_{t10} = 1.5 \pm 0.072$, $PPR_{t45} = 1.5 \pm 0.04$; mean ± SEM; PPR_{t10} vs PPR_{t45}, RM ANOVA, Tukey's post hoc test, $P > 0.05$, N = 5).

All three Ca_V3 isoforms are found in PNs with weak $Ca_V3.2$ channels staining[39] and more pronounced $Ca_V3.1$ and $Ca_V3.3$ channels expression[39,40]. PFs bursts-induced calcium transients in mature PNs are mostly mediated by $Ca_V3.1$ channels[21] and $Ca_V3.1$ KO mice showed LTP impairment[15]. We therefore investigated whether $Ca_V3.1$ channels play a role in MLI_{dep}-LTP in acute cerebellar slices from $Ca_V3.1$ KO mice[41]. Under the same experimental condition which led to MLI_{dep}-LTP in WT mice, $Ca_V3.1$ KO mice showed no MLI_{dep}-LTP (Fig. 2b, N = 5).

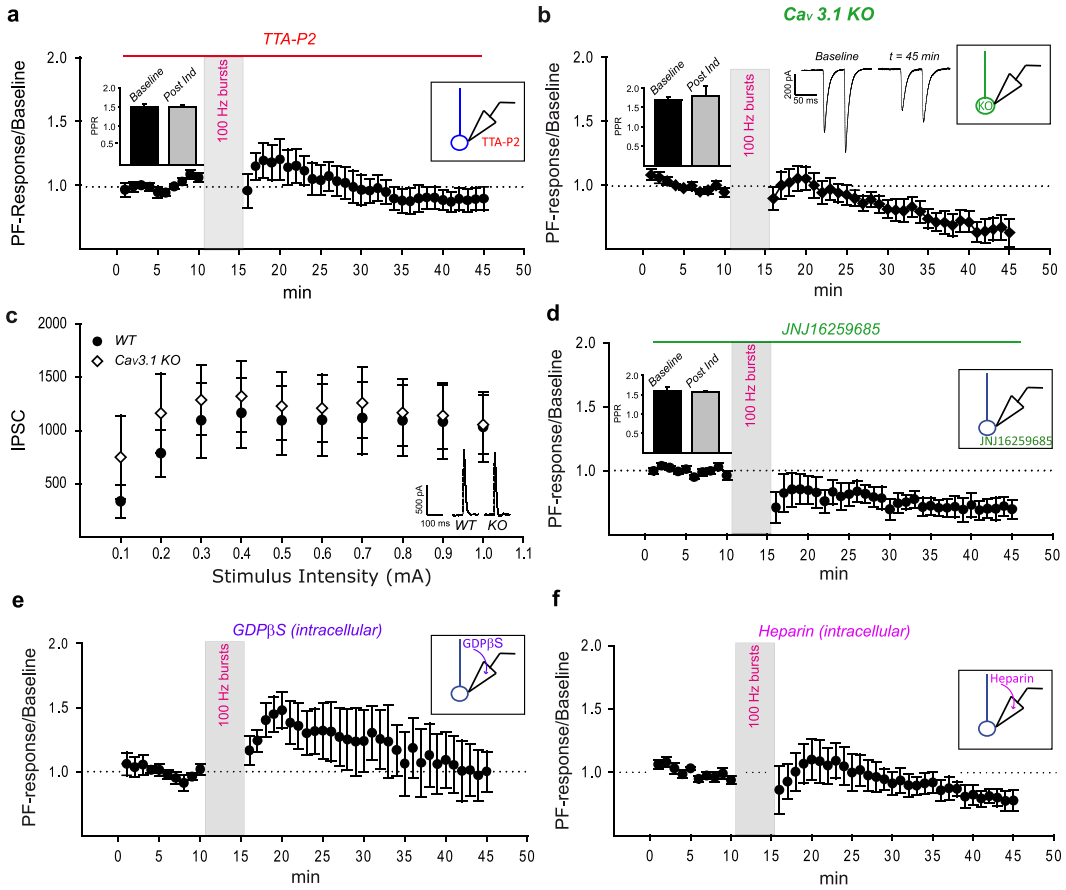

Figure 2. Molecular pathway to MLI_{dep}-LTP. MLI_{dep}-LTP was effectively prevented by the broad spectrum low threshold voltage-gated T-type calcium channels specific antagonist TTA-P2 (**a**, mean ± SEM, N = 5, RM ANOVA $P < 0.001$). To identify the Ca_V3 isoform required for the GABA-dependent potentiation, long-term plasticity experiments were performed in $Ca_V3.1$ KO mice. MLI_{dep}-LTP is absent in $Ca_V3.1$ KO mice (**b**, mean ± SEM, N = 5, RM ANOVA $P < 0.001$) under the same experimental condition that leads to $GABA_A$ receptor-dependent potentiation of PF to PN transmission in WT mice and traces from a representative experiment are shown in the middle inset. PF-induced inhibitory responses were recorded in PNs from WT and $Ca_V3.1$ KO mice (**c**, inset) and input/output curves obtained (**c**: WT, black circle: N = 8; KO, white diamond: N = 10, mean ± SEM). No statistically significant difference was detected among the two curves ($P > 0.05$, t-test at all stimulus intensities). MLI_{dep}-LTP also depends on mGluR1 and intracellular calcium stores; high frequency PFs stimulation failed to induce MLI_{dep}-LTP when activation of the metabotropic glutamate receptor mGluR1was prevented by bath application of the specific antagonist JNJ16259685 (**d**, mean ± SEM, N = 5, RM ANOVA $P < 0.001$). Inclusion of the non-hydrolysable GDP analog GDPβS (**e**, mean ± SEM, N = 3) or heparin (**f**, mean ± SEM, N = 6, RM ANOVA P = 0.006) in the intracellular recording solution also impaired MLI_{dep}-LTP. PPRs value (mean ± SEM) for the baseline (t = 10 min) and the post induction phase (t = 45 min) under each condition are shown in the left insets in panel **a**,**b**,**d**.

Also, PPRs value showed no statistically significant difference to baseline (Fig. 2b inset, $PPR_{t10} = 1.68 \pm 0.1$, $PPR_{t45} = 1.8 \pm 0.26$, mean ± SEM; PPR_{t10} vs PPR_{t45}, RM ANOVA, Tukey's post hoc test, $P > 0.05$, N = 5).

In order to exclude any effect of $Ca_V3.1$ absence on MLI to PN transmission that could potentially interfere with MLI_{dep}-LTP induction, the total PF-induced inhibition was measured in WT and $Ca_V3.1$ KO mice. Input/output curves showed no significant difference in $Ca_V3.1$ KO mice compared to WT animals (Fig. 2c, minimum stimulus intensity: WT = 382.88 ± 152.41 pA, N = 8; KO = 748.95 ± 391.01 pA, N = 10, P = 0.379, t-test) supporting a normal MLI to PN transmission. The absence of MLI_{dep}-LTP is therefore a direct consequence of impaired calcium influx in $Ca_V3.1$ KO PNs dendrites[15] rather than a secondary effect due to altered inhibition.

A functional coupling between mGluR1 receptors and $Ca_V3.1$ channels has been identified in PNs with the activation of the G-coupled receptor leading to the potentiation of calcium influx through T-type calcium channels[21] and therefore mGluR1activation may be required for the described long-term potentiation. Indeed, blocking mGluR1 by bath application of the specific antagonist JNJ16259685 (2 μM) prevented MLI_{dep}-LTP (Fig. 2d, N = 5) with no statistically significant change in PPRs when compared to baseline (Fig. 2d inset, $PPR_{t10} = 1.59 \pm 0.09$, $PPR_{t45} = 1.57 \pm 0.03$, mean ± SEM, N = 5; PPR_{t10} vs PPR_{t45} $P > 0.05$, RM ANOVA, Tukey's test). Strikingly, blocking the receptor also revealed a mGluR1-independent LTD (normalized PF-$Rsp_{t45} = 0.7 \pm 0.07$, normalized PF-$Rsp_{t1} = 1 \pm 0.02$, P = 0.025 RM ANOVA, Tukey's post hoc test). As expected by MLI_{dep}-LTP impairment

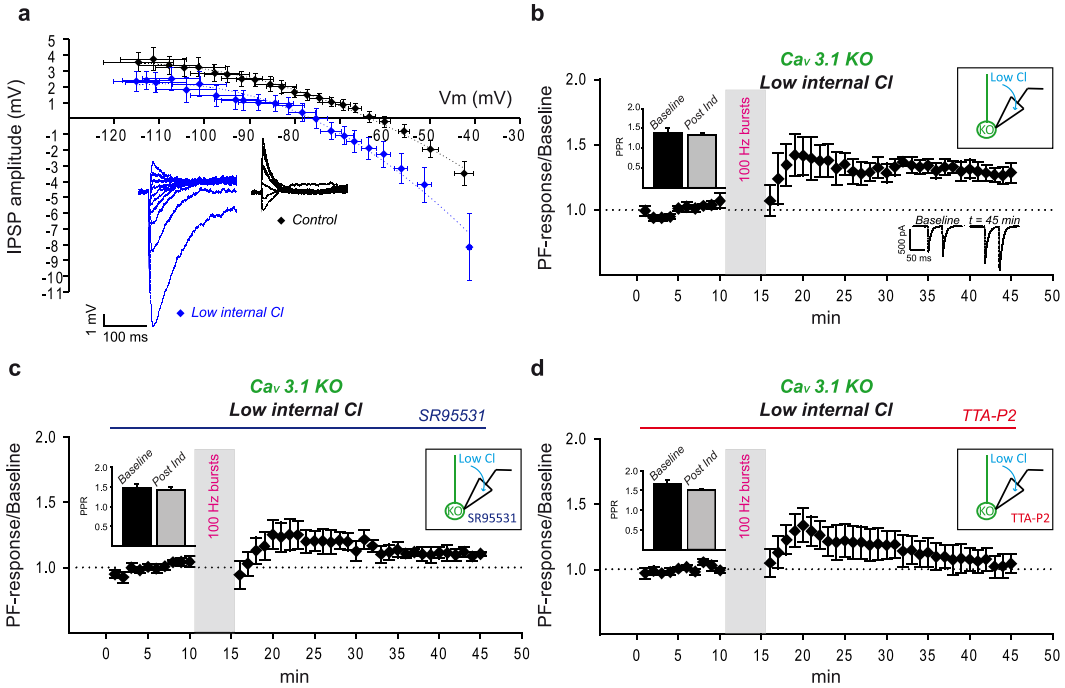

Figure 3. MLI_{dep}-LTP is $Ca_V3.1$ dependent and it relies on $GABA_A$ receptor and T-type calcium channels cooperation. Change in intracellular chloride concentration affects IPSPs/V_m curves in PNs from $Ca_V3.1$ KO mice. Lowering intracellular chloride caused a 13 mV hyperpolarizing shift of IPSP/Vm curves (**a**, blue diamond, N = 7, mean ± SEM) compared to control condition (**a**, black diamond, N = 7, mean ± SEM). IPSPs recorded at different V_m from two representative PNs are shown in the inset of panel **a** in control (black) and low chloride (blue) condition. Dot lines represent the polynomial fit of IPSP/Vm curves obtained under the two experimental conditions. MLI_{dep}-LTP was rescued when the low internal chloride recording solution was used (**b**, mean ± SEM, N = 5, RM ANOVA $P < 0.001$) and traces from one exemplificative experiment are shown in the inset at the bottom of the panel. The rescued MLI_{dep}-LTP was dependent on $GABA_A$ receptor (**c**: mean ± SEM, N = 5, RM ANOVA $P < 0.001$) and T-type calcium channels (**d**: mean ± SEM, N = 5, RM ANOVA $P < 0.001$) activation. PPRs value (mean ± SEM) for the baseline (t = 10 min) and the post induction phase (t = 45 min) under each condition are showed in the left insets in panel **c**,**d**.

caused by mGluR1 inactivation in PNs, the inclusion of the non-hydrolysable GDP analog GDPβS (2 mM) in the patch pipette also interfered with long term plasticity (Fig. 2e, N = 3). mGluR1 activation induces release of calcium from intracellular stores which could therefore be implicated in MLI_{dep}-LTP. When calcium release from intracellular store via IP3 receptors was prevented by inclusion of heparin (50 μg/ml) in the patch pipette[42], MLI_{dep}-LTP was also impaired (Fig. 2f, N = 6) suggesting that calcium influx via Ca_V3 channels and internal stores might cooperate for MLI_{dep}-LTP induction.

These experiments support the requirement of a postsynaptic molecular cascade for the expression of MLI_{dep}-LTP at PF to PN synapses; we showed that MLI_{dep}-LTP is Ca_V3 channels, mGluR1 and internal calcium stores dependent.

Ionotropic GABA receptors and Ca_V3 channels cooperation is required for MLI_{dep}-LTP. Ca_V3 channels open in response to small depolarization of the cell, quickly inactivate and recovery from inactive state depends on cell membrane re-hyperpolarization after channel opening[22]. The three Ca_V3 channel isoforms are characterized by different activation curves with $Ca_V3.1$ (half activation V_a: −60 ± 0.9 mV at 37 °C) and $Ca_V3.2$ channels (half activation V_a: −51.5 ± 1 mV at 37 °C) opening at more depolarized membrane potential compared to $Ca_V3.3$ channels (half activation V_a: −73.5 ± 1.3 mV at 37 °C)[43] which therefore requires stronger hyperpolarization to de-inactivate. Modulation of $GABA_A$-mediated transmission could therefore impact Ca_V3 channels availability and affect MLI_{dep}-LTP. We investigated this hypothesis by lowering the chloride concentration in the internal solution for MLI_{dep}-LTP experiments in $Ca_V3.1$ KO mice to obtain a stronger $GABA_A$ receptor-mediated hyperpolarization in PNs as shown by the 13 mV negative shift of the IPSP reversal potential when compared to control condition (control, N = 7: −63 mV; low chloride, N = 7: −76 mV) (Fig. 3a); a stronger hyperpolarization might enhance $Ca_V3.3$ channels availability and therefore improve Ca_V3 channels-mediated intracellular calcium rise in the $Ca_V3.1$ KO during bursts of PFs stimulation and facilitate MLI_{dep}-LTP induction. Indeed, under these experimental conditions, high frequency PFs stimulation generated a long lasting increase of transmission in $Ca_V3.1$ KO mice (Fig. 3b, t = 45, normalized PF-Rsp = 1.29 ± 0.17, mean ± SEM, N = 5). The recovery of LTP depended on $GABA_A$ activation (KO-MLI_{dep}-LTP) since it was absent in presence of SR95531 (Fig. 3c, normalized $EPSC_{t10}$ = 1.11 ± 0.01, normalized $EPSC_{t45}$ = 1.05 ± 0.04, $P > 0.05$ RM ANOVA, Tukey's post hoc test, N = 5). More importantly, TTA-P2 bath application (Fig. 3d) also prevented KO-MLI_{dep}-LTP (normalized

PF-Rsp$_{t45}$ = 1.04 ± 0.07, normalized PF-Rsp$_{t10}$ = 0.99 ± 0.02, P > 0.05 RM ANOVA, Tukey's post hoc test, N = 5) indicating that the enhanced availability of an alternative PN-expressed Ca_V3 isoform could compensate for the lack of $Ca_V3.1$ channels.

Under all experimental condition tested, PPRs showed no difference when compared to baseline value (Fig. 3c inset, control: PPR$_{t10}$ = 1.38 ± 0.13, PPR$_{t45}$ = 1.34 ± 0.04, N = 5; Fig. 3d inset, SR95531: PPR$_{t10}$ = 1.47 ± 0.09, PPR$_{t45}$ = 1.42 ± 0.08, N = 5; Fig. 3e inset, TTA-P2: PPR$_{t10}$ = 1.65 ± 0.1, PPR$_{t45}$ = 1.49 ± 0.04, N = 5; mean ± SEM, PPRt$_{10}$ vs PPR$_{t45}$, P > 0.05, RM ANOVA, Tukey's test).

Ca_V3 channels-mediated calcium transient is under the control of ionotropic GABA receptors. The recovery of MLI$_{dep}$-LTP in $Ca_V3.1$ KO mice supports a functional coupling between $GABA_A$ receptors and Ca_V3 channels important for LTP at PF to PN synapses. The influence of inhibition on Ca_V3-mediated calcium transient elicited by high frequency PFs stimulation was therefore tested in PNs from WT mice by calcium imaging (Fig. 4). For these experiments, the calcium indicator Oregon Green BAPTA 6F (400 μM) was added to the low chloride internal solution and loaded into the recorded PN via the patch pipette. To prevent calcium release from intracellular stores heparin (50 μg/ml)[42] was also included in the patch clamp intracellular recording solution. The variation of intracellular calcium concentration was monitored in current clamped PNs (Fig. 4aa–ba) while PFs were stimulated by a single 100 Hz burst (15 pulses). Stimulus intensity was set to induce PFs-mediated responses (Fig. 4ab) similar to those recorded during the LTP induction protocol. The raise in intracellular calcium concentration caused by high frequency PFs stimulation (Fig. 4aa, left panel) was largely Ca_V3 channels-mediated as shown by fluorescence attenuation following TTA-P2 bath application (Fig. 4aa, right panel); the relative change in fluorescence (ΔF/F) was strongly influenced by TTA-P2 with a 64% reduction of its peak value by the antagonist (Fig. 4ac, ΔF/F$_{Control}$ = 1.37 ± 0.5, ΔF/F$_{TTA\text{-}P2}$ = 0.47 ± 0.09, mean ± SEM, P = 0.041, ANOVA, Bonferroni post hoc test, N = 5). Interestingly, the Ca_V3 channels-mediated component of the calcium transient was completely lost when inhibition was blocked. In presence of SR95531 (Fig. 4ba, left panel), the induced increase in intracellular calcium was TTA-P2 insensitive (Fig. 4ba, right panel and Fig. 4bb, N = 5) and therefore mediated by high threshold voltage gated calcium channels.

Plasticity experiments were then conducted with the low chloride intracellular recording solution; when high frequency PFs stimulation was applied at low intracellular chloride concentration (Fig. 4c), MLI$_{dep}$-LTP was slightly bigger (Fig. 4c, EPSC$_{/baseline}$t$_{65}$ = 1.63 ± 0.27, mean ± SEM, N = 6) compared to normal chloride (Fig. 1d, EPSC$_{/baseline}$t$_{65}$ = 1.49 ± 0.2, N = 7) but with no statistically significant difference (normal vs low chloride, t = 65 min, P = 0.678, t-test); PPRs showed no statistically significant difference when compared to baseline value (Fig. 4c inset, PPR$_{t10}$ = 1.66 ± 0.07, PPR$_{t65}$ = 1.59 ± 0.11, mean ± SEM, N = 6, P > 0.05, RM ANOVA, Tukey's test).

These findings demonstrate that ionotropic GABA receptors activation is required for Ca_V3 channels-mediated calcium rise in PNs during high frequency PFs stimulation.

In agreement with the recovery of MLI$_{dep}$-LTP observed in $Ca_V3.1$ KO mice, the calcium transient recorded in PNs from KO mice was largely Ca_V3 channels-mediated only when elicited by PFs stimulation at low intracellular chloride concentration (Fig. 4d, *low chloride*); bath application of TTA-P2 strongly reduced calcium influx in low chloride (normalized ΔF/F$_{MAX\text{-}Control}$ = 1 ± 0.27, normalized ΔF/F$_{MAX\text{-}TTAP2}$ = 0.42 ± 0.13, mean ± SEM, N = 5, P = 0.017, paired t-test) while no statistically significant difference (normalized ΔF/F$_{MAX\text{-}Control}$ = 1 ± 0.23, normalized ΔF/F$_{MAX\text{-}TTAP2}$ = 0.79 ± 0.08, mean ± SEM, N = 5, P = 0.446, paired t-test) was detected in the presence of the antagonist when the regular internal solution was used (Fig. 4d, *normal chloride*).

Taken together these results support the fundamental role of Ca_V3 channels-mediated calcium influx in MLI$_{dep}$-LTP induction at PF to PN synapses and the requirement of $GABA_A$ receptors activation to ensure the availability of Ca_V3 channels for opening during bursts of PFs activation.

Discussion

In the cerebellar cortex, GCs activation by MFs input leads to excitatory (monosynaptic) and inhibitory (di-synaptic) events in PNs and their interaction in the induction of LTP at PFs excitatory synapses is described in this article. We showed that high frequency PFs stimulation caused LTP at PF to PN synapses only when MLIs-mediated GABAergic transmission was intact (Fig. 1).

MLI$_{dep}$-LTP is induced by a postsynaptic mechanism as showed by its recovery in $Ca_V3.1$ KO mice (Fig. 3b) and its impairment by the intracellular block of GPCRs (Fig. 2e) and IP3 receptors (Fig. 2f); MLI$_{dep}$-LTP is $GABA_A$ receptors (Fig. 1), Ca_V3 channels (Fig. 2a,b), mGluR1 receptors (Fig. 2d,e) and intracellular calcium store (Fig. 2f) dependent.

Ca_V3 channels-dependent LTP has been previously reported to be induced at PF to PN synapses in the presence of the $GABA_A$ receptor antagonist bicuculline[15] in apparent discrepancy with our results. Nevertheless, PNs have been shown to express the ionotropic GABA receptor bicuculline-insensitive ρ subunits[44,45] suggesting that bicuculline might not be able to completely eliminate inhibition in PNs. Indeed, we were able to record a bicuculline-insensitive IPSC component in PNs following PFs stimulation (Supplementary Information); after bath application of bicuculline (20 μM), 6% of the total IPSQs was still present (Supplementary Figure S1 panel a and panel b) and it was completely blocked by the following application of SR95531 (5 μM). The fact that LTP was successfully induced in the presence of bicuculline suggests that this residual bicuculline-insensitive component of the ionotropic GABA receptors-mediated response was sufficient to mediate Ca_V3 channels recovery from inactivation at least in WT mice. In agreement, MLI$_{dep}$-LTP was unaffected by bath application of bicuculline (Supplementary Figure S1 panel c and panel d).

The MLI network can be modulated by long-term plasticity and PF to MLI synapses can be potentiated[32] at low frequency stimulation (2–8 Hz) while high frequency stimulation induces LTD[30,31]. Also, high frequency PFs stimulation causes LTP at inhibitory MLI to MLI synapses[34] via increase of GABA release[33]. High frequency PFs stimulation could therefore reduce inhibitory inputs to PNs via decreased MLIs excitation and/or by increasing

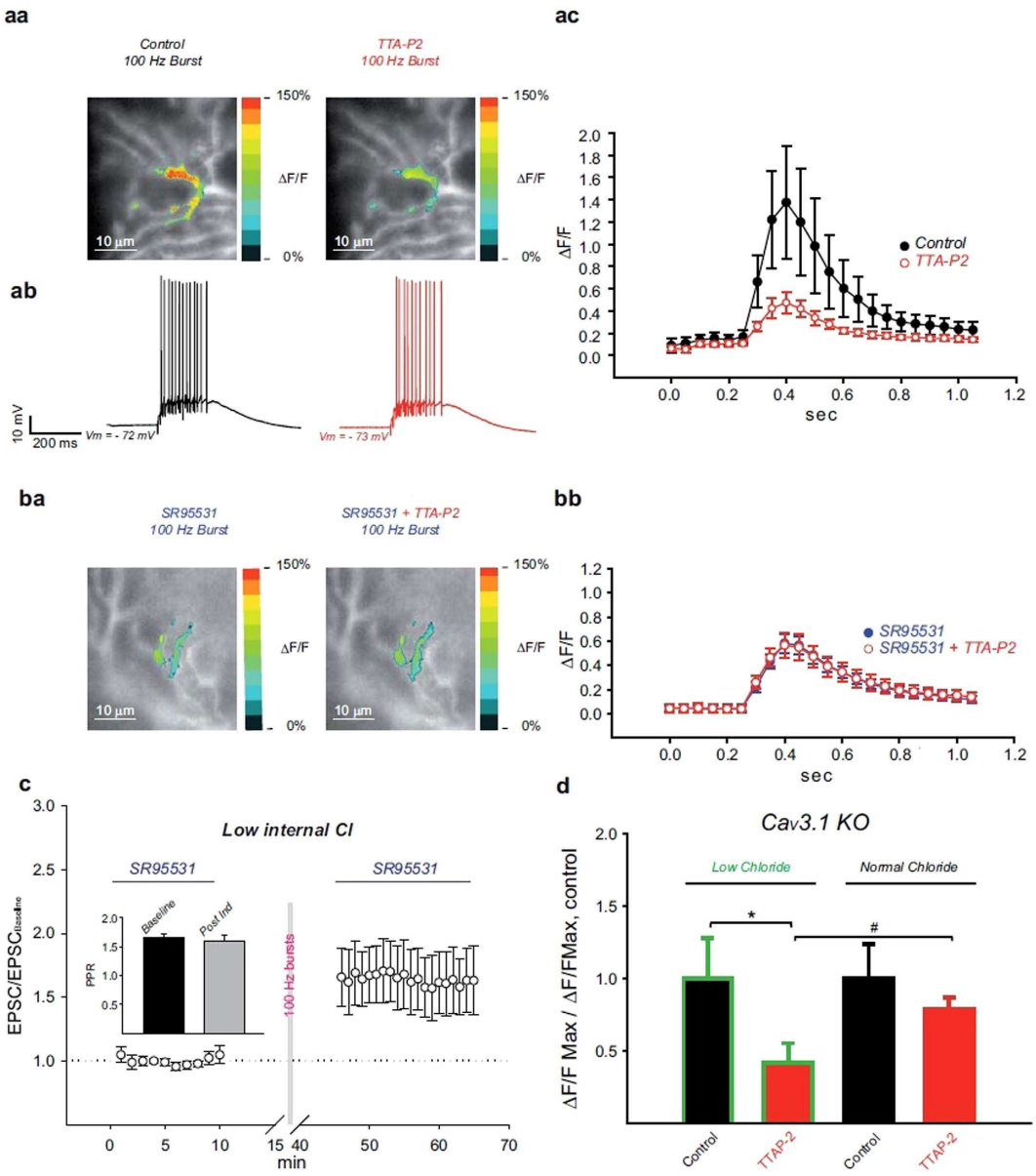

Figure 4. Ca_V3-mediated calcium influx is controlled by inhibition. High frequency PFs stimulation caused depolarization (**ab**) and calcium increase in PNs (**aa**, left panel; **ba**, left panel); for each representative cell showed, the average ΔF/F signals was obtained at the peak of the response under the different experimental conditions (pseudocolor) and an it was superimposed on the image of the PN at resting state (grayscale). While TTA-P2 bath application strongly affected the calcium transient recorded in control condition (**aa**, right panel), the antagonist showed no effect in presence of SR95531 (**ba**, right panel). Quantified relative change in fluorescence (ΔF/F) showed a large TTA-P2 sensitive component revealing that calcium influx is mostly mediated by Ca_V3 activation but only in control condition (**ac**, mean ± SEM, N = 5, ANOVA $P < 0.001$). Ca_V3-mediated calcium influx is lost when inhibition was blocked by bath application of SR95531 (**bb**, mean ± SEM, N = 5, ANOVA $P < 0.001$). High frequency PFs stimulation in low internal chloride induced MLI_{dep}-LTP (**c**, mean ± SEM, N = 6, RM ANOVA $P < 0.001$); PPRs (mean ± SEM) value for the baseline (t = 10 min) and the post-induction phase (t = 65 min) are shown in the panel **c** inset. The effect of different intracellular chloride concentrations on the PFs-induced calcium transient was evaluated in PNs from $Ca_V3.1$ KO mice (**d**). The TTA-P2 sensitive component of the calcium transient observed in low chloride (*Low chloride*: control = 1 ± 0.23, mean ± SEM, N = 5; TTA-P2: 0.42 ± 0.13, mean ± SEM, N = 5, P = 0.017, paired t-test) was lost when the normal chloride internal solution was used (*Normal Chloride*, control: 1 ± 0.23, mean ± SEM, N = 5; TTA-P2: 0.79 ± 0.08, mean ± SEM, N = 5, P = 0.446, paired t-test). Before cell averaging, the maximal ΔF/F value obtained before and after TTA-P2 bath application for each cell was normalized to the mean ΔF/F value obtained in control condition. *statistically significant difference, paired t-test. #statistically significant difference, t-test.

inhibition onto MLIs. The decreased inhibition in PNs could result in indirect potentiation of PFs-mediated responses in these neurons. No significant $GABA_A$-mediated component in the PFs-mediated responses was observed under our experimental conditions and therefore, if present, indirect potentiation should have had little influence on our recordings. This was confirmed by investigating the specific impact of high frequency PFs stimulation on excitatory transmission by blocking GABAergic inputs before and after the induction protocol. Excitatory transmission at PF to PN showed postsynaptic potentiation to level comparable to what previously observed (Fig. 1d). $GABA_A$ receptor activation is therefore required for MLI_{dep}-LTP at PF to PN synapses only during the induction phase. This and the intracellular pharmacological block of MLI_{dep}-LTP (Fig. 2e,f) strongly argue against indirect potentiation and they support involvement of inhibition in LTP induction at PF to PN synapses.

By investigating the molecular pathway leading to MLI_{dep}-LTP we have provided evidence for a tight cooperation among GABAergic transmission and low threshold voltage-gated calcium channels in PNs (Figs 3 and 4). We propose an active postsynaptic role for GABAergic transmission in MLI_{dep}-LTP induction with inhibition modulating T-type Ca_V3 calcium channels availability (i.e. by favoring de-inactivation). This hypothesis is supported by the recovery of MLI_{dep}-LTP in $Ca_V3.1$ KO mice by the intracellular modulation of the chloride electrochemical gradient in PNs (Fig. 3b). As shown by KO- MLI_{dep}-LTP dependency on TTA-P2 (Fig. 3d), an alternative Ca_V3 channels isoform is recruited when $GABA_A$ receptor activation favored hyperpolarization toward more negative potentials (Fig. 3a). Accordingly, the TTA-P2-sensitive component of the calcium transient was restored in $Ca_V3.1$ KO mice when the intracellular chloride was decreased (Fig. 4d). Furthermore, Ca_V3-mediated calcium influx and MLI_{dep}-LTP was detected in PNs from WT mice only when inhibitory GABAergic transmission was intact (Figs 4a,b and 1).

MLIs-mediated postsynaptic response causes membrane potential re-hyperpolarization in depolarized PNs both in the dendritic compartment and at the soma[46,47]. Since high frequency PFs stimulation is able to bring PNs membrane voltage to firing threshold (Fig. 4ab), the recovery of MLI_{dep}-LTP (Fig. 3b) and Ca_V3 channels-mediated calcium transient (Fig. 4d) in $Ca_V3.1$ KO mice suggests that activation of $GABA_A$ receptors favor re-hyperpolarization toward a level suitable for Ca_V3 channels de-inactivation. Ca_V3 channels inactivation has been shown to be effectively removed by $GABA_A$-mediated IPSPs in DCN neurons[35–37]; the IPSP reversal potential in these neurons (−75 mV)[37] is close the one obtained under our experimental condition in low chloride (Fig. 3a) supporting an effective Ca_V3 channels de-inactivation also in our experiments.

$Ca_V3.3$ channels are highly expressed in PNs and they require a stronger hyperpolarization to recovery from inactivation; based on its expression pattern and biophysical characteristics, $Ca_V3.3$ channels are therefore the isoform most likely to be involved in the rescue of MLI_{dep}-LTP in $Ca_V3.1$ KO mice although a role of $Ca_V3.2$ channels cannot be excluded at this time[48]. The reversal potential of GABAergic currents (E_{GABA}: −85/−87 mV) measured in mature PNs[49,50] predict a strong hyperpolarization in PNs caused by $GABA_A$ receptors activation suggesting that $Ca_V3.3$ channels might be also recruited under physiological conditions and it might also participate with $Ca_V3.1$ in MLI_{dep}-LTP induction. $Ca_V3.3$ channels sole requirement is nevertheless unlikely. Cerebellar long-term plasticity is a calcium-dependent mechanism[7] and PFs-mediated increment of calcium in PNs spines is mostly mediated by $Ca_V3.1$channels even though in $Ca_V3.1$ KO mice a residual T-type dependent influx is still present[21]. Furthermore, $Ca_V3.1$ channels-mediated calcium influx is potentiated by mGluR1 activation and MLI_{dep}-LTP dependency on this metabotropic glutamate receptor (Fig. 2d,e) further supports the requirement for the $Ca_V3.1$ channel isoform in MLI_{dep}-LTP. Interestingly, the impairment exhibited by $Ca_V3.1$ KO mice in long term VOR phase-reversal training seems less severe when compared to the one of WT mice systemically injected with TTA-P2[15] suggesting that $Ca_V3.3$ channels might also participate in cerebellar-mediated motor learning in $Ca_V3.1$ KO mice and slightly attenuate their phenotype.

When MLI_{dep}-LTP was compromised, decrease efficiency in PFs transmission was also revealed unmasking a pathway leading to depression at PF to PN synapses. Interestingly, this long term depression was still present when mGluR1 was inactivated (Fig. 2d). At PF to PN synapses, mGluR1 plays a central role in LTD[51–55] but long term depression is nevertheless also reliably induced by nitric oxide (NO) uncaging when coupled to PNs depolarization[56] suggesting that this PF-released anterograde messenger[57] together with the depolarization-induced intracellular calcium raise in PNs might be sufficient to permanently decrease the synaptic transmission strength at these synapses. Indeed a NO synthase (NOS) dependent LTD has been previously described at PF to PN synapses[58]; this LTD requires NMDA receptors activation[58] and it is mGluR1 independent[59]. NO is likely to be released under our experimental conditions and therefore it might play a role in the depression observed whenever MLI_{dep}-LTP was impaired.

A simple model describing the first events leading to MLI_{dep}-LTP at PF to PN synapses can be proposed (Fig. 5): high frequency PFs stimulation activates AMPA receptors and causes PN dendrites depolarization counterbalanced by the $GABA_A$-induced hyperpolarization elicited by MLIs; membrane depolarization triggers T-type calcium channels activation and their availability for opening is controlled by inhibition. In order to induce MLI_{dep}-LTP at PF to PN synapses, Ca_V3 channels require mGluR1 activation that potentiates $Ca_V3.1$ channels-mediated calcium influx via a PLC independent pathway[21]. Via the G_q/PLC pathway, mGluR1 activation also leads to the release of calcium from the intracellular stores via activation of IP3 receptors; intracellular released calcium also seems to be required for MLI_{dep}-LTP.

While high frequency stimulation of PFs induced a mGluR1-dependent LTP *in vivo*[18], low frequency (1 Hz) stimulation of PFs in the molecular layer of cerebellar slices induced a long lasting enhancement of transmission at PF to PN synapses which was unaffected by the pharmacological inactivation of this metabotropic receptor[9]. Together with our results, these findings support the existence of two distinct pathways leading to LTP which are differently engaged by PFs activity. Low frequency stimulation induces a mGluR1 independent potentiation which is unaffected by GABAergic ionotropic transmission impairment[19] but it depends on NO release[6] and PP2B activation[10]. When PFs are stimulated at high frequency, long term potentiation requires MLIs activation

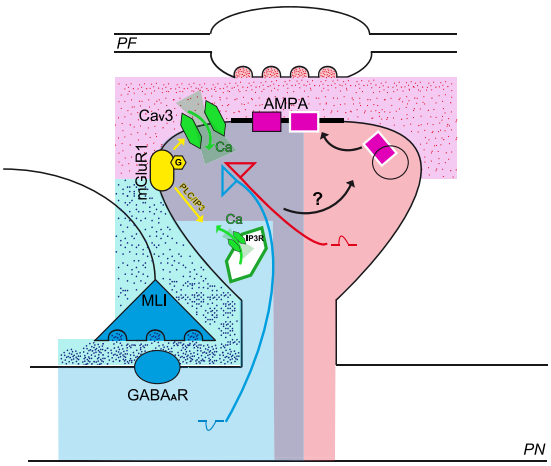

Figure 5. MLI_{dep}-LTP model. Schematic representation of the parallel fiber (*PF*) to Purkinje neuron (*PN*) synapse with a PF varicosity drawn in the upper part and the corresponding PN spine shown below. Molecular layer interneuron inhibitory synapse (MLI) is also shown in the scheme. Following high frequency parallel fibers (PF) stimulation, $GABA_A$-mediated hyperpolarization (blue shadow) limits AMPA-induced depolarization (pink shadow) to a range suitable for Ca_V3 activation (light violet shadow). AMPA-mediated depolarization (red arrow) activates Ca_V3 calcium channels dependently on their availability regulated by inhibition (blue arrow) and Ca_V3-mediated calcium influx is enhanced by mGluR1 activation (yellow arrow). mGluR1 activation also leads to calcium release from intracellular stores via IP3 receptors. The described molecular steps initiate the cascade that leads to MLI_{dep}-LTP and downstream events are still to be determined.

and it is dependent on ionotropic GABA receptors and mGluR1 activation which cooperate to ensure a reliable activation of low threshold voltage-gated calcium channels. We therefore describe here a complementary pathway regulating PF to PN synaptic efficacy in a context of high frequency GCs inputs. Since GCs inputs recorded *in vivo* range from few to several hundred hertz[27], both mechanisms might coexist in order to control plasticity in different conditions or they might underlie specific pathways expressed in different groups of GC to PN synapses as suggested by the discovery that zebrin band specific physiological mechanisms could regulate cerebellar information processing[60,61].

Suggestions on the possible role played by MLI_{dep}-LTP in cerebellar physiology come from previous findings obtained *in vivo*. When PFs in the cat forelimb movements-related C3 zone are electrically stimulated with the same paradigm used in this paper, a bidirectional change in PFs receptive field of PNs is induced depending on the co-activation of CF input to the recorded cell. While co-activation leads to depression, an enlargement of PFs receptive field is observed when PFs are the sole excitatory pathway stimulated. Following PFs stimulation, PNs in the C3 zone are driven by cutaneous stimulation from several parts of the body in agreement with what could be expected following awakening of silent connection between PFs and PNs[62]. In attempt to mimic protocols performed *in vivo*, LTP has been established in this study without pharmacological perturbation of synaptic transmission and intracellular signal transductions. Thus, our work might provide a detailed description of the initial molecular events which lead to the PFs receptor field enlargement observed *in vivo*. Consequently, it is tempting to speculate that the described MLI-dependent LTP could be the result of the summation of newly awaken PF to PN synapses rather than the sole increased membrane expression of AMPA receptors at activated synapses.

Methods

Ethical approval. All animal procedures were performed in accordance with the University of Strasbourg animal care committee's regulations and they were approved by the Ethical Committee of the University of Strasbourg (A67-2018-38).

Electrophysiology. Patch clamp experiments were conducted on acute coronal slices from cerebellum of adult C57BL/6 male mice (P27-P46) and age-matched $Ca_V3.1$ knockout (KO) male mice from homozygous breeding. Mice were anesthetized by exposure to isoflurane, decapitated and the cerebellum dissected in ice cold bubbled (95% O_2/5% CO_2) aCSF containing (in mM): NaCl 120, KCl 3, $NaHCO_3$ 26, NaH_2PO_4 1.25, $CaCl_2$ 2, $MgCl_2$ 1 and glucose 16. 300 μm thick slices were obtained with a vibratome (Microm 650 V: Thermo Scientific Microm, Waltham, Massachusetts) in ice cold slicing medium containing (in mM): KGluconate 130, KCl 14.6, EGTA 2, HEPES 20, Glucose 25, pH 7.3 and supplemented with D-APV 50 μM and minocycline 50 nM. Recovery for 1–5 seconds at 35 °C was allowed in bubbled transfer buffer containing (in mM): sucrose 230, KCl 2.5, $NaHCO_3$ 26, NaH_2PO_4 1.25, $CaCl_2$ 0.8, $MgCl_2$ 8, glucose 25 and supplemented with D-APV 50 μM and minocycline 50 nM. Slices were then transferred to a holding chamber containing bubbled aCSF and kept at 35 °C for at least 40 minutes before they were moved to room temperature for the remaining experimental time.

For patch clamp recordings slices were moved to a recording chamber at 34 °C and continuously perfused with bubbled aCSF eventually supplemented with antagonists as stated in the main text. Borosilicate glass pipettes were pulled using a vertical puller (Narishige PC-10: Narishige, Tokyo, Japan) to a final resistance of 4–4.5 MΩ and filled with the following internal solution (in mM): KGluconate 130, KCl 10, $MgCl_2$ 1, HEPES 10, Na_2ATP

4, NaGTP 0.4, sucrose 16, pH 7.3. For experiments in low internal chloride concentration the following internal solution was used (in mM): KGluconate 136, KCl 4, $MgCl_2$ 1, HEPES 10, Na_2ATP 4, NaGTP 0.4, sucrose 16, pH 7.3. Once whole-cell configuration was established, a period of at least 20 minutes was waited before the start of the experiment. PNs were clamped at −60 mV and PFs-induced responses elicited by electrical stimulation delivered by a patch pipette positioned in the molecular layer distant from the recorded cell. The stimulation pipette was filled with the following solution (in mM): NaCl 120, KCl 3, HEPES 10, NaH_2PO_4 1.25, $CaCl_2$ 2, $MgCl_2$ 1, glucose 10, pH 7.3. The PF-induced response was monitored over time by a test protocol of paired stimulation pulses (20 Hz) applied every 20 seconds. Three consecutive induced responses were averaged to obtain a mean trace of the evoked response per minute of recording. The induction protocol was applied in current-clamp mode with cells held at −68 mV.

Data were collected with a MultiClamp 700B (Molecular Devices, Sunnyvale, California), filtered at 2 kHz and digitized at 20 kHz. Data from each cell were normalized to the mean baseline value before cell averaging. Data are expressed as mean ± SEM.

A small hyperpolarize step (−10 mV) was applied before each stimulation to follow series resistance during the experiment. Series resistance was compensated by 70–80% and cells were discarded if significant changes were detected.

For input/output curves, cerebellar coronal acute slices from adult C57BL/6 and $Ca_V3.1$ KO mice were prepared as previously described and the following intracellular recording solution was used in whole cell patch clamp experiments (in mM): cesium methanesulfonate 135, NaCl 6, $MgCl_2$ 1, HEPES 10, MgATP 4, Na_2GTP 0.4, EGTA 1.5, QX314Cl 5, pH 7.3. The glutamatergic transmission was kept intact during the recordings to allow the full recruitment of all MLIs contributing to the GABA-mediated inhibitory response; to minimize the EPSCs contribution to the induced response, the recorded PNs was clamped at −10 mV and the PF-mediated inhibitory response was elicited by molecular layer electrical stimulation; the stimulation electrode was pulled with a vertical puller (Narishige PC-10) to a final 5 MΩ resistance when filled with the following solution (in mM): NaCl 120, KCl 3, HEPES 10, NaH_2PO_4 1.25, $CaCl_2$ 2, $MgCl_2$ 1, glucose 10, pH 7.3. Input/output curves were obtained by progressively increasing the strength of stimulation by 0.1 mA increments. At each intensity, PFs-mediated responses were recorded for three consecutive stimuli (one every 10 seconds) and traces averaged before analysis.

IPSPs were recorded in current clamp mode in presence of NBQX 5 μM. For IPSP/Vm curves, PNs were held at −40 mV and the membrane potential progressively hyperpolarized by 22 steps with a 200 pA increment.

Calcium imaging. 300 μm sagittal slices were prepared from adult (4–5 weeks) C57BL/6 and $Ca_V3.1$ KO male mice as previously described and calcium imaging experiments were performed at room temperature. The calcium indicator Oregon Green 488 BAPTA 6F ($K_D = \sim 3$ μM, Molecular Probes) and heparin were added to the low chloride or regular internal solution to a final concentration of 400 μM and 50 μg/ml respectively and they were loaded into PNs via the patch clamp pipette. After whole cell establishment, the calcium indicator was allowed to diffuse for at least 20 minutes before starting the experiment. PNs where held at a potential close to −70 mV in current clamp configuration and PF stimulation was achieved by electrical stimulation via a glass stimulation pipette placed in the molecular layer. A single 100 Hz burst stimulation (15 pulses) was applied while calcium images were acquired every 50 ms by a sCMOS CCD camera (Xyla 5.5, Andor Technology Ltd, UK) with a 20 ms exposure time. Stimulation was repeated at long interval (at least 3 minutes between trials) to avoid plasticity in the recorded cell and collected images analyzed by using ImageJ[63]. Relative change in fluorescence (ΔF/F) was quantified in ROIs including the entire dendritic tree area in which PF-induced increase in calcium concentration was detected. Average ΔF/F value for each cell was obtained from 5 consecutive imaging sections before and after TTA-P2 500 nM bath application with or without SR95531 5 μM.

Statistics. For plasticity experiments, PF-induced responses and paired-pulse ratios obtained at different time point were compared by one-way repeated measure (RM) ANOVA followed by Tukey's post hoc test.

References

1. Ito, M. *The cerebellum and neural control*. Raven Press (1984).
2. McCormick, D. A. & Thompson, R. F. Cerebellum: essential involvement in the classically conditioned eyelid response. *Science* **223(4633),** 296–299 (1984).
3. Thach, W. T., Goodkin, H. P. & Keating, J. G. The cerebellum and the adaptive coordination of movement. *Annu Rev Neurosci* **15,** 403–442 (1992).
4. Boyden, E. S., Katoh, A. & Raymond, J. L. Cerebellum-dependent learning: the role of multiple plasticity mechanisms. *Annu Rev Neurosci* **27,** 581–609 (2004).
5. Ito, M., Sakurai, M. & Tongroach, P., Climbing fibre induced depression of both mossy fibre responsiveness and glutamate sensitivity of cerebellar Purkinje cells. *J Physiol* **324,** 113–134 (1982).
6. Lev-Ram, V., Wong, S. T., Storm, D. R. & Tsien, R. Y. A new form of cerebellar long-term potentiation is postsynaptic and depends on nitric oxide but not cAMP. *Proc Natl Acad Sci USA* **99(12),** 8389–8393 (2002).
7. Coesmans, M., Weber, J. T., De Zeeuw, C. I. & Hansel, C. Bidirectional parallel fiber plasticity in the cerebellum under climbing fiber control. *Neuron* **44(4),** 691–700 (2004).
8. Belmeguenai, A. & Hansel, C. A role for protein phosphatases 1, 2A, and 2B in cerebellar long-term potentiation. *J Neurosci* **25(46),** 10768–10772 (2005).
9. Belmeguenai, A. *et al.* Alcohol impairs long-term depression at the cerebellar parallel fiber-Purkinje cell synapse. *J Neurophysiol* **100(6),** 3167–3174 (2008).
10. Schonewille, M. *et al.* Purkinje cell-specific knockout of the protein phosphatase PP2B impairs potentiation and cerebellar motor learning. *Neuron* **67(4),** 618–628 (2010).
11. Marr, D. A theory of cerebellar cortex. *J Physiol* **202(2),** 437–470 (1969).
12. De Zeeuw, C. I. *et al.* Expression of a protein kinase C inhibitor in Purkinje cells blocks cerebellar LTD and adaptation of the vestibulo-ocular reflex. *Neuron* **20(3),** 495–508 (1998).
13. Hansel, C. *et al.* alphaCaMKII Is essential for cerebellar LTD and motor learning. *Neuron* **51(6),** 835–843 (2006).
14. Boyden, E. S. *et al.* Selective engagement of plasticity mechanisms for motor memory storage. *Neuron* **5(6),** 823–834 (2006).

15. Ly, R. *et al.* T-type channel blockade impairs long-term potentiation at the parallel fiber-Purkinje cell synapse and cerebellar learning. *Proc Natl Acad Sci USA* **110(50),** 20302–20307 (2013).
16. Mittmann, W., Koch, U. & Hausser, M. Feed-forward inhibition shapes the spike output of cerebellar Purkinje cells. *J Physiol* **563** (Pt 2), 369–378 (2005).
17. Schreurs, B. G. & Alkon, D. L. Rabbit cerebellar slice analysis of long-term depression and its role in classical conditioning. *Brain Res* **631(2),** 235–240 (1993).
18. Wang, X., Chen, G., Gao, W. & Ebner, T. Long-term potentiation of the responses to parallel fiber stimulation in mouse cerebellar cortex *in vivo*. *Neuroscience* **162(3),** 713–722 (2009).
19. Wulff, P. *et al.* Synaptic inhibition of Purkinje cells mediates consolidation of vestibulo-cerebellar motor learning. *Nat Neurosci* **12(8),** 1042–1049 (2009).
20. Isope, P. & Murphy, T. H. Low threshold calcium currents in rat cerebellar Purkinje cell dendritic spines are mediated by T-type calcium channels. *J Physiol* **562** (Pt 1), 257–269 (2005).
21. Hildebrand, M. E. *et al.* Functional coupling between mGluR1 and Cav3.1 T-type calcium channels contributes to parallel fiber-induced fast calcium signaling within Purkinje cell dendritic spines. *J Neurosci* **29(31),** 9668–9682 (2009).
22. Perez-Reyes, E. Molecular physiology of low-voltage-activated t-type calcium channels. *Physiol Rev* **83(1),** 117–161 (2003).
23. Thomson, A. M. Inhibitory postsynaptic potentials evoked in thalamic neurons by stimulation of the reticularis nucleus evoke slow spikes in isolated rat brain slices–I. *Neuroscience* **25(2),** 491–502 (1988).
24. Suzuki, S. & Rogawski, M. A. T-type calcium channels mediate the transition between tonic and phasic firing in thalamic neurons. *Proc Natl Acad Sci USA* **86(18),** 7228–7232 (1989).
25. Chadderton, P., Margrie, T. W. & Hausser, M. Integration of quanta in cerebellar granule cells during sensory processing. *Nature* **428(6985),** 856–860 (2004).
26. Jorntell, H. & Ekerot, C. F. Properties of somatosensory synaptic integration in cerebellar granule cells *in vivo*. *J Neurosci* **26(45),** 11786–11797 (2006).
27. Arenz, A., Silver, R. A., Schaefer, A. T. & Margrie, T. W. The contribution of single synapses to sensory representation *in vivo*. *Science* **321(5891),** 977–980 (2008).
28. Rancillac, A. & Barbara, J. G. Frequency-dependent recruitment of inhibition mediated by stellate cells in the rat cerebellar cortex. *J Neurosci Res* **80(3),** 414–423 (2005).
29. Gao, Z., van Beugen, B. J. & De Zeeuw, C. I. Distributed synergistic plasticity and cerebellar learning. *Nat Rev Neurosci* **13(9),** 619–635 (2012).
30. Liu, S. Q. & Cull-Candy, S. G. Synaptic activity at calcium-permeable AMPA receptors induces a switch in receptor subtype. *Nature* **405(6785),** 454–458 (2000).
31. Soler-Llavina, G. J. & Sabatini, B. L. Synapse-specific plasticity and compartmentalized signaling in cerebellar stellate cells. *Nat Neurosci* **9(6),** 798–806 (2006).
32. Rancillac, A. & Crepel, F. Synapses between parallel fibres and stellate cells express long-term changes in synaptic efficacy in rat cerebellum. *J Physiol* **554** (Pt 3), 707–720 (2004).
33. Liu, S. J. & Lachamp, P. The activation of excitatory glutamate receptors evokes a long-lasting increase in the release of GABA from cerebellar stellate cells. *J Neurosci* **26(36),** 9332–9339 (2006).
34. Lachamp, P. M., Liu, Y. & Liu, S. J. Glutamatergic modulation of cerebellar interneuron activity is mediated by an enhancement of GABA release and requires protein kinase A/RIM1alpha signaling. *J Neurosci* **29(2),** 381–392 (2009).
35. Engbers, J. D. *et al.* Distinct roles for I(T) and I(H) in controlling the frequency and timing of rebound spike responses. *J Physiol* **589** (Pt 22), 5391–5413 (2011).
36. Llinas, R. & Muhlethaler, M. Electrophysiology of guinea-pig cerebellar nuclear cells in the *in vitro* brain stem-cerebellar preparation. *J Physiol* **404,** 241–258 (1988).
37. Aizenman, C. D. & Linden, D. J. Regulation of the rebound depolarization and spontaneous firing patterns of deep nuclear neurons in slices of rat cerebellum. *J Neurophysiol* **82(4),** 1697–1709 (1999).
38. Dreyfus, F. M. *et al.* Selective T-type calcium channel block in thalamic neurons reveals channel redundancy and physiological impact of I(T)window. *J Neurosci* **30(1),** 99–109 (2010).
39. Molineux, M. L. *et al.* Specific T-type calcium channel isoforms are associated with distinct burst phenotypes in deep cerebellar nuclear neurons. *Proc Natl Acad Sci USA* **103(14),** 5555–5560 (2006).
40. Talley, E. M. *et al.* Differential distribution of three members of a gene family encoding low voltage-activated (T-type) calcium channels. *J Neurosci* **19(6),** 1895–1911 (1999).
41. Petrenko, A. B., Tsujita, M., Kohno, T., Sakimura, K. & Baba, H. Mutation of alpha1G T-type calcium channels in mice does not change anesthetic requirements for loss of the righting reflex and minimum alveolar concentration but delays the onset of anesthetic induction. *Anesthesiology* **106(6),** 1177–1185 (2007).
42. Finch, E. A. & Augustine, G. J. Local calcium signalling by inositol-1,4,5-trisphosphate in Purkinje cell dendrites. *Nature* **396(6713),** 753–756 (1998).
43. Iftinca, M. *et al.* Temperature dependence of T-type calcium channel gating. *Neuroscience* **142(4),** 1031–1042 (2006).
44. Boue-Grabot, E. *et al.* Expression of GABA receptor rho subunits in rat brain. *J Neurochem* **70(3),** 899–907 (1998).
45. Rozzo, A. *et al.* Expression and dendritic mRNA localization of GABAC receptor rho1 and rho2 subunits in developing rat brain and spinal cord. *Eur J Neurosci* **15(11),** 1747–1758 (2002).
46. Midtgaard, J. Stellate cell inhibition of Purkinje cells in the turtle cerebellum *in vitro*. *J Physiol* **457,** 355–367 (1992).
47. Oldfield, C. S., Marty, A. & Stell, B. M. Interneurons of the cerebellar cortex toggle Purkinje cells between up and down states. *Proc Natl Acad Sci USA* **107(29),** 13153–13158 (2010).
48. Engbers, J. D. *et al.* Intermediate conductance calcium-activated potassium channels modulate summation of parallel fiber input in cerebellar Purkinje cells. *Proc Natl Acad Sci USA* **109(7),** 2601–2606 (2012).
49. Eilers, J., Plant, T. D., Marandi, N. & Konnerth, A. GABA-mediated Ca2+ signalling in developing rat cerebellar Purkinje neurones. *J Physiol* **536** (Pt 2), 429–437 (2001).
50. Chavas, J. & Marty, A. Coexistence of excitatory and inhibitory GABA synapses in the cerebellar interneuron network. *J Neurosci* **23(6),** 2019–2031 (2003).
51. Aiba, A. *et al.* Deficient cerebellar long-term depression and impaired motor learning in mGluR1 mutant mice. *Cell* **79(2),** 377–388 (1994).
52. Conquet, F. *et al.* Motor deficit and impairment of synaptic plasticity in mice lacking mGluR1. *Nature* **372(6503),** 237–243 (1994).
53. Hartell, N. A. Induction of cerebellar long-term depression requires activation of glutamate metabotropic receptors. *Neuroreport* **5(8),** 913–916 (1994).
54. Shigemoto, R., Abe, T., Nomura, S., Nakanishi, S. & Hirano, T. Antibodies inactivating mGluR1 metabotropic glutamate receptor block long-term depression in cultured Purkinje cells. *Neuron* **12(6),** 1245–1255 (1994).
55. Ichise, T. *et al.* mGluR1 in cerebellar Purkinje cells essential for long-term depression, synapse elimination, and motor coordination. *Science* **288(5472),** 1832–1835 (2000).
56. Lev-Ram, V., Makings, L. R., Keitz, P. F., Kao, J. P. & Tsien, R. Y. Long-term depression in cerebellar Purkinje neurons results from coincidence of nitric oxide and depolarization-induced Ca2+ transients. *Neuron* **15(2),** 407–415 (1995).

57. Shibuki, K. & Kimura, S. Dynamic properties of nitric oxide release from parallel fibres in rat cerebellar slices. *J Physiol* **498** (Pt 2), 443–452 (1997).
58. Casado, M., Isope, P. & Ascher, P. Involvement of presynaptic N-methyl-D-aspartate receptors in cerebellar long-term depression. *Neuron* **33(1),** 123–130 (2002).
59. Bidoret, C., Ayon, A., Barbour, B. & Casado, M. Presynaptic NR2A-containing NMDA receptors implement a high-pass filter synaptic plasticity rule. *Proc Natl Acad Sci USA* **106(33),** 14126–14131 (2009).
60. Zhou, H. *et al.* Cerebellar modules operate at different frequencies. *Elife* **3,** e02536 (2014).
61. Cerminara, N. L., Lang, E. J., Sillitoe, R. V. & Apps, R., Redefining the cerebellar cortex as an assembly of non-uniform Purkinje cell microcircuits. *Nat Rev Neurosci* **16(2),** 79–93 (2015).
62. Jorntell, H. & Ekerot, C. F., Reciprocal bidirectional plasticity of parallel fiber receptive fields in cerebellar Purkinje cells and their afferent interneurons. *Neuron* **34(5),** 797–806 (2002).
63. Rasband, W. S. *ImageJ*, U. S. National Institutes of Health, Bethesda, Maryland, USA (1997–2014).

Acknowledgements

We thank the TIGER project funded by INTERREG IV Rhin Supérieur program and European Funds for Regional Development (FEDER, #A31). This work was supported by the Centre National pour la Recherche Scientifique, the Université de Strasbourg, the Agence Nationale pour la Recherche and Grant ANR-2010-JCJC-1403-1 MicroCer and by the Fondation pour la Recherche Médicale (Grant Equipe FRM 2014 DEQ20140329514). We thank Dr. John J. Renger and Dr. Victor Uebele (Merck Research Laboratories, West Point USA) for kindly providing the T-type calcium channels specific antagonist TTA-P2. We thank Ludovic Spaeth for his technical assistance.

Author Contributions

F.B. designed research, performed research, analyzed data wrote the paper. K.D. performed research. S.R. provided technical assistance. K.S. and M.K. provided $Ca_V3.1$ KO mice. B.P. wrote the paper. P.I. designed research and wrote the paper.

Additional Information

Supplementary information accompanies this paper at http://www.nature.com/srep

Competing financial interests: The authors declare no competing financial interests.

How to cite this article: Binda, F. *et al.* Inhibition promotes long-term potentiation at cerebellar excitatory synapses. *Sci. Rep.* **6**, 33561; doi: 10.1038/srep33561 (2016).

Cellular/Molecular

Late-Life Environmental Enrichment Induces Acetylation Events and Nuclear Factor κB-Dependent Regulations in the Hippocampus of Aged Rats Showing Improved Plasticity and Learning

Romain Neidl,[1,2]* Anne Schneider,[1,2]* Olivier Bousiges,[1,2,3] Monique Majchrzak,[1,2] Alexandra Barbelivien,[1,2] Anne Pereira de Vasconcelos,[1,2] Kevin Dorgans,[4] Frédéric Doussau,[4] Jean-Philippe Loeffler,[5] Jean-Christophe Cassel,[1,2] and Anne-Laurence Boutillier[1,2]

[1]Laboratoire de Neurosciences Cognitives et Adaptatives, Université de Strasbourg, F-67000 Strasbourg, France, [2]Laboratoire de Neurosciences Cognitives et Adaptatives, Centre National de la Recherche Scientifique, UMR 7364, F-67000 Strasbourg, France, [3]Hôpitaux Universitaires de Strasbourg, F-67000 Strasbourg, France, [4]Institut des Neurosciences Cellulaires et Intégratives, Centre National de la Recherche Scientifique, Unité Propre de Recherche 3212, F-67084 Strasbourg, France, and [5]Institut National de la Santé et de la Recherche Médicale U1118, Mécanismes centraux et périphériques de la neurodégénérescence, Université de Strasbourg, F-67085 Strasbourg, France

Aging weakens memory functions. Exposing healthy rodents or pathological rodent models to environmental enrichment (EE) housing improves their cognitive functions by changing neuronal levels of excitation, cellular signaling, and plasticity, notably in the hippocampus. At the molecular level, brain derived-neurotrophic factor (BDNF) represents an important player that supports EE-associated changes. EE facilitation of learning was also shown to correlate with chromatin acetylation in the hippocampus. It is not known, however, whether such mechanisms are still into play during aging. In this study, we exposed a cohort of aged rats (18-month-old) to either a 6 month period of EE or standard housing conditions and investigated chromatin acetylation-associated events [histone acetyltranferase activity, gene expression, and histone 3 (H3) acetylation] and epigenetic modulation of the *Bdnf* gene under rest conditions and during learning. We show that EE leads to upregulation of acetylation-dependent mechanisms in aged rats, whether at rest or following a learning challenge. We found an increased expression of *Bdnf* through *Exon-I*-dependent transcription, associated with an enrichment of acetylated H3 at several sites of *Bdnf* promoter I, more particularly on a proximal nuclear factor κB (NF-κB) site under learning conditions. We further evidenced p65/NF-κB binding to chromatin at promoters of genes important for plasticity and hippocampus-dependent learning (e.g., *Bdnf*, *CamK2D*). Altogether, our findings demonstrate that aged rats respond to a belated period of EE by increasing hippocampal plasticity, together with activating sustained acetylation-associated mechanisms recruiting NF-κB and promoting related gene transcription. These responses are likely to trigger beneficial effects associated with EE during aging.

Key words: acetylation; aging; chromatin immunoprecipitation; environmental enrichment; NF-κB; spatial memory

Significance Statement

Aging weakens memory functions. Optimizing the neuronal circuitry required for normal brain function can be achieved by increasing sensory, motor, and cognitive stimuli resulting from interactions with the environment (behavioral therapy). This can be experimentally modeled by exposing rodents to environmental enrichment (EE), as with large cages, numerous and varied toys, and interaction with other rodents. However, EE effects in aged rodents has been poorly studied, and it is not known whether beneficial mechanisms evidenced in the young adults can still be recruited during aging. Our study shows that aged rats respond to a belated period of EE by activating specific epigenetic and transcriptional signaling that promotes gene expression likely to facilitate plasticity and learning behaviors.

Introduction

Aging is characterized by a gradual cognitive decline often associated with weakened cerebral plasticity (e.g., synaptic plasticity, neurogenesis) in brain regions involved in memory formation. Deregulations of specific transcriptional programs involved in plasticity processes could be one cause of the age-related cognitive decline (Blalock et al., 2003; Burger et al., 2008; Peleg et al., 2010). The regulation of these genetic programs is operated by the coordinated action of transcription factors and coactivators. Importantly, their accessibility and recruitment to chromatin is modulated in part by histone posttranslational modifications, of which acetylation is a well documented trigger of memory formation (Gräff and Tsai, 2013; Peixoto and Abel, 2013; Lopez-Atalaya and Barco, 2014). In the hippocampus, histone tails are actually acetylated following learning experience (Sultan and Day, 2011; Castellano et al., 2012; Bousiges et al., 2013), some of these changes being associated with the transcription of several plasticity genes required for memory formation (Bousiges et al., 2010; Gräff and Tsai, 2013; Peixoto et al., 2015). It is currently thought that aging may alter these mechanisms. For instance, H4K12 acetylation and associated genetic programs become unresponsive to experience in the hippocampal region of aged mice (Peleg et al. 2010). Another study suggests that loss of coordinated control of epigenetic landscape may account for age-associated dysfunctions rather than a specific histone modification (Castellano et al., 2012; Sewals et al., 2015). Such impairments may lead to age-associated memory deficits. Interestingly, some of these deficits could be reversed by treatment with a histone deacetylase (HDAC) inhibitor [suberoylanilide hydroxamic acid (SAHA)], as demonstrated *in vivo* with the rescue of learning-induced gene expression, enhancement of associative learning (Peleg et al., 2010), and, as described more recently, age-induced aberrant exon usage associated with a neuron-specific decrease in H4K12ac (Benito et al., 2015). Thus, compensating for acetylation deficiencies during aging with such inhibitor molecules could have an important impact on plasticity and memory functions.

Aged-induced learning and memory deficits can also be attenuated by sustained exposure of rodents to environmental enrichment (EE; Harati et al., 2011, 2012; Simpson and Kelly, 2011). EE promotes various plasticity mechanisms in the hippocampus, including long-term potentiation, *Bdnf* gene upregulation, enhanced dendritic branching, and stimulation of adult neurogenesis (van Praag et al., 2000; Nithianantharajah and Hannan, 2006; O'Callaghan et al., 2009; Simpson and Kelly, 2011; Novkovic et al., 2015). An important step toward the understanding of beneficial effects of EE was to show that, at the molecular level, EE correlated with increased histone-tail acetylation in young rodents (Fischer et al., 2007). Furthermore, mice deficient for an epigenetic enzyme such as the acetyltransferase CBP presented marked deficiencies in EE-induced neurogenesis and were less responsive to EE-mediated enhancement of spatial navigation capabilities (Lopez-Atalaya et al., 2011). Thus, epigenetic regulations, particularly histone acetylation, represent a molecular mean by which EE can translate into long-lasting changes and plasticity. However, molecular effects induced by EE have been poorly studied in aged rodents, and it is not known to which extent beneficial mechanisms evidenced in young adults can still be recruited during aging.

The present study investigated whether EE, when provided to rats at a late stage during their life (i.e., between the age of 18 and 24 months), could impact on acetylation-related regulations relevant to cognitive functions. Our results show that in aged rats, late EE improved plasticity, spatial memory acquisition, activated several acetylation-dependent processes [global histone acetyltranferase (HAT) activity, *Pcaf* expression, histone H3 acetylation], and fostered the expression of *Bdnf Exon-I* transcripts in the dorsal hippocampus. We also found that EE could favor p65/nuclear factor κB (NF-κB)-dependent regulations in aged rats. Indeed, EE induced p65/NF-κB enrichment on the proximal region of *Bdnf* promoter I and *CamK2D* promoter, both genes showing enhanced expression in response to EE. Thus, our data provide molecular evidence accounting for beneficial cognitive effects in aged rodents exposed to a belated EE.

Materials and Methods

Animals and housing conditions. Five-week-old female Long–Evans rats (Janvier Labs; $n = 107$ total) were housed in pairs in transparent cages ($46 \times 26 \times 15$ cm) until the age of 18 months [standard conditions (SCs)]. At this age, they were further kept in SCs or randomly assigned to enriched conditions (ECs) for 6 months. Enriched rats were gathered in groups of 10–12 in two contiguous wire mesh cages ($112 \times 40 \times 40$ cm) with various objects (tunnels, ramps, shelters, wooden objects, but no running wheel) changed five times a week. Food and water were available *ad libitum* in a temperature-controlled (22 ± 1°C) and humidity-controlled (55 ± 5%) room under a 12 h light/dark cycle. At the end of differential housing, the now 24-month-old rats were placed in individual transparent cages for 20 d before undergoing spatial training (tr) or not. Subsequently, they were killed for molecular biology experiments. All animals with detectable pathologies (e.g., hydrocephalus, palpable tumors) that might influence the principal outcome measures were killed or excluded a posteriori from the study. Experimental protocols and animal care were in compliance with national (Council Directive 87-848; October 19, 1987; Ministère de l'Agriculture et de la Forêt, Service Vétérinaire de la Santé et de la Protection Animale) and international (Directive 86-609; November 24, 1986; European Community and new guidelines of the European Parliament 2010/63/UE of September 22, 2010) laws and policies (Personal Authorization No. 67-167 for A.B., No. 67-289 for M.M., No. 67-215 for J.-C.C.).

Morris water maze training. The Morris water maze (MWM) consisted of a circular pool (160 cm diameter) filled with opaque water (20°C) placed in an experimental room containing extramaze cues and paintings on the walls (for details, see Lopez et al., 2012). The platform (11 cm diameter) was placed 1 cm underneath the water surface. Rats were first subjected to a 1 d habituation with a visible platform followed by a 3 d training (4 trials/day) with a hidden platform according to our previous study in young adult rats (Bousiges et al., 2010). For each trial, the rat was placed in the pool at a randomly designed starting point and given a maximum of 60 s to reach the submerged platform. When the rat had climbed onto the platform, it was left on it for 10 s, then removed, and then the next trial was started. When the rat failed to find the platform

Received Aug. 28, 2015; revised Feb. 16, 2016; accepted March 7, 2016.

Author contributions: R.N., F.D., J.-P.L., J.-C.C., and A.-L.B. designed research; R.N., A.S., O.B., M.M., A.B., A.P.d.V., K.D., and A.-L.B. performed research; R.N., A.S., M.M., A.B., and A.-L.B. analyzed data; R.N., A.S., and A.-L.B. wrote the paper.

This work was supported by the CNRS, Institut National de la Santé et de la Recherche Médicale, University of Strasbourg, and several contracts and associations: the Ligue Européenne Contre la Maladie d'Alzheimer [LECMA Project 10702 (A.L.B.); Project 10702 (O.B., R.N.)], Agence Nationale de la Recherche [ANR-12-MALZ-0002 (A.L.B., A.S.)], Alsace Alzheimer 67 (A.L.B., Dr. F. Blanc (Hôpitaux Universitaires Strasbour, France), J.-C.C.), and the Fondation Unistra-don Pierre Fabre (A.S.). R.N. is the recipient of a doctoral fellowship from the French government. We thank O. Bildstein, O. Egesi, and G. Edomwonyi for their assistance in animal care and B. Cosquer, K. Herbeaux, A. Bombardier, and M. J. Ruivo for their excellent technical assistance. We thank Prof. B. Frenguelli (University of Warwick, Coventry, UK) for his useful comments on an earlier version of this manuscript, and Dr. Karine Merienne (University of Strasbourg, Strasbourg, France) for her critical reading of this manuscript.

*R.N. and A.S. contributed equally to this work.

The authors declare no competing financial interests.

Correspondence should be addressed to Dr. Anne-Laurence Boutillier, Laboratoire de Neurosciences Cognitives et Adaptatives, UMR7364, Université de Strasbourg-CNRS, Faculté de Psychologie, 12 Rue Goethe, F-67000 Strasbourg, France. E-mail: laurette@unistra.fr.

DOI:10.1523/JNEUROSCI.3239-15.2016

 0270-6474/16/364352-11$15.00/0

within 60 s, it was gently guided to it by the experimenter and was left there for 10 s. Parameters were recorded using a video-tracking system (Noldus). The distance to the platform, corrected according to the method described by Lindner (1997), and the percentage of thigmotaxis [(time spent in the periphery/total latency to reach the platform) × 100] were calculated.

Tissue collections for biochemical studies. Rats subjected to learning in the MWM (training groups) were killed 1 h after the last training trial (Bousiges et al., 2010). Freshly dissected tissues were immediately frozen at −80°C until being processed for biochemical studies (RNA, total protein) or were immediately processed (chromatin and nuclear protein extractions).

Real-time reverse transcription-PCR. Total RNA was extracted from the dorsal hippocampus using TRizol reagent (Invitrogen) as reported previously (Bousiges et al., 2010). cDNA synthesis was performed on 1 μg of total RNA (iScript cDNA synthesis kit; Bio-Rad). Quantitative PCR (qPCR) analysis was performed on a Bio-Rad iCycler System using SsoAdvanced Green Supermix. A specific standard curve was performed in parallel for each gene, and each sample was quantified in duplicate. PCR conditions were 3 min at 94°C, followed by 40 cycles of 45 s at 94°C and 10 s at 58−62°C. Data were analyzed using the iCycler software and normalized to the RNA polymerase II mRNA. *CamK2D* primers were F_tcagtggtgagaagatgcatg and R_cagattctagcttccctttccag (for all others, see Bousiges et al., 2010).

Protein preparation, Western blot analyses, and HAT activity measurements. Total protein preparations were analyzed by Western blot as described previously (Bousiges et al., 2010). Primary antibodies were as follows: acetyl-histone H3 (06-599; Millipore), total histone H3 (ab1791, Abcam), p65 (ab31481, Abcam), K310acp65 (ab52175, Abcam), actin (Sigma-Aldrich), BDNF (AB9612, Millipore), and GFAP (MAB360, Millipore). The secondary antibodies were from Jackson Immunoresearch. Blots were revealed with Clarity ECL (Bio-Rad). Results were quantified using ImageLab software. HAT activity was measured on nuclear protein extracts prepared as by Bousiges et al. (2010), with a fluorimetric assay kit (Active Motif). All samples were tested in duplicates. The activity was analyzed in a fluorescent microplate reader at 360–390 and 450–470 nm.

Immunohistochemistry. Animals were deeply anesthetized with pentobarbital (60 mg/kg) and perfused transcardially with 150 ml ice-cold paraformaldehyde (4% in 0.1 M PB, 4°C). Brains were then rapidly removed from the skulls and postfixed for 4 h in the same fixative at 4°C. Fixed brains were then kept in sucrose at 4°C for 48 h. The freezing of the brains was performed in isopentane for 1 min at −40°C. The brains were stored in a −08°C freezer until being processed further. Coronal sections, 20 μm in thickness, were made through the dorsal hippocampus using a cryostat (Microm HM560). The tissue sections were permeabilized in 1× PBS/2% Triton for 15 min. Nonspecific labeling was blocked by 1× PBS/0.1% Triton/5% horse serum for 30 min, and sections were then incubated overnight with the indicated antibodies [doublecortin (DCX), sc-8066, Santa Cruz Biotechnology; synaptophysin (SYP), S5768, Sigma]. After three washes, they were incubated with the appropriate secondary antibody. For immunofluorescence (SYP), sections were incubated with donkey anti-mouse conjugated with fluorescent far red (FR) dye (1 h, room temperature), followed by three washes with 1× PBS/0.1% Triton; the nuclei were stained with DAPI (1:1000 dilution) for 5 min. After two PBS washes, the sections were mounted. For immunohistochemistry (DCX), sections were incubated with anti rabbit horseradish peroxidase-conjugated antibody for 1 h. After three washes with 1×PBS/0.1% Triton, the revelation was performed with diaminobenzidine (0.05% DAB, 0.04 M Tris, pH 7.5, 0.03% H_2O_2), and sections were mounted with Roti Histokit II (Roth). Images were acquired with a Zeiss (ApoTome2) imaging system.

Synaptic densities counting. Images from SYP immunofluorescence were analyzed blind using the spot detector plug-in of ICY software (F. de Chaumont, Institut Pasteur, Paris). To estimate the number of presynaptic terminals in both CA3 and CA1 areas, fluorescence puncta were filtered by size (spots >100 or <5 pixels were rejected), and spots were binarized to get an optimal visual control.

Chromatin immunoprecipitation. Freshly dissected tissues were chopped with a razor blade and rapidly put in 5 ml PBS containing 1% formaldehyde for 15 min at room temperature followed by the addition of glycine (0.125 M final concentration). Samples were prepared as in the study by Bousiges et al. (2010) and sonicated with a Diagenode Bioruptor (30 cycles of 30 s ON/30 s OFF on high power). Sonicated chromatin was diluted 10 times in chromatin immunoprecipitation (ChIP) dilution buffer (0.01% SDS, 1.1% Triton X-100, 1.2 mM EDTA, 16.7 mM Tris-Cl, pH 8.1, 167 mM NaCl). A fraction of supernatant (50 μl) from each sample was saved before immunoprecipitation (IP) and served as "total input chromatin." Supernatants were incubated overnight (4°C) with 2–5 μg of primary antibody (H3K9/K14ac, 06-599, Millipore; p65, ab31481, Abcam; or no antibody as negative control), followed by a mix of protein A/G Dynabeads (Invitrogen) for 3 h. After several washing steps (low salt, high salt, LiCl, and TE buffers), complexes were eluted in 300 μl of Elution buffer (1% SDS, 0.1 M $NaHCO_3$). The cross-linking was reversed (overnight at 65°C), and the DNA was subsequently purified with RNase (30 min, 37°C) and proteinase K (2 h, 45°C) and then subjected to phenol/chloroform extraction and ethanol precipitation. After a last wash with 70% ethanol, pellets were resuspended in 50 μl of nuclease-free milliQ water and analyzed by semiquantitative PCR (MyCycler system, Bio-Rad; 95°C for 4 min, 95°C for 40 s, 58−62°C for 40 s, 72°C for 40 s for 30–36 cycles) or by qPCR (CFX96, Bio-Rad; 98°C for 3 min, and 98°C for 15 s, 63°C for 45 s for 50 cycles, then 98°C for 10 s; melt curve, 65 to 98°C; increment, 0.5°C, 5 s). IP enrichment and specificity were checked with control genes either expressed ubiquitously (*Gapdh*) or not expressed in the hippocampus (*TsH2B*).

Primers for *Bdnf* promoter I are from Tian et al. (2009): neural-restrictive silencer element (NRSE), F_ccaaagcccaccttctggagct R_gccctagatctctgagcgaagaggtata; cAMP response element (CRE), F_aacttttctaagaagtttccttttttacca, R_tgagccagttacgtgaccaact; NF-κB, F_gcagttggacagtcattggtaacc, R_acgcaaacgccctcattctg. The promoter of rat *CamK2D* was found with the UCSC genome browser and Transcriptional Regulatory Element Database (TRED) and the Fasta sequence entered in Jaspar, computational regulatory genomics software, to identify the predictive recognition sites of p65/NF-kB. Primers were then designed with Primer3Plus bioinformatics software to the proximal region as noted in Figure 4*A*. *CamK2D* promoter primers were F_gggtctgggagcactaaaca and R_ggacagagatctcgcagtga.

Statistical analyses. Data were analyzed using a two-way ANOVA ("housing" and "training" conditions) followed, where appropriate, by *post hoc* comparisons using the Newman–Keuls multiple range test or a Student's *t* test for the data obtained in one condition only (training or housing).

Results

Late-life EE improved adult neurogenesis and synaptic densities in aged rats

A cohort of rats was raised in standard conditions for 18 months, and half of them were then either exposed to enriched conditions for the next 6 months or left in their standard conditions (Fig. 1*A*). We first asked whether belated EE had an impact on hippocampal plasticity and verified several criteria such as the formation of neuronal progenitors in the dentate gyrus and the synaptic density in two hippocampal areas. We performed immunohistochemistry studies on DCX, a marker of new yet immature neurons in the adult brain. Overall, a significant increase in the number of DCX-positive neurons (almost twofold, $p < 0.05$) was observed in the subgranular zone of the hippocampus of aged rats raised during 6 months in ECs compared to SCs (Fig. 2*B*). Another typical hallmarks of aged, memory-impaired animals is the alteration of hippocampal synaptic plasticity at CA3–CA1 synapses (Kumar, 2011). In addition, levels of the synaptic marker synaptophysin were found to be increased by EE in young (Fischer et al., 2007) and aged (Frick and Fernandez, 2003) mice. We thus measured synaptic densities by synaptophysin immunolabeling in the stratum radiatum of the dorsal hippocampal CA1 region (Fig. 2*C*, inset, DAPI) and in the CA3 region (Fig. 2*C*). The intrinsic fluorescence of lipofuscin classically observed in aged brain tissues (Fig. 2*C*, inset, FITC) was circumvented by using a

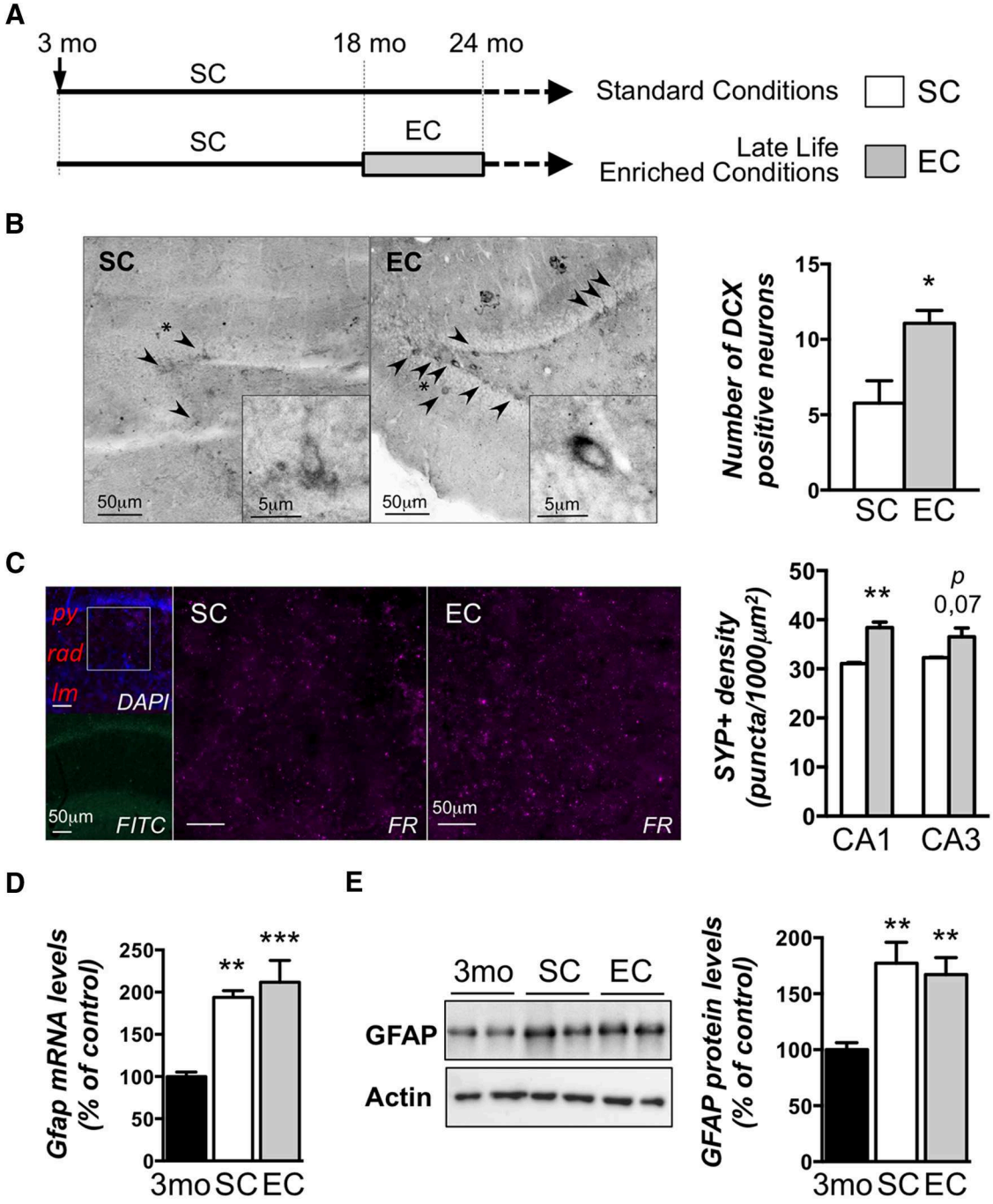

Figure 1. Enriched environment housing conditions applied in late life for aged rats increases plasticity in the hippocampus without impacting inflammation. ***A***, Experimental design. A cohort of 5-week-old rats was housed in pairs over 18 months (standard conditions). Then, rats were randomly kept in standard conditions or assigned to enriched conditions for another 6 month period, after which the 24-month-old rats were placed in individual cages for 20 d. ***B–E***, A subgroup was used for baseline assessments: immunostological (***B***, ***C***) or biochemical (***D***, ***E***) analyses. Three-month-old rats (3mo) placed in standard conditions were used as young controls (***D***, ***E***). ***B***, Hippocampal neurogenesis was evaluated by immunohistochemical detection of the immature neuronal marker DCX in the dentate gyrus subgranular zone from aged rat groups (SC and EE) under basal conditions. Arrowheads indicate DCX positive neurons, and asterisks indicate the neuron focused on in the inset. DCX-positive neurons were counted, and data are expressed as mean ± SEM ($n = 4$ per group). *$p < 0.05$ (SC vs EE; Student's t test). A significant increase of the number of DCX-positive cells in the dentate gyrus of aged rats exposed to EE compared to those reared in standard conditions is observed. ***C***, Synapse densities were visualized by synaptophysin immunolabeling (FR) in the CA1 and CA3 regions of the dorsal hippocampus. Typical photographs observed in the CA1 area are shown for SC and EC rats. The inset in the photograph on the left (top, DAPI) represents the region of CA1 that was investigated. py, Pyramidal layer; rad, stratum radiatum; lm, stratum lacunosum moleculare. The FITC photograph below shows the background fluorescence of lipofuscin typically observed in the brains of aged animals. The synapse density is represented as the number of puncta per square 1000 micrometers counted in each photograph (3–5 slices/animal; $n = 3–4$/group). **$p = 0.0025$. ***D***, mRNA expression of the glial marker GFAP was evaluated by RT-qPCR in the dorsal hippocampi of young adult rats (3mo) housed in standard conditions and aged rats (24 months of age) housed either in standard conditions or enriched conditions. Values were normalized to the RNA polymerase II expression levels. Data are expressed as mean ± SEM ($n = 7–8$ per group) with the percentage relative to the young control group arbitrarily set at 100%. **$p < 0.01$; ***$p < 0.001$ [NK *post hoc* comparisons after one-way ANOVA, significantly different from control (3mo) group]. ***E***, GFAP protein levels were assessed by Western blot in nuclear protein extracts from the dorsal hippocampi of the three previously described groups. Typical blots are shown in duplicates. Blots were quantified, and the results are expressed as mean ± SEM ($n = 4–5$ per group) with the percentage relative to the control group arbitrarily set at 100%. **$p < 0.01$ [NK *post hoc* after one-way ANOVA, significantly different from the control (3mo) group].

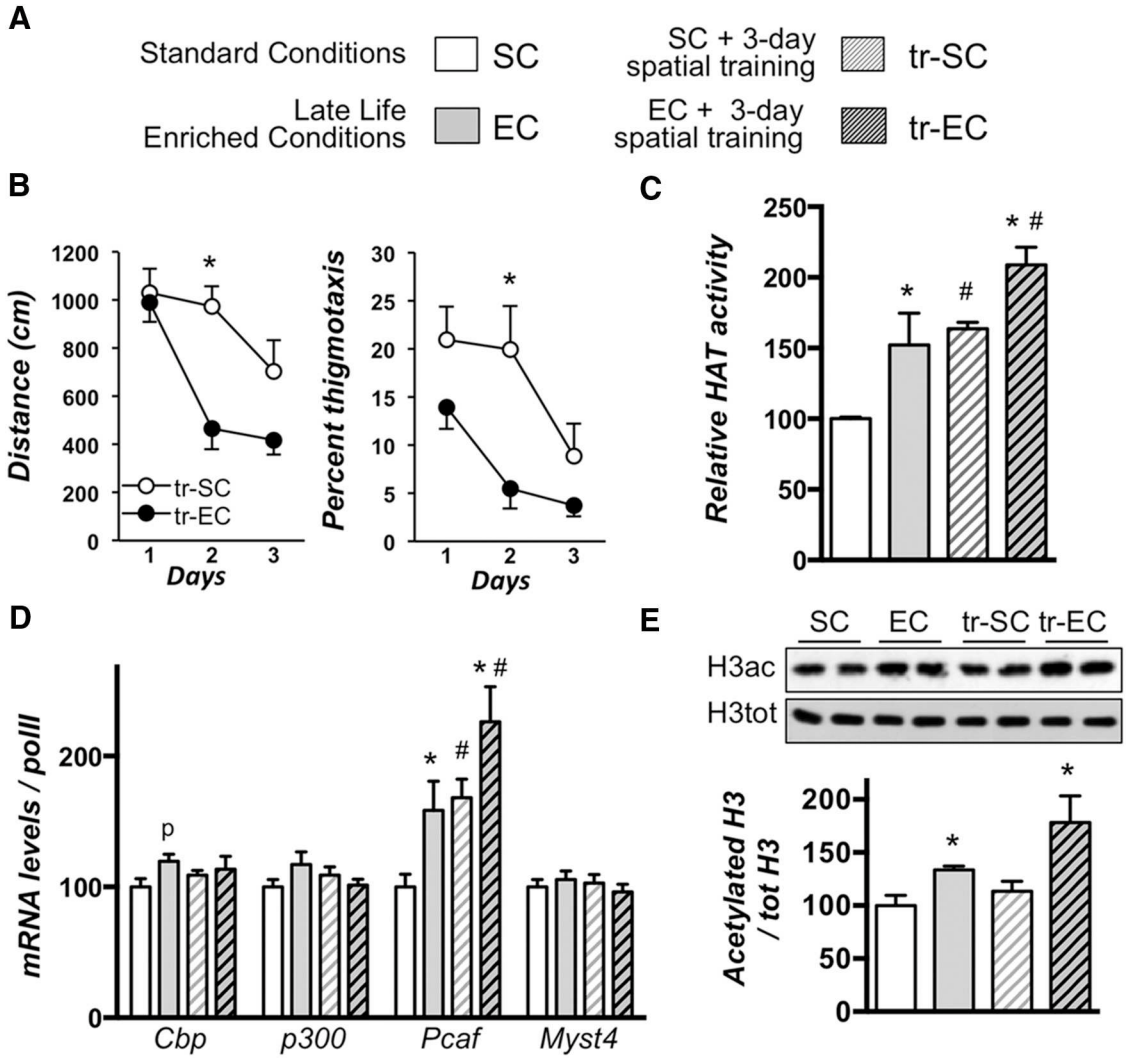

Figure 2. Late-life enrichment improves spatial learning and increases acetylation-related events in the dorsal hippocampus. ***A***, Experimental design. A cohort of 5-week-old rats was raised and housed in the same conditions than those of Figure 1. Half of each cohort was then trained (tr-SC, tr-EC) during 3 d for acquisition of reference memory in the MWM (see Material and Methods), the other half being used for baseline assessments. Thereafter, all rats were killed and their brains processed for biochemical analyses within the same range of time. ***B***, Average distance (centimeters) to reach the platform (left) and percentage of thigmotaxis (right) during the 3 d acquisition period (learning based on 4 trials per day) in the water maze. ***C***, HAT activity was measured on nuclear protein extracts from the dorsal hippocampi of the different aged rat groups ($n = 4–5$ per group) in basal (SC, white bars; EC, gray bars) and trained (tr-SC, hatched white bars; tr-EC, hatched dark bars) conditions. The color code used herein will be the same in the following figures. ***D***, mRNA expression for several HATs (*Cbp*, *p300*, *Pcaf*, and *Myst4*) was evaluated by RT-qPCR in the dorsal hippocampi of all groups of aged rats ($n = 7–10$ per group). Values were normalized to RNA polymerase II expression levels. ***E***, Total and acetylated histone H3 protein levels were assessed by Western blot in total protein extracts from the dorsal hippocampi of aged rats ($n = 4–5$ per group) as noted. Typical blots are shown in duplicates and quantifications of the ratio (acH3/total H3) are shown below (***C***–***E***). Data are expressed as mean ± SEM, with the percentage relative to the SC control group set at 100%. $^{*}p < 0.05$ (for housing, SC vs EC); $^{\#}p < 0.05$ (for training comparison; *post hoc* comparisons using the Newman–Keuls multiple range test). *p* denotes $p = 0.07$ when the EC group was compared to the SC group.

secondary antibody with an emission in the FR light wavelength. EC rats displayed a significantly higher number of synaptic contacts in CA1 as indicated by a higher number of synaptophysin-positive (SYP+) puncta/1000 μm^2 ($p < 0.01$), whereas a tendency to increase was observed in CA3 ($p = 0.07$). This suggests that a cellular adaptation of the neuronal network is induced by the 6 month period of EE. However, we found that the aged brains displayed a higher level of inflammation compared to young rats, as attested by GFAP measurements, a process that was not counteracted by the enrichment (Fig. 1*D*,*E*). This result emphasizes that the cellular content of aged hippocampi may be comparable in the two environmental conditions (aged rat groups), but is different from that found in the young rats. Therefore, biochemical measurements were performed in tissue samples of aged rats only. Overall, late-life EE produced more plasticity in the aged brain without changing the inflammation process.

EE improved spatial learning and increased acetylation-related events in aged rats

Another cohort of rats was raised in SCs or ECs as in Figure 1*A*, among which the half was trained in the MWM for 3 d (tr-SC and tr-EC) to induce learning-related signaling (Fig. 2*A*). Trained rats were killed 1 h after training, and nontrained rats were killed at the same time. We first monitored the effect of late EE on the spatial training itself. The results obtained are shown in Figure 2*B*. The average distance traveled to reach the platform decreased in both groups (tr-SC and tr-EC) from day 1 to day 3. The ANOVA showed significant housing and day of training effects for the distance traveled ($F_{(1,11)} = 13.13$, $p < 0.01$ and

$F_{(2,22)} = 11.14$, $p < 0.001$, respectively) and the percentage of thigmotaxis ($F_{(1,11)} = 10.45$, $p < 0.01$ and $F_{(2,22)} = 6.62$, $p < 0.01$, respectively). However, the overall distance swum was higher in the tr-SC than in the tr-EC rat group. *Post hoc* comparisons showed that at day 2, the tr-SC rats swam a longer distance to reach the platform than the tr-EC rats ($p < 0.01$) and stayed closer to the walls ($p < 0.05$), suggesting that rats raised in standard conditions displayed slower acquisition performance than those raised in EE. It is noteworthy that rats raised in the same EE conditions show a significantly improved retention performance when tested 24 h after 5 d of acquisition (Fuchs et al., 2016). Together, our data show that a belated EE has a beneficial effect on hippocampal plasticity by increasing adult neurogenesis, synaptic densities, and spatial learning abilities in aged rats.

We then evaluated the impact of EE on acetylation regulations in the dorsal hippocampus of these aged rats, measuring different outcomes: global HAT enzyme activity (Fig. 2*C*), global acetylation of H3 (*D*), and gene expression of several HAT enzymes (*E*), in basal and trained conditions. Our results indicated significant housing ($F_{(1,12)} = 20.68$, $p < 0.01$) and training ($F_{(1,12)} = 13{,}55$, $p < 0.001$) effects on HAT activity, and no interaction between the two factors (Fig. 2*C*). *Post hoc* comparisons indicated that EE led to increased global HAT activity in the dorsal hippocampus of aged rats under basal conditions (SC vs EC, $p < 0.05$) and under the condition of ongoing learning (tr-SC vs tr-EC, $p < 0.05$). We showed previously that spatial memory induces the upregulation of *Cbp*, *p300*, and *Pcaf* acetyltransferase transcripts in the dorsal hippocampus of young adult rats (Bousiges et al., 2010). Interestingly, in aged rats, we found that only *Pcaf* mRNA levels were significantly responsive to training (SC vs tr-SC, $p < 0.05$; Fig. 2*D*). *Pcaf* was also upregulated in response to housing conditions (SC vs EC, $p < 0.05$; tr-SC vs tr-EC, $p < 0.05$), while *Cbp* only tended to increase in response to EE ($p = 0.07$). The effect of EE was further evaluated on bulk histone H3 acetylation. We detected a significant increase in acetylated H3 levels in aged rats in response to EE in both basal and training conditions (SC vs EC, $p < 0.05$; tr-SC vs tr-EC, $p < 0.05$; Fig. 2*E*). However, contrasting with our previous findings in young adults (Bousiges et al., 2010), spatial training did not activate H3 acetylation in aged rats (Fig. 2*E*, SC vs tr-SC), suggesting a possible age-related impairment of this regulation.

Altogether, these data point to PCAF as a selective EE-responsive HAT able to contribute to increased HAT activity and histone H3 acetylation levels in the dorsal hippocampus of aged rats. Importantly, EE counteracted the lack of acetylation on H3 observed in tr-SC rats.

EE induced an up-regulation of bdnf expression through specific promoter I-dependent acetylation at different enhancer sites

EE beneficial effects are known to involve *Bdnf* transcription (Novkovic et al., 2015), even in the aged rat (O'Callaghan et al., 2009). We thus measured the expression of specific *bdnf* transcripts (*total*, *Exon-I*, *Exon-IV*, and *Exon-VI*) by RT-qPCR in the dorsal hippocampus of aged rats. As shown in Figure 3*A*, training was able to induce a moderate but significant increase of total *Bdnf* transcripts (SC vs tr-SC, $p < 0.05$). Interestingly, a dramatic upregulation of *Bdnf Exon-I* mRNA levels (SC vs tr-SC, $p < 0.05$) was observed in the dorsal hippocampus of aged rats in response to training, but no significant difference was seen for *Bdnf Exon-IV* and *Exon-VI* mRNA levels. Whereas EE did not significantly affect total *Bdnf* mRNA levels in the absence of training, despite a tendency to increase (SC vs EC, $p = 0.07$), a significant housing effect was observed in the training condition (tr-SC vs tr-EC, $p < 0.05$), suggesting that housing could enhance dynamic processes. The other *Bdnf* exons tested (*Exon-IV* and *Exon-VI*) were not responsive to EE in aged rats, yet EE induced a specific and marked increase in *bdnf Exon-I* expression in the dorsal hippocampus, under both basal and training conditions (SC vs EC, $p < 0.05$; tr-SC vs tr-EE, $p < 0.05$). Consistently, we found increased production of the 28 KDa pro-BDNF protein in trained rats in response to EE by Western blot analyses (Fig. 3*B*); however, mature BDNF levels could not be detected in our extracts.

To establish a functional link between acetylation-dependent mechanisms and specific gene transcription, we next evaluated the putative elements responsive to EE of the proximal *bdnf* promoter I region by ChIP. This promoter was well characterized in previous studies (Lubin et al., 2008; Tian et al., 2009), which indicated a correlation between NMDA receptors stimulation and *Bdnf Exon-I* transcriptional activation with increased acetylated-H3 levels on specific sites: NRSE, CRE, and NF-κB-responsive element. These sites are depicted in Figure 3*C*. We thus performed a series of ChIP experiments, targeting the proximal region of *bdnf* promoter I with acetylated-H3 histone antibodies using chromatin extracts from the dorsal hippocampus of a new group of aged rats (SC vs EC and tr-SC vs tr-EC). Figure 3*D* shows the specificity and the enrichment of the immunoprecipitation: no enrichment was detected using primers against a gene that is not expressed in the hippocampus, but only in the testis (*TsH2B*), and an enrichment of ~80-fold was found when testing binding to *Gapdh*, a highly expressed gene. On *Bdnf* promoter I (Fig. 3*E*), we detected a marked enrichment of acetylated-H3 levels induced by training on the NRSE- and CRE-binding sites in the aged rats reared in standard conditions (SC vs tr-SC, NRSE, $p < 0.05$; CRE, $p < 0.05$; NF-κB, $p = 0.09$), suggesting that *Bdnf* expression is activated to some extent through these elements in aged rats. Interestingly, EE did not impact the three responsive sites to a comparable extent under basal and trained conditions: a significant increase in acetylated-H3 levels was measured at the three sites (NRSE, CRE, and NF-κB) under basal conditions in EE housed rats (SC vs EC, NRSE, $p < 0.05$; CRE, $p < 0.05$; NF-κB, $p < 0.05$), whereas only the NF-κB binding site displayed an additional enrichment of acetylated-H3 over training (tr-SC vs tr-EC, $p < 0.05$). Thus, the additional effect found on this NF-κB site suggests that this site could contribute to the *Bdnf Exon-I* transcriptional upregulation observed in aged enriched rats during the formation of spatial memory.

EE exposure increases the binding of p65/NF-κB to target gene promoters and acetylation of p65/NF-κB during spatial training of aged rats

Having pointed to an EE-induced H3 acetylation at a proximal NF-κB site of *Bdnf* promoter I during training, our next goal was to assess whether this site was enriched with bound p65/NF-κB. Figure 4*A* shows that both CRE and NF-κB sites retained more p65/NF-κB protein during training when rats were exposed to EE (tr-SC vs tr-EE, CRE, $p < 0.01$; NF-κB, $p < 0.05$), whereas this was not the case on the NRSE site. Increased NF-κB on the CRE site may result from close proximity of the two sites (Fig. 3*C*). Our results thus indicate that NF-κB is a target for EE that could be relevant for improving hippocampal plasticity.

Interestingly, PCAF, p300, and CBP acetylate the NF-κB subunit p65 (Sheppard et al., 1999; Chen et al., 2001, 2002; Hoberg et al., 2006), and K310 acetylation is required for full transcriptional activity (Chen et al., 2002). We investigated whether EE housing conditions could impact on p65/NF-κB expression and acetyla-

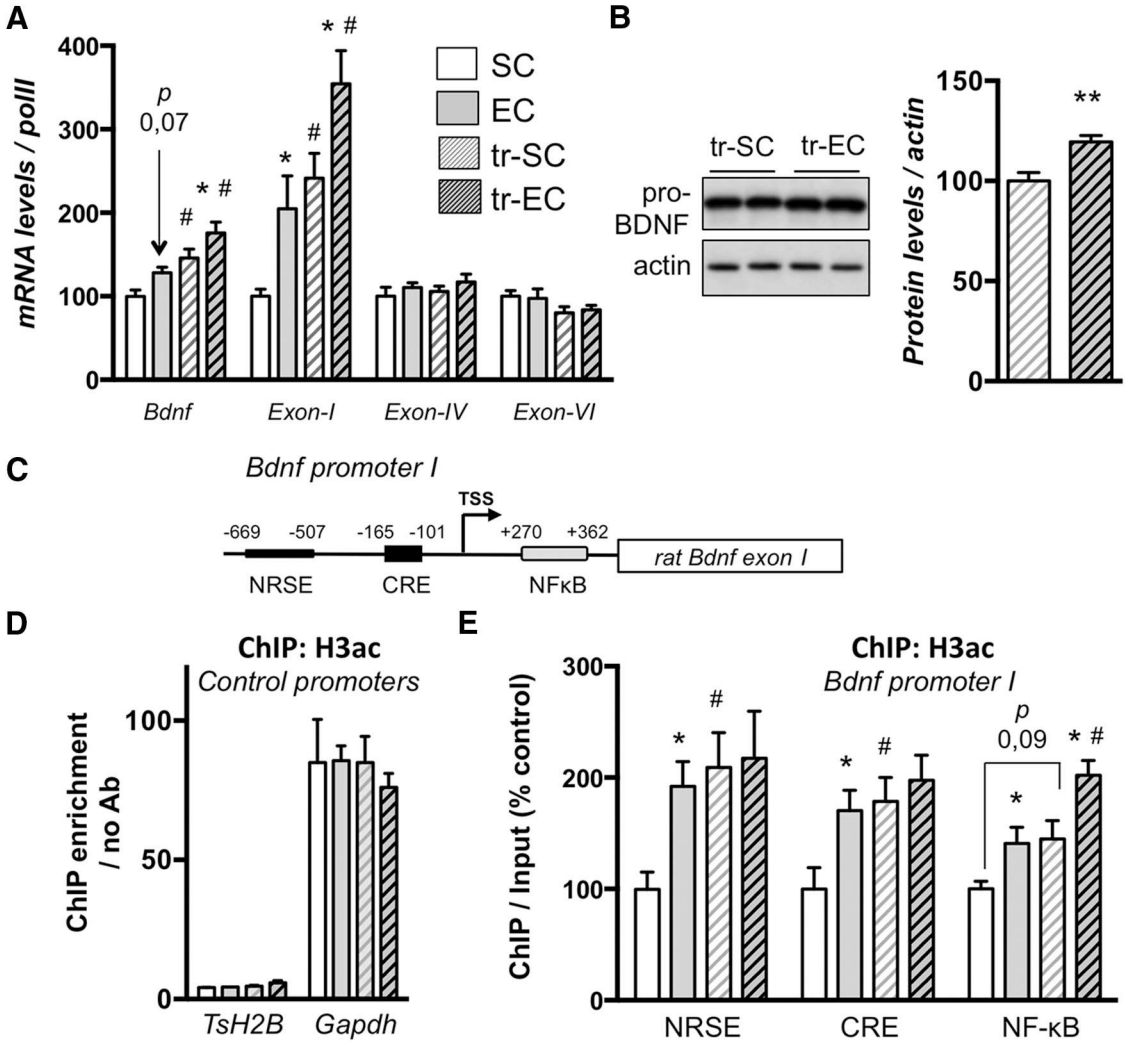

Figure 3. Late-life enrichment improves learning-induced *Bdnf* expression from *Exon-1*-dependent transcription and acetylation of the NF-κB regulatory promoter region. ***A***, mRNA expression for total *Bdnf* and several specific exons (*Exon-I*, *Exon-IV*, and *Exon-VI*) was evaluated by RT-qPCR in the dorsal hippocampi of all groups of aged rats as noted. Values were normalized to RNA polymerase II expression levels. Data are expressed as mean ± SEM ($n = 7$–10 per group), with the percentage relative to the SC control group set at 100%. $^{*}p < 0.05$ (housing, SC vs EC); $^{\#}p < 0.05$ (training; *post hoc* comparisons using the Newman Keuls multiple range test). $p = 0.07$ when the EC group was compared to the SC group for total *Bdnf* transcripts. ***B***, Western blot analyses of pro-BDNF and actin levels performed on lysates from dorsal hipocamppi of MWM-trained aged SC or EC rats. Representative results are presented as duplicates (left), and their quantification is expressed as mean ± SEM ($n = 6$ per group), with the percentage relative to the tr-SC control group arbitrarily set at 100%. Enrichment housing induces pro-BDNF expression. $^{**}p < 0.01$ (Student's *t* test to compare the effect of housing on trained aged rats (tr-EC vs tr-SC). ***C***, Relative location of enhancer elements within the rat *Bdnf Exon-I* specific promoter (adapted from Tian et al., 2009). The three sites examined (NRSE, CRE, and NF-κB) are located with their respective position in the proximal region of the promoter [transcription start site (TSS)]. ***D***, ***E***, ChIP performed with an antibody against acetylated-histone H3 on chromatin isolated from dorsal hippocampi of aged rat groups. The quantity of immunoprecipitated DNA was assessed by qPCR for control genes (testis H2B histone *TsH2B* and *Gapdh*) relative to the no antibody control to establish the enrichment of the IP (***D***) and *Bdnf I* promoter regions of interest as noted (***E***). The net quantities of enriched DNA were corrected with their corresponding input DNA. Data are expressed as mean ± SEM ($n = 4$ per group), with the percentage relative to the SC control group arbitrarily set at 100%. $^{*}p < 0.05$ (housing, SC vs EC); $^{\#}p < 0.05$ (training; *post hoc* comparisons using the Newman–Keuls multiple range test). *p* denotes $p = 0.09$ when training was compared to basal in SC for the NF-κB site.

tion status on K310 by Western blot analyses. As shown in Figure 4*B*, p65/NF-κB protein levels were not changed by EE, whereas its acetylation at K310 was significantly induced by EE exposure ($p < 0.01$).

Last, we further looked at genes implicated in spatial memory and that may be responsive to p65/NF-κB, among which *CamK2D* is a good candidate (Federman et al., 2013). We checked for p65/NF-κB binding on its proximal promoter in a region enriched on potential p65/NF-κB sites (Fig. 5*A*, left) and found an increase in p65/NF-κB binding (right). Finally, we found a significant increase of *CamK2D* gene transcription in EE-exposed rats compared to rats raised in standard conditions (Fig. 5*B*). Therefore, we propose that EE housing beneficial effects observed on aging are produced in part by boosting acetylation and NF-κB-dependent regulations, by the mean of increased HAT activity and expression (e.g., *Pcaf*), and increased transcription of genes important for spatial memory and hippocampal plasticity (e.g., *Bdnf*, *CamK2D*; Fig. 5*C*).

Discussion

As aging may have detrimental effects on memory function, much effort is made to develop mild therapeutic strategies such as behavioral therapies for preventing/delaying cognitive symptoms. Enrichment of physical and social environments belongs to such strategies. Herein, we present evidence that a belated 6 month EE exposure of rats exerts beneficial effects on plasticity and memory compared to their counterparts raised in standard conditions. These effects are in part transduced through specific

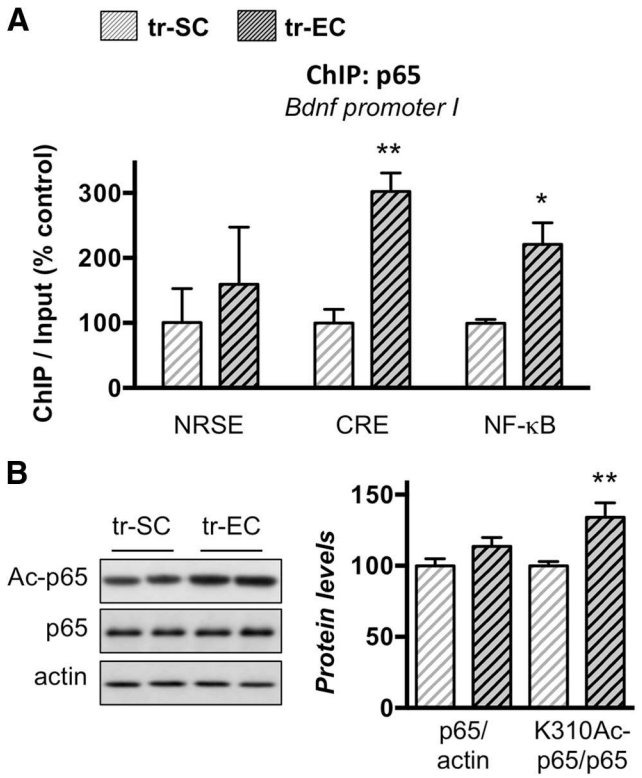

Figure 4. Late-life enrichment induces p65/NF-κB binding on the *Bdnf* promoter I and acetylation of p65/NF-κB protein. ***A***, ChIP performed with an antibody against p65/NF-κB on chromatin isolated from dorsal hippocampi of SCs or ECs aged rat groups that were trained in the MWM for 3 d as described. The quantity of immunoprecipitated DNA was assessed by qPCR for the three sites (NRSE, CRE, NF-κB) present in the *Bdnf* promoter I. The net quantities of enriched DNA were corrected with their corresponding input DNA. Data are expressed as mean ± SEM ($n = 3$ per group) with percentage relative to the tr-SC control group arbitrarily set at 100%. EE promotes p65/NF-κB binding to the proximal region of the *Bdnf* promoter I. ***B***, Western blot analyses of p65, acetylated-p65 at K310 (Ac-p65), and actin levels performed on lysates from dorsal hipocamppi of MWM-trained aged SC or EC rats. Representative results are presented as duplicates (left), and their quantification is expressed as mean ± SEM ($n = 6$ per group) with percentage relative to the tr-SC control group arbitrarily set at 100%. Enrichment housing induces acetylation of p65. *$p < 0.05$; **$p < 0.01$ (Student's *t* test to compare the effect of housing on trained aged rats, tr-EC vs tr-SC; ***A***, ***B***).

cellular signaling regulating chromatin acetylation and NF-κB-dependent transcription and leading to the expression of genes important for memory and plasticity, such as *Bdnf* and *CamK2D*.

In our study, EE was found to induce global HAT activity, with a significant increase of *Pcaf* expression and of bulk histone H3 acetylation, events likely to lead to increased chromatin H3 acetylation at the *Bdnf* promoter I and to the production of pro-BDNF in the dorsal hippocampus of aged rats. Several studies have reported increased plasticity mechanisms in the hippocampus of rodents exposed to EE, including upregulation of *Bdnf* expression (van Praag et al., 2000; Novkovic et al., 2015), as well as in mouse and rat models of aging (O'Callaghan et al., 2009; Grinan-Ferre et al., 2015). Only a few previous studies addressed the question of exon-specific expression, and it seems that short-term enrichment can activate *Bdnf* expression through multiple promoters in young adult animals (Zajac et al., 2010; Branchi et al., 2011; Jha et al., 2011; Kuzumaki et al., 2011). We found that *Bdnf Exon-I* transcripts were highly upregulated in EE-exposed aged rats. The *Bdnf* promoter I was found more responsive to histone acetylation changes compared to *Bdnf* promoter IV in HDAC inhibitor-treated neuronal primary cultures (Hara et al., 2009; Tian et al., 2009). In addition, this particular transcript increases after a single new context exposure (Lubin et al., 2008). As a short EE exposure capable of inducing recovery of hippocampal-dependent memory was associated with increased global histone H3/H4 acetylation levels in the dorsal hippocampus of young adult mice (Fischer et al., 2007), our data also provide evidence that EE is able to increase H3 acetylation in aged rats. Furthermore, sustained acetylated-H3 occupancy at *Bdnf* promoter I has been shown to lead to a persistent increase of *Bdnf Exon-I* transcripts over time (Hara et al., 2009). Thus, our data show that EE can still favor a dynamic epigenetic regulation of *Bdnf* through increased chromatin acetylation at promoter I in the aged rats, despite that mature old rats are known to benefit less than their young counterparts from the social and physical stimulation provided by EE (Mora-Gallegos et al., 2015). Of note, PCAF can acetylate histone H3K9 (Nagy et al., 2010) and is implicated in learning and memory in young and old mice (Maurice et al., 2008). Thus, PCAF could be a molecular link by which EE can modify chromatin structure. As synaptic plasticity and memory deficits that occur during aging are associated with altered histone acetylation mechanisms (Peleg et al., 2010; Benito et al. 2015), our data emphasize that a 6 month period of EE in aged rats could improve hippocampal plasticity, in part through *Pcaf*- and *Bdnf* promoter I–mediated regulations.

Our data also point to NF-κB as an important player in EE-induced plasticity-related transcription that is still adjustable in the aged rats. Indeed, we evidenced an increase in p65/NF-κB occupancy at plasticity-related gene promoters, e.g., *Bdnf* and *camK2D*. The role of the transcription factor p65/NF-κB in memory is now well documented (Mattson and Meffert, 2006; Alberini, 2009; Gutierrez and Davies, 2011). For instance, it has been associated with the control of excitatory synapse and dendritic spine formation and morphology in hippocampal neurons, a process that requires, in part, NF-κB-dependent transcription of *Psd-95*, but also the local presence of p65 in the dendritic spines (Boersma et al., 2011). Interestingly, a previous study demonstrated that the target gene *Camk2D* that bears canonical NF-κB sites displayed increased p65 occupancy in this region during object recognition memory consolidation (Federman et al., 2014). Importantly, NF-κB regulation of memory was associated with increased acetylation at these sites, which occurred in a NF-κB-dependent manner (Federman et al., 2014). Our results also demonstrate an increased p65/NF-κB binding to the canonical NF-κB sites present within the rat promoter after spatial learning, and it is associated with an enhancement of *CamK2D* transcripts (Fig. 5*A*,*B*). However if the acetylation status of these sites was not determined in our study, the *Bdnf* promoter I presented an additive H3ac enrichment on the NF-κB site after training and EE. Interestingly, such additive effect of housing and training was observed in aged rats for several parameters (Figs. 2*D*, *Pcaf*; *C*, HAT activity; 3*A*, *Bdnf Exon-1*), suggesting that both housing and training induced the same outcome may be by different means. Also, the effects of 6 months of EE were most often observed after training as well (e.g., *Bdnf Exon-1 i*nduction). It is noteworthy that "housing" reflects a chronic stimulation, whereas "training" reflects an acute one. Thus, it is likely that responses that might appear similar at the molecular level in the first place would actually differ in strength as well as in duration. Nevertheless, regarding *bdnf* promoter I, the additive effect of housing and training was only observed on the NF-κB site.

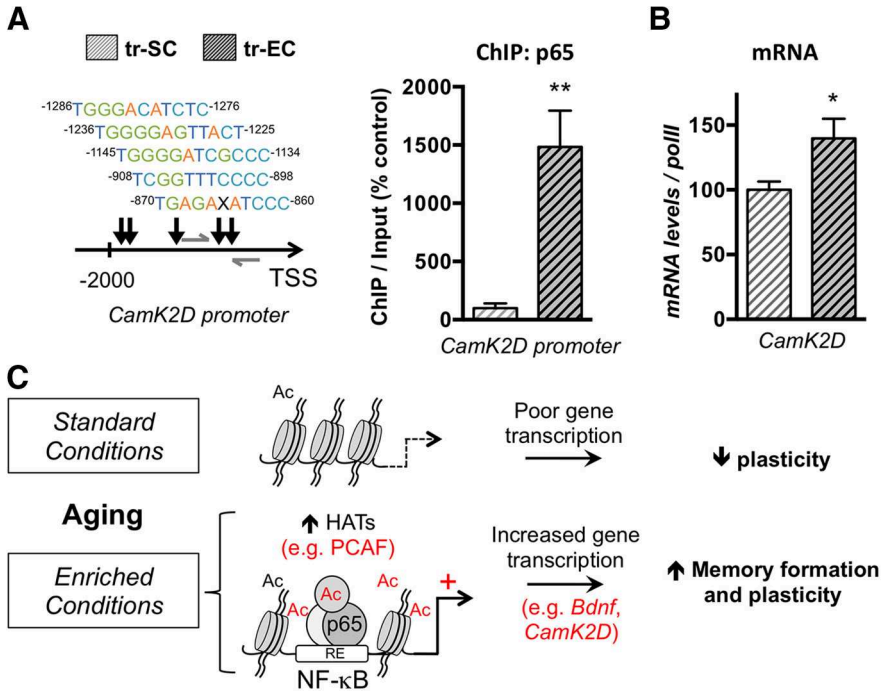

Figure 5. Late-life enrichment induces p65/NF-κB binding at NF-κB sites of spatial training-induced genes. ***A***, ChIP performed with an antibody against p65/NF-κB on chromatin isolated from dorsal hippocampi of SC or EC aged rat groups that were trained in the MWM for 3 d as described. Left, The scheme depicts the rat *CamK2D* proximal promoter and the potential p65/NF-κB binding sites ("X" represents any of the 4 bases) with their distance relative to the transcription start site (TSS), as found with TRED software. Right, The quantity of immunoprecipitated DNA was assessed by qPCR with specific primers (gray arrows on the scheme). The net quantities of enriched DNA were corrected with their corresponding input DNA. Data are expressed as mean ± SEM ($n = 3$ per group), with the percentage relative to the tr-SC control group set at 100%. EE promotes p65/NF-κB binding to the proximal region of the rat *CamK2D* promoter. ***B***, RT-qPCR evaluation of *CamK2D* transcripts in the dorsal hippocampi of trained groups of aged rats, enriched (EC) or not (SC). Values were normalized to RNA polymerase II expression levels. Data are expressed as mean ± SEM ($n = 6$ per group), with the percentage relative to the tr-SC control group set at 100%. EE significantly induced *CamK2D* expression. $^{*}p < 0.05$; $^{**}p < 0.01$ (Student's *t* test to compare the effect of housing on trained aged rats, tr-EC vs tr-SC). ***C***, Proposed model, Animals raised in standard conditions during their whole life present decreased plasticity with aging. EE induces acetylation-related events (in part through increased PCAF expression) and promotes histone (H3) and non-histone (p65/NF-κB) acetylation that leads to increased NF-κB-dependent gene transcription of specific plasticity and memory related genes, such as *Bdnf* and *CamK2D*. Ac, Acetylation.

Accordingly, NF-κB binding was found increased at the *Bdnf* promoter I (Fig. 4*A*). This suggests that EE ultimately impacts chromatin acetylation at different sites, and particularly at NF-κB-dependent sites in the hippocampus, to further modulate the response during experience (here, *Bdnf* expression after spatial training). This more "plastic" genome induced by EE, as also attested by the increased number of doublecortin-positive neurons and synapse densities in the hippocampus (Fig. 1*B*,*C*), may be relevant for differences in the strength and duration of gene (*Bdnf*) expression. In addition, increased acetylation of the p65/NF-κB protein might reinforce this mechanism (Fig. 4*B*). Indeed, p65 transcriptional activity is regulated by acetylation of lysine 310 and by several HATs, including CBP, P300, and PCAF (Sheppard et al., 1999; Chen et al., 2001, 2002; Schmitz et al., 2004). K310ac-p65 has been implicated in hippocampus-dependent memory formation (Meffert et al., 2003; Yeh et al., 2004). The fact that PCAF is highly dynamic in response to training and EE in aged rats could be associated with increased K310ac-p65. Interestingly, a previous study described a loss of p65/NF-κB occupancy at active genes downregulated in Kat2a/GCN5 cKO mice, in which memory functions are severely impaired (Stilling et al., 2014). Kat2a/GCN5 is an acetyltransferase from the same family as PCAF, also called Kat2b (Allis et al., 2007). Stilling et al. (2014) point to a concomitant action of NF-κB and Kat2a/GCN5 at the promoter region of target genes, which activates gene expression via acetylation of the p65 subunit and nearby histone tails (Stilling et al., 2014). Such a regulation between PCAF and p65/NF-κB could be at play in aged rats that were enriched. Of note, another study demonstrated that *cbp*+/− mice displayed impaired neuroadaptive transcriptional response to EE in the hippocampus and pointed to NF-κB binding site motifs (among two others) present on EE-inducible promoters in the wild type, but not in the *cbp*+/− phenotype (Lopez-Atalaya et al., 2011). Thus, HAT activation and NF-κB regulation stand as possible adaptive responses to EE.

EE could also trigger chromatin acetylation through HDAC inhibition. BDNF was shown to increase S-nitrosylation of HDAC2, thereby inhibiting its deacetylase activity (Nott et al., 2008). Interestingly, a genomewide study showed that *in vivo* HDAC inhibition with molecules such as Trichostatin A preferentially impacted NF-κB-dependent regulations in the hippocampus of treated mice (Lopez-Atalaya et al., 2013). Benito et al. (2015) demonstrated that oral administration of SAHA, another HDAC inhibitor, could ameliorate age-associated memory impairment in spatial reference memory by partly reinstating physiological exon usage through H4K12ac levels in neuronal cells. However, Sewal et al. (2015) showed that acute HDAC inhibition administration in animals having water maze experience could improve memory and extend the transcription profile in the hippocampus of young but not old rats. Thus, it is possible that the beneficial effects provided by EE in the aged rat shown in our study not only occur through NF-κB- and acetylation-related events, but also through other EE-induced pathways activated concomitantly (e.g., Phosphorylation). In addition, it will be important to discriminate the participation of glial (inflammation) versus neuronal cells (plasticity) in these processes.

Altogether, our data support the involvement of the NF-κB complex and acetylation regulations in driving hippocampal plasticity in response to enriched housing conditions in aged rats, in part through PCAF activity and the regulation of memory-dependent genes responsive to NF-κB (e.g., *Bdnf*, *CamK2D*; Fig. 5*D*). Future work investigating the relationship between EE-induced plasticity genes expression (as *Bdnf*) and particular transcriptional regulators such as NF-κB may provide insights into the development of new therapeutic strategies to prevent/damper age-related cognitive decline. Our results further support cognitive/behavioral therapeutic strategies during aging, as we show they can still be effective through specific pathways even when applied late in lifetime.

References

Alberini CM (2009) Transcription factors in long-term memory and synaptic plasticity. Physiol Rev 89:121–145. CrossRef Medline

Allis CD, Berger SL, Cote J, Dent S, Jenuwien T, Kouzarides T, Pillus L, Reinberg D, Shi Y, Shiekhattar R, Shilatifard A, Workman J, Zhang Y (2007) New nomenclature for chromatin-modifying enzymes. Cell 131: 633–636. CrossRef Medline

Benito E, Urbanke H, Ramachandran B, Barth J, Halder R, Awasthi A, Jain G, Capece V, Burkhardt S, Navarro-Sala M, Nagarajan S, Schütz AL, Johnsen SA, Bonn S, Lührmann R, Dean C, Fischer A (2015) HDAC inhibitor-dependent transcriptome and memory reinstatement in cognitive decline models. J Clin Invest 125:3572–3584. CrossRef Medline

Blalock EM, Chen KC, Sharrow K, Herman JP, Porter NM, Foster TC, Landfield PW (2003) Gene microarrays in hippocampal aging: statistical profiling identifies novel processes correlated with cognitive impairment. J Neurosci 23:3807–3819. Medline

Boersma MC, Dresselhaus EC, De Biase LM, Mihalas AB, Bergles DE, Meffert MK (2011) A requirement for nuclear factor-kappaB in developmental and plasticity-associated synaptogenesis. J Neurosci 31:5414–5425. CrossRef Medline

Bousiges O, Vasconcelos AP, Neidl R, Cosquer B, Herbeaux K, Panteleeva I, Loeffler JP, Cassel JC, Boutillier AL (2010) Spatial memory consolidation is associated with induction of several lysine-acetyltransferase (histone acetyltransferase) expression levels and H2B/H4 acetylation-dependent transcriptional events in the rat hippocampus. Neuropsychopharmacology 35:2521–2537. CrossRef Medline

Bousiges O, Neidl R, Majchrzak M, Muller MA, Barbelivien A, Pereira de Vasconcelos A, Schneider A, Loeffler JP, Cassel JC, Boutillier AL (2013) Detection of histone acetylation levels in the dorsal hippocampus reveals early tagging on specific residues of H2B and H4 histones in response to learning. PLoS One 8:e57816. CrossRef Medline

Branchi I, Karpova NN, D'Andrea I, Castrén E, Alleva E (2011) Epigenetic modifications induced by early enrichment are associated with changes in timing of induction of BDNF expression. Neurosci Lett 495:168–172. CrossRef Medline

Burger C, Lopez MC, Baker HV, Mandel RJ, Muzyczka N (2008) Genome-wide analysis of aging and learning-related genes in the hippocampal dentate gyrus. Neurobiol Learn Memory 89:379–396. CrossRef

Castellano JF, Fletcher BR, Kelley-Bell B, Kim DH, Gallagher M, Rapp PR (2012) Age-related memory impairment is associated with disrupted multivariate epigenetic coordination in the hippocampus. PLoS One 7:e33249. CrossRef Medline

Chen LF, Mu Y, Greene WC (2002) Acetylation of RelA at discrete sites regulates distinct nuclear functions of NF-kappaB. EMBO J 21:6539–6548. CrossRef Medline

Chen Lf, Fischle W, Verdin E, Greene WC (2001) Duration of nuclear NF-kappaB action regulated by reversible acetylation. Science 293:1653–1657. CrossRef Medline

Federman N, de la Fuente V, Zalcman G, Corbi N, Onori A, Passananti C, Romano A (2013) Nuclear factor kappaB-dependent histone acetylation is specifically involved in persistent forms of memory. J Neurosci 33:7603–7614. CrossRef Medline

Federman N, Zalcman G, de la Fuente V, Fustinana MS, Romano A (2014) Epigenetic mechanisms and memory strength: a comparative study. J of physiology, Paris 108:278–285. CrossRef

Fischer A, Sananbenesi F, Wang X, Dobbin M, Tsai LH (2007) Recovery of learning and memory is associated with chromatin remodelling. Nature 447:178–182. CrossRef Medline

Frick KM, Fernandez SM (2003) Enrichment enhances spatial memory and increases synaptophysin levels in aged female mice. Neurobiol Aging 24: 615–626. CrossRef Medline

Fuchs F, Cosquer B, Penazzi L, Mathis C, Kelche C, Majchrzak M, Barbelivien A (2016) Exposure to an enriched environment up to middle age allows preservation of spatial memory capabilities in old age. Behav Brain Res 299:1–5. CrossRef Medline

Gräff J, Tsai LH (2013) Histone acetylation: molecular mnemonics on the chromatin. Nature reviews Neuroscience 14:97–111. CrossRef Medline

Griñan-Ferré C, Pérez-Cáceres D, Gutiérrez-Zetina SM, Camins A, Palomera-Avalos V, Ortuño-Sahagún D, Rodrigo MT, Pallàs M (2015) Environmental enrichment improves behavior, cognition, and brain functional markers in young senescence-accelerated prone mice (SAMP8). Mol Neurobiol 27:1–16. CrossRef Medline

Gutierrez H, Davies AM (2011) Regulation of neural process growth, elaboration and structural plasticity by NF-kappaB. Trends Neurosci 34:316–325. CrossRef Medline

Hara D, Miyashita T, Fukuchi M, Suzuki H, Azuma Y, Tabuchi A, Tsuda M (2009) Persistent BDNF exon I-IX mRNA expression following the withdrawal of neuronal activity in neurons. Biochem Biophys Res Commun 390:648–653. CrossRef Medline

Harati H, Majchrzak M, Cosquer B, Galani R, Kelche C, Cassel JC, Barbelivien A (2011) Attention and memory in aged rats: Impact of lifelong environmental enrichment. Neurobiol Aging 32:718–736. CrossRef Medline

Harati H, Barbelivien A, Herbeaux K, Muller MA, Engeln M, Kelche C, Cassel JC, Majchrzak M (2012) Lifelong environmental enrichment in rats: impact on emotional behavior, spatial memory vividness, and cholinergic neurons over the lifespan. Age (Dordr) 35:1027–1043. CrossRef

Hoberg JE, Popko AE, Ramsey CS, Mayo MW (2006) IkappaB kinase alpha-mediated derepression of SMRT potentiates acetylation of RelA/p65 by p300. Mol Cell Biol 26:457–471. CrossRef Medline

Jha S, Dong B, Sakata K (2011) Enriched environment treatment reverses depression-like behavior and restores reduced hippocampal neurogenesis and protein levels of brain-derived neurotrophic factor in mice lacking its expression through promoter IV. Transl Psychiatry 1:e40. CrossRef Medline

Kumar A (2011) Long-term potentiation at CA3-CA1 hippocampal synapses with special emphasis on aging, disease, and stress. Front Aging Neurosci 20:3–7. CrossRef Medline

Kuzumaki N, Ikegami D, Tamura R, Hareyama N, Imai S, Narita M, Torigoe K, Niikura K, Takeshima H, Ando T, Igarashi K, Kanno J, Ushijima T, Suzuki T (2011) Hippocampal epigenetic modification at the brain-derived neurotrophic factor gene induced by an enriched environment. Hippocampus 21:127–132. CrossRef Medline

Lindner MD (1997) Reliability, distribution, and validity of age-related cognitive deficits in the Morris water maze. Neurobiol Learn Mem 68:203–220. CrossRef Medline

Lopez J, Herbeaux K, Cosquer B, Engeln M, Muller C, Lazarus C, Kelche C, Bontempi B, Cassel JC, de Vasconcelos AP (2012) Context-dependent modulation of hippocampal and cortical recruitment during remote spatial memory retrieval. Hippocampus 22:827–841. CrossRef Medline

Lopez-Atalaya JP, Barco A (2014) Can changes in histone acetylation contribute to memory formation? Trends Genet 30:529–539. CrossRef Medline

Lopez-Atalaya JP, Ciccarelli A, Viosca J, Valor LM, Jimenez-Minchan M, Canals S, Giustetto M, Barco A (2011) CBP is required for environmental enrichment-induced neurogenesis and cognitive enhancement. EMBO J 30:4287–4298. CrossRef Medline

Lopez-Atalaya JP, Ito S, Valor LM, Benito E, Barco A (2013) Genomic targets, and histone acetylation and gene expression profiling of neural HDAC inhibition. Nucleic Acids Res 41:8072–8084. CrossRef Medline

Lubin FD, Roth TL, Sweatt JD (2008) Epigenetic regulation of BDNF gene transcription in the consolidation of fear memory. J Neurosci 28:10576–10586. CrossRef Medline

Mattson MP, Meffert MK (2006) Roles for NF-kappaB in nerve cell survival, plasticity, and disease. Cell Death Differ 13:852–860. CrossRef Medline

Maurice T, Duclot F, Meunier J, Naert G, Givalois L, Meffre J, Célérier A, Jacquet C, Copois V, Mechti N, Ozato K, Gongora C (2008) Altered memory capacities and response to stress in p300/CBP-associated factor (PCAF) histone acetylase knockout mice. Neuropsychopharmacology 33: 1584–1602. CrossRef Medline

Meffert MK, Chang JM, Wiltgen BJ, Fanselow MS, Baltimore D (2003) NF-kappa B functions in synaptic signaling and behavior. Nat Neurosci 6:1072–1078. CrossRef Medline

Mora-Gallegos A, Rojas-Carvajal M, Salas S, Saborio-Arce A, Fornaguera-Trias J, Brenes JC (2015) Age-dependent effects of environmental enrichment on spatial memory and neurochemistry. Neurobiol Learn Memory 118:96–104. CrossRef

Nagy Z, Riss A, Fujiyama S, Krebs A, Orpinell M, Jansen P, Cohen A, Stunnenberg HG, Kato S, Tora L (2010) The metazoan ATAC and SAGA coactivator HAT complexes regulate different sets of inducible target genes. Cell Mol Life Sci 67:611–628. CrossRef Medline

Nithianantharajah J, Hannan AJ (2006) Enriched environments, experience-dependent plasticity and disorders of the nervous system. Nat Rev Neurosci 7:697–709. CrossRef Medline

Nott A, Watson PM, Robinson JD, Crepaldi L, Riccio A (2008)

S-Nitrosylation of histone deacetylase 2 induces chromatin remodelling in neurons. Nature 455:411–415. CrossRef Medline

Novkovic T, Mittmann T, Manahan-Vaughan D (2015) BDNF contributes to the facilitation of hippocampal synaptic plasticity and learning enabled by environmental enrichment. Hippocampus 25:1–15. CrossRef Medline

O'Callaghan RM, Griffin EW, Kelly AM (2009) Long-term treadmill exposure protects against age-related neurodegenerative change in the rat hippocampus. Hippocampus 19:1019–1029. CrossRef Medline

Peixoto L, Abel T (2013) The role of histone acetylation in memory formation and cognitive impairments. Neuropsychopharmacology 38:62–76. CrossRef Medline

Peixoto LL, Wimmer ME, Poplawski SG, Tudor JC, Kenworthy CA, Liu S, Mizuno K, Garcia BA, Zhang NR, Giese K, Abel T (2015) Memory acquisition and retrieval impact different epigenetic processes that regulate gene expression. BMC Genom 16 [Suppl 5]:S5.

Peleg S, Sananbenesi F, Zovoilis A, Burkhardt S, Bahari-Javan S, Agis-Balboa RC, Cota P, Wittnam JL, Gogol-Doering A, Opitz L, Salinas-Riester G, Dettenhofer M, Kang H, Farinelli L, Chen W, Fischer A (2010) Altered histone acetylation is associated with age-dependent memory impairment in mice. Science 328:753–756. CrossRef Medline

Schmitz ML, Mattioli I, Buss H, Kracht M (2004) NF-kappaB: a multifaceted transcription factor regulated at several levels. Chembiochem 5:1348–1358. CrossRef Medline

Sewal AS, Patzke H, Perez EJ, Park P, Lehrmann E, Zhang Y, Becker KG, Fletcher BR, Long JM, Rapp PR (2015) Experience modulates the effects of histone deacetylase inhibitors on gene and protein expression in the hippocampus: impaired plasticity in aging. J Neurosci 35:11729–11742. CrossRef Medline

Sheppard KA, Rose DW, Haque ZK, Kurokawa R, McInerney E, Westin S, Thanos D, Rosenfeld MG, Glass CK, Collins T (1999) Transcriptional activation by NF-kappaB requires multiple coactivators. Mol Cell Biol 19:6367–6378. CrossRef Medline

Simpson J, Kelly JP (2011) The impact of environmental enrichment in laboratory rats–behavioural and neurochemical aspects. Behav Brain Res 222:246–264. CrossRef Medline

Stilling RM, Rönicke R, Benito E, Urbanke H, Capece V, Burkhardt S, Bahari-Javan S, Barth J, Sananbenesi F, Schütz AL, Dyczkowski J, Martinez-Hernandez A, Kerimoglu C, Dent SY, Bonn S, Reymann KG, Fischer A (2014) K-Lysine acetyltransferase 2a regulates a hippocampal gene expression network linked to memory formation. EMBO J 33:1912–1927. CrossRef Medline

Sultan FA, Day JJ (2011) Epigenetic mechanisms in memory and synaptic function. Epigenomics 3:157–181. CrossRef Medline

Tian F, Hu XZ, Wu X, Jiang H, Pan H, Marini AM, Lipsky RH (2009) Dynamic chromatin remodeling events in hippocampal neurons are associated with NMDA receptor-mediated activation of Bdnf gene promoter 1. J Neurochem 109:1375–1388. CrossRef Medline

van Praag H, Kempermann G, Gage FH (2000) Neural consequences of environmental enrichment. Nat Rev Neurosci 1:191–198. Medline

Yeh SH, Lin CH, Gean PW (2004) Acetylation of nuclear factor-kappaB in rat amygdala improves long-term but not short-term retention of fear memory. Mol Pharmacol 65:1286–1292. CrossRef Medline

Zajac MS, Pang TY, Wong N, Weinrich B, Leang LS, Craig JM, Saffery R, Hannan AJ (2010) Wheel running and environmental enrichment differentially modify exon-specific BDNF expression in the hippocampus of wild-type and pre-motor symptomatic male and female Huntington's disease mice. Hippocampus 20:621–636. Medline

Partie1. Les terminaisons présynaptiques, unités structurales de la neurotransmission chimique

Les synapses transfèrent des informations électriques en libérant des neurotransmetteurs dans des gammes temporelles très courtes (moins d'une milliseconde) et ce, de manière extrêmement fiable. Les propriétés ultrastructurales et moléculaires des terminaisons présynaptiques sont à l'origine de leur capacité à transférer une information dans une fenêtre temporelle réduite.

Au sein des terminaisons synaptiques, les neurotransmetteurs sont contenus dans des vésicules synaptiques et le cycle des vésicules synaptiques est un processus hautement régulé :
1) Dans un premier temps, les mobilisation des vésicules de réserve permet un adressage spécifique à la zone active. 2) La zone active contient les sites de libération des neurotransmetteurs et les vésicules synaptiques sont arrimées et « primées » pour une fusion membranaire qui repose sur les complexes moléculaires SNARE. 3) Au cours d'une activité neuronale, des potentiels d'action viennent dépolariser les terminaisons présynaptiques. De telles dépolarisations génèrent des entrées calciques via les canaux calciques voltage-sensitifs présents au niveau des sites de libération ce qui déclenche la fusion membranaire en l'espace de quelques centaines de millisecondes. 4) Les membranes des vésicules synaptiques ainsi que leurs composants moléculaires sont récupérés via des processus d'endocytose compensatrice. Le recyclage des vésicules synaptiques s'effectue en périphérie des sites de libération et il est essentiel pour la stabilité des différentes populations de vésicules présynaptiques.

Au cours d'une activité synaptique, les neurotransmetteurs sont libérés dans la fente synaptique, leur fixation sur des récepteurs post-synaptiques ionotripiques induit un courant post-synaptique. La taille des courants post-synaptiques est en lien avec la quantité de neurotransmetteurs libérés par une dépolarisation présynaptique. En effet, il est possible d'estimer la quantité de neurotransmetteurs libérés par une mesure des courants post synaptiques (CPS). Cette mesure peut être résumée par une simple équation :

$i_{syn} = n \,.\, P_r \,.\, Q$

i_{syn}	la taille du CPS (en Ampères)
Q	l a taille d'un événement unitaire (en Ampères)
n	le nombre de sites de libération
P_r	la probabilité de fusion des vésicules synaptiques

Tandis que la taille du quantum (Q) est à la fois liée à des variables présynaptiques (la quantité de neurotransmetteurs au sein d'une vésicule synaptique) et postsynaptiques (la conductance unitaire des récepteurs post-synaptiques, leur saturation, leur présence ou non), la probabilité de libération de

neurotransmetteur à la suite d'un potentiel d'action (P_r) ainsi que le nombre de sites de libération (n) sont plus couramment admis comme des paramètres présynaptiques.

Au cours des prochains paragraphes, je décrirai les éléments de la physiologie synaptique qui déterminent les différents paramètres de la libération de neurotransmetteurs (N, P et Q). De plus, j'accorderai une importance très particulière aux mécanismes de plasticité synaptique à court terme. Il s'agit d'un processus qui façonne la sécrétion de neurotransmetteurs de manière extrêmement dynamique. Ainsi, nous verrons que les paramètres de la libération de neurotransmetteurs ne sont pas figés dans le temps. Comme l'hétérogénéité de fonctionnement présynaptique a été mon principal objet d'étude lors de ma thèse, nous verrons que les paramètres de libération et de plasticité présynaptique varient d'une synapse à l'autre.

1,1 Les vésicules synaptiques

Les vésicules synaptiques contiennent les neurotransmetteurs. On les considère comme des unités ultrastructurales homogènes dédiées à l'exocytose régulée. Des travaux récents visant à caractériser le protéome de vésicules synaptiques uniques ont permis de mieux cerner leurs particularité moléculaires (Takamori et al., 2006).

Premièrement, ces études ont démontré que les neurotransmetteurs sont densément stockés dans les vésicules synatiques (~40nm) par des transporteurs vésiculaires (par exemple, les VGluT 1-3 sont les transporteurs vésiculaires du glutamate tandis que GAT est le transporteur du GABA). Ces derniers utilisant des gradients de protons, une V-ATPase est nécessaire pour l'acidification luminale et par conséquent, le transport des molécules à l'intérieur des vésicules synaptiques. Cette quantité est également qualifiée de *quantum,* qui à priori stable d'une vésicule à l'autre même s'il a été démontré qu'elle peut être sujet à diverses modulations (Takamori, 2016).

Deuxièmement, ces études montrent que les vésicules synaptiques présentent une très grande diversité de protéines associées, telles que les vSNAREs (VAMP, synaptobrevin), différents isoformes de Synapsines, des Rho-GTPases et des protéines sensibles au calcium telles que les Synaptotagmines, senseurs calciques déclenchant la fusion vésiculaire.

Par conséquent, les vésicules synaptiques sont en interaction permanente avec l'environnement intra-synaptique ainsi qu'avec les complexes macromoléculaires de la fusion vésiculaire. De plus, il existe une très grande diversité de protéines et d'isoformes de ces protéines, associées aux vésicules synaptiques. Cette diversité est possiblement liée au sous-type de synapse purifiée et elle peut possiblement émerger d'une variabilité inter-synaptique comme nous le verrons plus tard.

Depuis leur biosynthèse jusqu'à leur fusion, le trafic des vésicules synaptiques est régulé de manière très précise ; les vésicules subissent différentes étapes successives de maturation. Dans les paragraphes suivants, je décrirai la machinerie présynaptique qui permet la maturation des vésicules synaptiques en éléments pleinement libérables au cours d'une activité neuronale.

1.2 La zone active présynaptique

La zone active présynaptique est entièrement dédiée aux mécanismes de libération des neurotransmetteurs. Elle contient la machinerie moléculaire de la neurotransmission et se situe en vis-à-vis des densités post-synaptiques et plus particulièrement des récepteurs post-synaptiques. Comme elle contient les sites de fusion des vésicules synaptiques, la zone active est un élément clé du couplage excitation/sécrétion (Südhof, 2012). Lorsqu'un potentiel d'action dépolarise la terminaison présynaptique, des canaux calciques sensibles au voltage produisent une entrée d'ions calciques dans le volume intra-terminal. Les courants calciques sont détectés par des complexes moléculaires ce qui déclenche la fusion de certaines vésicules synaptiques ancrées à la zone active. Comme nous le verrons plus tard, la neurotransmission synchrone et rapide s'effectue grâce à un couplage physique entre vésicules synaptiques et canaux calciques.

Avant de fusionner, les vésicules synaptiques suivent différentes étapes de maturation qui les rapprochent des sites de libération de la zone active. Dans un premier temps, elles sont adressées à la cytomatrice de la zone active via des ancrages moléculaires. Puis, les vésicules synaptiques sont rapprochées du feuillet interne de la membrane cytoplasmique où elles sont arrimées aux sites de libération à l'aide de complexes macromoléculaires. Enfin, le « priming » des vésicules synaptiques est un ensemble d'ajustements moléculaires qui augmentent la probabilité de fusion vésiculaires à la suite d'une activation synaptique.

1.2.1 L'adressage des vésicules synaptiques à la zone active

L'adressage des vésicules synaptiques à la zone active est une étape importante du cycle des vésicules synaptiques car l'ensemble de la machinerie moléculaire dédiée à la fusion vésiculaire se situe dans cette zone. Les micrographies synaptiques de microscopie électronique décrivent des zones de 400~700nm de diamètre denses aux électrons. Celles-ci sont enrichies en éléments du cytosquelette (comme la tubuline ou les filaments d'active), diverses protéines stabilisatrices du cytosquelette (les Synapsines, Spectrine pour les microfilaments, tau et MAP6 pour les microtubules) ainsi que de protéines permettant l'oligomérisation ()comme les septines). Un tel réseau de filaments piège les vésicules synaptiques aux abords de la zone active en impose une proximité physique entre les vésicules synaptiques et leur site de fusion. De plus, la cytomatrice est stabilisée par des protéines transmembranaires qui permettent la cohésion entre éléments pré et post-synaptiques via des échafaudages moléculaires et qui agissent également comme transducteurs

du signal (comme les N-CAM, par exemple). Cet enrichissement bien précis montre que la zone active est une zone dynamique au rôle essentiel dans le trafic des vésicules synaptiques (Laßek, Weingarten, & Volknandt, 2014). En effet, des études de microscopie électronique ont démontré qu'il existe un réseau filamenteux et dense reliant les vésicules synaptiques les une au autres en les maintenant proches des sites de libération (Siksou et al., 2007). La caractérisation de ces filaments montrent qu'il s'apparentent à des protéines présynaptiques spécifiques telles que Synapsin et Bassoon ; celles-ci contribuent en effet à l'assemblage vésiculaire au sein des terminaisons.

1.2.2 Le *docking* des vésicules synaptiques aux sites de libération

L'apport et la stabilisation des vésicules synaptiques au niveau de la zone activé (aussi dénommé phase de *docking*) est une étape essentielle à la neurotransmission. En effet, la zone active présynaptique est dotée d'une population de vésicules synaptiques prête à fusionner lors d'une activation synaptique. Ces vésicules peuvent être étudiées grâce aux outils de microscopie électroniques ; on peut discerner les vésicules *dockées* car elles sont très rapprochées de la membrane cytoplasmique présynaptique (à moins de 10nm) (Schneggenburger, Han, & Kochubey, 2012) . Des complexes moléculaires spécifiques régulent les phases de *docking* des vésicules synaptiques et le nombre de vésicules *dockées* déterminera en partie les propriétés de libération de synapses unitaires (Szule et al., 2012; Weyhersmüller, Hallermann, Wagner, & Eilers, 2011).

Grace à des techniques d'imagerie innovantes, une étude a récemment démontré que plusieurs sites de libération peuvent coexister au sein d'une même terminaison présynaptique (Maschi & Klyachko, 2017). Les sites de libération ont une identité physique et que des événements de fusion vésiculaire successifs ont lieu au niveau des mêmes domaines membranaires d'un essai à l'autre. Ainsi, la zone active et ses sites de libération sont maintenus dans le temps ; on peut parler de sites de *docking*. Ces derniers sont composés d'éléments cytosquelettiques tels que les microfilaments d'actine mais sont également composés de protéines synapse-spécifiques telles que Rim1, Munc13, Bassoon, Piccolo et Synapsine.

1.2.3 *Priming* moléculaire et *priming* positionnel des vésicules synaptiques

Lorsque les vésicules synaptiques sont *dockées* à la membranes cytoplasmique, elles subissent une étape d'amorçage (*priming*), où des ajustements moléculaires les rendent compétentes à la fusion membranaire. Rim et Munc13 sont des molécules clé dans la régulation des événements de *priming* vésiculaire bien que ce ne soient pas les seules molécules impliquées dans ce processus.

-*Priming positionnel :* Plusieurs protéines telles que Rim et Munc13 sont enrichies au niveau des sites de

libération et sont considérés comme des éléments fondamentaux de la zone active présynaptique. Elles contribuent à la construction de sites de libération car elles interviennent dans le maintien de la proximité entre canaux calciques voltage-dépendants et vésicules synaptiques ; cette proximité va déterminer le caractère synchrone et extrêmement rapide de la neurotransmission. Ainsi, réguler la distance entre vésicules synaptiques et canaux calciques va définir la probabilité de fusion des vésicules synaptiques (p_r). Un resserrement de la distance vésicule-canal augmentera la probabilité de libération et amplifiera l'aspect synchrone de la neurotransmission.

-Priming moléculaire : Certaines molécules présynaptiques optimisent le couplage excitation/sécrétion via des ajustements de la distance et des liens moléculaires entre les membranes lipidiques des vésicules et de la membrane présynaptique. Munc13 est une protéine liant le calcium qui régule l'ancrage des vésicules aux sites de libération via son interaction avec la syntaxine : la protéine membranaire de la fusion vésiculaire. Munc13 interagit également avec β-spectrin ; ce type d'interactions avec le cytosquelette permet de stabiliser les vésicules présynaptiques (Garner, Kindler, & Gundelfinger, 2000).

Rim est également une protéine liant le calcium connue notamment pour son interaction avec Rab3, une petite protéine associée aux vésicules synaptiques impliquée dans la fusion vésiculaire. Rim interagit directement avec les canaux calciques présynaptiques de la zone active grâce à son partenaire moléculaire, Rim-BP (Rim Binding Protein). Ainsi, Rim est suspectée de jouer un rôle essentiel dans la régulation des distances vésicule/canaux calciques au niveau des sites de libération (Kaeser et al., 2011).

Rim et Munc13 sont des protéines très sensibles à l'activité synaptique car elles disposent de domaines liant le calcium d'autres domaines d'interaction aux esther de phorbol (comme le diacyl-glycerol, DAG : une métabolite des récepteurs métabotropiques Gq). En effet, de telles protéines sont aptes à moduler la probabilité de libération des vésicules synaptiques en modifiant les propriétés de *priming moléculaire* et de *priming positionnel*. Ainsi, un ajustement du gain de la neurotransmission peut passer par la modulation ciblée de protéines telles que Rim et Munc13.

Université de Strasbourg

École Doctorale des Sciences de la Vie et de la Santé STRASBOURG

Kevin DORGANS

« Ultrastructural, molecular and functional heterogeneities of cerebellar granule cell presynaptic terminals »

Résumé en Français

Le cervelet est une structure cérébrale impliquée dans la régulation motrice et l'apprentissage moteur. Dans le cortex cerebelleux, les informations sensorimotrices sont transmises par les cellules en grain. Mon travail de thèse démontre que les connections synaptiques de ces neurones ont des propriétés hétérogènes. D'une synapse à l'autre, j'ai pu observer des variations d'ultrastructure, de composition moléculaire et de fonctionnement au cours de trains de potentiels d'action à haute fréquence. Plus particulièrement, j'ai caractérisé les propriétés de « plasticité à court terme » des synapses unitaires des cellules en grain :

1) Elles sont très différentes d'une synapse à l'autre et peuvent être classées en différentes sous-catégories.
2) Certaines catégories de fonctionnement synaptique reposent sur l'expression de molécules telles que la Synapsine2.
3) La réponse d'un neurone post-synaptique à de hautes fréquences de stimulation dépend de la nature de la synapse activée.

Mots-clé : neurone, synapse, cervelet, cellule en grain, interneurone de la couche moléculaire, neurotransmission, plasticité synaptique à court terme, Synapsine2, patch-clamp, microscopie électronique

Résumé en Anglais

Cerebellum is a brain structure involved in motor regulation and motor learning. In the cerebellar cortex, sensorimotor information is transmitted by granule cells. During my PhD, I demonstrated that the properties of individual granule cell synaptic connections are highly heterogeneous. From one synapse to another, I observed ultrastructural, molecular and functional variability at the level of unitary contact. More precisely, I assessed the properties of short term plasticity at individual synapses during high frequency trains of stimulation :

1) Short term plasticities are highly heterogeneous from one synapse to another and can be classified in sub-categories.
2) Some categories of short-term plasticity profiles relie on the expression of molecules such as Synapsin2.
3) The response of post-synaptic neuron to high-frequency inputs is dependent on the nature of the activated synaptic contact.

Keywords : neuron, synapse, cerebellum, granule cell, molecular layer interneuron, neurotransmission, short-term synaptic plasticity, Synapsin2, patch-clamp, electron microscopy